2021

Optimization of energy-constrained resources in radial distribution networks with solar PV

Mohammad Nawaf Nazir

University of Vermont

Recommended Citation

Nazir, Mohammad Nawaf, "Optimization of energy-constrained resources in radial distribution networks with solar PV" (2021). *Graduate College Dissertations and Theses*. 1377.
https://scholarworks.uvm.edu/graddis/1377

Optimization of energy-constrained resources in radial distribution networks with solar PV

A Dissertation Presented

by

Nawaf Nazir

to

The Faculty of the Graduate College

of

The University of Vermont

In Partial Fulfillment of the Requirements
for the Degree of Doctor of Philosophy
Specializing in Electrical Engineering

Defense Date: December 17, 2020
Dissertation Examination Committee:

Prof. Mads R. Almassalkhi, Ph.D., Advisor
Prof. Jeffrey S. Marshall, Ph.D., Chairperson
Prof. Paul D. H. Hines, Ph.D.
Prof. Hamid R. Ossareh, Ph.D.
Prof. Daniel K. Molzahn, Ph.D.
Cynthia J. Forehand, Ph.D., Dean of Graduate College

ABSTRACT

The research objective of the proposed dissertation is to make best use of available distributed energy resources to meet dynamic market opportunities while accounting for AC physics of unbalanced distribution networks and the uncertainty of distributed solar photovoltaics (PV). With ever increasing levels of renewable generation, distribution system operations must shift from a mindset of static unidirectional power flows to dynamic, unpredictable bidirectional flows. To manage this variability, distributed energy resources (DERs; e.g.,solar PV inverters, inverter-based batteries, electric vehicles, water heaters, A/Cs) need to be coordinated for reliable and resilient operation. This introduces the challenge of coordinating such resources at scale and within confines of the existing distribution system. It also becomes important to develop efficient and accurate models of the distribution system to achieve desired operating objectives such as tracking a market reference, reduction in operation cost or voltage regulation. This work surveys, discusses the challenges and proposes solutions to the modeling and optimization of realistic distribution systems with significant penetration of renewables and controllable DERs, including energy storage. To contain this increase in system complexity as result of the large number of controllable DERs available, the distribution system has to be adapted from a passive Volt-Var focused operator to a more active manager of resources. To approach this challenge, in this work, we propose two main approaches. The first is a utility centric approach, where the utility controls the dispatch of flexible resources based on solving an optimization problem. This approach would require the utility to have all the network and resource data and also the control over customer devices. Another approach is a more aggregator centric approach, where an aggregator is an entity that represents an aggregation of many diverse DERs or a Virtual Battery (VB). In this approach, it is the role of the aggregator to dispatch DERs, whereas the utility provides certain bounds and limits (calculated offline), which the aggregator (which dispatches resources in real-time) must operate under. The benefits of such an approach lie in improved data-privacy and real-time dispatch. We present simulation results validating the proposed methods on various standard IEEE and realistic distribution feeders.

Dedicated to my parents and my sisters,
for their unconditional love and support.

ACKNOWLEDGEMENTS

First and foremost, I would like to thank my Advisor, Prof. Mads Almassalkhi for his continuous support and mentorship during the four years of my PhD. Dr. Almassalkhi has always been encouraging in his efforts to help me pursue my research work and to work harder to achieve my career goals. He has helped cultivate in me important notions of critical thinking and scientific rigor. Through our discussion and his constructive feedback, I have learnt how to tackle and solve complex problems. Due to his support, I was able to do internships at two national labs during the course of my PhD, which was a great learning experience. He has always fully supported my research ideas and encouraged me to publish in high quality journals and present at prestigious conferences. I'm truly grateful for having the opportunity to be able to learn and grow under the guidance of Dr. Almassalkhi.

I would also like to thank my committee members for taking the time to guide me in this dissertation and for their helpful feedback through this entire process. I would especially like to thank Prof. Jefferey Marshall for agreeing to be the chair of my defense committee. I would also like to thank Prof. Hamid Ossareh for his guidance throughout my PhD. Prof. Ossareh has been a great source of knowledge on control systems and has helped me sharpen my skills in this area. I would also like to thank Prof. Paul Hines and Prof. Daniel Molzahn for their support and constructive feedback on my research work.

Outside my committee, I would like to thank Dr. Soumya Kundu at PNNL and Dr. Emiliano Dall'Anese at NREL for their mentorship during my internships at these national labs. I would also like to thank my collegues at UVM, including my good friends Adil Khurram, Joycer Osorio, Sarnaduti Brahma, Molly Rose and Andrew

Klem.

Finally I would like to thank my family, my parents and two sisters, for their unconditional love and support. They have always been supportive of my career goals and have always encouraged me to pursue higher education.

TABLE OF CONTENTS

List of Abbreviations

AC	Alternating current
ACOPF	Alternating current optimal power flow
AMI	Advanced metering infrastructure
ANSI	American national standards institute
BESS	Battery energy storage system
BTM	Behind the meter
BFM	Branch flow model
CAISO	California independent system operator
CB	Capacitor bank
CIA	Convex inner approximation
DC	Direct current
DER	Distributed energy resources
DSO	Distribution system operator
DSP	Distributed system platforms
EV	Electric vehicles
GLD	Gridlab-D
IEC	International electrotechnical commission
ISO	Independent system operator
IL	Inner loop
IEEE	Institute of electrical and electonic engineers
IoT	Internet of things
KKT	Karush-Kuhn-Tucker
LPF	Linear power flow

LQR	Linear quadratic regulator
LMP	Locational marginal price
MILP	Mixed integer linear program
MIP	Mixed integer program
MISOCP	Mixed integer second order cone program
NP-hard	Non-deterministic polynomial-time hard
NLP	Nonlinear program
OLTC	On-load tap changer
OPF	Optimal power flow
ORU	Orange and Rockland Utility
OL	Outer loop
PV	Photo-Voltaic
PWL	Piece-wise linear
PSD	Positive semi-definite
PF	Power factor
QC	Quadratic program
QCQP	Quadratically constrained quadratic program
QoS	Quality of service
RMSE	Root mean square error
SOCP	Second order cone program
SDP	Semi-definite program
SCD	Simultaneous charging and discharging
SoC	State of charge
SCADA	Supervisory control and data acquisition
TCL	Thermostatically controlled loads

TSO	Transmission system operator
VB	Virtual battery
VP	Voltage positioning
VPO	Voltage positioning optimization

List of Figures

List of Tables

Chapter 1

Introduction

The goal of this work is to dispatch energy-constrained resources within limits of realistic distribution networks, i.e., grid-aware dispatch of DERs. One of the routes to solve this problem, which makes sense under a utility-centric scenaio, is to develop efficient and scalable receding horizon optimal power flow (OPF) formulations. In this regard I have focused on developing convex relaxations of OPF that can manage energy-constrained grid resources, while providing guarantees on feasibility and optimality of solution. Through such techniques OPF can be scaled, but in order to achieve real-time operation (milliseconds), a convex inner approximation (CIA) of the OPF is presented, that implicitly embeds grid physics into resource bounds, enabling realtime grid-aware dispatch. The motivations for pursuing this work are presented next.

1.1 Motivation

Mitigating climate change is one of the greatest challenge of our time and will require a transition to cleaner sources of energy [12]. This will require massive integration of terawatts (TWs) of renewable generation into the electric grid, as the electricity sector represents a significant contributor towards greenhouse gas emissions. In order to manage with the intermittent nature of renewable generation, batteries can play a pivotal role in supporting this increased renewable generation. Batteries are already replacing natural gas backup generators as the cost of batteries keeps decreasing [13]. Apart from physical batteries, distributed energy resources (DERs), such as solar PV inverters and demand-side appliances (such as electric water heaters and air-conditioners) can also provide the required flexibility and improve system reliability. In particular, flexible demand is projected to exceed by more than 200 GW in the United States by 2030 [14]. DERs have the potential to enable significantly more renewable generation and furthermore reduce duck-curve ramping effects [15]. In order to tap into this huge flexibility potential, millions of devices at the distribution level would need to be coordinated. However, recruiting individual customers to DER programs and deploying this technology to individual customer devices remains a challenge and a major hurdle in the widespread adoption of DER technologies. In recent years, the ubiquitous connectivity with low-cost IoT (Internet of things) devices has made large-scale adoption of DER programs possible. As a result costs for sensing and actuation have significantly declined paving the way for cost-effective control of DERs [16]. An illustration on the adoption of renewable energy as a result of increased connectivity of DERs is shown in Fig. 1.1. The figure also shows how convergence of electric networks with other networks such as cyber, social media and financial markets, can lead to increased value creation for customers. The challenges introduced due to renewable energy and DERs will be discussed in detail in the succeeding section.

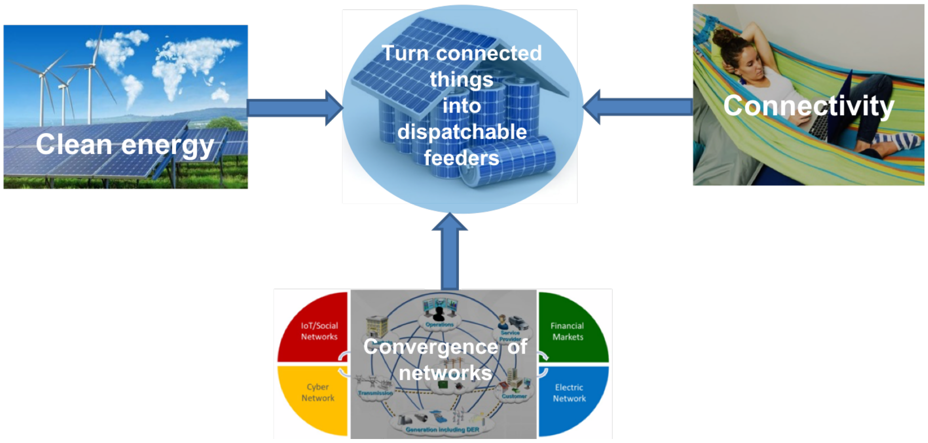

Figure 1.1: Summary of the process of using flexibility of DERs together with the improved communication and connectivity and convergence of networks, to enable large scale integration of renewables in the energy grid.

1.2 RELIABILITY CHALLENGES INTRODUCED DUE TO INCREASED RENEWABLE GENERATION

Traditionally in energy systems power flows from large generators in transmission system to the loads in distribution system. Load changes at the distribution utility level were slow and predictable through a daily load profile and hence could be easily managed. However, due to decreasing costs in renewable energy generation (such as solar PV) and climate change concerns, the amount of renewable energy in the distribution grid is increasing. Some states in the U.S. like California, Hawaii and Vermont have very ambitious renewable energy targets which include having >50% of their energy demand met through renewable generation. This will make reliability in distribution networks a challenge due to the highly volatile nature of renewable generation such as solar PV as depicted by the 10 sec resolution of solar power output in Fig. 1.2a. Furthermore, the slow and predictable variation in loads will be replaced by the fast and uncertain variability in renewable generation. Such volatility in generation can result in violation of network limits, affecting system reliability metrics [17]. With ever-increasing levels of renewable generation, distribution system operations must shift from a mindset of static unidirectional flows to dynamic, unpredictable bidirectional flows. This bidirectional flow of power introduces many challenges in the operation of distribution systems, including requirements on steep ramping. This is illustrated through the California duck curve in Fig. 1.2b showing the large variability in net-load over the same day for different years and the steep ramping requirements introduced due to increased solar generation. This bidirectional flow can also lead to voltage violations harming system reliability. The availability of flexible grid resources, however, has the potential to provide solutions to these challenges. This will require fast timescale control and coordination of distribution grid resources in order to maintain system reliability.

1.3 Role of flexibility in mitigating challenges

To maintain reliability under significant renewable (and intermittent) generation, the utility grid operators can leverage the power and energy flexibility inherent to DERs.

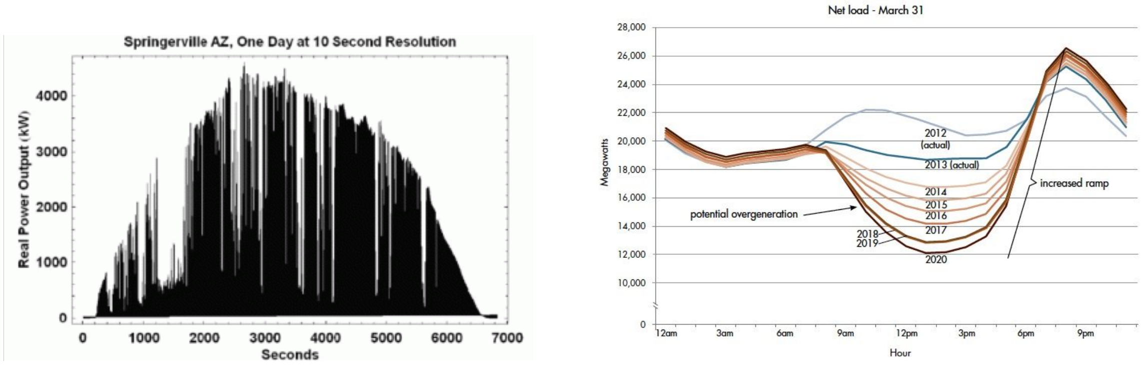

(a) (b)

Figure 1.2: (a) Figure showing the highly variable nature of solar generation over a day at 10 second resolution [1]. (b) California duck curve showing a snapshot of a 24-hour period in California during springtime, illustrating the difference in electricity demand and the amount of available solar energy throughout the day. Source: California Independent System Operator (CAISO).

This has prompted significant interests and investments in demonstration of substation automation technology, DERs, such as energy storage and smart inverters, and autonomous demand response [18,19]. However, unlike traditional generation, DERs, such as batteries are energy constrained, which give rise to the need for multi-period decision making and predictive optimization. When interacting with wholesale markets, it is useful to coordinate DERs in aggregate. Previous work in literature has shown that these DERs such as water heaters, thermostatically controlled loads, electric vehicles, etc, can be aggregated together. Since the aggregation is dispatched as a single entity by a centralized coordinator, and is subject to power and energy limits, the aggregate is often referred to as a "virtual battery" (VB) [20,21]. In such a manner, each neighbourhood or feeder can be represented as a VB, as depicted by the illustration in Fig. 1.3 [2]. However, flexible demand needs to consider the human in the loop, i.e., quality of service should always be maintained. This is further highlighted by the work in [22], which employed data-driven methods to identify behavior of customers, showing that a large proportion of thermostat users would often override large deviations away from quality service (e.g., temperature). The quality of service (QoS) shows up in the VB model as the state of charge (SoC) and it becomes important to manage and satisfy the SoC constraints of VBs [20] and also physical batteries. To tackle some of these issues, previous works in [21, 23] have developed techniques to identify the parameters of such VB models, whereas the work in [2] has illustrated a full scale validation of power balancing services provided from VBs. Furthermore, the role of the distribution network is also important to consider and will be discussed next.

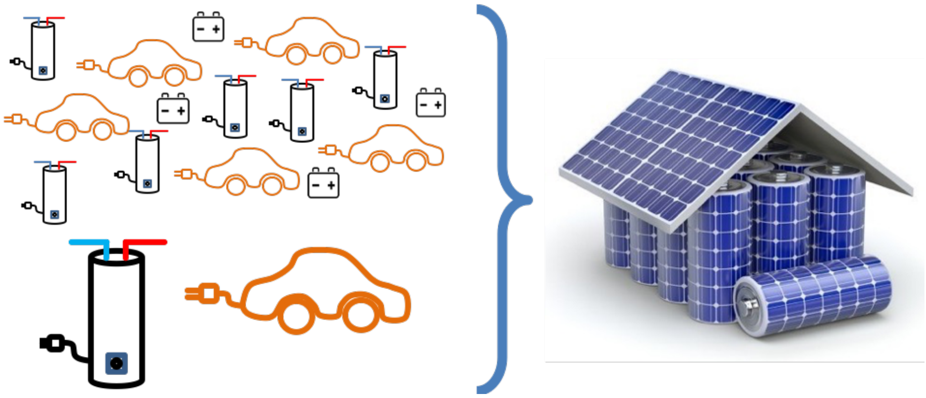

Figure 1.3: Aggregation of distributed energy resources (DERs) like physical batteries, electric vehicles and flexible demand such as water heaters, into a aggregate virtual battery [2]

1.4 ROLE OF THE GRID/NETWORK

An important question in distribution grid management is the role the grid or the network should play in the coordinated dispatch of DERs. As of now the Distribution System Operator (DSO) is a passive Volt-Var focused operator that uses Transformers and Capacitor banks (usually 10s-100s) in the distribution system to maintain voltages within acceptable limits. These mechanical devices are mostly scheduled and set manually. But with extreme distributed solar PV, wind and smart inverters in the distribution system and the requirement to provide dynamic energy services, more controllable devices (10,000s smart devices) would need to be scheduled. This would increase the complexity of the distribution system operation by a factor of more than 100. The goal then is to contain this complexity through optimization algorithms. The optimal power flow (OPF) is a useful tool to coordinate the grid resources subject to the grid and device constraints. The power flow equations, based on the Kirchhoff's current and voltage laws, relate voltages in the system to power injections. The non-convexity of 3-phase AC OPF, however, generally complicates gradient-based optimization solvers. Furthermore, the addition of storage leads to the coupling of different time-steps, which further complicates the OPF models. Also with increased behind the meter solar PVs, customers will become so called "Prosumers", with the ability to supply power back to the grid in times of need. Hence, the distribution system can act as an energy service provider with the ability to provide market services to the energy grid. In order to overcome these challenges, the DSO will need to evolve from passive/reactive management, to a more active management of grid resources [24] with the ability to dispatch flexibility located across a network as depicted in Fig. 1.4. Future distribution networks will have to adapt in order to increase value through interaction of intelligent devices on the grid and prosumerization of customers [25]. In lieu of these challenges and possible direction of solutions, the goal of this work is to present a framework for the best utilization of available grid resources to meet dynamic energy market opportunities while accounting for AC physics of the network and the uncertainty of renewables. In achieving these goals, I rely on a number of key terms and concepts that are described next.

Figure 1.4: Virtual batteries (VBs) placed across a distribution network.

1.5 KEY TERMS AND CONCEPTS

- **Distributed energy resources (DERs)**: For the purpose of this work, DERs are defined as any resource on the distribution system that either produces electricity or has flexibility in consuming electricity, but is not included as part of the Bulk electric system (BES). According to this definition, DERs can include flexible resources such as solar PV inverters, battery energy storage system (BESS) and vehicle-to-grid (V2G), and also flexible demands-side resources such as water heaters and A/Cs, since they can also be dispatched similar to battery storage. This is in line with NERC's recent recommendation that demand-side management of aggregated resources be included in the definition of a DER [17].

- **Virtual batteries (VBs)**: In this work, a VB is considered an energy-based abstraction of a group of a relatively small number of directly controlled loads (e.g., 100-200 distributed loads like air-conditioners, electric water heaters). A VB, via direct manipulation of appliance statuses, can intelligently shift loads in time (i.e., defer demand) to achieve a desired active power set-point. Since comfort/device constraints limit the duration of the shift, the VB is akin to a simple energy storage system. It is assumed that the flexible loads reside in the low-voltage secondary network, while the local VB coordination (computation and control) takes place at the primary service transformer level.

- **Distribution system operator (DSO)**: In this work, we assume that the DSO, or the distribution utility, acts as the coordinator and aggregator of DERs and manages the entire scheme. It is the DSO that manages grid resources by solving an OPF, in order to achieve certain distribution network objectives. In this regard, it is reasonable to assume that the DSO has access to SCADA data and is aware of the grid topology to solve the AC OPF.

- **Transmission system operator (TSO)**: In this work, TSO is an entity similar to an Independent system operator (ISO) and is responsible for managing the bulk electricity markets. In this regard, the TSO provides pricing signals to the DSO, which in-turn manages the distribution grid resources accordingly.

- **AC admissible**: The original AC OPF problem in distribution systems is non-convex, making it NP-hard to solve. In this works, relaxations and approximations of the original AC OPF are presented, which lead to a scalable solution. However, it is important that the solution obtained from the modified formulation, not violate any constraints in the original model. A solution of a modified (either through relxations or approximations) OPF is said to be AC admissible, if the solution applied to the original, non-convex AC OPF, is feasible, i.e., does not violate any constraints.

1.6 Comprehensive literature review

To manage the variability in renewable generation, distributed energy resources (DERs; e.g. inverter-based batteries, water heater, A/Cs) need to be coordinated for reliable and resilient operation. This introduces the challenge of coordinating DERs at scale and within confines of the existing distribution system.

The variability introduced by renewable resources necessitates the detailed analysis of distribution systems for optimal operation of the grid. It becomes important to develop efficient and accurate models of the distribution system to achieve desired operating objectives such as reduction in operation cost, network loss reduction or voltage regulation. This can be accomplished through receding horizon OPF of distribution systems with energy-constrained DERs. The inclusion of energy storage distinguishes this work from the state of science in distribution system OPF [26]. This section surveys and discusses the challenges with and proposes methods for modeling and optimizing a three-phase distribution system with significant penetration of renewables and controllable DERs, including energy storage.

1.6.1 Objectives of distribution system OPF

The aim of the optimal power flow (OPF) problem is to attain certain distribution system objectives while satisfying all the network and device constraints. This objective can take on a variety of forms such as the optimal sizing of capacitor banks to reduce voltage deviation [27], reduction in line losses [28] or the use of various reactive power sources to improve voltage regulation in the system [29].

With the increase in renewable power generation on the distribution level, there has been an increased coupling of transmission and distribution systems wherein the aggregation of distributed energy resources (DERs) can provide regulation services to the transmission system [30]. In this situation, the OPF problem is used to track a reference grid power request. Another outcome of increased DER penetration has been the use of DERs in voltage droop control [31, 32]. Furthermore, some recent works [33], [34], have considered the coupling between the economic dispatch and frequency regulation problems and their joint optimization in transmission system. This method represents an interesting avenue for distribution system market design (objective) and dynamic load balancing. These recent developments highlight the importance of the OPF problem to distribution systems and related state-of-the-art techniques for OPF.

1.6.2 Co-optimization of continuous and discrete assets

The distribution grid is made of many different types of flexible (such as solar PV, EVs) and mechanical assets (such as transformers) as depicted by the illustration in Fig. 1.5. With increasing penetration of solar PV, some distribution feeders are experiencing highly variable net-load flows and even reverse flows. The intermittent nature of solar energy can cause under and over-voltages in the system [35–38] leading to unacceptable operation. To optimize distribution systems under such conditions, the scheduling of mechanical devices, such as OLTCs and capacitor banks, needs to take into account forecasted solar PV and actual grid conditions. These discrete mechanical assets are subject to physical wear and tear and, thus, are usually only operated a few times during the day with heuristic open-loop policies [39]. However, with increasing solar PV penetration, it becomes important to optimize the schedule for the mechanical assets against bidirectional and variable power flows [40]. Heuristics have been proposed to solve this problem, but given the large number of devices encountered in practical systems, they represent a computational challenge [41].

Due to the discrete state of these devices, including them into an optimization problem renders the problem NP-hard [42]. These discrete decision variables take the problem outside the realm of convex optimization and hence mixed-integer programming tools are used with a convex integer relaxation. To incorporate discrete devices into convex OPF formulations, the McCormick relaxations [43] and linearization techniques have been used to incorporate these devices [44, 45]. In [42], the authors use SDPs (semi-definite programs) to capture the transformer ratios and then the solutions are rounded to the nearest discrete tap values, whereas in [46] the load tap changers and shunt capacitors are both modeled by linear constraints using discrete variables, facilitating the linearly constrained mixed-integer formulation. However, this rounding can cause infeasibility issues, which are analyzed in [47] and the authors provide an MISOCP formulation, which is computationally tractable and converges to a feasible optimal solution. In [48], the authors propose a technique to use variable McCormick bounds for improved accuracy and reduction in computation time. In [49], a distributed algorithm for solving mixed-integer linear programs (MILPs) is proposed.

Computationally efficient and provably feasible algorithms that consider both the switching mechanical assets and continuous inverter-based assets are still an open problem. This work builds upon the papers discussed in this section, but leverages the notion that discrete devices and continuous resources can offer their flexibility at different time-scales, which gives rise to a natural prioritization of reactive power resources.

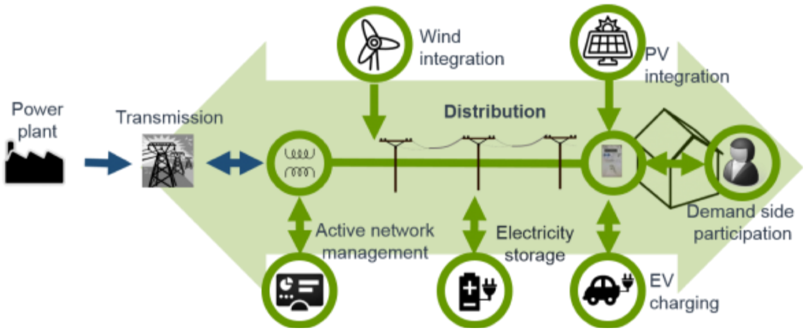

Figure 1.5: Complexity of distribution systems due to the different types of resources to be controlled [3]

1.6.3 Nonconvexity of OPF

The optimal power flow (OPF) is a useful tool to coordinate the grid resources subject to the nonlinear power flow equations and network constraints [50]. For constant power loads, the AC power flow equations relate the voltages in the network with the power injections. However, the non-convexity of the power flow equations generally complicates gradient-based optimization solvers unless simplifying assumptions are made to the model. An example of the non-convex nature of the power flow feasible space is shown in Fig. 1.6. Furthermore, the assumption of constant power loads is generally not valid in distribution systems due to voltage dependencies. Instead, the loads should be modeled as a ZIP model which further complicates the modeling [51, 52].

Traditionally, *DistFlow* algorithms based on *branch flow power models*, which is an exact nonlinear formulation of the distribution network power flow equations, are used to solve the OPF problem in distribution networks [27]. The full ACOPF model represents an NP-hard, non-convex problem. Recently, there have been efforts to use convex relaxation techniques to solve the OPF problem [53, 54]. Previous works in literature have shown that for certain (e.g. radial) network toplogies, the convex relaxations, such as second order cone programs (SOCP) and semi-definite programs (SDP) can be exact [55, 56].

In [53], an SDP formulation of the OPF problem is given, which is the dual of the original problem. It gives the necessary and sufficient conditions for a zero duality gap, i.e., the primal and dual solutions have the same optimal value. It is shown that the zero duality gap holds for many practical IEEE systems after adding resistance to every transformer and when load over-satisfaction is allowed. However, the method only accounts for the balanced single phase equivalent case. Furthermore, SDP solvers are still not numerically robust [57].

In [54], the authors investigate the geometry of the injection regions and its relationship to the optimization of power flows in radial distribution networks. It is shown that under the assumption that the phase angle difference across each line is small, the Pareto-optimal points of the injection region remain unchanged by taking the convex hull. In [58] and [59], the application of conic relaxations and SDP relaxations is extended to meshed networks. However, SDP relaxation techniques have their drawbacks, as described in [60] and [61]. Some of these issues can be overcome by using moment-based relaxations [62], which improves accuracy at the cost of significant computational overhead. Some recent work has also used the QC (quadratic constraint) based convex relaxations due to their advantage over SDP and SOCP relaxations [63].

Linear approximate models can also be powerful when they are sufficiently accurate. One particular approximation is the simplification of the *DistFlow* model [27] to *LinDistFlow*, which is a linear formulation of the branch flow model obtained by neglecting the line losses. In [64], a novel linear approximation of the implicit relation between nodal voltages and nodal power injections is considered around a generic solution of the power flow equations for a balanced network. A method to obtain an analytical solution to the non-linear power flow equations is presented in [65]. It gives sufficient conditions for the existence of such a solution to the power flow problem (again, for a balanced network). It also obtains a bound on the approximation error based on the grid parameters. Linear models, even though simple and computationally efficient, do not provide guarantees on optimality and feasibility, which are important for scheduling/dispatch problems, such as battery dispatch.

In this work, we develop an SOCP-NLP coupled algorithm that provides a near optimal but guaranteed feasible solution. The optimized solutions obtained from the relaxed SOCP model, are used to initialize a nonlinear program (NLP) of the actual AC power flow to obtain a physically realizable solution.

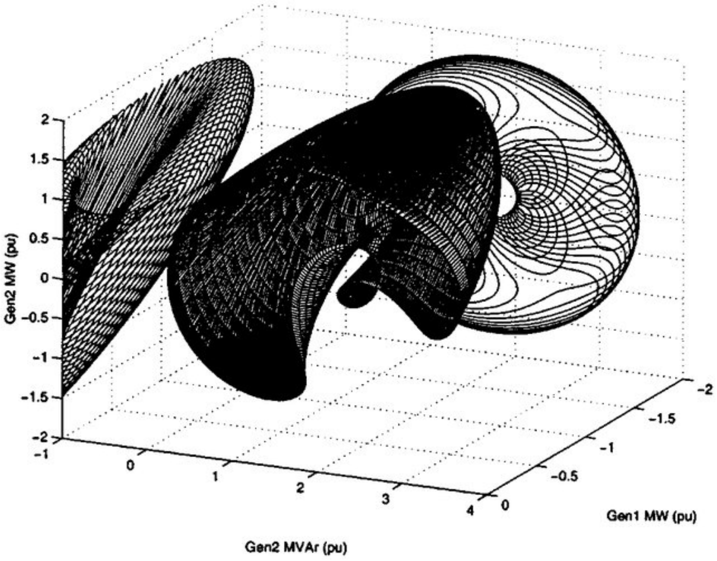

Figure 1.6: Figure showing the non-convexity of the feasible space of the optimal power flow problem [4].

1.6.4 THREE-PHASE OPF MODELS

The assumption of a single-phase balanced network fails to hold when analyzing three-phase unbalanced distribution networks. Many works in literature such as [66] have shown the importance of considering the imbalances in a distribution network for accurate analysis. It has been shown in [67] that the solution space of the three-phase OPF is non-convex and the solution space of the OPF problem and its convex hull are different. The full ACOPF model represents an NP-hard, non-convex problem. *DistFlow* algorithms, which are traditinally used to solve the OPF, only consider balanced single phase equivalent models. Distribution networks are inherently unbalanced which makes it important to study the full three-phase models of these networks [68].

Linear approximate models have also been developed for three-phase distribution networks. One particular approximation is an extension of the *DistFlow* model [27] to unbalanced power flows, *Dist3Flow*, which is obtained by linearization and assumptions of fixed per-phase imbalances [69, 70]. These linear models again do not provide guarantees on optimality and feasibility.

In [71,72] the authors use SDP rank constraint relaxation to the three phase model of a distribution network, however, SDP solvers are still not numerically robust [57]. In [72], the authors propose two SDP relaxations (with branch injection and branch flow models) of the three-phase OPF problem and a linear approximation of the power flow (LPF). It is found that the LPF is accurate when line loss is small compared with power flow and voltages are nearly balanced. In [73], the Feasible Point Pursuit - Successive convex approximations algorithm - a powerful approach for general non-convex quadratically constrained quadratic programs to solve the three-phase AC OPF problem is leveraged.

These three-phase OPF techniques either involve linearization, which introduces modeling (and prediction) errors or are based on SDP relaxations, which are numerically sensitive and suffer when LMPs are negative. Development of a provably feasible convex model for 3-phase distribution systems remains an open problem. In this work, we develop an SOCP-NLP algorithm that provides a near optimal but guaranteed feasible solution. The optimized solutions obtained from the relaxed SOCP model, are used to initialize a nonlinear program (NLP) of the actual AC power flow to obtain a physically realizable solution. Furthermore, the active-power solutions that form the energy trajectory and are obtained from the SOCP are fixed in the NLP, leading to a decoupling of the different time-steps. As a result, the NLP solves each time-step separately (and possibly in parallel), leading to a scalable framework.

1.6.5 Multi-period OPF

To maintain grid operating conditions under significant renewable (and intermittent) generation, the utility grid operators can leverage the power and energy flexibility inherent to many DERs. However, unlike traditional generation, DERs, such as batteries are energy constrained, which give rise to the need for multi-period decision-making and predictive optimization.

In [74,75], the authors have used multi-period SDP relaxation techniques to solve this problem for transmission networks, however, SDP solvers are still not numerically robust [57]. In [76], the authors have utilized a single phase OPF AC-QP algorithm that is initialized with an SOCP relaxation. However, this multi-period OPF formulation neglects the non-unity charge and discharge efficiency of the battery, which can create solutions to the OPF problem that are physically unrealizable due to simultaneous charging and discharging of batteries. In order to avoid solutions involving simultaneous charge and discharge of batteries in the system, complementarity constraints have to be added to the models. These complementarity constraints ensure that the batteries in the system do not simultaneously charge and discharge. But these constraints involve the use of integers and make the problem non-convex.

One solution to this problem would be the use of mixed-integer formulation but this would increase the computation time substantially. Thus, the approach is to relax these constraints and analyze under which conditions the optimal solution satisfies the complementarity constraint. In [7,77], the authors provide conditions under which simultaneous charging and discharging can be avoided in the optimal solution for an economic dispatch problem. In [77], Karush-Kuhn-Tucker (KKT) conditions are analyzed for a linear DC model of the economic dispatch problem and show that, under reasonable economic assumptions, simultaneous charging and discharging is avoided. Optimal consideration for storage in the OPF problem is still an open problem. The sufficient conditions provided for mitigating simultaneous charge and discharge in [7], [77] need to be adapted for distribution networks since many of the conditions (such as positive LMPs) may not hold in practice [78].

In this work, we develop a three-phase convex SOCP relaxation of the multi-period OPF problem. We also provided sufficient conditions to avoid simultaneous charging and discharging of batteries in distribution networks with non-unity charging and discharging efficiencies.

1.6.6 Coordination and aggregation of DERs

Coordinated control of demand-side, distributed energy resources (DERs), such as grid-tied PV inverters, distributed battery storage, and thermostatically controlled loads (TCLs; e.g., water heaters and air conditioners) is part of the solution that supports a renewable energy future [14, 79–81]. Much of the recent literature on the coordination of DERs has focused on distributed control methodologies to turn large-scale aggregations of DERs into dispatchable grid assets as depicted in Fig. 1.7 (similar to [82–84]). To control and dispatch the DERs, much of the literature has also focused on optimizing the energy storage operation over ISO/TSO market signals, but this does not directly consider the underlying AC network and the distribution system operator (DSO) constraints (e.g., voltage or power limits), see for example [85, 86].

To avoid violating operational limits of the grid and to ensure system reliability with DERs at scale, coordination between a DSO and DER owners and aggregators will become critical. This has spurred a multitude of concepts and models for how DSOs can interact with DERs, aggregators, and whole-sale (transmission) markets [87–89]. In this work, we focus on the so-called "Market DSO" model, e.g., see [87], where the DSO performs coordination and aggregation of DERs to deliver grid services. While such a setup could preclude independent DER aggregators (i.e., increases regulatory complexity), the model simplifies the interaction between whole-sale market signals and the DSO and the ideas herein can be adapted further to enable independent "grid-aware" DER aggregators [90]. For other market-based DER coordination schemes, "transactive energy" can engender holistic TSO-DSO-Aggregator participation of DERs [91]. Some of these schemes focus on broadcasting prices directly to devices. However, with large-scale participation of DERs, transactive energy is susceptible to harmful load synchronization effects, power oscillations, and volatile prices, as shown in [92].

Other grid-aware approaches include optimization-based methods to account for AC network constraints [93], where DER control is achieved by solving an optimization problem based on AC network models and tracking a Karush-Kuhn-Tucker (KKT) point that satisfies the KKT optimality conditions. However, for non-convex AC OPF, the KKT conditions may not be sufficient to guarantee global optimality. Other optimization schemes can provide market services with DERs without exact grid models nor real-time measurements [94]. However, these methods do not directly incorporate multi-period energy constraints and the KKT point can be sensitive to exogenous disturbances. Formulations based on convex relaxations can provide guarantees on feasibility and optimality of solutions when the cost function is monotonic [95]. However, optimal tracking of a power reference signal has a non-monotonic cost function, which means that one cannot guarantee that the predicted solutions are network-admissible.

To address these challenges concerning real-time, optimal, and network-admissible coordination of DERs, this work presents a hierarchical (multi-layer) framework for coordinating demand-side flexibility in the form of DERs. The hierarchical coordination consists of a novel, convex OPF relaxation, which is provably tight at optimality under realistic conditions and generates grid-aware, feasible set-points for the DERs. Prior work on hierarchical control of DERs in microgrids (e.g. [96]) has mainly considered using frequency and voltage droop characteristics to generate active and reactive power set-points for DERs using local measurements of frequency and voltage and compensating for the deviations, but in this work, we compensate for the deviation in the head node power of the feeder from the economic set-point, thus taking into account the economic trajectory.

1.6.7 Convex inner approximation of OPF

Since Carpentier's original OPF formulation [50] and subsequent improvements in optimization solvers, the OPF problem has become a powerful methodology for optimizing the dispatch of various grid resources. This is because OPF-based methods

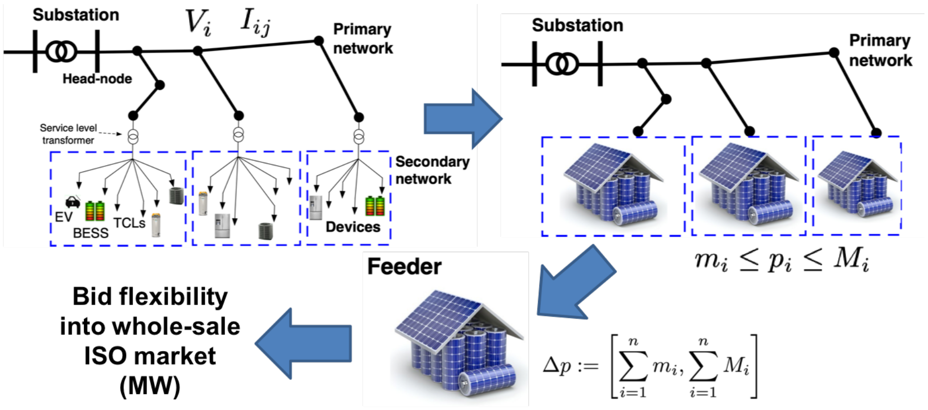

Figure 1.7: Figure showing aggregation of flexibility at the secondary and primary level of a feeder in order to bid the flexibility into the ISO market.

can account for the underlying grid physics, static network constraints on voltages and apparent branch flows, and resource limitations. However, it was also recognized early on that the nonlinear AC power flow equations that model the underlying grid physics render the AC OPF non-convex [97].

To overcome the computational challenges associated with non-convex AC network models, many recent techniques involve using linear or convex approximations [98]. Traditional optimization techniques for dispatching resources include linear OPF-based *LinDist* models [27]. These models work well close to the expected conditions of the system (e.g., low losses). The authors in [99] quantified the errors associated with more general linear power flow approximations. Recently, improved linear approximations of the power flow equations have been proposed that provide improved accuracy over a wider range of operation [64, 100]. However, the solution space of the AC power flow equations is highly non-convex, which means that such methods cannot guarantee network-admissible solutions under all net-load conditions.

Beyond linear approximations, recent attention in literature has focused on convex relaxations of the AC power flow equations, including second-order cone programs, semi-definite programs, and quadratic relaxations [101]. Several works in literature such as [102] have shown that, under certain analytical conditions, these relaxations can be exact and the solution of the relaxed convex problem then represents the global optimum of the original non-convex AC OPF problem. However, these conditions fail to hold under extreme solar PV injections when the network experiences reverse power flows, which engenders a non-zero duality gap solution that may not be network admissible, i.e., not feasible in the original AC OPF formulation [103].

However, in many practical applications, guaranteeing network admissibility is more critical than finding the globally optimal solution. For such applications, finding an inner approximation of the non-convex power flow space can result in efficient and network admissible dispatch of flexibility. An illustration of the concept of convex inner approximation is shown in Fig. 1.8. The authors in [104], develop an optimization-based method to certify whether a DER dispatch scheme can result in constraint violations. However, they do not discuss the network-admissible range of DER dispatch. The authors in [105] provide a convex restriction technique that guarantees an admissible solution, which they utilize in [106] to determine a feasible path from a known initial operating point to a desired final operating point. In [107], the convex OPF formulation is based on an augmented second-order cone relaxation. The authors in [108] solve a large number of non-convex OPF problems to determine nodal injection bounds. However, these methods either rely on non-convex techniques or they cannot ensure that the full range of DER dispatch is network-admissible, which is the main focus herein.

The work herein presents a computationally tractable convex inner approximation for the optimal power flow (OPF) problem that characterizes a feeders aggregate DERs hosting capacity and enables a realtime, grid-aware dispatch of DERs for radial distribution networks. From this approach, we achieve an OPF formulation that exhibits computational solve times similar to that of linear formulations with the added (and crucial benefit) that the formulation guarantees admissible solutions.

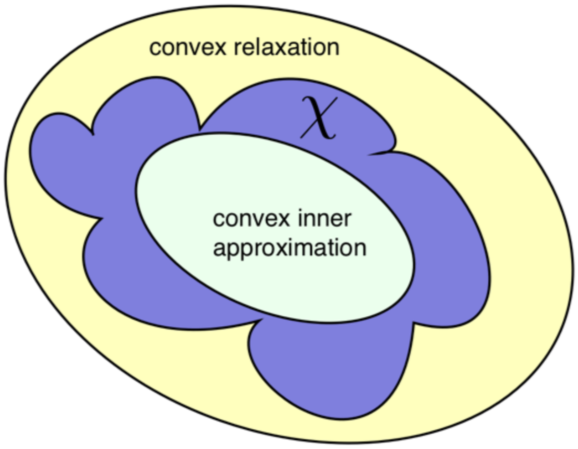

Figure 1.8: Figure illustrating the idea of convex inner approximation in relation to the original non-convex feasible space χ and its convex relaxation.

1.6.8 Stochastic Optimal power flow

Renewable energy sources, such as solar PV, are inherently stochastic in nature and the corresponding variability poses a challenge to grid operators [109]. The severity of the problem is illustrated in Fig. 1.9, which is from a recent Velco load profile [5], showing the large difference in net-load between a sunny day and a cloudy day. To overcome these challenges, grid operators can leverage responsive DERs to provide demand-side flexibility. The inclusion of flexible demand from energy-constrained DERs, such as battery storage, couples the time-steps, which requires multi-period decision-making and predictive optimization.

In addition, accounting for the uncertainties in solar generation and demand forecasts calls for a robust dispatch of flexible DERs. Choosing an acceptable violation probability is perceived as an intuitive and transparent way of determining a probabilistic security level [110]. Chance-constraint-based optimization is one such tool that is employed to robustly dispatch flexible resources in order to satisfy AC power flow constraints. The nonlinearities associated with the AC physics, however, renders the chance-constrained optimization problem challenging to solve due to non-convexities. Thus, to certify reliable operation of distribution systems under high penetrations of solar PV, techniques are desired that take into account both the AC nonlinearities and the uncertainty from solar PV forecasts.

The non-convexity of the solution space of the three-phase AC OPF [67], means that a direct application of chance-constraints to the non-convex optimization problem is not possible. Previous works on chance constraint formulations have considered a linear power flow model, which under chance constraint formulation becomes a second-order cone program (SOCP) that can be solved in a computationally-efficient manner [111, 112]. In [113] the authors utilize a scenario-based approach with an AC-QP formulation to provide a-posteriori probabilistic guarantees. However, the single-phase equivalent, linearized DC OPF models utilized in these works can be inaccurate for distribution feeders. The authors in [114] implement a formulation of chance constraints using an affine policy, which allows them to include corrective control policies. They utilize convex relaxations to reformulate the chance constrained AC OPF problem as a semi-definite program (SDP). However, they do not consider the multi-period coupling and the reformulation only holds for Gaussian distributions. Futhermore, SDPs can be numerically sensitivie [57]. The authors in [115] present an algorithm which alternates between solving a deterministic AC optimal power flow problem and assessing the impact of uncertainty. The authors developed a two-stage approach where the full AC load flow is solved based on a forecast and in the second step the uncertainty is accounted for through chance-constraints applied to the network linearized at the operating point obtained in step one. However, they only consider a single-phase equivalent model and ignore multi-period coupling. Furthermore, the non-convex AC OPF problem is not guaranteed to converge to a global optimum and the solve time increases exponentially with system size for NLPs.

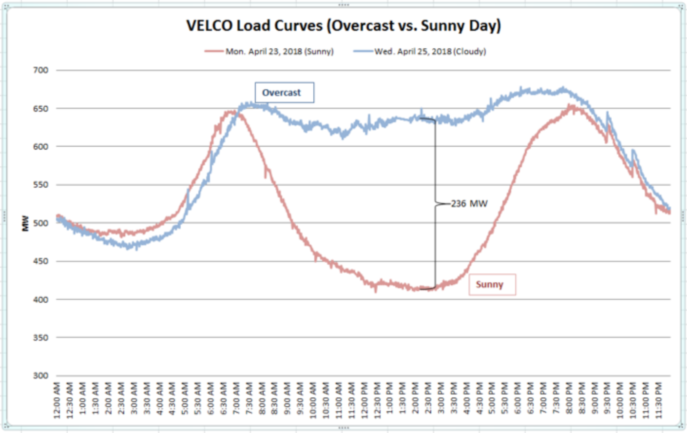

Figure 1.9: Velco load curve showing the large variability in net-demand between a sunny day versus an overcast day [5]. This figure illustrates the large variability that can result from increased volatile solar penetration in distribution systems.

In this work, we build upon the work on chance constraint formulation in [115] by decoupling the solution to the deterministic multi-period AC OPF problem and the linearized chance constraint problem. This work presents a convex, multi-period, AC-feasible Optimal Power Flow (OPF) framework that robustly dispatches flexible demand-side resources in unbalanced distribution feeders against uncertainty in very-short timescale solar Photo-Voltaic (PV) forecasts. The novel, robust OPF formulation accounts for both the nonlinear power flow constraints and the uncertainty in forecasts. This is achieved by linearizing an optimal trajectory and using first-order methods to systematically tighten voltage bounds.

1.6.9 CONCLUSIONS

This section presented a survey of the recent developments in solving the Optimal power flow problem for unbalanced distribution systems. Particular emphasis was given to the case of three-phase distribution models with both mechanical switching assets and continuously operated renewable and storage assets. Recent developments in the field of multi-period OPF are presented, which highlight the need for the development of fast and efficient algorithms for these applications.

1.7 OPEN PROBLEMS TACKLED IN THIS WORK

- Lack of computationally efficient algorithms for co-optimization of discrete and continuous controllable assets in distribution systems.
- Lack of AC admissible convex models for general 3-phase multi-period OPF in distribution systems under solar PV uncertainty.
- Lack of convex formulations for coordinated control of distributed energy resources in order to track grid reference signals, subject to grid constraints.
- Lack of convex inner approximation methods that guarantee admissibility of solutions.

- Lack of tools that can assist in dynamic hosting capacity studies and enable real-time grid-aware control of DERs.

1.8 ORIGINAL CONTRIBUTIONS AND PAPERS

The main contribution of this work is to transform the distribution system from a passive Volt-Var focused operator to a more active manager of distributed energy resources (DERs). In this work we tackle the major challenges that arise as a result of this transformation, namely with respect to feasibility and optimality guarantees and coordinating large number of resources at scale. These contributions can lead to a more robust and resilient operation of the electric grid even under very high penetration of variable renewable generation and uncertain forecasts. The work in this document is grouped into two overarching contributions:

- **Making OPF scalable for different distribution systems operational objectives:** The non-convexity of the AC OPF together with the multi-period coupling introduced due to energy-constrained DERs, make the OPF problem hard to scale, especially under the stochasticity introduced due to highly variable and uncertain renewable generation. To improve the scalability of AC OPF in distribution networks and help manage the forecast uncertainty, a number of methods are proposed in this work.

  One of the main challenges in distribution system AC OPF is to manage the co-optimization of continuous and discrete assets. In this work, we consider the natural timescale-separation between (slow) mechanical and (fast) inverter-based controllable grid assets. Mechanical resources on slow time-scale act as a form of reactive reserve, allowing the DERs to fully participate in valuable market services on a fast timescale. This way mechanical assets maximize margins and optimize value of DERs. This effectively prioritizes the responsive reactive resources for the faster time-scales to counter variability in net-load (demand minus solar PV).

To account for the three-phase multi-period nature of OPF in distribution systems, which represents an NP-hard non-convex problem, this work develops a multi-period three-phase SOCP-NLP algorithm that provides near optimal but guaranteed feasible solution. The optimized solutions obtained from the convex relaxed SOCP model, are used to initialize a nonlinear program (NLP) of the actual AC power flow to obtain a physically realizable solution. Furthermore, the active-power solutions that form the energy trajectory and are obtained from the SOCP are fixed in the NLP, leading to a de-coupling of the different time-steps. As a result, the NLP solves each time-step separately (and possibly in parallel), leading to a scalable framework. We also provide sufficient conditions to avoid simultaneous charging and discharging of batteries in distribution networks with non-unity charging and discharging efficiencies.

To approach the challenge of coordination and aggregation of DERs in order to track grid reference signals and hence provide grid market services, this work presents a hierarchical framework for network-admissible coordination of aggregated DERs. The coordination is achieved by solving an optimization problem to disaggregate a feeder's desired reference trajectory into constraint-aware set-points for the DERs. Specifically, a novel, provably-tight, convex relaxation of the optimal power flow (OPF) problem is presented to optimally dispatch the DERs to track the feeders desired power trajectory.

To certify reliable operation of distribution systems under high penetrations of solar PV, techniques are desired that take into account both the AC nonlinearities and the uncertainty from solar PV forecasts. In this work, we decouple the solution to the deterministic multi-period AC OPF problem and the linearized chance constraint problem. A deterministic, multi-period, SOCP+NLP problem is solved to obtain a three-phase, AC feasible optimized state (voltage, current) trajectory. Based on the trajectory, Taylor series expansions of the power flow equations are computed around the operating points from each time-step. The sensitivity of the network constraints (voltage and branch flows) to the uncertain injections (demand and solar PV) can be computed. From these sensitivity factors, the uncertainty determines the degree of constraint tightening, which robustifies the SOCP and NLP formulations.

To verify the efficacy of the developed OPF tools, we also conducted large-scale hierarchical simulation of feeders with significant penetration of renewables and DERs. In this work, DERs were used to optimize system operations with respect to economic signals from wholesale energy and ancillary service markets. We present a novel hierarchical scheme that actively controls behind-the-meter DERs to reliably manage each unbalanced distribution feeder and exploits the available flexibility to ensure reliable operation and economically optimize the entire distribution network. Each layer of the scheme employs advanced optimization methods at different timescales to ensure that the system operates within both grid and device limits. The hierarchy is validated in a large-scale realistic simulation based on data from the industry.

The following publications resulted from this contribution on making OPF scalable:

- **Nawaf Nazir**, Mads Almassalkhi, “Receding-horizon optimization of unbalanced distribution systems with time-scale separation for discrete and continuous control devices”, Power System Computation Conference (PSCC), Dublin, Ireland, June, 2018
- **Nawaf Nazir**, Pavan Racherla and Mads Almassalkhi, “Optimal multi-period dispatch of distributed energy resources in unbalanced distribution feeders”, IEEE Transactions on Power Systems, vol. 35, no. 4, pp. 2683-2692, July 2020.
- Sarnaduti Brahma, **Nawaf Nazir**, Hamid Ossareh and Mads Almassalkhi, “Optimal and resilient coordination of virtual batteries in distribution feeders”, IEEE Transactions on Power Systems.
- **Nawaf Nazir** and Mads Almassalkhi, “Stochastic multi-period optimal dispatch of energy storage in unbalanced distribution feeders”, Power Systems Computations Conference (PSCC), Porto, Portugal, June, 2020.
- Mads Almassalkhi, Sarnaduti Brahma, **Nawaf Nazir**, Hamid Ossareh, Pavan Racherla, Soumya Kundu, Sai Pushpak Nandanoori, Thiagarajan Ramachandran, Ankit Singhal, Dennice Gayme, Chengda Ji, Enrique Mallada, Yue Shen, and Pengcheng You, Dhananjay Anand, "Hierarchical, Grid-Aware, and Economically Optimal Coordination of Distributed Energy Resources in Realistic Distribution Systems", Energies Journal, Special Issue on Building-to-Grid Integration through Intelligent Optimization

and Control.

- **Realtime grid-aware dispatch through convex inner approximation:** The linear OPF and the convex relaxation based OPF can improve the scalability of AC OPF in distribution systems, however, in order to solve a large OPF problem in realtime (order to milliseconds), a different approach is required. In many applications, feasibility guarantees at optimality are more valuable than solving to a globally optimal solution. This work proposes a convex inner approximation of the power flow equations that results in a network-admissible solution, i.e., all physical network limits are respected at (global) optimality, while solving in polynomial time. Hence, the method is robust against modeling errors introduced from approximations of the non-linear power flow equations.

  This convex inner approximation method is also applied to control discrete assets. An voltage positioning optimization (VPO) method is presented that utilizes mechanical resources to position the predicted voltages close to nominal values, while minimizing the use of inverter-based resources (i.e., DERs), making them available for control at a faster time-scale (after the uncertainty reveals itself). The convex, inner approximation of the OPF problem is adapted to a mixed-integer linear program that minimizes voltage deviations from nominal (i.e., maximizes voltage margins). The resulting OPF solution respects all the network constraints and is, hence, robust against modeling simplifications.

  The developed convex inner approximation method is then applied to develop grid-aware aggregation and realtime disaggregation of flexibility. This is useful in many applications, such as to determine the admissible range for dispatching distributed energy resources (DERs), i.e., the DER hosting capacity. Another application is that of disaggregating the dispatch of a large, aggregated Virtual battery (VB) resource into the dispatch of multiple smaller nodal resources that are distributed spatially across a network. Such a method overcomes the inherent scalability issues of receding horizon OPF and engenders realtime grid-aware control of DERs. The following publication resulted from this contribution on developing a convex inner approximation and its application to realtime grid-aware DER dispatch:

- **Nawaf Nazir** and Mads Almassalkhi, “Convex inner approximation of the feeder hosting capacity limits on dispatchable demand”, IEEE Conference on Decision and Control (CDC) 2019, Nice, France.
- **Nawaf Nazir** and Mads Almassalkhi, “Voltage positioning using co-optimization of controllable grid assets in radial networks”, IEEE Transactions on Power Systems.
- **Nawaf Nazir** and Mads Almassalkhi, "Grid-aware aggregation and realtime disaggregation of distributed energy resources in radial networks", under review, IEEE Transactions on Power Systems.

1.9 ORGANISATION OF DOCUMENT

The rest of this document is organized as follows: Section 2 describes the modeling of distribution systems. Within section 2, section 2.1 describes the modeling of unbalanced three-phase distribution networks, whereas section 2.2 provides the modeling of balanced single phase equivalent distribution networks. Section 2.3 describes the modeling of discrete assets such as OLTCs and capacitor banks in distribution systems, section 2.4 describes the operational objectives in distribution systems and section 2.5 provides an overview of network reduction in distribution systems and how it improves scalability. In section 3, we provide a DSO centric approach to the dispatch of flexibility through receding horizon OPF solutions, with section 3.1 providing a method for the optimal dispatch of discrete assets in three-phase distribution networks and section 3.2 provides a method for the dispatch of energy storage in three-phase distribution networks. Section 3.3 describes a method to account for uncertainty of solar PV when dispatching flexibility and finally section 3.4 presents a hierarchical scheme for the coordination of DERs in order to provide grid market services. In section 4, we present an DSO-aggregator hybrid approach for the coordination of flexibility, with section section 4.1 introducing the concept of convex inner approximation and its advantage over other optimal power flow techniques. Using this convex inner approximation methods, section 4.2 presents a method that manages the discrete assets such as OLTCs and capacitor banks to position the voltage close to nominal, whereas section 4.3 develops a method to embed grid physics into aggregate feeder flexibility and enables a real-time disaggregation in response to market signals. This document is finally concluded with section 5 providing the final remarks and outlining the scope for future research in this area.

Chapter 2

Modeling of distribution systems

This section presents an overview of the modeling techniques utilized in distribution systems. Section 2.1 presents the modeling of three-phase distribution networks, whereas section 2.2 presents the modeling of balanced single phase equivalent distribution networks. Both of these models can be useful depending upon the details of the application [116]. Next section 2.3 provides the modeling of discrete devices such as transformers and capacitor banks. Section 2.4 describes the operational objectives in distribution system OPF and finally section 2.5 introduces the network reduction techniques utilized in this work.

2.1 Modeling three-phase distribution feeders

The power flow equations relate the voltages in the network with the power injections. Traditionally, *DistFlow* method is used to model the power flow equations in distribution networks [27]. However, these methods assume a balanced network model, which is not the case when 3-phase distribution networks with significant small-scale renewable generation are considered. Distribution systems are often unbalanced and it becomes necessary to study the three-phase model of the system for accurate analysis and control [68].

Thus, the aim of this section is to develop an AC power flow model of an unbalanced distribution feeder that relates the feeder's voltage and current signals with power injections. Specifically, we employ a branch flow model (BFM) to represent the AC physics in the unbalanced feeder [117].

In modeling 3-phase AC power flows, we need to leverage mathematical operators $|.|$, $\circ$, $(.)^*$ and $\text{diag}(.)$ to represent the cardinality of a set, the Hadamard product of matrices, the complex conjugate operator, and the diagonal operator, respectively. Then, given a radial, 3-phase feeder with N nodes, denote $\mathcal{N} = \{1, 2, \ldots, N\}$ as the set of all nodes, $\phi = \{a, b, c\}$ as the set of phases at each node, $\mathcal{L} = \{1, 2, \ldots, L\} = \{(m, n)\} \subset (\mathcal{N} \times \mathcal{N})$ as the set of L branches, and $\mathcal{G} = \{1, 2, \ldots, G\} \subseteq \mathcal{N}$ as the set of all nodes with DERs. Let vector $V_n(t) \in \mathbb{C}^{|\phi|}$ be the complex voltage at node n and time t, with $W_n(t) = V_n(t)V_n(t)^*$, $i_l(t) \in \mathbb{C}^{|\phi|}$ be the current in branch l at time t, with $I_l(t) = i_l(t)i_l(t)^*$, $S_l(t) = V_n(t)i_l(t)^*$ be the apparent power in branch l at time t. Further, let $Z_l = R_l + jX_l \in \mathbb{C}^{|\phi| \times |\phi|}$ be the impedance matrix of branch l. Let $S_n^{\text{net}}(t) \in \mathbb{C}^{|\phi|}$ be the complex net power injection at node n at time t and is based on complex solar PV inverter injections and electric demand, $S_n^{\text{S}}(t), S_n^{\text{L}}(t) \in \mathbb{C}^{|\phi|}$, respectively. In addition, let $P_n^{\text{b}}(t) = P_n^{\text{d}}(t) - P_n^{\text{c}}(t) \in \mathbb{R}^{|\phi|}$ be the active power delivered from a battery at node n at time t, with $P_n^{\text{d}}(t) \in \mathbb{R}^{|\phi|}$ being the battery discharge power and $P_n^{\text{c}}(t) \in \mathbb{R}^{|\phi|}$ being the battery charging power. Also let $q_n^{\mathrm{b}}(t) \in \mathbb{R}^{|\phi|}$ be the reactive power delivered from the battery inverter. Herein, we assume that each resources is connected to a single phase. Based on the above notation, the physics of 3-phase AC power flows are given by the following equations:

$$0 = W_n(t) - W_m(t) + (S_l(t)Z_l^* + Z_l S_l(t)) - Z_l I_l(t) Z_l^* \quad \forall l \in \mathcal{L} \tag{2.1a}$$

$$0 = \mathrm{diag}(S_l(t) - Z_l I_l(t) - \sum_p S_p(t)) + S_n^{\mathrm{net}}(t) \quad \forall l \in \mathcal{L} \tag{2.1b}$$

$$\begin{bmatrix} W_n(t) & S_l(t) \\ S_l(t)^* & I_l(t) \end{bmatrix} = \begin{bmatrix} V_n(t) \\ i_l(t) \end{bmatrix} \begin{bmatrix} V_n(t) \\ i_l(t) \end{bmatrix}^* \quad \forall l \in \mathcal{L} \tag{2.1c}$$

$$0 = \mathrm{real}\{S_n^{\mathrm{net}}(t) - S_n^{\mathrm{S}}(t) + S_n^{\mathrm{L}}(t)\} - P_n^{\mathrm{b}}(t) \quad \forall n \in \mathcal{G} \tag{2.1d}$$

$$0 = \mathrm{imag}\{S_n^{\mathrm{net}}(t) - S_n^{\mathrm{S}}(t) + S_n^{\mathrm{L}}(t)\} - q_n^{\mathrm{b}}(t) \quad \forall n \in \mathcal{G} \tag{2.1e}$$

In (2.1), (2.1a) relates the voltage drop in the network with the branch power flows, (2.1b) represents the power balance equation at each node which ensures that the power entering a node equals the power leaving, and (2.1c) is the non-linear power flow constraint that relates voltages and currents to new matrix variables $W_n(t)$, $I_l(t)$ and $S_l(t)$. In (2.1d) and (2.1e), the active and reactive nodal power balance equations are defined.

2.2 MODELING BALANCED DISTRIBUTION FEEDERS

Balanced equivalent models can be sufficiently accurate depending upon the application and the distribution network under consideration [116]. Consider a radial, balanced distribution network as a graph $\mathcal{G} = \{\mathcal{N}, \mathcal{E}\}$, where $\mathcal{N}$ is the set of nodes and $\mathcal{E}$ is the set of branches, such that $(i, j) \in \mathcal{E}$, if nodes $i, j \in \mathcal{N}$ are connected, and $|\mathcal{E}| = n,\ |\mathcal{N}| = n + 1$. Node 0 is assumed to be the head-node (i.e., substation) node with a fixed voltage V_0 and define $\mathcal{N}^+ := \mathcal{N} \setminus \{0\}$. Let V_i be the voltage phasor at node i and I_{ij} the current phasor in branch $(i, j) \in \mathcal{E}$. Then, we define $v_i := |V_i|^2$ and $l_{ij} := |I_{ij}|^2$. Let $S_{ij} = P_{ij} + \mathbf{j}Q_{ij}$ denote the sending end power flow from bus i to bus j where P_{ij} and Q_{ij} denote the active and reactive power flows respectively and let $s_i = p_i + \mathbf{j}q_i$ denote the power injection into bus i where p_i and q_i denote the active and reactive power injections, respectively. Next, denote r_{ij} and x_{ij} as the resistance and reactance of the branch $(i, j) \in \mathcal{E}$, respectively, which gives complex branch impedance $z_{ij} = r_{ij} + \mathbf{j}x_{ij}$.

Then, based on the *DistFlow* model for radial networks [27], the variables (s, S, v, l, s_0) at any time-step k are described by the following equations:

$$S_{ij}[k] = s_i[k] + \sum_{h:h\rightarrow i} (S_{hi}[k] - z_{hi} l_{hi}[k]), \quad \forall (i, j) \in \mathcal{E} \tag{2.2}$$

$$0 = s_0[k] + \sum_{h:h\rightarrow 0} (S_{h0}[k] - z_{h0} l_{h0}[k]) \tag{2.3}$$

$$v_i[k] - v_j[k] = 2\mathrm{Re}(\overline{z}_{ij} S_{ij}[k]) - |z_{ij}|^2 l_{ij}[k], \quad \forall (i, j) \in \mathcal{E} \tag{2.4}$$

$$l_{ij}[k] = \frac{|S_{ij}[k]|^2}{v_i[k]}, \quad \forall (i,j) \in \mathcal{E} \tag{2.5}$$

Apart from the nonlinear relation (2.5) of l to S and v, (2.2)-(2.4) represent a linear relationship between the nodal power injections s, the branch power flows S, and the nodal voltages v. Thus, in an AC OPF optimization formulation, (2.5) would be a non-convex equality constraint, which begets a non-convex formulation.

2.2.1 MATRIX NOTATION FOR MODELING BALANCED DISTRIBUTION FEEDERS

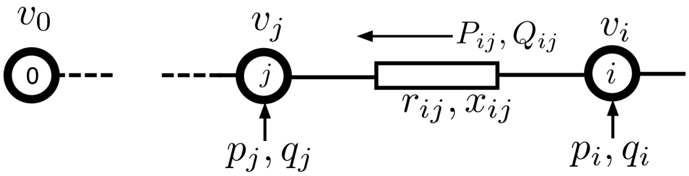

Figure 2.1: Diagram of a radial distribution network from [6].

Clearly, the line losses in (2.5) are nonlinear, and since it is an equality constraint, this makes the *DistFlow* model non convex. In the remainder of this section, we develop a mathematical model of the radial network that expresses the constrained variables as a linear function of the power injections and the branch currents. Through this approach, we are able to separate the model into linear and nonlinear components.

From the incidence matrix B of the radial network and following the method adopted in [6], (2.2) and (2.3) can be expressed through the following matrix equations:

$$P = p + AP - ARl \qquad Q = q + AQ - AXl, \tag{2.6}$$

where $P = [P_{ij}]_{(i,j)\in\mathcal{E}}$, $Q = [Q_{ij}]_{(i,j)\in\mathcal{E}}$, $p = [p_i]_{i\in\mathcal{N}^+}$, $q = [q_i]_{i\in\mathcal{N}^+}$, $R = \text{diag}\{r_{ij}\}_{(i,j)\in\mathcal{E}}$, $X = \text{diag}\{x_{ij}\}_{(i,j)\in\mathcal{E}}$, $l = [l_{ij}]_{(i,j)\in\mathcal{E}}$ and $A = [0_n \quad I_n]B - I_n$, where I_n is the $n \times n$ identity matrix and 0_n is a column vector of n rows.

Defining $C = (I_n - A)^{-1}$, $D_{\text{R}} = (I_n - A)^{-1}AR$, and $D_{\text{X}} = (I_n - A)^{-1}AX$, allows us to simplify (2.6) to:

$$P = Cp - D_{\text{R}}l \qquad Q = Cq - D_{\text{X}}l, \tag{2.7}$$

Remark 1. *The matrix* $(I_n - A)$ *is nonsingular since* $I_n - A = 2I_n - [0_n \quad I_n]B = 2I_n - B_n$*, where* $B_n := [0_n \quad I_n]B$ *is the* $n \times n$ *matrix obtained by removing the first row of* B*. For a radial network, the vertices and edges can always be ordered in such a way that* B *and* B_n *are upper triangular with* $\textit{diag}(B_n) = 1_n$*, which implies that* $2I_n - B_n$ *is also upper triangular and* $\textit{diag}(2I_n - B_n) = 1_n$*. Thus,* $\det(2I_n - B^{'}) = 1 > 0$ *and* $I_n - A$ *is non-singular.*

Similarly, (2.4) can be applied recursively to the distribution network in Fig. 2.1 to get the matrix equation:

$$[v_i - v_j]_{(i,j)\in\mathcal{E}} = 2(RP + XQ) - Z^2 l \tag{2.8}$$

where $Z^2 := \text{diag}\{z_{ij}^2\}_{(i,j)\in\mathcal{E}}$. Based on the incidence matrix B, the left hand side of

(2.8) can be formulated in terms of the fixed head node voltage as:

$$C^\top [v_i - v_j]_{(i,j)\in\mathcal{E}} = V - v_0\mathbf{1}_n \tag{2.9}$$

where $V := [v_i]_{i\in\mathcal{N}^+}$. Based on (2.9), (2.8) can be expressed as:

$$V = v_0\mathbf{1}_n + 2(C^\top RP + C^\top XQ) - C^\top Z^2 l \tag{2.10}$$

Substituting (2.7) into (2.10), we obtain a compact relation between voltage and power injections shown below.

$$V = v_0\mathbf{1}_n + M_\mathrm{p}p + M_\mathrm{q}q - Hl \tag{2.11}$$

where $M_\mathrm{p} = 2C^\top RC, \quad M_\mathrm{q} = 2C^\top XC$ and
$H = C^\top(2(RD_\mathrm{R} + XD_\mathrm{X}) + Z^2)$

Remark 2. *The matrix H is non-negative, when the underlying distribution network is either inductive (X is non-negative), capacitive (X is non-positive) or purely resistive (X is zero matrix). This fact helps in obtaining the convex inner approximation described later in the paper in section 4.2. Substituting the values of C, D_R and D_X into the expression of H, gives:*

$$H = (I_n - A)^{-\top}[2(R(I_n - A)^{-1}AR + X(I_n - A)^{-1}AX) + Z^2].$$

To show H is non-negative, we just need to focus on A and $(I_n - A)^{-1}$. Due to the definition, A is non-negative and $I_n - A$ has positive diagonal entries and non-positive *off-diagonal entries and is, hence, a Z-matrix. Also,* $I_n - A = 2I_n - B_n$ *and* $2I_n - B_n$ *is an upper triangular matrix. Hence its eigenvalues are positive, so it is also a non-singular M-matrix (i.e., a Z-matrix whose eigenvalues have non-negative real part). Non-singular M-matrices are a subset of a class of inverse-positive matrices, i.e., matrices with inverses belonging to the class of non-negative matrices (all the elements are either equal to or greater than zeros) [118, Corollary 3.2]. Hence,* $(I_n - A)^{-1}$ *is a non-negative matrix. As* A *is also a non-negative matrix, then* H *is clearly non-negative whenever matrix* R *is non-negative and either* X *is non-negative (i.e., all lines are inductive),* X *is non-positive (i.e., all lines are capacitive) or* X *is zero (i.e., all lines are purely resistive).*

Apart from the nonlinear relation (2.5) of l to P, Q and V, (2.7) and (2.11) is a linear relationship between the nodal power injections p, q, the branch power flows P ,Q and node voltages V. The nonlinearity in the network is represented by (2.5), as the current term l is related to the power injections and node voltages in a nonlinear fashion. Including this term into the optimization model would render the optimization problem non-convex, however, neglecting this term could result in an inadmissible linear OPF solution. In the next section, we model the discrete grid resources such as OLTCs and capacitor banks.

2.3 MODELING DISCRETE ASSETS IN DISTRIBUTION FEEDERS

2.3.1 DISCRETE DEVICE NOMENCLATURE

Consider the distribution grid defined in Section 2.2, where $\mathcal{C} \subseteq \mathcal{N}^+$ represent the sets of nodes with capacitor banks, and $\mathcal{T} \subseteq \mathcal{E}$ is the set of branches with on-load tap change transformers (OLTC) or voltage regulators. The tap-ratio for the OLTC/regulator at branch $m \in \mathcal{T}$ is denoted by t_m with the tap position defined by $n_m^{\text{tr}} \in \mathbb{Z}$, e.g. $n_m^{\text{tr}} \in \{-16, \ldots, 0, \ldots, +16\}$. The number of capacitor bank units is $n_i^{\text{cp}} \in \mathbb{Z}$ at node $i \in \mathcal{C}$ and b_i as the capacitor bank admittance at node $i \in \mathcal{C}$.

2.3.2 OLTC AND CAPACITOR BANK MODELING

The voltage relation between the nodes across an OLTC is given by:

$$0 = v_i - t_m^2 v_j \quad \forall m \in \mathcal{T} \tag{2.12}$$

$$0 = t_m - (1 + \tau_m n_m^{\text{tr}}) \quad \forall m \in \mathcal{T} \tag{2.13}$$

The constraints (2.12) and (2.13) define the relation between the tap ratio and the tap position with $\tau_m \in \mathbb{R}$ being the tap step. Note that the equality constraint (2.12) represents a non-convex constraint and makes the OPF problem NP-hard. The non-linearity related to the OLTC taps is approximated with piecewise linear (PWL) constraints in (2.15a)-(2.15d) to obtain an accurate representation as described in [46] and summarized next. The coupling between v_i, v_j, t_m can be expressed as:

$$v_i = t_m^2 v_j \approx t_{m,0}^2 v_j + \sum_{p=1}^{n_m^{\mathrm{tr}} - \underline{n_m^{\mathrm{tr}}} + 1} \Delta t_{m,p} v_j, \tag{2.14}$$

where $\Delta t_{m,p} = t_{m,p}^2 - t_{m,p-1}^2$, $\{t_{m,0}, t_{m,1}, t_{m,2}, \ldots, t_{m,K}\}$ represent the fixed tap ratio settings of the OLTC connected at branch m and $n_m^{\mathrm{tr}} - \underline{n_m^{\mathrm{tr}}} + 1$ is the index of tap position n_m^{tr}. Next, we use binary variables $\{s_1^m, s_2^m, \ldots, s_K^m\}$ with adjacency conditions $s_p^m \geq s_{p+1}^m$, $p = 1, 2, \ldots, K-1$ to represent the operating status of the OLTC branch and the following group of mixed-integer linear constraints exactly describe the OLTC connected at branch m in (2.14):

$$v_i = t_{m,0}^2 v_j + \sum_{p=1}^{K} \Delta v_p^m \tag{2.15a}$$

$$0 \leq \Delta v_p^m \leq s_p^m \overline{v} \Delta t_{m,p} \tag{2.15b}$$

$$\Delta t_{m,p}(v_j - (1 - s_p^m)\bar{v}) \leq \Delta v_p^m \leq \Delta t_{m,p} v_j \tag{2.15c}$$

$$s_{p+1}^m \leq s_p^m,\ p = 1, 2, \ldots, K-1. \tag{2.15d}$$

The relation between capacitor bank admittance (b_i) and reactive power injected by capacitor banks (Q_i^{cp}) is given by (2.16), whereas the relation between capacitor bank admittance and number of capacitor bank units with $y_{\mathrm{c},i} \in \mathbb{R}$ being the admittance of a single capacitor bank unit is given by (2.17)

$$0 = Q_i^{\mathrm{cp}} - v_i b_i \quad \forall i \in \mathcal{C} \tag{2.16}$$

$$0 = b_i - y_{\mathrm{c},i} n_i^{\mathrm{cp}} \quad \forall i \in \mathcal{C} \tag{2.17}$$

If Q_i^{cp} represents the reactive power injection from capacitor banks at node i, then:

$$Q_i^{\text{cp}} = v_i b_i = \sum_{p=1}^{n_i^{\text{cp}}} (v_i b_{i,p}) \tag{2.18}$$

represents the bilinearity, where $\{b_{i,1}, b_{i,2}, \ldots, b_{i,K}\}$ are the admissible admittance values of controllable capacitor banks at node i. Similar to the formulation in (2.15a)-(2.15d), for the capacitor bank at node i, (2.18) can be equivalently expressed by the following set of linear constraints [46]:

$$Q_i^{\text{cp}} = \sum_{p=1}^{K} Q_{i,p}^{\text{s}} \tag{2.19a}$$

$$0 \leq Q_{i,p}^{\text{s}} \leq u_p^i \bar{v} b_{i,p} \tag{2.19b}$$

$$b_{i,p}(v_i - (1 - u_p^i)\bar{v}) \leq Q_{i,p}^{\text{s}} \leq v_i b_{i,p} \tag{2.19c}$$

$$u_{p+1}^i \leq u_p^i,\ p = 1, 2, \ldots, K - 1. \tag{2.19d}$$

where binary $\{u_1^i, u_2^i, \ldots, u_K^i\}$ represent the operating status of the capacitor bank units on node i.

2.4 Operational Objectives in distribution system OPF

The general distribution system OPF problem can be expressed as:

$$\min_x f(x) \tag{2.20a}$$

$$s.t.\ g(x) \leq 0 \tag{2.20b}$$

$$h(x) = 0 \tag{2.20c}$$

where $f(x)$ is the objective or the cost to be minimized. A review on the different objectives in distribution systems operations is provided in section 1.6.1. Specifically, the following practical objectives are common in three-phase distribution networks:

- $f(W) = \sum_i (W_i - W^{nom})^2$ (e.g., minimizing voltage deviation from nominal)
- $f(I) = \sum_l (\mathrm{diag}(R_l \circ I_l))$ (e.g., minimizing network line loss)
- $f(P_0)$=$(P_0 - P^{\mathrm{ref}})^2$ (i.e., tracking a grid/head-node reference power set-point)
- $f(P^{\mathrm{d}} + P^{\mathrm{c}}) = \sum_i (P_i^d + P_i^c)$ (e.g., minimizing battery degradation)
- $f(P^{\mathrm{d}} - P^{\mathrm{c}}) = (P^{\mathrm{d}} - P^{\mathrm{c}} - P^{\mathrm{ref}})^2$ (i.e., tracking VB reference trajectory)

Furthermore, (2.20c) represents the power flow equations which form an equality constraint and (2.20b) represents the network constraints (e.g., voltage, current, power flow limits). For (2.20) to be a convex optimization problem, $f(x)$ and $g(x)$ have to be convex functions and in the equality constraint, $h(x)$ has to be affine [119]. However, the power flow equations represented by $h(x) = 0$ in (2.20) are non-linear, making the OPF problem non-convex. A major contribution of this work is to propose relaxations to these non-linear equations, in order to achieve a convex formulation. The reasoning behind this approach is that convex optimization problems can be solved very efficiently and reliably and they scale as a polynomial with the increase in problem size, as compared to non-convex problems that in general scale exponentially. Due to this reason, convexity is a key issue when setting up any optimization problem [120].

Energy systems especially are an important area for the application of various optimization techniques. This is due to the challenging nature of the optimization in energy systems due to: (a) their non-convexity(which results from the non-linear power flow equations, the discrete nature of switching assets and nonlinearity of several other devices), (b) the large scale of the problem (due to the possibly hundreds of thousands of controllable set-points) and (c) due the requirements on solve-time (which can range from seconds to minutes to hours to several days depending on the particular application). Due to all the above mentioned challenges, energy systems are an ideal candidate for testing the applicability, reliability and performance of various convex and non-convex optimization techniques. In this work, we compare and leverage several convex optimization methods such as linear programs (LPs), quadratic programs (QPs), second order conic programs (SOCPs) and semi-definite programs (SDP) for continuous optimization. For discrete optimization, we utilize several mixed-integer programming (MIP) methods, such as mixed-integer linear program (MILP) and mixed-integer second order cone program (MISOCP). We also illustrate the benefits and drawbacks of these methods when applied to various optimization problems in distribution networks.

2.5 Network reduction

A distribution feeder may be made up of several thousands of nodes, with each node having possibly hundreds of controllable DERs. With the non-linearity of the power flow equations and the large scale of these networks, scalability becomes an issue. In order to maintain the scalability of the algorithms, network reduction is employed on the large-scale three-phase feeders. This network reduction is accomplished through Kron reduction [121]. The Kron reduction is based on creating clusters of proximal nodes with similar voltage sensitivities to current injections [122]. Within each cluster, a "super-node" is designated to represent the cluster in the reduced network [123]. The maximum absolute percent error (Max-APE) in intra-cluster voltage magnitudes compares how representative the super node voltages in the reduced network are of the cluster's voltages under AC load flow analysis. It is shown in [124] that the Max-APE is smaller than the 2% RMSE Furthermore, this error can be considered as a model mismatch in a stochastic formulation to make the solution robust against modeling errors. Within each cluster, solar PV and demand are also aggregated up to the corresponding super-node. The aggregate of flexible devices within a super-node then represents a VB, which in this work is made up of less than 200 flexible DERs. Figure 2.2 shows the process of network reduction in electrical circuits by partitioning the network into clusters and then representing each cluster as a super-node, with aggregate flexible VBs and aggregate demand.

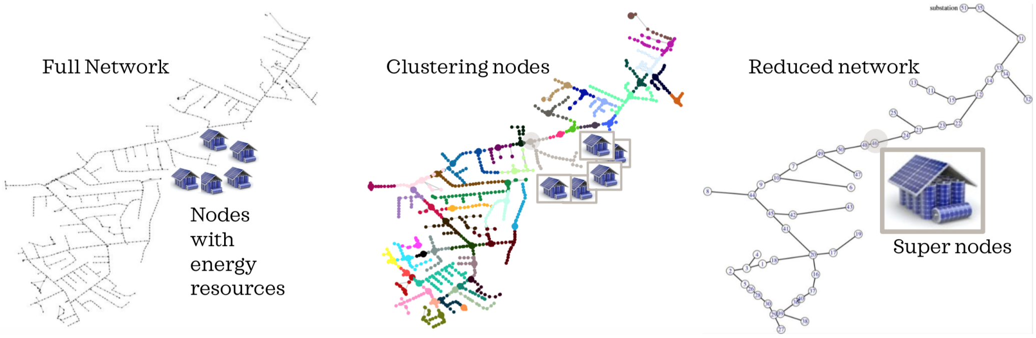

Figure 2.2: Process for network reduction of electrical circuits by partitioning the network into clusters of similar nodes with the same color. The largest nodes in each cluster is the designated super-node.

CHAPTER 3

RECEDING HORIZON OPF IN DISTRIBUTION SYSTEMS

This section presents a utility-centric approach, where the utility controls the dispatch of flexible resources based on solving a receding horizon optimal power flow (OPF) problem. This approach assumes that the utility or DSO has all the required network and resource data and also control over flexible customer devices. Based on these assumptions, section 3.1 presents a three-phase OPF for the dispatch of discrete assets, whereas section 3.2 presents a three-phase multi-period OPF for the dispatch of flexible energy storage. Section 3.3 considers the uncertainty in the solar PV when solving the OPF problem and finally section 3.4 presents a hierarchical framework for the coordination and control of distributed energy resources (DERs) in order to provide grid market services.

3.1 THREE-PHASE MULTI-PERIOD OPF OF DISCRETE ASSETS

This section presents a method for the co-optimization of discrete and continuous devices in an unbalanced three-phase distribution network with significant renewable generation, focusing on the dispatch of discrete devices. To overcome the challenge of dispatching both slower mechanically-actuated grid assets and flexible and response VBs, a hierarchical control scheme is presented where the discrete mechanical assets are dispatched at a slow time-scale (called the outer loop or OL) as a mixed-integer program (MIP) and a fast inner loop or IL for the dispatch of flexible VBs. The optimization programs for discrete and continuous devices are assumed to operate at two different time scales as they manage controllable grid resources with different levels of responsiveness and flexibility. The outer loop utilizes a linearized three-phase model of the distribution network to dispatch mechanical assets with the goal of maximizing voltage margins. The aim is to position the nodal voltages within a "nominal range", while minimizing the use of flexible reactive power resources, which can then be made available to the inner loop when the uncertainty reveals itself. The set-points of mechanical assets obtained from the outer loop are then adopted in the inner loop for the dispatch of flexible VBs.

3.1.1 INTRODUCTION

The distribution grid is also made up of many different types of discrete and continuous operated devices. Discrete devices like the capacitor/reactor banks and line

regulators (ON/OFF) and load-tap-changing (LTC) transformers are an integral part of the distribution management system. These devices operate at different time scales (hourly) as compared to the flexible VBs, which necessitates the use of a separate optimization loop to coordinate them. Furthermore, the mechanical assets also have operational constraints on tap changes per hour to limit wear and tear, which necessitates separation. Heuristics have been proposed to solve this problem, but given the large number of devices encountered in practical systems, they represent a computational challenge [41].
Due to the non-convexity of three-phase OPF, linear approximate models are often used to solve OPF problem. One particular approximation is an extension of the *DistFlow* model to three-phase unbalanced power flows, *Dist3Flow*, that is obtained by linearization and certain assumptions on the per-phase imbalances [69, 70]. Also, due to the discrete nature of mechanical devices, including them into an optimization problem renders the problem NP-hard [42]. Previously, McCormick relaxation and linearization techniques have been used to incorporate these devices into the OPF problem for a balanced network [45]. This paper builds upon these works but leverages the notion that discrete devices and continuous VBs can offer their flexibility at different time-scales and, hence, can be optimized in separate loops. This is further illustrated in Fig. 3.1a which shows the hierarchical framework for the dispatch of grid assets and Fig. 3.1b which illustrates the concept of voltage margins.

The main contributions of this work are as follows:

- In this work, the authors present a novel hierarchical OPF scheme for distribution systems operations that separates out the slow mechanical (called the

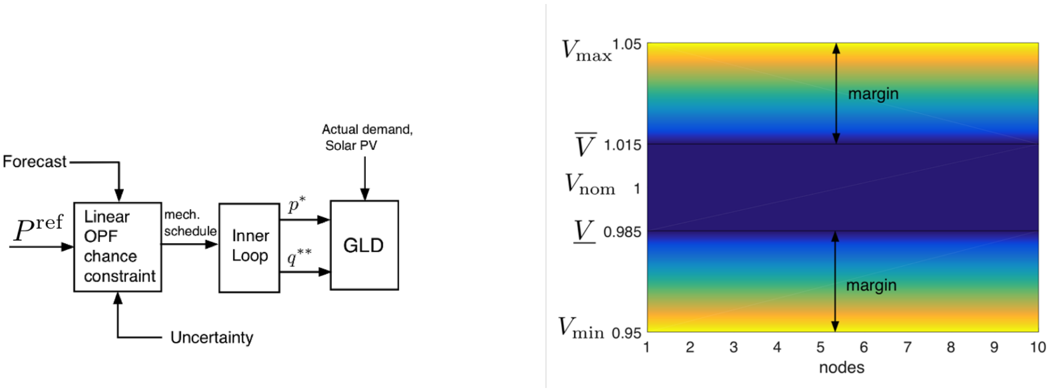

(a) (b)

Figure 3.1: Voltage positioning in a distribution network. (a) The outer-loop (OL) is cast as a voltage positioning (VP) problem, which employs a convex model to maximize voltage margins and validated with GridLab-D (GLD). (b) Voltage margins are represented as the minimum distance from a nominal range $[\underline{V}, \overline{V}]$ *to* $V_{\min}$ *and* $V_{\max}$.

outer loop scheme) and a fast flexible VB (called the inner loop scheme) grid assets on two different timescales.

- For the dispatch of slow discrete devices such as OLTCs and capacitor banks, a linearized three-phase OPF model (*Dist3Flow*) is used to position voltage robustly against uncertain net-load, i.e., position nodal voltages within a nominal range. It is shown through simulation results that the voltage positioning performs the role of robust dispatch under uncertainty.

The rest of this section is organised as follows. Section 3.1.2 provides the MIP formulation of the outer loop to optimize the operation of mechanical assets. Simulation results on realistic feeders are presented in Section 3.1.3 and finally the conclusions are presented in Section 3.1.4.

3.1.2 FORMULATION OF THE VOLTAGE POSITIONING OPTIMIZATION

In this optimization problem, we schedule the discrete assets by solving a multi-period (12-24 hourly periods) mechanical asset scheduling problem for a three-phase feeder model to position the voltage close to nominal values. In addition to scheduling mechanical assets, this optimization problem also positions energy of the batteries (i.e., schedules active power exchanges) to take into account the variability of solar PV generation and forecast energy demands (and, possibly, energy market interactions). Note that the reactive capability of the flexible resources like solar PV is reserved (minimized in the optimization) for corrective control in the inner loop dispatch.
Since discrete decision variables only take integer values, this optimization problem turns into a mixed-integer problem, which is NP-hard. Branch and bound techniques can be effective on mixed-integer programs if their continuous versions are convex. In order to reduce the computational complexity of the outer loop, a three-phase linearized model of the network is used and the problem is reduced to a mixed-integer linear program (MILP) [69]. A linear power flow model is suitable due to the longer prediction horizon and slower (hourly) timescale. This problem is solved in a receding horizon fashion where the solar and load forecasts are used to obtain the operation of discrete assets.

In order to formulate the optimization problem, we utilize the three-phase distribution network model presented in section 2.1 with the simplification of neglecting the non-linear terms in order to obtain a simplified three-phase linear model.

Define the prediction horizon as $\mathcal{T} = \{0, 1, \ldots, T-1\}$, then the optimization problem is formulated as:

$$
\begin{aligned}
\min \sum_{t\in\mathcal{T}} \sum_{n} & (\mathbf{1^T} q_n^{\mathrm{S}}(t))^2 + (\mathbf{1^T} q_n^{\mathrm{b}}(t))^2 + \rho_{\mathrm{v}} \mathbf{1^T} V_{\mathrm{v,n}}(t) && \text{(3.1a)}\\
\text{s.t. } 0 =& W_n(t) - W_m(t) + (S_l(t)Z_l^* + Z_l S_l(t)) \;\; \forall l \in \mathcal{L} && \text{(3.1b)}\\
0 =& \mathrm{diag}(S_l(t) - Z_l I_l(t) - \sum_p S_p(t)) + S_n^{\mathrm{net}}(t) \quad \forall l \in \mathcal{L} && \text{(3.1c)}\\
0 =& \mathrm{real}\{S_n^{\mathrm{net}}(t) - S_n^{\mathrm{S}}(t) + S_n^{\mathrm{L}}(t)\} - P_n^{\mathrm{b}}(t) \quad \forall n \in \mathcal{G} && \text{(3.1d)}\\
0 =& \mathrm{imag}\{S_n^{\mathrm{net}}(t) - S_n^{\mathrm{S}}(t) + S_n^{\mathrm{L}}(t) - q_n^{\mathrm{b}}(t) - Q_n^{\mathrm{cp}}(t)\} \qquad \forall n \in \mathcal{G} && \text{(3.1e)}\\
& |\mathrm{diag}(S_l(t))| \leq S_{\max,l} \qquad \forall l \in \mathcal{L} && \text{(3.1f)}\\
& - V_{\mathrm{v},n}(t) + \underline{V_n}^2 \leq \mathrm{diag}(W_n(t)) \leq \overline{V_n}^2 + V_{\mathrm{v},n}(t) \; \forall n \in \mathcal{N} && \text{(3.1g)}\\
& V_{\min,n}^2 \leq \mathrm{diag}(W_n(t)) \leq V_{\max,n}^2 \; \forall n \in \mathcal{N} && \text{(3.1h)}\\
& |S_n^{\mathrm{S}}(t)| \leq G_{\max,n} \qquad \forall n \in \mathcal{G} && \text{(3.1i)}\\
& B_n(t+1) = B_n(t) - P_n^{\mathrm{b}}(t)\Delta t \quad \forall n \in \mathcal{G} && \text{(3.1j)}\\
& (P_n^{\mathrm{b}}(t))^2 + (q_n^{\mathrm{b}}(t))^2 \leq H_{\max,n}^2 \qquad \forall n \in \mathcal{G} && \text{(3.1k)}\\
& B_{\min,n} \leq B_n(t) \leq B_{\max,n} \qquad \forall n \in \mathcal{G} && \text{(3.1l)}\\
& P_{\min,n} \leq P_n^{\mathrm{b}}(t) \leq P_{\max,n} \qquad \forall n \in \mathcal{G} && \text{(3.1m)}\\
& (2.15a) - (2.15d), (2.19a) - (2.19d) && \text{(3.1n)}
\end{aligned}
$$

for $t \in \mathcal{T}$. The objective function in (3.1a) minimizes the use of reactive power from flexible VBs and solar PV inverters where $q_n^{\mathrm{S}} = imag\{S_n^{\mathrm{S}}\}$ and $V_{\mathrm{v},n}$ being the voltage slack that is penalized in order to position the voltage W_n within the tighter voltage bounds $\underline{V_n}$ and $\overline{V_n}$ as shown in (3.1h). The parameter ρ_{v} is the trade-off parameter to determine penalty on voltage slack compared to flexible reactive power utilization, e.g., a small value of ρ_v would minimize the reactive power from flexible VBs while allowing the nodal voltages to vary beyond the tighter voltage bounds through the voltage slack, whereas a large value of ρ_v would penalize the voltage slack resulting in the nodal voltages lying within the tighter voltage bounds, but in the process utilizing flexible reactive power. Further, (3.1b)-(3.1e) represent the linear power flow equations for the three-phase network, obtained by neglecting the non-linear loss term in (3.1b). The term Q_n^cp in (3.1e) represents the reactive power injection from capacitor banks. Inequality (3.1f) bounds the line power flow below apparent power limit $S_{\mathrm{max},l} \in \mathbb{R}^{|\phi|}$, while (3.1g) captures the voltage bounds with $V_{\mathrm{min},n} \in \mathbb{R}^{|\phi|}$ and $V_{\mathrm{max},n} \in \mathbb{R}^{|\phi|}$ as the lower and upper voltage limits and inequality (3.1i) bounds the apparent power of the solar inverter. Inequalities (3.1k)-(3.1m) define bounds on VB apparent power, state of charge (SoC), and active power dispatch, respectively. Specifically, $H_{\mathrm{max},n} \in \mathbb{R}^{|\phi|}$ defines the apparent power limit of the corresponding VB's complex power injection and $B_{\mathrm{min},n}, B_{\mathrm{max},n} \in \mathbb{R}^{|\phi|}$ and $P_{\mathrm{min},n}, P_{\mathrm{max},n} \in \mathbb{R}^{|\phi|}$ are the VB's lower and upper energy and power bounds, respectively. The relation between the battery SoC and battery power is given by (3.1j), where Δt is the width of the discrete timesteps. In this work, we employ the simplifying assumption that VBs have unity charge/discharge efficiencies, which avoids the technicalities around simultaneous charging and discharging, which is reasonable for VBs as explained in [9] and represents ongoing work [125]. Analysis on storage with non-unity charge and discharge efficiency will be presented in the section 3.2. Finally, (2.15a)-(2.15d) represent modeling of capacitor and (2.19a)-(2.19d) represent the transformer model, both presented in section 2.3.

The optimization problem in (3.1) represents a MISOCP problem which can be efficiently solved through commercial solvers such as Gurobi [126]. The next section presents simulation results on practical distribution systems utilizing the voltage positioning formulation presented here.

3.1.3 Simulation Results

For the validation of the proposed voltage positioning (VP) scheme we consider a realistic 1200 three-phase Orange and Rockland utility (ORU) feeder. Through network reduction technique presented in section 2.5, this feeder is reduced to a 131 node three-phase network. In this formulation the aim is to prevent deviations from nominal (1.0 pu in this case) by having a pre-defined narrow range (± 0.02 pu in this case) and penalize solutions that are beyond this level through the voltage slack. This way the voltage margin is now a priced resource in the outer loop VP problem. The simulation setup is depicted in Fig. 3.2. Since the reactive power from flexible VBs also helps manage voltages, there is a natural trade-off between voltage devia-

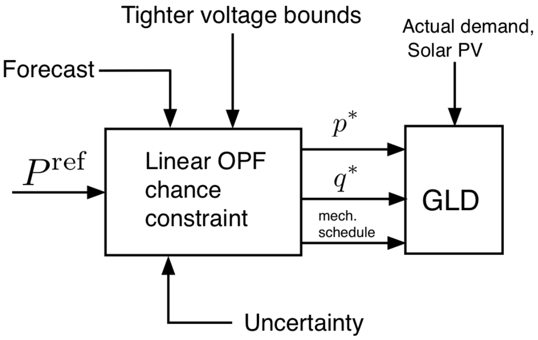

Figure 3.2: Setup for the stochastic simulation of outer loop with validation of the results done in GridLab-D (GLD).

tions from nominal and the use of flexible reactive power, so we can price reactive power resources as well. We capture this trade-off in the VP problem by considering the sensitivity of voltage deviations and reactive power injections in designing a "narrow-enough" range of acceptable deviations. The simulation results show that the MISOCP solves in less than 90 seconds with 0% constraint violations and with less than 5% optimality gap. The optimality gap and solve time results are depicted in Fig. 3.4a and Fig. 3.4b respectively. The VP formulation is also robustified by considering the uncertainty in solar PV and demand. A chance constrained problem is formulated and its results are compared with the deterministic VP problem. As shown in Fig. 3.3, the VP alone can manage stochastic conditions and ensure robust optimized dispatch of mechanical assets. This case study shows the inbuilt robustness in the VP formulation to account for uncertainty in forecast.

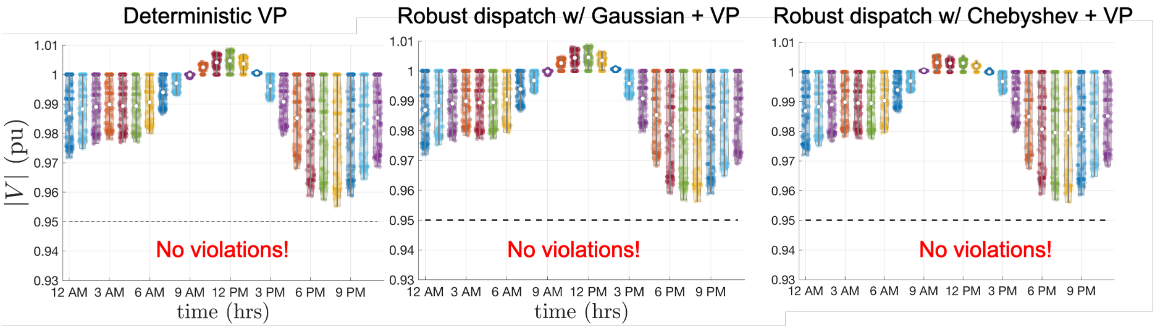
Deterministic VP
Robust dispatch w/ Gaussian + VP
Robust dispatch w/ Chebyshev + VP

Figure 3.3: Comparing the deterministic VP formulation (on left) against two different robust formulations (Gaussian in the middle; unimodular Chebyshev on the right) for a 131-node reduced ORU (Orange and Rockland utility) network for a full day with peak solar PV generation around noon. Clearly, all are robust to the uncertainty. So there is no reason to further robustify the deterministic VP formulation.

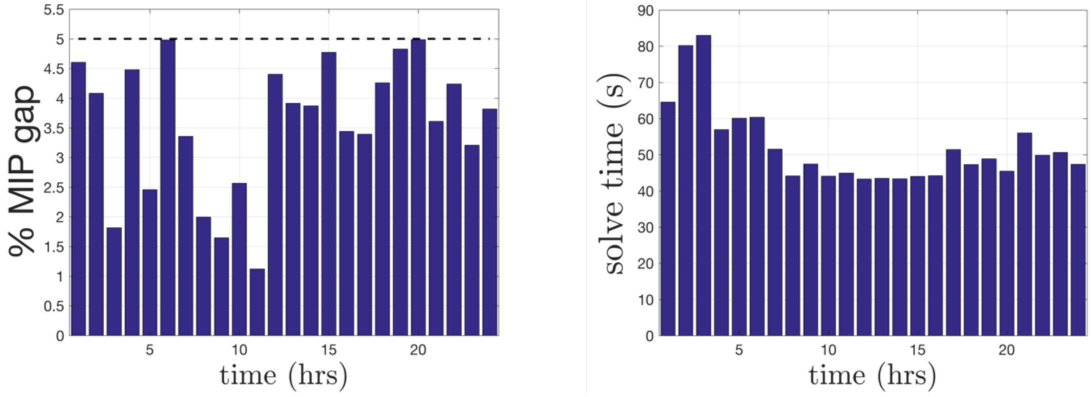

(a) (b)

Figure 3.4: (a) MIP gap of the MISOCP formulation showing a worst case of 5% (b) Solve time of the VP problem with a worst case of 90 seconds.

3.1.4 Conclusions

This work presents a technique to optimally solve an unbalanced three-phase distribution network by co-optimizing the slow and fast control assets using multi-period optimal power flow techniques. A multi-period mixed-integer linear program solves the OPF for the slow mechanical assets as a voltage positioning (VP) problem that aims to utilize the mechanical assets in positioning the voltage close to nominal values, while at the same time minimizes the use of flexible reactive power resources. Validation of the proposed scheme is demonstrated through GridLab-D on a realistic reduced ORU network and the results illustrate the robustness of the VP problem and show that it achieves the objective of minimizing voltage deviations under uncertainty.

3.2 Three-phase multi-period OPF of flexible energy resources

This section presents an efficient algorithm for the multi-period optimal dispatch of flexible energy storage in an unbalanced distribution feeder with significant solar PV penetration. The three-phase, non-convex optimal power flow (OPF) problem is formulated as a convex second-order cone program (SOCP) for the dispatch of batteries in a receding-horizon fashion in order to counter against the variable, renewable generation. The solution of the SOCP is used to initialize a nonlinear program (NLP) in order to ensure a physically realizable solution. The phenomenon of simultaneous charging and discharging of batteries is rigorously analyzed and conditions are derived that guarantee it is avoided. Simulation scenarios are implemented with GridLab-D for the IEEE-13, IEEE-123 test feeders and several Orange and Rockland (ORU) feeders that illustrate not only AC feasibility of the solution, but also near-optimal performance and solve-times within a minute.

3.2.1 Introduction

The rapid growth in distributed solar PV generation over the past decade has prompted significant interests and investments in demonstration of substation automation technology, distributed energy resources or DERs, such as energy storage and smart inverters, and autonomous demand response [19, 127]. To maintain grid operating conditions under significant renewable (and intermittent) generation, the utility grid operators can leverage the power and energy flexibility inherent to many DERs. However, unlike traditional generation, DERs, such as batteries are energy constrained, which give rise to the need for multi-period decision-making and predictive optimization.

The optimal power flow (OPF) is a useful tool to coordinate the grid resources subject to the nonlinear power flow equations and network constraints [50]. For constant power loads, the AC power flow equations relate the voltages in the network with the power injections. It has been shown in [67] that the solution space of the three-phase OPF is non-convex and the solution space of the OPF problem and its convex hull are different. The full ACOPF model represents an NP-hard, non-convex problem. Distribution networks are also inherently unbalanced which makes it important to study the full three-phase models of these networks [68].

In this section, we develop a multi-period SOCP-NLP algorithm that provides a near optimal but guaranteed feasible solution. We also present analysis on simultaneous charging and discharging to different objective functions and provide comprehensive simulation results on 100+ node feeder systems to illustrate computational effectiveness of the proposed optimization algorithms. The optimized solutions obtained from the relaxed SOCP model, are used to initialize a nonlinear program (NLP) of the actual AC power flow to obtain a physically realizable solution. Furthermore, the real-power solutions that form the energy trajectory and are obtained from the SOCP are fixed in the NLP, leading to a decoupling of the different time-steps. As a result, the NLP solves each time-step separately (and possibly in parallel), leading to a scalable framework. Validation is performed with GridLab-D [128].

Thus, main contributions of this work are as follows:

1. A novel approach to obtain a near-optimal feasible solution by temporal de-

coupling of the NLP initialized with the solution from a multi-period three-phase SOCP convex relaxation is presented. By fixing the active-power solutions, the time-steps of the NLP are decoupled leading to a scalable framework

2. Rigorous analysis is performed on the convex formulation and general conditions are derived that guarantee that the phenomenon of simultaneous charging and discharging of batteries is avoided for different types of network objectives.

The rest of this section is organized as follows. Section 3.2.2 develops the three-phase OPF problem and the convex formulation for the dispatch of batteries to attain network objectives. The role of the objective function on the conditions for which simultaneous charging and discharging of batteries is avoided are analyzed in Section 3.2.3. Section 3.2.4 guarantees a physically realizable battery multi-period dispatch by coupling the relaxed SOCP with the exact NLP formulation. Simulation-based analysis and validation results are discussed in Section 3.2.5 for the IEEE-123 node system, realistic utility systems and GridLab-D. Conclusions are presented in Section 3.2.6.

3.2.2 Convex formulation of Multi-period 3-phase OPF

The aim of this section is to develop a convex formulation of the multi-period optimal power flow in three-phase distribution networks that can be used for the dispatch of DERs in the network. Figure 3.5 illustrates the types of DERs available to the optimizer at each node and the corresponding notation. A common objective in distribution networks is to minimize the real power losses, while keeping the system within its operational grid constraints [129]. Another common objective is to track some reference grid signal at the feeder head-node. This program optimizes the batteries (i.e., the real and reactive powers) in the network, whose architecture is shown in figure 3.5, over the minute-to-minute time-scale. Such fast solution times for large networks requires formulation that can be solved in polynomial time. Thus, we focus on the following convex formulation. A three-phase second order cone program (SOCP) is developed to solve the multi-period optimization problem.

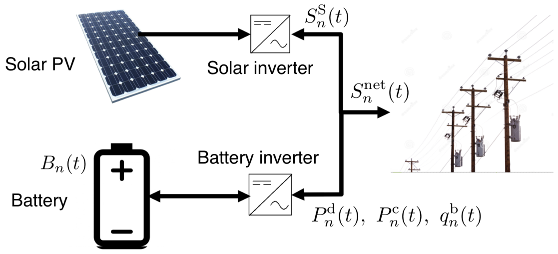

Figure 3.5: Distributed storage architecture. The batteries are controlled through a four quadrant control scheme and can supply and consume both real and reactive power. Each distributed storage is composed of a renewable source of energy such as solar power and a battery bank, each with its own inverter.

If $x = \{P_n^{\mathrm{d}}(t), P_n^{\mathrm{c}}(t), q_n^{\mathrm{b}}(t), S_n^{\mathrm{S}}(t)\}$ be the set of independent optimization variables $\forall\, t \in \mathcal{T},\ n \in \mathcal{N}$, then the problem of optimally dispatching the batteries to minimize objective function $f(x)$ can be formulated as:

$$\min_{P_n^{\mathrm{d}}(t), P_n^{\mathrm{c}}(t), q_n^{\mathrm{b}}(t), S_n^{\mathrm{S}}(t)} \quad f(x) \tag{3.2a}$$

s.t.

$$\begin{bmatrix} W_n(t) & S_l(t) \\ S_l(t)^* & I_l(t) \end{bmatrix} = \begin{bmatrix} V_n(t) \\ i_l(t) \end{bmatrix} \begin{bmatrix} V_n(t) \\ i_l(t) \end{bmatrix}^* \qquad \forall l \in \mathcal{L}, \tag{3.2b}$$

$$0 = W_n(t) - W_m(t) + (S_l(t)Z_l^* + Z_l S_l(t)) - Z_l I_l(t) Z_l^* \quad \forall l \in \mathcal{L}, \tag{3.2c}$$

$$0 = \mathrm{diag}(S_l(t) - Z_l I_l(t) - \sum_p S_p(t)) + S_n^{\mathrm{net}}(t) \quad \forall l \in \mathcal{L}, \tag{3.2d}$$

$$0 = \mathrm{real}(S_n^{\mathrm{net}}(t) - S_n^{\mathrm{S}}(t) + S_n^{\mathrm{L}}(t)) - P_n^{\mathrm{d}}(t) + P_n^{\mathrm{c}}(t) \qquad \forall n \in \mathcal{G}, \tag{3.2e}$$

$$0 = \mathrm{imag}(S_n^{\mathrm{net}}(t) - S_n^{\mathrm{S}}(t) + S_n^{\mathrm{L}}(t)) - q_n^{\mathrm{b}}(t) \qquad \forall n \in \mathcal{G}, \tag{3.2f}$$

$$|\mathrm{diag}(S_l(t))| \leq S_{\mathrm{max},l} \qquad \forall l \in \mathcal{L}, \tag{3.2g}$$

$$V_{\mathrm{min},n}^2 \leq \mathrm{diag}(W_n(t)) \leq V_{\mathrm{max},n}^2 \; \forall n \in \mathcal{N}, \tag{3.2h}$$

$$|S_n^{\mathrm{S}}(t)| \leq G_{\mathrm{max},n} \qquad \forall n \in \mathcal{G}, \tag{3.2i}$$

$$(P_n^{\mathrm{d}}(t) - P_n^{\mathrm{c}}(t))^2 + (q_n^{\mathrm{b}}(t))^2 \leq H_{\mathrm{max},n}^2, \qquad \forall n \in \mathcal{G}, \tag{3.2j}$$

$$0 = B_n(t+1) - B_n(t) - \eta_{\mathrm{c},n} P_n^{\mathrm{c}}(t)\Delta t + \frac{P_n^{\mathrm{d}}(t)}{\eta_{\mathrm{d},n}}\Delta t \qquad \forall n \in \mathcal{G}, \tag{3.2k}$$

$$B_{\mathrm{min},n} \leq B_n(t) \leq B_{\mathrm{max},n} \qquad \forall n \in \mathcal{G}, \tag{3.2l}$$

$$0 \leq P_n^{\mathrm{d}}(t) \leq P_{\mathrm{max},n} \qquad \forall n \in \mathcal{G}, \tag{3.2m}$$

$$0 \leq P_n^{\mathrm{c}}(t) \leq P_{\mathrm{max},n} \qquad \forall n \in \mathcal{G}, \tag{3.2n}$$

$$P_n^{\mathrm{d}}(t) \circ P_n^{\mathrm{c}}(t) = 0 \qquad \forall n \in \mathcal{G} \tag{3.2o}$$

where the above equations hold $\forall t \in \mathcal{T}$. In the optimization problem (3.2a)-(3.2o), (3.2a) represents the objective function, which, e.g., can be to minimize line losses, i.e., $f(x) = \sum_{l=1}^{L} \sum_{t=t_0}^{T} \sum_{\phi=1}^{|\phi|} (\mathrm{diag}(R_l \circ I_l(t)))$. The constraint that relates the voltages and currents in the network to the variables $W_n(t)$, $I_l(t)$ and $S_l(t)$ are in (3.2b) while (3.2c) is the power flow equation relating the voltage drop in the network with the branch power flows. Constraint (3.2d) represents the power balance equation at each node which makes sure that the power coming into a node equals power going out, (3.2e) and (3.2f) are the real and reactive nodal power balance equations, (3.2g) is the line power flow constraint with $S_{\mathrm{max},l} \in \mathbb{R}^{|\phi|}$ being the apparent power limit of line l,

Table 3.1: Variables used in the model formulation.

Variable type	**Variables**
Decision	$P_n^{\mathrm{d}}(t)$, $P_n^{\mathrm{c}}(t)$, $q_n^{\mathrm{b}}(t)$, $S_n^{\mathrm{S}}(t)$
Dependent	$W_n(t)$, $S_l(t)$, $I_l(t)$, $S_n^{\mathrm{net}}(t)$, $B_n(t)$
Constant parameters	Z_l, $S_n^{\mathrm{L}}(t)$, $S_{\max,l}$, $V_{\min,n}$, $V_{\max,n}$, $G_{\max,n}$, $\eta_{\mathrm{c},n}$, $\eta_{\mathrm{d},n}$, $H_{\max,n}$, Δt, $B_{\min,n}$, $B_{\max,n}$, $P_{\max,n}$

(3.2h) is the voltage limit constraint at each node with $V_{\min,n} \in \mathbb{R}^{|\phi|}$ and $V_{\max,n} \in \mathbb{R}^{|\phi|}$ the lower and upper voltage limit respectively at node n, and (3.2i) represents the apparent power limit of the solar inverter at node n. Constraints (3.2j)-(3.2o) describe the battery power, state of charge (SoC) and charge/discharge complementarity constraints with $H_{\max,n} \in \mathbb{R}^{|\phi|}$ as the apparent power limit of the battery inverter at node n and $B_{\min,n} \in \mathbb{R}^{|\phi|}$ and $B_{\max,n} \in \mathbb{R}^{|\phi|}$ as the lower and upper state of charge limit of the battery respectively at node n and Δt is the prediction horizon step. The variable types used in the formulation are presented in Table 3.1.

The optimization model from (3.2a)-(3.2o) is nonlinear due to the equality constraints in (3.2b) and (3.2o), which can also be equivalently expressed as an integer constraint using binary variables as shown in [44]. These constraints make the problem NP-hard. The nonlinear equality constraint in (3.2b) can equivalently be expressed by the following two constraints [72]:

$$\begin{bmatrix} W_n(t) & S_l(t) \\ S_l(t)^* & I_l(t) \end{bmatrix} \succeq 0, \quad rank \begin{bmatrix} W_n(t) & S_l(t) \\ S_l(t)^* & I_l(t) \end{bmatrix} = 1 \tag{3.3}$$

The inequality constraint in equation (3.3) is an positive semi-definte (PSD) convex constraint, whereas the rank constraint is non-convex. Removing the rank constraint in (3.3) leads to a convex SDP formulation, however, it is desirable to find a second order cone relaxation that can be solved with numerically robust solvers such as GUROBI [126]. SOCP relaxation can be applied to the PSD constraint in equation (3.3) as in [130, 131] to obtain the following relaxed SOC constraints:,

$$\left\| \frac{2W_n(t)(i,j)}{W_n(t)(i,i) - W_n(t)(j,j)} \right\|_2 \leq W_n(t)(i,i) + W_n(t)(j,j) \tag{3.4}$$

$$\left\| \frac{2I_l(t)(i,j)}{I_l(t)(i,i) - I_l(t)(j,j)} \right\|_2 \leq I_l(t)(i,i) + I_l(t)(j,j) \tag{3.5}$$

$$\left\| \frac{2S_l(t)(i,j)}{W_n(t)(i,i) - I_l(t)(j,j)} \right\|_2 \leq W_n(t)(i,i) + I_l(t)(j,j) \tag{3.6}$$

If the complementarity constraint given in equation (3.2o) is also relaxed, the optimization model becomes convex and can be solved with GUROBI (as a QCQP) or MOSEK (as an SOCP). However, the reader will notice that removing (3.2o) means that a feasible solution may charge and discharge a battery simultaneously, which is not physically realizable. Therefore, we need to analyze conditions under which the complementarity condition is satisfied at optimality. Section 3.2.3 provides conditions for avoiding simultaneous charging and discharging in batteries which are not dependent on the size of inverters.

3.2.3 Relaxing battery complementarity constraint

This section focuses on the phenomenon of simultaneous charging and discharging (SCD) of batteries in (3.2). As detailed in [44] and [7, Appendix] and illustrated in Fig. 3.6, SCD begets a family of battery dispatch solutions $(P_n^{\mathrm{d}}(t), P_n^{\mathrm{c}}(t))$ whose nodal net-injections, $P_n^{\mathrm{d}}(t) - P_n^{\mathrm{c}}(t)$, are identical but whose effect on the battery's predicted state of charge introduces a undesirable prediction error proportional to $\sum_{t\in\mathcal{T}} P_n^{\mathrm{d}}(t)P_n^{\mathrm{c}}(t)$. To avoid SCD, one can enforce complementarity condition (3.2o) between charging and discharging decision variables of each battery. However, (3.2o) renders the SOCP problem non-convex. One approach to eliminate the challenging constraint is to introduce a binary (charge/discharge) variable to formulate an equivalent mixed-integer SOCP (MISOCP) problem. However, despite recent advances in MIP solvers, the MISOCP is computationally challenging as the number of batteries or the time-horizon increases. Instead, this work omits (3.2o) entirely and then analyzes under which conditions the optimal solution satisfies the complementarity constraint. This ensures that a (near) globally optimal solution can be achieved in a computationally efficient manner.

In this section, we provide general conditions that provably guarantee no SCD and hold for different practical optimization objectives and use-cases. Specific operating conditions are identified where SCD is provably optimal (which is undesired) and explicit methods are then presented that enforce complementarity.

The approach herein first augments the objective function to reduce the effects of SCD's fictitious energy losses, i.e., fictitious in the sense that the predicted state of charge will be different from the actual state of charge since the battery cannot operate with SCD (e.g., see Fig. 3.6), and is as follows:

$$f(x) + \alpha \sum_{t=t_0}^{T} \sum_{n=1}^{|G|} \sum_{\phi=1}^{|\phi|} P_n^{\mathrm{d}}(t) \left(\frac{1}{\eta_{\mathrm{d},n}} - \eta_{\mathrm{c},n} \right), \tag{3.7}$$

where $f(x)$ is given in (3.2a).

Loss-minimization on the IEEE-13 node network with network parameters provided in [132], Fig. 3.7 illustrates the effects of SCD with a single battery. Without the complementarity constraint imposed, the optimizer may waste energy through charge/discharge inefficiencies to achieve a lower state of charge of the battery as shown in Fig. 3.8a

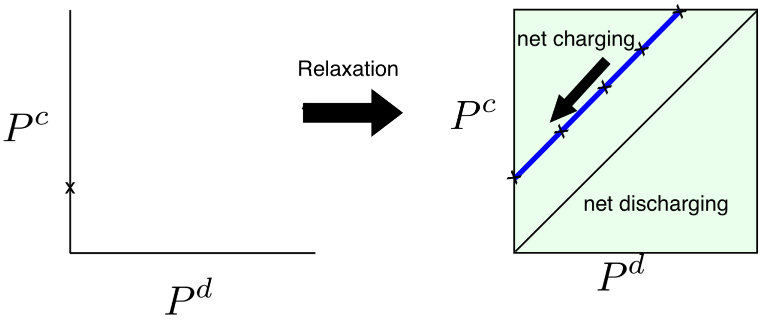

Figure 3.6: Illustration of simultaneous charging and discharging (SCD) from relaxing the battery's complementarity constraint. (Left) SCD is enforced, so any net injection value, $P^d - P^c$*, gives rise to only one solution. (Right) the same net injection value gives rise to a family of solutions shown in blue where the battery's state of charge (SoC) are different due to SCD's so-called "fictitious energy losses."*

The addition of the battery power term in the objective function avoids SCD as shown in Fig. 3.7 with a negligible effect on the original objective function as illustrated with Fig. 3.8b, where a comparison is presented with the exact mixed integer formulation. The solutions have the same optimized line losses as shown in Fig. 3.8b and the addition of battery power term incentivizes the solution to points that satisfy the complementarity constraint.

To formalize this result, Theorem 1 below provides specific conditions under which the convex formulation with a differentiable objective function, $f(x)$ can avoid SCD with (3.7). Specifically, the result holds for the following practical objectives in distribution networks:

- $f(W) = \sum_i (W_i - W^{nom})^2$ (e.g., minimizing voltage deviation from nominal)

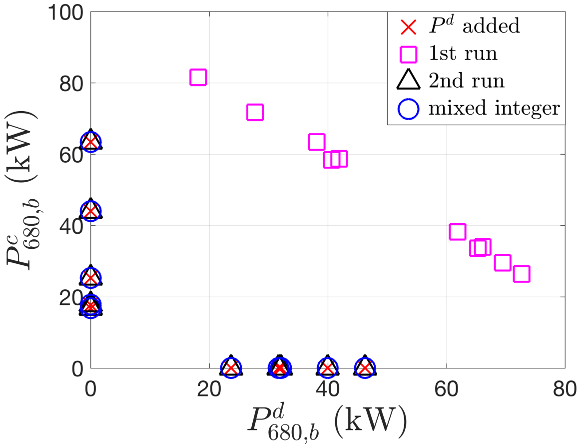

Figure 3.7: Comparison of simultaneous charge and discharge in battery at node 680, phase B for IEEE-13 node system between the cases with battery power term in objective, the 1st and 2nd run of the two-step algorithm presented in [7] and the mixed integer formulation. The reason for simultaneous occurrence of charge and discharge is that the objective function only has terms for the losses in the distribution lines and does not take into account the fictitious energy loss in the battery due to charging and discharging. Thus, all solutions with the same value for $P^d - P^c$, are equivalent in the optimization solution, which begets simultaneous charging and discharging.

- $f(I) = \sum_l(\text{diag}(R_l \circ I_l))$ (e.g., minimizing network line loss)

- $f(P_0)$=$(P_0 - P^{\text{ref}})^2$ (i.e., tracking a grid/head-node reference power set-point)

- $f(P^{\text{d}} + P^{\text{c}}) = \sum_i(P_i^d + P_i^c)$ (e.g., minimizing battery degradation)

- $f(P^{\text{d}} - P^{\text{c}}) = (P^{\text{d}} - P^{\text{c}} - P^{\text{ref}})^2$ (i.e., tracking VB reference trajectory)

Theorem 1. *For the SOCP optimization problem (3.2a)-(3.2n) with modified objective function (3.7), the SCD relaxation is exact if the following conditions hold at each node n and phase ϕ:*

C1: $\frac{\partial f(x)}{\partial P^c} + \frac{\partial f(x)}{\partial P^d} \geq 0$,

C2: α *in (3.7) is strictly positive* (> 0)*,*

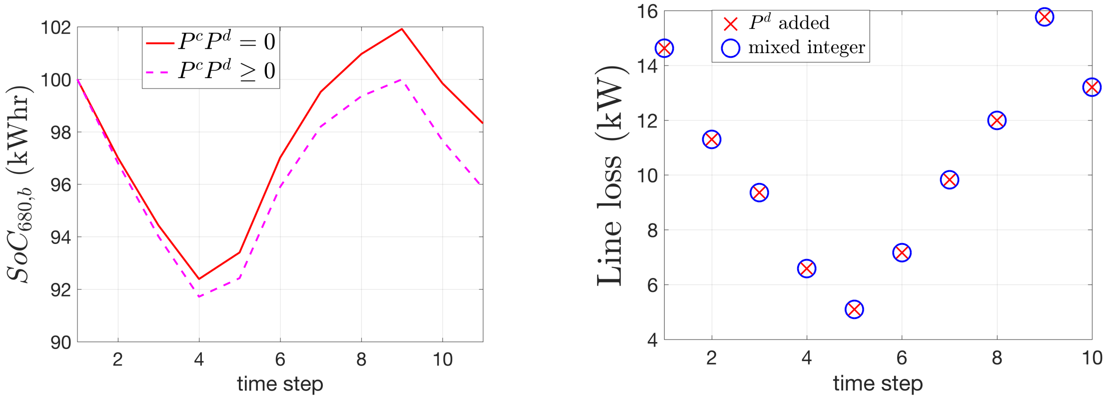

(a) (b)

Figure 3.8: (a) Comparison of state of charge of battery at node 680, phase B for IEEE-13 node system with and without battery power term in objective. Due to the occurrence of simultaneous charge and discharge, energy is fictitiously consumed in the battery leading to a lower net state of charge. (b) Comparison of objective value (line loss) between the convex formulation and mixed integer formulation over a prediction horizon. The figure shows that the addition of battery power term to the objective of the convex formulation has negligible effect on the objective value of minimizing line losses.

C3: $\Gamma(t) := \sum_{\tau=t}^{T}(\beta_{1,n,\phi}(\tau) - \beta_{2,n,\phi}(\tau)) \geq -\alpha$, $\beta_{1,n,\phi}(\tau), \beta_{2,n,\phi}(\tau) \in \mathbb{R}_+$ *be Lagrange multipliers for the upper and lower bounds of inequality (3.2l), respectively.*

The proof of Theorem 1 is provided in Appendix 5.A. Theorem 1 showed that with the modified objective function given by (3.7), SCD can be avoided under certain conditions in order to obtain a physically realizable solution from the optimizer.

The addition of the battery power term in the objective does, however, modify the objective function resulting in a sub-optimal solutions compared to the original objective. When the battery is charging, i.e., $P^{\mathrm{d}} = 0$, the modified objective is the same as the original objective resulting in the same optimal value. When the battery is discharging, i.e., $P^{\mathrm{d}} > 0$, the modified objective is different from the original objective, however, as α can be chosen to be small the effect on the optimal value is negligible.

Figure 3.7 shows the comparison between the solution $(P^{\mathrm{d}}, P^{\mathrm{c}})$ obtained from the convex formulation and the mixed-integer formulation and shows that the solutions match. This is also shown in Fig. 3.8b which compares the optimal value (line loss) between the two formulations and shows that the objective values match.

Remark 3. *Theorem 1 holds for the given objectives when conditions C1, C2 and C3 are satisfied. However, condition C3 can be restrictive, especially under a high penetration of renewable generation. Furthermore, certain objective functions like tracking battery state of charge require stricter conditions as shown in Corollary 1 in Appendix 5.B. For such cases, the following methods are proposed to obtain a physically realizable solution that avoids simultaneous charging and discharging of batteries.*

- *Large α: In the case where $\Gamma(t) < 0$, α can be chosen large enough to ensure that condition C1 is satisfied. The value of $\Gamma(t)$ may be estimated based upon the solar and load conditions. However, the drawback of this approach is that a large value of α would clearly shift the optimal solution.*

- *Two-step battery dispatch: as presented in [7], the first run permits SCD and the the second enforces complimentarity based on the net-effect of the first solution to obtain a physically realizable solution. This method can provide a near optimal feasible solution as shown in Fig. 3.7 but doubles the run-time. Future work will further explore how this two-step technique can provide optimality certificates and will improve its implementation to avoid the doubling of the solve time.*

- *Simplified battery model: In this method, the battery model in (3.2k) is replaced* *by an approximated battery model that uses a single standing-loss efficiency* η_{eq} *instead as shown below:*

$$B_n(t+1) = \eta_{eq} B_n(t) - \Delta t P_n^b(t)$$

where $P_n^b(t) \in \mathbf{R}^{|\phi|}$ *is the net battery power injection. The value of* η_{eq} *can be estimated based upon expected battery schedule and the values of* η_d *and* η_c*. Future work will explore a mapping between the two battery models as a way to estimate* η_{eq} *to minimize modeling error over the horizon with respect to the actual battery model in (3.2k).*

Based on the results of this section, a convex formulation of the multi-period three-phase OPF can be obtained that satisfies the complementarity condition between charging and discharging of batteries under certain conditions. When the conditions are not satisfied, this work proposes techniques to obtain a near optimal solution that enforces complementarity. However, the second order cone relaxation of the nonlinear power flow equations may engender solutions that are not physically realizable. To guarantee realizability, the next section presents a nonlinear programming (NLP) formulation of the OPF problem that is initialized with the relaxed SOCP solution. Note that the NLP initialization goes beyond just a warm-start and includes a novel mechanism to account for the multi-period formulation inherent to an energy storage trajectory.

3.2.4 Multi-period coupling of SOCP with NLP

The original OPF formulation given by (3.2a)-(3.2o) is non-convex because of the nonlinear power flow constraint in (3.2b) and the SCD complementarity constraint in (3.2o). The two constraints are relaxed to obtain an SOCP formulation of the OPF problem. The non-convex constraint (3.2o) is relaxed as explained in section 3.2.3, which provides conditions under which the SOCP solution is tight (with respect to the complementarity condition). However, the relaxation of the nonlinear power flow model in (3.2b) with the second-order cone constraints (3.4)-(3.6) can result in non-physical solutions to the OPF problem as has recently been shown in [67].

Thus, if we seek a physically realizable solution for a general objective function, we need a nonlinear programming (NLP) formulation. Thus, we seek to leverage the multi-period solution available from the SOCP. However, NLPs are not scalable and the solve time increases dramatically with the increase in problem size (and coupling) [119]

To overcome this challenge, we propose a time-decoupled approach by fixing the battery's active power set-points in the NLP based on the solution obtained from the SOCP. This allows the NLP to focus on reactive power set-points and voltage limits, which aligns with recent analysis [97]. In [97], it is shown how reactive power and voltage limits lead to disconnections in the power flow solution space resulting in a non-zero duality gap for the relaxed OPF. Based on these observations, an SOCP-NLP coupled algorithm is developed as shown in Fig. 3.9, where the solution obtained from the SOCP is passed to the NLP solver. Prior work in literature, such as [130], have proposed the idea of using the solution of a convex relaxation as an initial starting point for solving the full, nonlinear ACOPF. However, herein we extend the notion of a "warm start" to the multi-period domain. Specifically, we decouple the multi-period NLP by fixing the active power set-points of the batteries to the solution of the convex relaxation (SOCP). Keeping the active power solutions constant leads to fixing the state of charge of the batteries and, as a result, results in a decoupling of the time-steps of the prediction horizon in the NLP. Thus, each time-step can be solved independently and in parallel (as independent NLPs), which leads to a scalable implementation compared to solving the multi-period NLP.

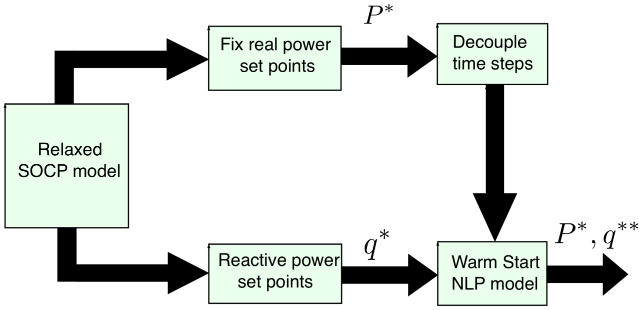

Figure 3.9: Coupling of SOCP with NLP by fixing real power solutions from SOCP and hence decoupling the NLP to obtain a feasible solution.

This is further explained through Fig. 3.10 where for each time-step of the prediction, the reactive power range available to the NLP is constrained by the SOCP's solution. That is, Figure 3.10 illustrates the decomposition approach presented herein by showing the effect of the SOCP's optimized active power trajectory on the feasible set of the reactive power of the NLP problem.

Remark 4. *The decoupling of the time-steps reduces the feasible set of the optimization problem and, hence, increases the optimal value. Thus, the decoupled problem represents an upper bound on the time-coupled nonlinear problem, which in turn is*

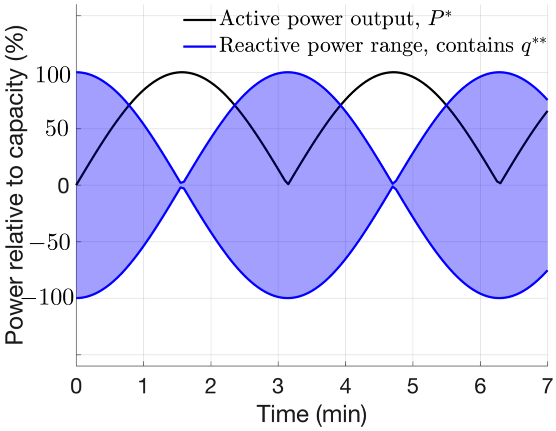

Figure 3.10: Available reactive power variation range for NLP across multiple time steps based on the active power trajectory provided by the SOCP.

lower bounded by the SOCP as shown below:

$$SOCP_{opt} \leq NLP_{opt} \leq DNLP_{opt} \tag{3.8}$$

where NLP_{opt} represents the optimal value of the time-coupled nonlinear program and $DNLP_{opt}$ the optimal value of the time-decoupled nonlinear program (DNLP).

The DNLP problem at each time-step t of the prediction horizon can then be expressed as:

$$\min_{x} \sum_{l=1}^{L} \sum_{\phi=1}^{|\phi|} \mathrm{diag}(R_l \circ I_l(t)) \tag{3.9a}$$

$$s.t: \ (3.2b) - (3.2j) \tag{3.9b}$$

$$P_n^{\mathrm{d}}(t) = P^{\mathrm{d}*} \tag{3.9c}$$

$$P_n^{\mathrm{c}}(t) = P^{\mathrm{c}*} \tag{3.9d}$$

where $P^{\mathrm{c}*} \in \mathcal{R}^{|\phi|}$ and $P^{\mathrm{d}*} \in \mathcal{R}^{|\phi|}$ are the charge and discharge power of the battery obtained from the SOCP at node n and time t, such that $P^{*} = P^{\mathrm{d}*} - P^{\mathrm{c}*}$. The NLP given by equations (3.9a)-(3.9d) is solved separately at each step of the prediction horizon to obtain a feasible plus (near) optimal solution with guaranteed feasibility and a bound on the optimality, as the relaxed SOCP provides a lower bound on the optimal value of the original nonlinear problem [119]. Utilizing this SOCP-NLP coupled optimization framework, a scalable solution of three-phase OPF problem can be obtained rapidly, plus the framework provides bounds and guarantees on feasibility and optimality of the solution, where the upper-bound on the global optimality gap is computed from

$$\%\ \text{optimality gap} \leq \frac{DNLP_{opt} - SOCP_{opt}}{DNLP_{opt}} \times 100. \tag{3.10}$$

In the next section, simulation tests are conducted on unbalanced IEEE test feeders and realistic distribution feeders to verify the feasibility of the proposed formulation and investigate the global optimality gap. The validation is conducted by using forward-backward sweep in GridLab-D.

3.2.5 Test case results and validation

3.2.5.1 Case study description

Simulation-based analysis of the multiperiod SOCP-NLP algorithm presented above is first conducted on the unbalanced 123-node IEEE test feeder with a base voltage of 2.4kV and base apparent power of 1 MVA. The algorithm is implemented in receding-horizon fashion. That is, the SOCP results in an open-loop, optimal battery and inverter control schedule, which is used by the NLP to calculate a physically realizable schedule that is implemented by GridLab-D (i.e., the “plant”) to determine the resulting AC power flows. The forecasts of demand and renewable generation are then updated and the SOCP-NLP implementation repeats. A sample forecast of aggregate solar, demand and net-demand over a prediction horizon is shown in Fig. 3.11a.

Distributed storage and solar PV units are added at random to 16 nodes in the network which can supply active and reactive power through four quadrant operation. Each storage unit has an energy capacity of 40 kWh and an apparent power rating of 50 kVA, whereas each solar PV unit has a rating of 100 kVA. The solar and load profile over the 30-step prediction horizon, with each step being 1 minute duration, are constructed from the minutely forecast data available [133]. The choice of the length of prediction horizon is based on a trade-off between objective function value (performance) versus solve time. As illustrated in Fig. 3.11b, as the prediction horizon is increased, the objective value reduces, i.e., the performance increases. This is due to the fact that considering the multi-time step optimization results in predicted set-points over the horizon which lead to improved system performance. Let mean load, μ_l, be the base load of the IEEE-123 node system and μ_s be the mean solar and equal to 100kW Discrete control devices such as switches, capacitor banks and transformers are fixed at their nominal value for this study. A three phase OPF is run in a receding horizon fashion with a prediction horizon of 30 time-steps, for the dispatch of controllable assets of the network to minimize the network losses. The set-points provided by the solution of the SOCP are used to initialize an NLP to provide a feasible solution. The SOCP is modeled in JuMP [134], with Julia and solved using GUROBI [126]. The multi-period SOCP has 108,000 variables, 48,000

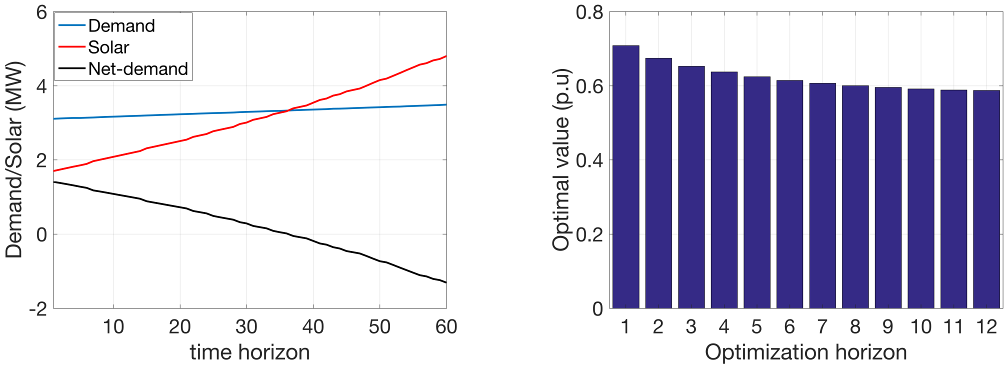

(a) (b)

Figure 3.11: (a) Aggregate solar, demand and net-demand profile over a prediction horizon. (b) Trade-off between performance (optimal value) versus solve-time (length of prediction horizon.

linear constraints and 81,000 SOC constraints. The NLP is also modeled in JuMP, but solved with IPOPT [135] using `HSL_MA86` solver [136]. The single-period NLP has 3,600 variables, 1,600 linear constraints, 700 SOC constraints and 2,000 non-linear constraints.

3.2.5.2 Data management

To enable the presented framework, it is assumed that the minutely PV production forecast data and the demand profile data over the 30 minute horizon, as shown in Fig. 3.11a, is available to the central dispatcher. In this work, we assume a perfect forecast, whereas section 3.3 will investigate the role of uncertainty and robustness to forecast error. Such minutely solar PV forecasts are available today at minutely forecasts with a 60-minute prediction horizon [133]. It is also assumed that the dispatcher knows about the power rating and capacity of the available PV units and the updated state of charge of the distributed storage units. This dispatcher

Table 3.2: Different solar and load cases.

	Low load: 50% load	High load: 100% load
Low solar: 50% Solar	Case LL	Case HL
High solar: 100% Solar	Case LH	Case HH

could be a distribution system operator (DSO; e.g., NY REV's DSIP [89]), so it is reasonable to assume that such system information is available. Furthermore, it is assumed that the DSO knows the network topology, so it can formulate and solve the optimization problem based on network parameters and dispatch available flexible resources accordingly.

3.2.5.3 Test case results on IEEE-123 node network

The results obtained under four different solar and load cases as shown in Table 3.2, where high load and high solar corresponds to the base values and low load and low solar corresponds to a mean value of 50% of base. These cases are utilized to show the feasibility, optimality, gap and solve time of the formulated algorithms.

The result in Table 3.3 show that the optimality gap of the obtained solution is always less than 3%, as the SOCP solution provides the lower bound to the global optimum. The RMSE and worst case values are calculated based on the optimal values of the SOCP and the NLP run in a receding horizon fashion through simulations over a horizon of one hour. To further investigate the optimality gap, Fig. 3.12a shows the optimality gap as the solar penetration level in the system is varied for the base load case. From the figure it can be seen that the optimality gap is always below 3% for the different solar penetration levels.

The feasiblity of the NLP solution is tested against GridLab-D and the validation is given in Fig. 3.12b for case HH, which shows that the voltages obtained from the NLP match closely with those obtained through a power flow performed in GridLab-D using backward-forward sweep. NLPs are not scalable and the solve time increases dramatically with the increase in problem size (and coupling) as can be seen from Fig. 3.14a for case HH, which shows the increase in solve time as the length of the prediction horizon increases. The computation time of the decoupled algorithm is illustrated in Table 3.4 showing that the mean total solve time at each time step for SOCP+NLP is always under 45 seconds, providing sufficient time for communication delays in order to guarantee a solve time of under one minute for the dispatch of distributed storage to counter the fast-time variation in renewable generation. The SOCP time is the time it takes to solve the multi-period optimization with a time-horizon of 30 steps, whereas the NLP time is the time it takes to solve each time-instant in a decoupled and parallel form. Figures 3.13a-3.13d shows the worst case difference in DER reactive power generation over the prediction horizon between the SOCP and the NLP, whereas Fig. 3.14b shows the variation in SOCP solve time as the size of the receding horizon is increased for case HH. In the figure, the edges of the box represent the 25th and 75th percentile of data, whereas the + sign represents the most extreme value in the dataset. It can be seen from Fig. 3.14b that the SOCP algorithm scales well with the increase in horizon size.

Table 3.3: Comparison of optimality gap values of SOCP and NLP.

Case	RMSE	Worst case
LL	0.43	1.25
HL	0.83	0.91
LH	1.14	1.33
HH	0.88	2.10

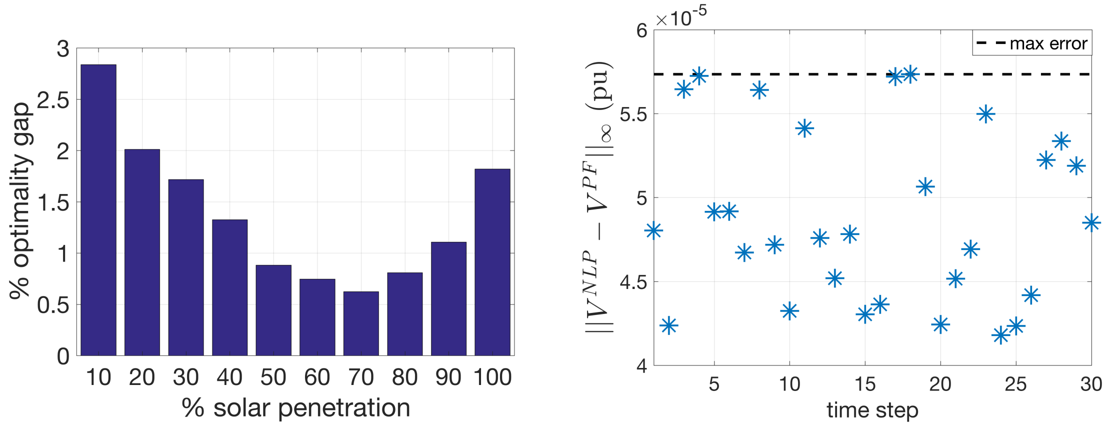

(a) (b)

Figure 3.12: (a) Variation of optimality gap with change in % solar penetration. (b) Worst case voltage error between NLP and power flow (PF) in GridLab-D over the time horizon showing the feasibility of the NLP solution.

Table 3.4: Comparing solver times for the SOCP-NLP algorithm.

Solver time (s)	Case LL	Case HL	Case LH	Case HH
$(\mu, \sigma)_{\mathrm{SOCP}}$	(42.4, 6.3)	(17.9, 1.5)	(31.4, 9.6)	(24.1, 2.2)
$(\mu, \sigma)_{\mathrm{NLP}}$	(1.8, 0.3)	(2.2, 0.8)	(1.9, 0.2)	(2.1, 0.7)
$(\mu, \sigma)_{\mathrm{total}}$	(44.2, 6.4)	(20.1, 1.6)	(33.3, 9.6)	(26.3, 2.5)

3.2.5.4 Tracking results on ORU network

Further simulation results are conducted on reduced Orange and rockland utility (ORU) feeders. In this study, we consider two ORU networks with 900 and 600 three-phase nodes that are reduced through the network reduction technique presented in section 2.5 to 90 and 60 node three-phase networks respectively. These two reduced networks are used to show the tracking performance of the SOCP-NLP algorithm developed in this section. Figure 3.15a shows the head-node tracking performance of the 90 node reduced network, whereas Fig. 3.15b shows the head-node tracking performance of the 60 node reduced network. From the results in Fig. 3.15, it can

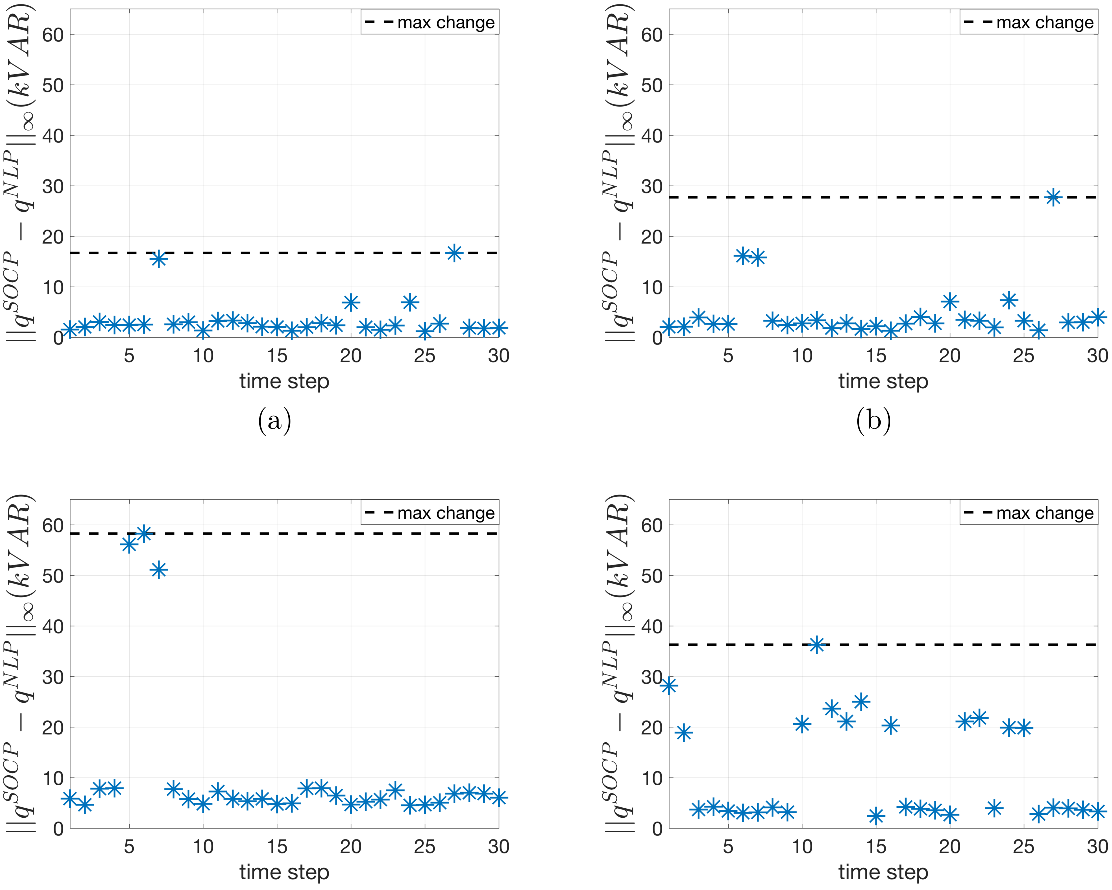

(a)

(b)

(c)

(d)

Figure 3.13: Comparison of reactive power generation obtained from NLP and SOCP for IEEE-123 node system under the following cases: (a) low load, low solar (b) high load, low solar (c) low load, high solar (d) high load, high solar.

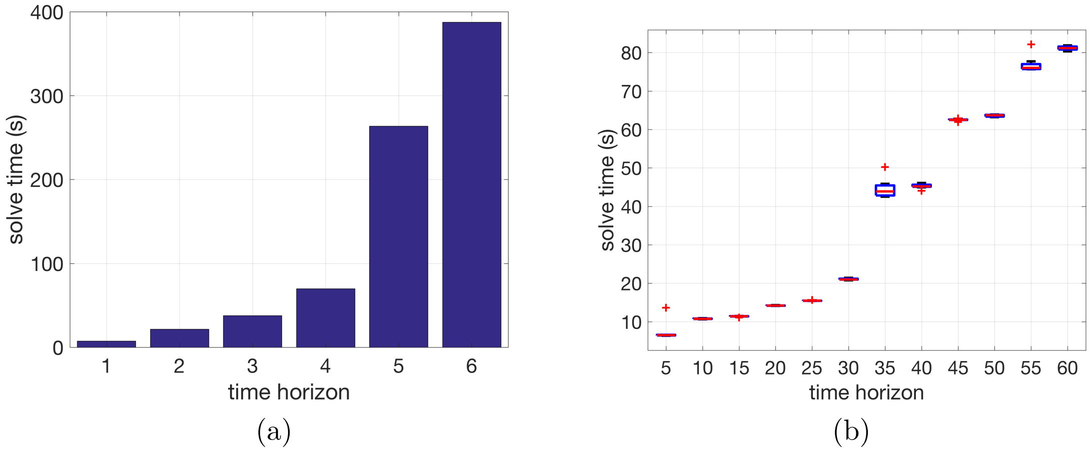

(a) (b)

Figure 3.14: (a) Solve time for the full-scale NLP for different prediction horizons. For prediction horizons > 6 time-steps, the solver did not converge. (b) SOCP solve time vs. length of prediction horizon.

be seen that the presented SOCP-NLP formulation has the desired grid-reference tracking ability.

3.2.6 Conclusions

This section presented a method for the optimal dispatch of batteries in an unbalanced three-phase distribution network. A second order cone relaxation is used to convert the non-convex power flow equation into a convex formulation that can be solved in polynomial time. As the solution obtained from the relaxed problem may not be feasible, an NLP is solved at each time-step by fixing the real power set-points and decoupling the time-steps to obtain a physically realizable solution. Furthermore, the phenomenon of simultaneous charging and discharging of batteries is analyzed and sufficient conditions are provided for different objective functions that provably avoid this phenomenon to obtain a feasible solution. Simulation tests are conducted

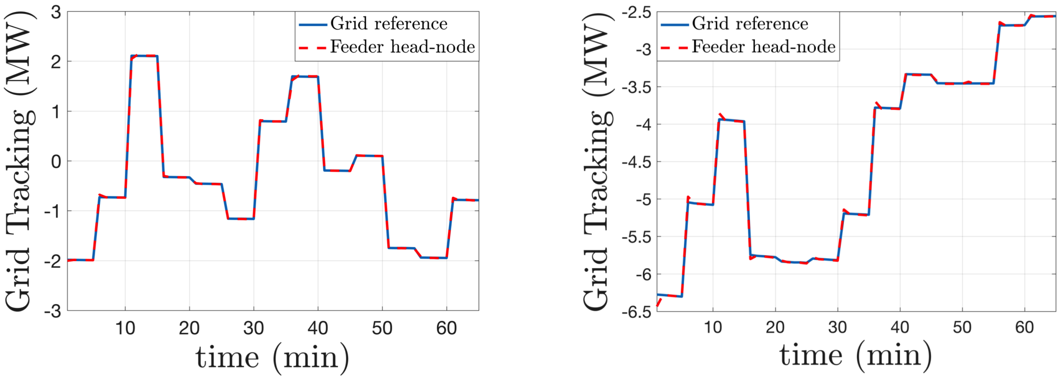

(a) (b)

Figure 3.15: Tracking the grid economic signal by the feeder head-node through the deterministic SOCP-NLP OPF problem for (a) ORU feeder with 90 reduced nodes (b) ORU feeder with 60 reduced nodes. The results show that the SOCP-NLP optimization is able to achieve desired tracking for these feeders.

on IEEE-13, IEEE-123 node and realistic ORU distribution feeders showing the feasibility of the obtained solution. The optimality gap is found to be within 3%. The approach is computationally tractable and solves in less than 45 seconds, which ensures that enough time is available for realistic communication delays. This permits an implementation of the optimization scheme on the minute timescale.

3.3 Stochastic multi-period OPF in unbalanced feeders

This section presents a convex, multi-period, AC-feasible Optimal Power Flow (OPF) framework that robustly dispatches flexible demand-side resources in unbalanced distribution feeders against uncertainty in very-short timescale solar Photo-Voltaic (PV) forecasts. This is valuable for power systems with significant behind-the-meter solar PV generation as their operation is affected by uncertainty from forecasts of demand and solar PV generation. The aim of this work is then to ensure the feasibility and reliability of distribution system operation under high solar PV penetration. We develop and present a novel, robust OPF formulation that accounts for both the nonlinear power flow constraints and the uncertainty in forecasts. This is achieved by linearizing an optimal trajectory and using first-order methods to systematically tighten voltage bounds. Case studies on a realistic distribution feeder shows the effectiveness of a receding-horizon implementation.

3.3.1 Introduction

Renewable energy sources, such as solar PV, are inherently stochastic in nature and the corresponding variability poses a challenge to grid operators [109]. To overcome these challenges, grid operators can leverage responsive DERs to provide demand-side flexibility. The inclusion of flexible demand from energy-constrained DERs, such as battery storage, couples the time-steps, which requires multi-period decision-making and predictive optimization.

In addition, accounting for the uncertainties in solar generation and demand forecasts calls for a robust dispatch of flexible DERs. Choosing an acceptable violation probability is perceived as an intuitive and transparent way of determining a probabilistic security level [110]. Chance-constraint-based optimization is one such tool that is employed to robustly dispatch flexible resources in order to satisfy AC power flow constraints. The nonlinearities associated with the AC physics, however, renders the chance-constrained optimization problem challenging to solve due to non-convexities. Thus, to certify reliable operation of distribution systems under high penetrations of solar PV, techniques are desired that take into account both the AC nonlinearities and the uncertainty from solar PV forecasts.

In this work, we build upon the work on chance constraint in the literature by decoupling the solution to the deterministic multi-period AC OPF problem and a linearized chance constraint problem. As shown in Fig. 3.16, a deterministic, multi-period, SOCP+NLP problem is solved by an centralized grid operator to obtain an optimal, three-phase, AC-feasible state (voltage and current) trajectory. Based on the trajectory, Taylor series expansions of the power flow equations are computed around the operating points from each time-step. The sensitivity of the network constraints (voltage and branch flows) to the uncertain injections (demand and solar PV) can be computed. From these sensitivity factors, the uncertainty determines the degree of constraint tightening, which robustifies the SOCP and NLP formulations. Validation of the presented robust optimization framework is completed in GridLab-D, where an AC load flow is solved based on actual, realized demand and solar PV injections. An illustration of the relative root-mean-square error (RMSE) in the solar PV forecasts is shown in Fig. 3.17a along with an illustration of the range of uncertainty around the expected solar PV generation over the prediction horizon in Fig. 3.17b. The forecast error is meant to be representative of the state-of-the-science in solar PV forecasts today [137, 138].The RMSE error in Fig. 3.17a showcases how the error in solar forecast grows over the prediction horizon (60 minutes in this case). Further, every 30 minutes a new solar forecast is available that follows a similar forecast error. Corresponding to the RMSE values in Fig. 3.17a, Fig. 3.17b shows the range of error in predicted forecast of solar PV over the prediction horizon.

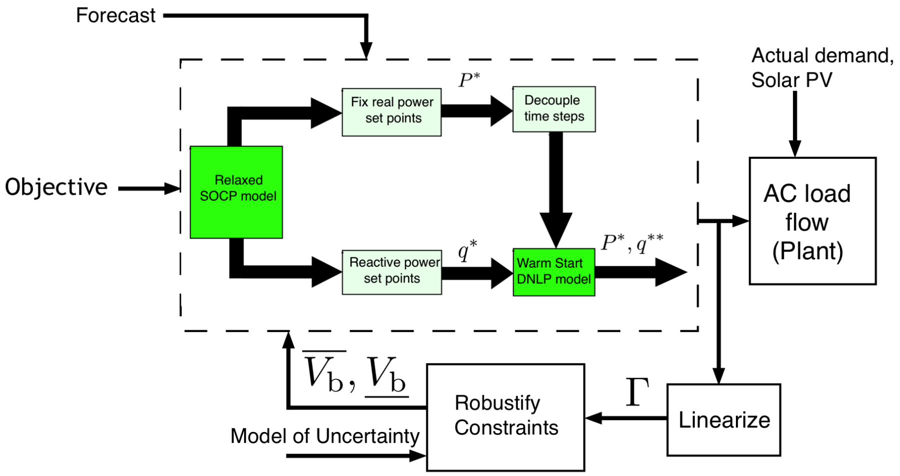

Figure 3.16: Block diagram showing the components of the complete robust version of the SOCP+NLP optimization problem together with three-phase, AC load flow "plant model" in GridLab-D (GLD). The The SOCP block performs multi-period optimization and fixes the active power set-points in the NLP to temporally decouple the NLP's ACOPF formulation and compute optimal reactive power set-points that are AC feasible.

Thus, the two key contributions of this work are as follows:

1. A novel approach to robustify a stochastic, multi-period feasible ACOPF optimization problem by leveraging the solution of the deterministic problem with a linearized chance-constrained tightening procedure based on the operating points determined by the NLP's optimal trajectory. Hence, the uncertainty in

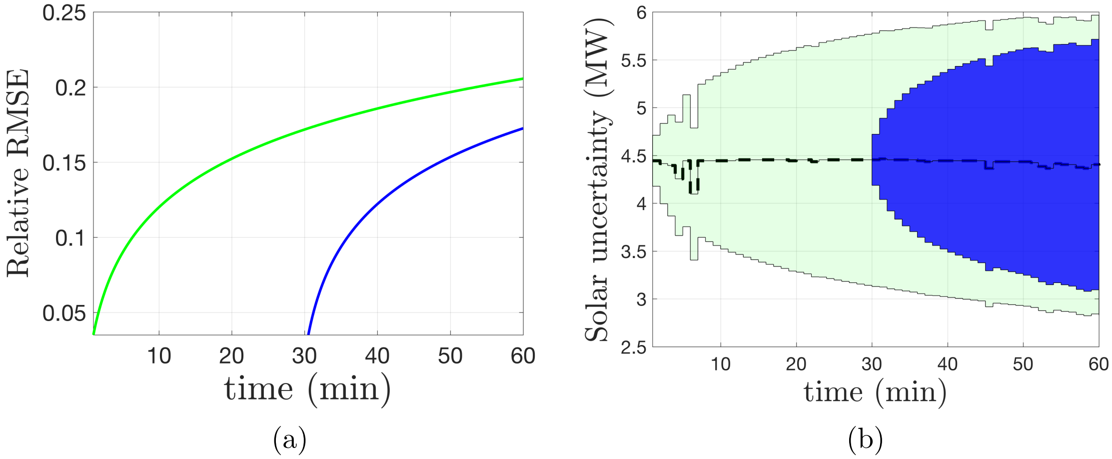

(a) (b)

Figure 3.17: Left: (a) Relative-RMSE over the forecast horizon from minutely solar PV forecasts. The forecasts are updated every 30 minutes and provide a 60-minute preview window. Right: (b) Error in predicted forecast of solar PV over the prediction horizon for the considered test network from 12:00 noon to 1:00 pm.

forecasted values determine the first-order tightening of constraints. The calculated change in these variables at each time-step due to the uncertainty is then added as safety buffer to the constraints in the deterministic SOCP+NLP scheme.

2. Simulation-based analysis employs a state-of-the-art solar PV forecasting scheme to validate the proposed robust ACOPF approach.

In the remainder of this section, a method to ensure a network-admissible, multi-period battery dispatch by coupling the convex, multi-period SOCP with an exact, time-decoupled NLP formulation together with the linearized chance-constrained formulation is presented in Section 3.3.2. Simulation-based analysis and validation results obtained with GridLab-D are discussed in Section 3.3.3 for a realistic distribution feeder. Finally, conclusions are discussed in Section 3.3.5.

In the next section, the physically realizable solution obtained from the SOCP-NLP formulation presented in section 3.2 is used to linearize the network model at the operating point. Based on the obtained linear model at each operating point over the prediction horizon, the uncertainty in demand and solar PV is used to calculate the predicted changes in voltage magnitudes and line power flows in the network. These values are then used to systematically tighten the limits to robustly solve the AC OPF at the next instant.

3.3.2 Robustify constraints

In this section, we describe the chance constraint method that is implemented to obtain the robust bounds on network constraints. In this work, we consider the uncertainty in demand and solar PV forecast. Other sources of uncertainty include the capacity and ratings of DERs, which is inherent due to the nature of aggregation of different energy resources to form a DER resource. However, the method presented in this work can also be extended to these types of uncertainties. A detailed analysis on accounting for uncertainty in DERs can be found in [139].

Based on the Taylor series expansion of the power flow equations around the operating point (determined previously from the deterministic optimization presented in section 3.2), sensitivity factors, similar to the ones in [140], can be obtained. These sensitivity factors then determine the fluctuations in the variables to the uncertainty Ω (which could represent either solar or demand uncertainty). For a constrained variable Y, the sensitivity with respect to the random variable Ω can be expressed as: $\Gamma_Y = \frac{\partial Y}{\partial \Omega}\Big|_{\Omega=0, Y=Y^*}$

The sensitivity factors allow us to approximate the constrained variables as linear functions of the random variable Ω, as a result the constraints in stochastic form can be expressed as:,

$$\mathbb{P}(Y + \Gamma_Y \Omega \leq Y_{max}) \geq 1 - \alpha_{\mathrm{Y}} \tag{3.11}$$

$$\mathbb{P}(Y + \Gamma_Y \Omega \geq Y_{min}) \geq 1 - \alpha_{\mathrm{Y}} \tag{3.12}$$

where α_{Y} represents the acceptable violation probability. The linear dependence of Ω enables the use of an analytical chance constraint reformulation [115]. Assuming that the uncertainty Ω is any general zero mean distribution (operating point is determined by the expected forecast) with covariance matrix Σ, then (3.11)-(3.12) can be expressed in a deterministic form as:

$$Y + f^{-1}(1 - \alpha_{\mathrm{Y}})||\Gamma_Y \Sigma^{1/2}||_2 \leq Y_{max} \tag{3.13}$$

$$Y - f^{-1}(1 - \alpha_{\mathrm{Y}})||\Gamma_Y \Sigma^{1/2}||_2 \geq Y_{min} \tag{3.14}$$

where $f^{-1}(1 - \alpha_{\mathrm{Y}})$ represents the safety factor function evaluated at $1 - \alpha_{\mathrm{v}}$, which prescribes the desired probabilistic guarantee. Thus, robustness against the uncertainties naturally begets an uncertainty margin that is product of the safety factor function and the variances and defines how much the constraint is tightened.[1] It can be observed from (3.13)-(3.14), that the uncertainty margin can be calculated before solving the optimization problem at the forecast value and then utilizing the margins obtained from chance-constraints to tighten the constraints on the deterministic problem. If we denote by λ_{Y} the uncertainty margin in the constraint, then (3.13)-(3.14)

---

[1] Note that this method can be extended beyond normal distributions to consider more general distributions with only knowledge of mean and variance of the distribution. However, the results obtained are more conservative in that case, e.g., with a Chebyshev approximation.

can be expressed as:

$$Y \leq Y_{max} - \lambda_{\mathrm{Y}}(\alpha_{\mathrm{Y}}, \Sigma, Y^*) =: \overline{Y_{\mathrm{b}}} \tag{3.15}$$

$$Y \geq Y_{min} + \lambda_{\mathrm{Y}}(\alpha_{\mathrm{Y}}, \Sigma, Y^*) =: \underline{Y_{\mathrm{b}}}, \tag{3.16}$$

where $\overline{Y_{\mathrm{b}}}$ and $\underline{Y_{\mathrm{b}}}$ represent the updated upper and lower robust bounds and $\lambda_{\mathrm{Y}}(\alpha_{\mathrm{Y}}, \Sigma, Y^*) := f^{-1}(1-\alpha_{\mathrm{Y}})||\Gamma_Y \Sigma^{1/2}||_2$ represents the uncertainty margin which depends on both the operating point and the acceptable violation probability factor α_{Y}.

From the tightened constraints on voltage and power limits, we ensure that any dispatch of DERs is robust against desired uncertainty levels. However, the tightened bounds may lead to infeasible dispatch, so to guarantee persistent feasibility in the scheme, we introduce slack variables Y_{v}^{+} and Y_{v}^{-} which guarantee feasibility of solution to the deterministic AC OPF with the tighter bounds under very high uncertainty. Based on these updates, the optimization problem under the tightened bounds can be expressed as:

$$\min_{P_n^{\mathrm{d}}(t), P_n^{\mathrm{c}}(t), q_n^{\mathrm{b}}(t), S_n^{\mathrm{S}}(t)} \quad f_1(x) \tag{3.17a}$$

$$\text{s.t.}$$

$$0 = W_n(t) - W_m(t) + (S_l(t) Z_l^* + Z_l S_l(t)) - Z_l I_l(t) Z_l^* \quad \forall l \in \mathcal{L}, \tag{3.17b}$$

$$0 = \mathrm{diag}(S_l(t) - Z_l I_l(t) - \sum_p S_p(t)) + S_n^{\mathrm{net}}(t) \quad \forall l \in \mathcal{L}, \tag{3.17c}$$

$$0 = \mathrm{real}(S_n^{\mathrm{net}}(t) - S_n^{\mathrm{S}}(t) + S_n^{\mathrm{L}}(t)) - P_n^{\mathrm{d}}(t) + P_n^{\mathrm{c}}(t) \qquad \forall n \in \mathcal{G}, \tag{3.17d}$$

$$0 = \mathrm{imag}(S_n^{\mathrm{net}}(t) - S_n^{\mathrm{S}}(t) + S_n^{\mathrm{L}}(t)) - q_n^{\mathrm{b}}(t) \qquad \forall n \in \mathcal{G}, \tag{3.17e}$$

$$\left\|\frac{2W_n(t)(i,j)}{W_n(t)(i,i)-W_n(t)(j,j)}\right\|_2 \leq W_n(t)(i,i)+W_n(t)(j,j), \tag{3.17f}$$

$$\left\|\frac{2I_l(t)(i,j)}{I_l(t)(i,i)-I_l(t)(j,j)}\right\|_2 \leq I_l(t)(i,i)+I_l(t)(j,j), \tag{3.17g}$$

$$\left\|\frac{2S_l(t)(i,j)}{W_n(t)(i,i)-I_l(t)(j,j)}\right\|_2 \leq W_n(t)(i,i)+I_l(t)(j,j), \tag{3.17h}$$

$$|\mathrm{diag}(S_l(t))| \leq \overline{L}_{\mathrm{b},l}(t,\alpha_{\mathrm{L}},\Sigma) \qquad \forall l \in \mathcal{L}, \tag{3.17i}$$

$$\underline{V}_{\mathrm{b},n}(t,\alpha_{\mathrm{v}},\Sigma) - V^{-}_{\mathrm{v},n}(t) \leq \mathrm{diag}(W_n(t)) \leq \overline{V}_{\mathrm{b},n}(t,\alpha_{\mathrm{v}},\Sigma) + V^{+}_{\mathrm{v},n}(t)\ \forall n \in \mathcal{N}, \tag{3.17j}$$

$$|S^{\mathrm{S}}_n(t)| \leq \overline{S}_{\mathrm{b},n}(t,\alpha_{\mathrm{s}},\Sigma) \qquad \forall n \in \mathcal{G}, \tag{3.17k}$$

$$(P^{\mathrm{d}}_n(t) - P^{\mathrm{c}}_n(t))^2 + (q^{\mathrm{b}}_n(t))^2 \leq H^2_{\max,n}, \qquad \forall n \in \mathcal{G}, \tag{3.17l}$$

$$0 = B_n(t+1) - B_n(t) - \eta_{\mathrm{c},n}P^{\mathrm{c}}_n(t)\Delta t + \frac{P^{\mathrm{d}}_n(t)}{\eta_{\mathrm{d},n}}\Delta t \qquad \forall n \in \mathcal{G}, \tag{3.17m}$$

$$B_{\min,n} \leq B_n(t) \leq B_{\max,n} \qquad \forall n \in \mathcal{G}, \tag{3.17n}$$

$$0 \leq P^{\mathrm{d}}_n(t) \leq P_{\max,n} \qquad \forall n \in \mathcal{G}, \tag{3.17o}$$

$$0 \leq P^{\mathrm{c}}_n(t) \leq P_{\max,n} \qquad \forall n \in \mathcal{G} \tag{3.17p}$$

where the above equations hold $\forall t \in \mathcal{T}$ and $\overline{L}_{\mathrm{b},l}(t,\alpha_{\mathrm{L}},\Sigma) := S_{\max,l} - \lambda_{\mathrm{L}}(\alpha_{\mathrm{L}},\Sigma,S_l(t)^*)$, $\overline{V}_{\mathrm{b},n}(t,\alpha_{\mathrm{v}},\Sigma) := V^2_{\max,n} - \lambda_{\mathrm{v}}(\alpha_{\mathrm{v}},\Sigma,W_n(t)^*)$, $\underline{V}_{\mathrm{b},n}(t,\alpha_{\mathrm{v}},\Sigma) := V^2_{\min,n} + \lambda_{\mathrm{v}}(\alpha_{\mathrm{v}},\Sigma,W_n(t)^*)$, $\overline{S}_{\mathrm{b},n}(t,\alpha_{\mathrm{s}},\Sigma) := G_{\max,n} - \lambda_{\mathrm{s}}(\alpha_{\mathrm{s}},\Sigma,S^{\mathrm{S}*}_n(t))$. In the above problem the objective is to minimize line losses and voltage slack, i.e., $f_1(x) := \sum_{t=t_0}^{T}(\sum_{l=1}^{L}(\mathbf{1^T}\mathrm{diag}(R_l \circ I_l(t))) + \gamma\sum_{n=1}^{N}\mathbf{1^T}(V_{\mathrm{v},n}(t)^+ + V_{\mathrm{v},n}(t)^-) + \alpha\sum_{n=1}^{|G|}\mathbf{1^T}P^{\mathrm{d}}_n(t)\left(\frac{1}{\eta_{\mathrm{d},n}} - \eta_{\mathrm{c},n}\right))$, where $V_{\mathrm{v},n}(t)^+$ and $V_{\mathrm{v},n}(t)^-$ represents the upper and lower voltage slack that is added to ensure feasibility. The parameter γ is chosen to be large in order to discourage the activation of the slack variables and only employ them when a solution would not be feasible. The parameter γ can be thought of as a trade-off parameter between risk and performance. If $\gamma << 1$ then the solution is close to the deterministic solution, whereas for

$\gamma >> 1$ we sacrifice performance for robustness. In-between these two extremes, the trade-off parameter γ represents a "price" on risk (i.e., cost of risk), which has been studied extensively in [9]. Simulation-based analysis can help inform grid operators on an appropriate value of γ for a specific system. Similarly, the NLP optimization is updated with the bounds obtained from the chance constraints, which comes next:

$$\min_{x} \; f_2(x) \tag{3.18a}$$

$$0 = W_n(t) - W_m(t) + (S_l(t)Z_l^* + Z_l S_l(t)) - Z_l I_l(t) Z_l^* \quad \forall l \in \mathcal{L} \tag{3.18b}$$

$$0 = \mathrm{diag}(S_l(t) - Z_l I_l(t) - \sum_p S_p(t)) + S_n^{\mathrm{net}}(t) \quad \forall l \in \mathcal{L} \tag{3.18c}$$

$$\begin{bmatrix} W_n(t) & S_l(t) \\ S_l(t)^* & I_l(t) \end{bmatrix} = \begin{bmatrix} V_n(t) \\ i_l(t) \end{bmatrix} \begin{bmatrix} V_n(t) \\ i_l(t) \end{bmatrix}^* \qquad \forall l \in \mathcal{L} \tag{3.18d}$$

$$0 = \mathrm{imag}\{S_n^{\mathrm{net}}(t) - S_n^{\mathrm{S}}(t) + S_n^{\mathrm{L}}(t)\} - q_n^{\mathrm{b}}(t) \qquad \forall n \in \mathcal{G} \tag{3.18e}$$

$$(P_n^{\mathrm{d}*}(t) - P_n^{\mathrm{c}*}(t))^2 + (q_n^{\mathrm{b}}(t))^2 \leq H_{\max,n}^2, \qquad \forall n \in \mathcal{G} \tag{3.18f}$$

$$|\mathrm{diag}(S_l(t))| \leq \overline{L}_{\mathrm{b},l}(t, \alpha_{\mathrm{L}}, \Sigma) \qquad \forall l \in \mathcal{L} \tag{3.18g}$$

$$\underline{V}_{\mathrm{b},n}(t, \alpha_{\mathrm{v}}, \Sigma) - V_{\mathrm{v},n}^{-}(t) \leq \mathrm{diag}(W_n(t) \leq \overline{V}_{\mathrm{b},n}(t, \alpha_{\mathrm{v}}, \Sigma) + V_{\mathrm{v},n}^{+}(t) \; \forall n \in \mathcal{N} \tag{3.18h}$$

$$|S_n^{\mathrm{S}}(t)| \leq \overline{S}_{\mathrm{b},n}(t, \alpha_{\mathrm{s}}, \Sigma) \qquad \forall n \in \mathcal{G} \tag{3.18i}$$

where $f_2(x) := \sum_{l=1}^{L} \mathbf{1^T}(diag(R_l \circ I_l(t))) + \gamma \sum_{n=1}^{N} \mathbf{1^T}(V_{\mathrm{v},n}(t)^+ + V_{\mathrm{v},n}(t)^-)$, (3.18b)-(3.18e) respresent the nonlinear power flow equations and (3.18f) represents the VB apparent power constraint with $P_n^{\mathrm{d}*}(t) \in \mathbb{R}^{|\phi|}$ and $P_n^{\mathrm{c}*}(t) \in \mathbb{R}^{|\phi|}$ being the optimal discharge and charge power of the VB at node n obtained from the solution of the robust SOCP given in (3.17a)-(3.17p). Thus the algorithm is a combination of robust, multi-period SOCP formulation in (3.17a)-(3.17p) and the robust, time-decoupled NLP in (3.18)

In this work, the forecast errors for solar PV and demand are assumed to pertain to uniform (unimodal) distributions. Due to this assumption, the conventional Gaussian safety factor function may not guarantee robust performance for the given α_{Y}. A Chebyshev approximation can be used, which guarantees robustness for *any* distribution of forecast errors with a given mean and covariance matrix, but the approximation is often very conservative [8]. In addition, it is reasonable to assume that intra-hour forecast errors will come from a unimodal distribution, which allows for a less conservative unimodal Chebyshev approximation, which still guarantees robust performance against any unimodal distribution (e.g., uniform distribution). The safety-factor function for the unimodal distribution presented herein is a simple analytical approximation based on the exact numerical solution from [8] and is given by:

$$f^{-1}(1-\alpha_{\mathrm{Y}}) \approx \left(\frac{1-\alpha_{\mathrm{Y}}}{e\alpha_{\mathrm{Y}}}\right)^{1/1.95} \tag{3.19}$$

This approximation is an inner approximation of $f^{-1}(1-\alpha_{\mathrm{Y}})$ (i.e., no less conservative) with a coefficient of determination, R^2, of 0.997 for $\alpha_{\mathrm{Y}} < 0.50$ and relative approximation errors of less than 5% for $\alpha_{\mathrm{Y}} < 0.10$. The effect of probabalistic violation level on the safety factor for different distributions is shown in Fig. 3.18, illustrating the conservativeness of Chebyshev safety factor in comparison to the Unimodal Chebyshev and Gaussian safety factor. The updated SOCP-NLP optimization problem can then be implemented in receding-horizon fashion together with the updated bound tightening. Numerical results are presented next.

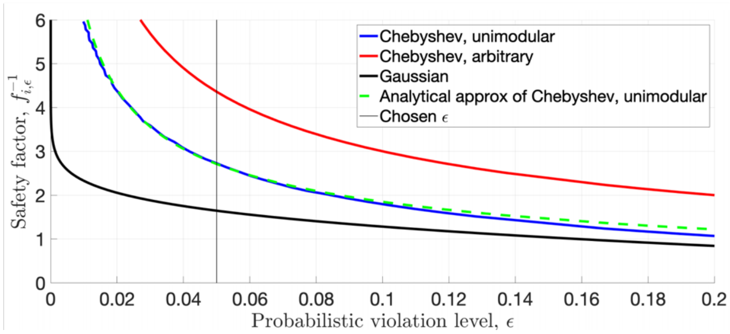

Figure 3.18: Effect of different information on safety factor function [8, 9]

3.3.3 SIMULATION RESULTS

In this section, we illustrate the effectiveness of the approach with simulation-based analysis on a realistic three-phase distribution feeder.

3.3.3.1 Case study description

Simulations are conducted on a reduced 131-node three-phase distribution feeder with a base voltage of 7.6kV and base apparent power rating of 1 MVA. The 131-node radial network is obtained through Kron-based network reduction from the full 1200 node circuit. Frrom the network reduction process, the reduced network consists of 130 representative "super nodes" with each connected to a "super net-load" (with demand minus solar PV injection) and the head-node represents the 0th super node.

The robust SOCP-NLP algorithm is implemented in a receding-horizon fashion with an optimization horizon of 30 time-steps with each time-step being 1 minute (i.e., 30 min prediction horizon). That is, the SOCP results in an open-loop, optimal battery and inverter control trajectory, which is used by the time-decoupled NLP instances to calculate an AC-feasible dispatch trajectory. The resulting operating trajectory is used to calculate the operating points from which a sensitivity-based bound tightening is performed on the network constraints as described in section 3.3.2. Discrete control devices such as switches, capacitor banks, and tap-changing transformers are fixed at their nominal value for this study. Analysis on the control of such discrete devices is provided in [44, 141].

3.3.3.2 Required data management

In the presented framework, the minutely PV production forecast data and demand profile data are available over the 30 minute optimization horizon to the central dispatcher. Such minutely solar PV forecasts are available for purchase by utilities and updated every 30 minutes with a 60-minute forecast [133]. A sample forecast of aggregated solar PV over one hour from 12:00 noon to 1:00 pm is shown in Fig. 3.17b, together with the uncertainty in solar PV generation based on the assumed uniform error distribution. From Fig. 3.17b, it can be seen how the error in forecast grows over the prediction horizon. Furthermore, the uncertainty in demand and solar PV forecast is assumed to be from a uniform distribution, which is unimodal. It is too strong an assumption to claim that forecast errors come from a Gaussian distribution, so instead, we employ the unimodal Chebyshev approximation above to generalize the result. Further details about the relative conservativeness of different distributions can be found in [9]. For the chance constraints, the acceptable voltage violation parameter α_{v} is chosen to be 0.10. The results presented here only consider the voltage constraint, however, the framework readily allows for tightening other constraints, such as current and power flow limits. In addition, it is reasonable to assume that the system operator or utility knows about the power rating and capacity of the available

PV units and the ratings and updated SoC of the DERs. The dispatcher could be a distribution system operator (DSO; e.g., NY REV's DSIP [89]), so it is reasonable to assume that such system information is available. Furthermore, we assume that the DSO is provided updated feeder topology, so they can formulate and solve the optimization problem based on network parameters and dispatch available flexible resources.

As the proposed method employs convex optimization formulations, the solution time is expected to be polynomial in the system size. In section 3.2, it was shown that the SOCP-NLP formulation can be solved in under a minute for a similar sized network. In fact, herein, the average solve time of the minutely implementations is $\approx$ 50 seconds, which allows sufficient time for communication delays. All simulations were conducted on a MacBook Pro with 2.2 GHz processor and 16 GB RAM.

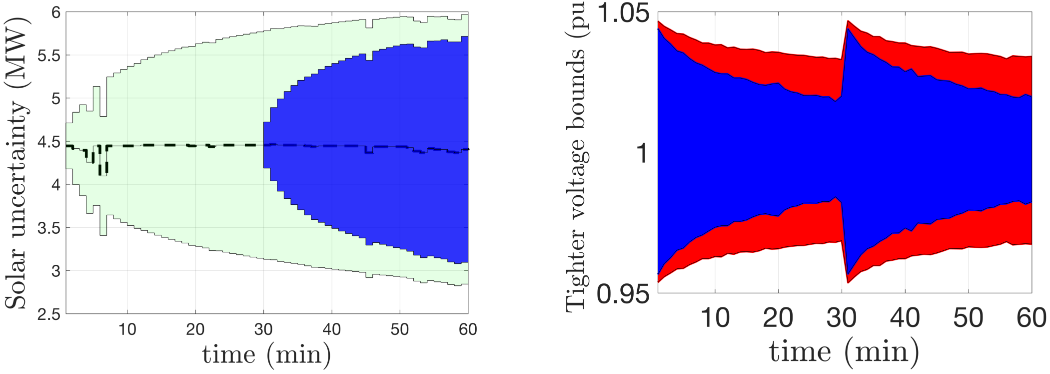

(a) (b)

Figure 3.19: (a) Error in predicted forecast of solar PV over the prediction horizon for the considered test network from noon to 1:00 pm, (b) Tightened voltage bounds obtained from chance constraint over the prediction horizon for Gaussian assumption (red) and Unimodal Chebyshev assumption (blue)

3.3.3.3 Test case results

The high solar penetration results in large variability in the net-demand, which, in a deterministic setting, can lead to violations of network constraints. Validation of the proposed stochastic framework is achieved by comparing the deterministic SOCP+NLP scheme, which does not account for uncertainty, against the one with the robustified constraints. The multi-period SOCP is solved using GUROBI [126], whereas the NLP is solved with IPOPT [135] with the `HSL_MA86` solver [136]. Based on the optimal dispatch (p^*, q^{**}), three-phase, AC load flows are computed in GridLab-D [128] with the realized (actual) demand and solar PV values. We illustrate the effectiveness of the robustified scheme by analyzing the voltage magnitudes from Gridlab-D over the 60-minute receding horizon from 12:00 noon to 1:00pm.

The resulting network voltages over the hour obtained from the deterministic method are depicted in the histogram shown in Fig. 3.20a, illustrating that voltage violations due to the uncertainty are significant and beyond the acceptable limit. The histogram of the voltages obtained through the stochastic formulation are shown in Fig. 3.20b, from where it can be seen that the violations are less than $\alpha_{\mathrm{v}} = 10\%$. This is due to the robust voltage bounds in the stochastic formulation, which account for the uncertainty in solar PV. Figure 3.19b shows how the voltage bounds are tightened over the prediction horizon depending upon the accuracy of forecast. Recall that the forecasts are updated only every 30 minutes, which explains the sudden changes at minute 30 in the simulation.

Further differences between the deterministic and stochastic formulation is shown through the comparison of the control variables. Fig. 3.21a shows the comparison in the aggregate dispatch of batteries, whereas Fig. 3.21b shows the comparison in

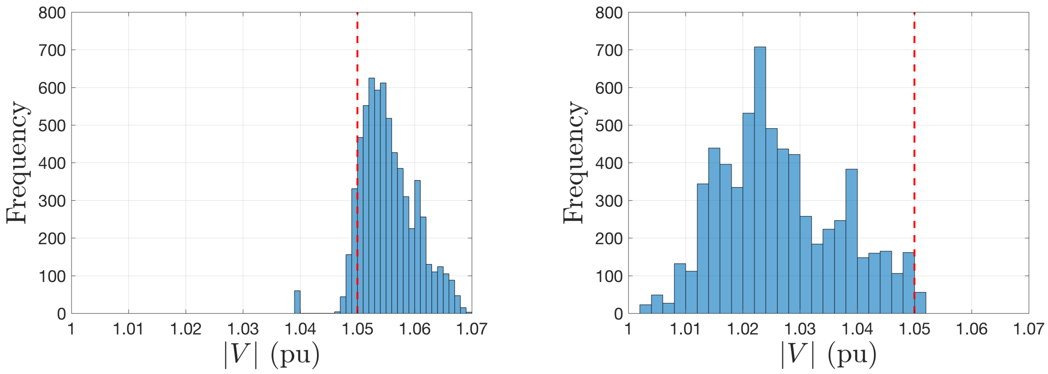

(a) (b)

Figure 3.20: Histogram of the voltages obtained from: (a) the deterministic AC OPF showing violation of voltage limits; (b) from the stochastic AC OPF showing acceptable voltages.

the aggregate state of charge. From these plots it can be seen that the stochastic formulation forces the batteries to dispatch their resources much differently in order to ensure that the voltage constraints are not violated under uncertainty. This is further illustrated in Fig. 3.22a, which shows how the stochastic formulation dispatches more reactive resources in order to counter the effect of the expected variability from the forecasts. However, the robust formulation is clearly more conservative which explains the increased utilization of flexible resources to ensure robust operation. This is illustrated in Fig. 3.22b and Fig. 3.23b, where in Fig. 3.22b a comparison of the objective function (i.e., total network losses) between the deterministic and the stochastic methods is provided, whereas in Fig. 3.23b a comparison of the net demand, i.e., demand plus losses is provided. Clearly, the stochastic approach results in reduced performance (i.e., increased losses). The worst case increase in net demand is found to be less than 3% in this case, with an RMSE of .0538 MW between the deterministic and stochastic method. However, unlike the deterministic approach, the robust implementation satisfies voltage magnitude constraints despite the uncertainty and

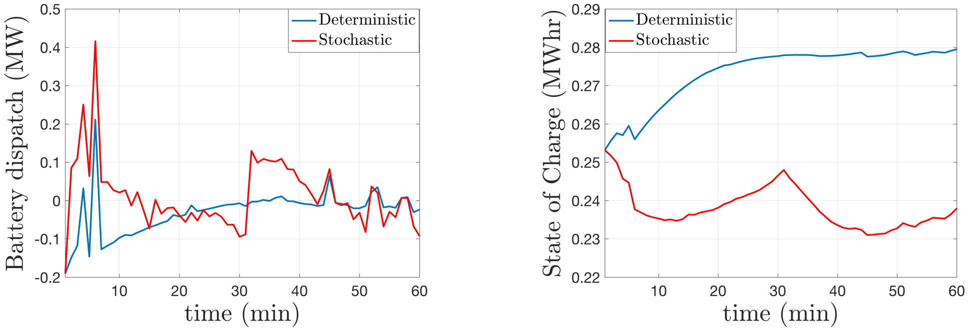

(a) (b)

Figure 3.21: Comparing deterministic and robust optimal solutions: (a) Aggregate battery dispatch; (b) Aggregate battery state of charge

within acceptable violation limit, α_{v}. This trade-off can be designed by choosing α_{v} appropriately. Furthermore, the stochastic method results in reduced network voltage imbalance as shown in Fig. 3.23a. Future work will look into the reasons for this improved performance in network imbalance.

3.3.3.4 Tracking simulation results

Next we utilize the stochastic formulation developed to track a grid reference similar to the tracking results presented in section 3.2. Figure 3.24a shows tracking of the grid signal at the head-node of the feeder under uncertain solar PV and demand, whereas Fig. 3.24b shows the histogram of the voltages over the tracking period. From Fig. 3.24 it can be seen that the stochastic formulation is able to maintain desired tracking while satisfying the network constraints (nodal violations) to be within the specified allowable violation levels. Furthermore, for the tracking formulation, Fig. 3.25a shows that the optimality gap for the SOCP-NLP formulation is no worse than 4%, with the solve time being under 30 seconds. Finally, Fig. 3.26 shows that the

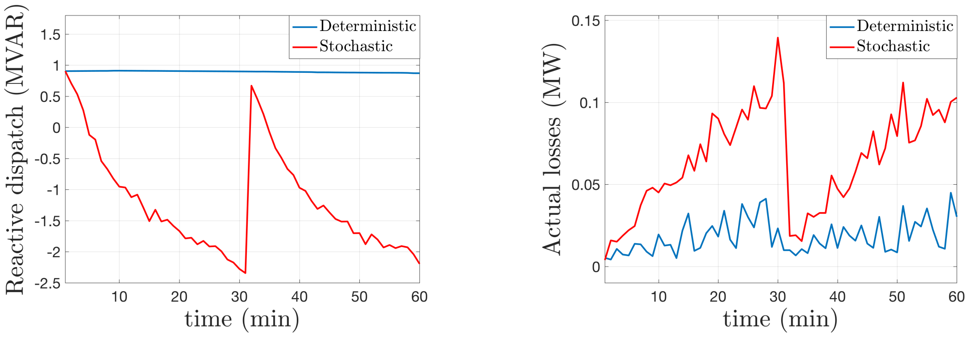

(a) (b)

Figure 3.22: Comparing deterministic and robust optimal solutions: (c) Aggregate reactive power dispatch; (d) Feeder network line losses (objective value)

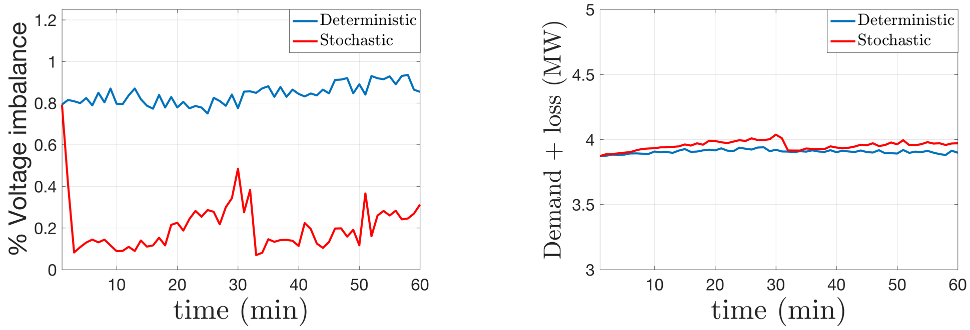

(a) (b)

Figure 3.23: Comparing deterministic and robust optimal solutions: (e) Average nodal voltage imbalance; (f) Total feeder demand with optimized losses. The stochastic implementation is more conservative and leads to a root-mean-square demand-plus-loss increase of just 0.054MW (less than 1.4%).

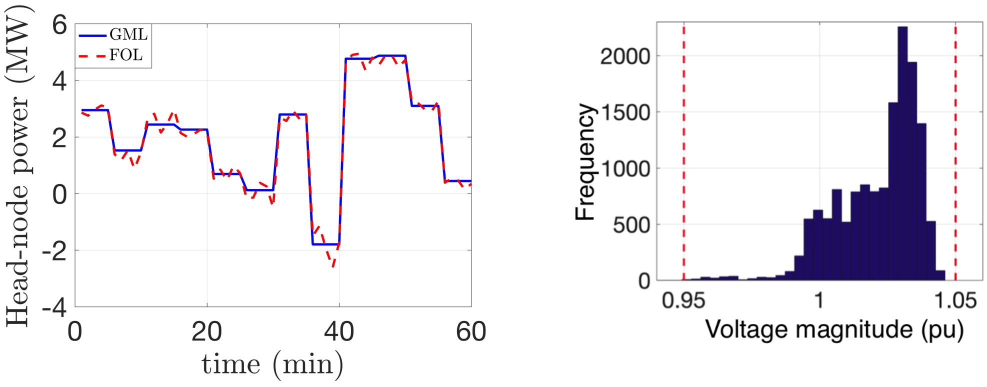

(a)

(b)

Figure 3.24: Left: (a) Tracking of the reference grid head-node power by the feeder through the control of VBs showing acceptable tracking performance for the period 1:00-2:00 pm Right: (b) Histogram of the voltages obtained from the stochastic AC OPF. Clearly, the voltages are within the ANSI limits given by the red dashed vertical lines.

difference in the objective (head-node tracking) in this case between the deterministic and stochastic formulation, which shows that robustness is achieved by sacrificing tracking performance, as expected. However, the overall difference between the two is still reasonable.

3.3.4 SENSITIVITY ANALYSIS

The above formulation and analysis is based on the assumption that the network parameters such as line impedance values are known and are also accurate. However, in practical distribution systems this may not be the case. Often these parameter values are unknown or mis-recorded. Hence, it is important to consider the system behaviour when there is error in the provided line impedance values. To accomplish this task, in this section we perform sensitivity analysis of the distribution system optimal power flow solution to the changes in line impedance. The aim of this sensitivity analysis

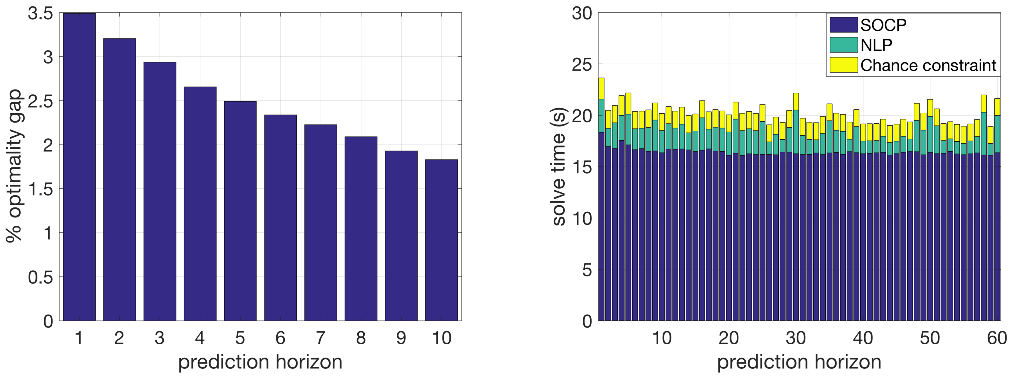

(a) (b)

Figure 3.25: Left: (a) Optimality gap of the SOCP-NLP formulation under stochasticity Right: (b) Solve time for the stochastic formulation over the prediction horizon.

is to determine the relative change in optimal solution as the parameters values are varied over a uniform distribution. Through such an analysis, we aim to determine a range of impedance values that provide satisfactory optimization solutions, i.e., the change in optimal solution is minimal over the distribution set.

To achieve this, we perform simulation based sensitivity analysis on the reduced 131-node three-phase ORU distribution feeder. We conduct four case studies where the impedance values are varied over a uniform distribution of 1%, 5%, 10% and 20%. The histogram of the distribution of the change in resistance and reactance values resulting from this is shown in Fig. 3.27. For each of these uniform distribution cases, we calculate % change in the battery dispatch from the base case (exact impedance values) as:

$$\%\text{battery dispatch change}(i) = 100\frac{(B_{\text{uni},i} - B_{\text{base},i})}{B_{\text{base},i}} \tag{3.20}$$

where $B_{\text{uni},i}$ represents the dispatch of battery i obtained when variation the line

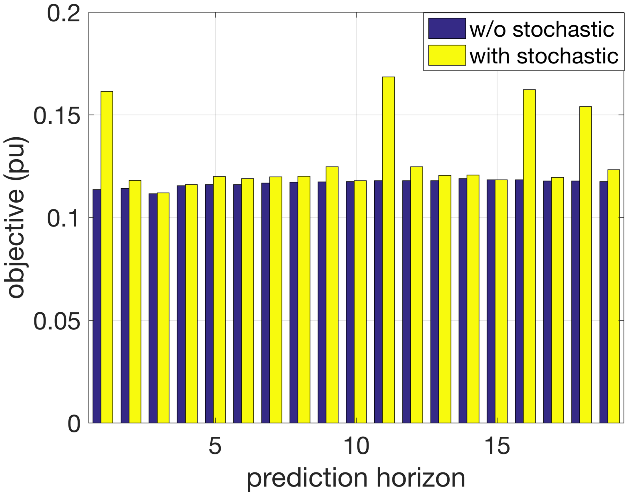

Figure 3.26: Case 4: Comparison of the objective value between the formulation without and with stochastic implementation. The objective function represents tracking objectives, which implies that robustness is achieved by sacrificing tracking performance, as expected. In this example, tracking reference was made very large, which means that small deviations away from the tracking reference signal leads to large changes in the objective function.

impedance over the uniform distribution and B_{base} represents the dispatch of battery i in the base case. The histogram of the distribution of the % change in battery dispatches is shown in Fig. 3.28, with Fig. 3.28a showing the distribution of change in battery dispatches when the impedance values are varied over a uniform distribution error of 1%, Fig. 3.28b for 5% error, Fig. 3.28c for 10% error and finally Fig. 3.28d for 20% error. The mean and standard deviation of the battery dispatch change in all the four cases is shown in Table 3.5. These results suggest that the sensitivity of the optimal solution to the impedance values is within manageable range and as a rule of thumb if $x\%$ is the change in impedance values, then that results in a standard deviation in battery dispatch of roughly $\frac{x}{4}\%$.

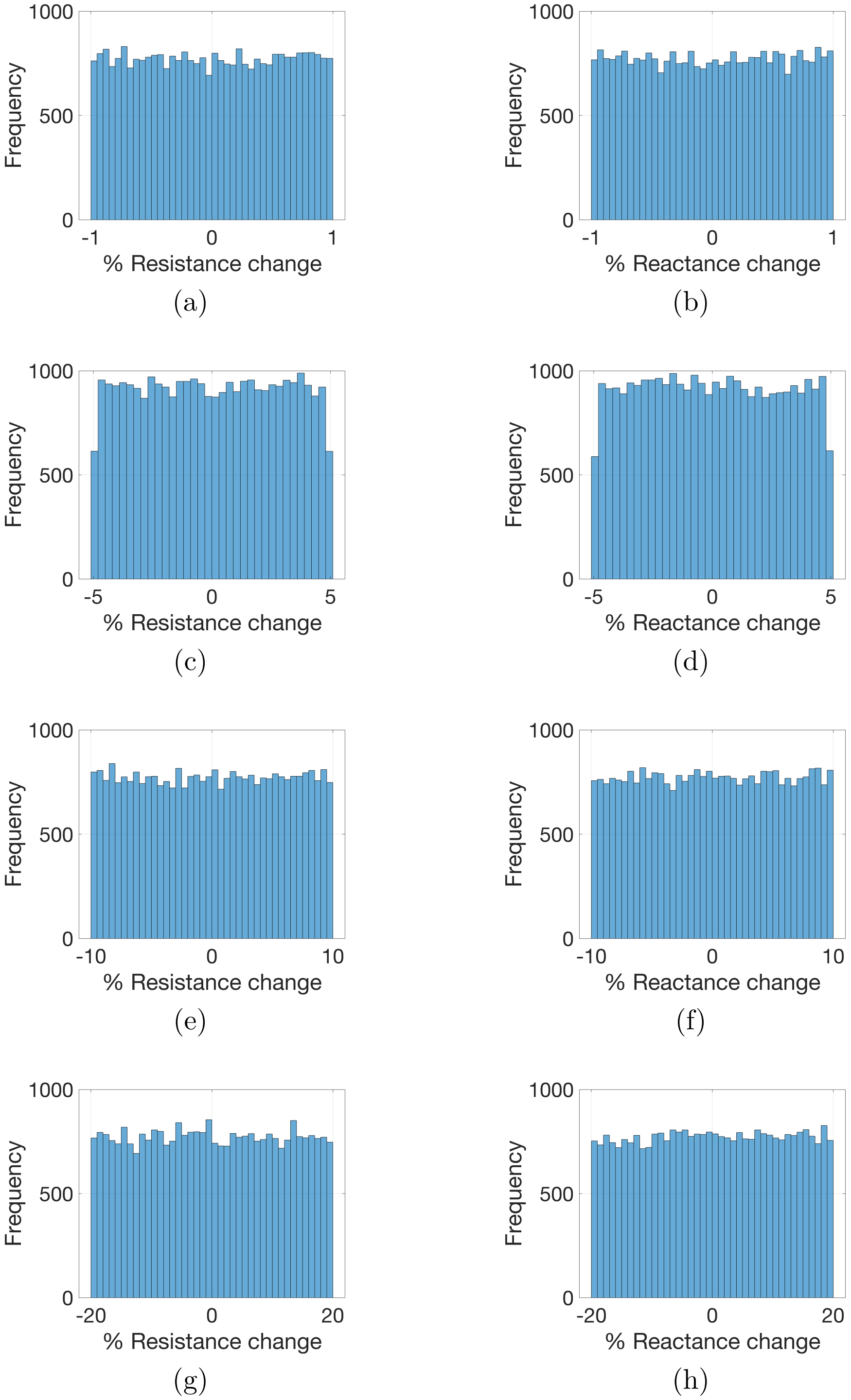

Figure 3.27: Histograms of the change in resistance and reactance from the base value from variation in line impedance in a uniform distribution of : (a), (b) 1%; (c), (d) 5%; (e), (f) 10%; (g), (h) 20%.

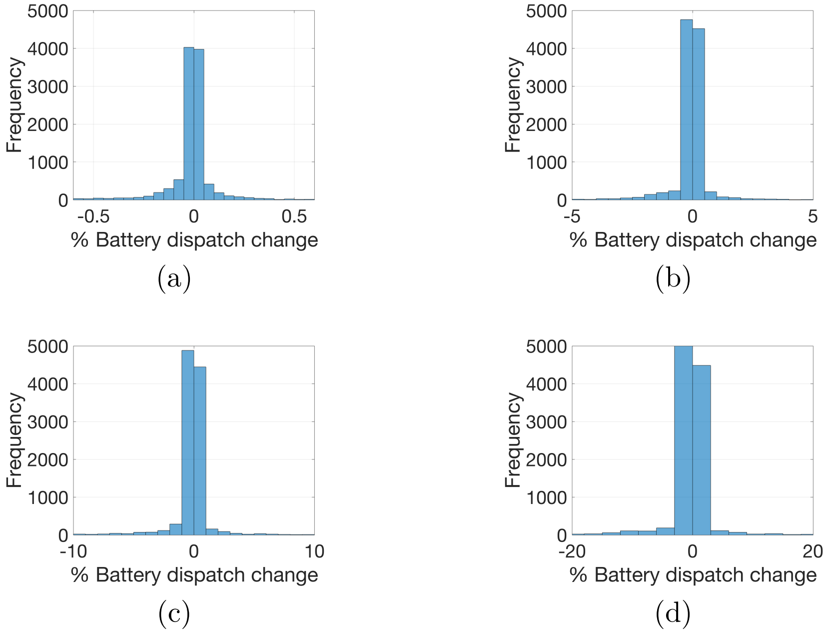

(a) (b) (c) (d)

Figure 3.28: Histograms of the change in battery dispatch from the base value from variation in line impedance in a uniform distribution of : (a) 1%; (b) 5%; (c) 10%; (d) 20%.

Table 3.5: Mean and standard deviation of battery dispatch change under variation in impedance values.

Change in impedance	Mean (%)	Standard deviation (%)
1%	-0.04	0.29
5%	-0.04	0.88
10%	-0.09	1.87
20%	-0.31	4.26

3.3.5 CONCLUSIONS

This work presented an efficient method for the optimal dispatch of DERs in an unbalanced distribution network while considering the uncertainty in demand and solar PV forecast. A two-stage technique is developed that accounts for both the non-linearity of power flow equations and the uncertainty in forecast. A deterministic multi-period

AC OPF is solved based on the forecast of demand and solar PV, whereas the linearized model obtained at the operating point of the NLP is used to calculate the tighter bounds on network constraints for the deterministic AC OPF. The simulation results and comparison with deterministic approach show the effectiveness of the proposed method in dealing with uncertainty.

3.4 Coordination of DERs for grid reference tracking

This section presents a novel method for network-admissible coordination of responsive grid resources aggregated to provide market services. Such responsive grid resources can be either physical batteries or virtual batteries (VBs). In this context, a VB represents a local aggregation of directly controlled loads, such as smart inverters, electric water heaters, and air-conditioners. The coordination is achieved by solving an optimization problem to disaggregate a feeder's desired reference trajectory into constraint-aware set-points for the energy resources. Specifically, a novel, provably-tight, convex relaxation of the AC optimal power flow (OPF) problem is presented to optimally dispatch the energy resources to track the feeder's desired power trajectory. Simulation results conducted on a modified IEEE test system demonstrate the effectiveness of the proposed energy resource coordination method.

3.4.1 Introduction

3.4.1.1 Background and Motivation

Coordinated control of demand-side, distributed energy resources (DERs), such as grid-tied PV inverters, distributed battery storage, and thermostatically controlled loads (TCLs; e.g., water heaters and air conditioners) is part of the solution that supports a renewable energy future [14, 79–81]. Much of the recent literature on the coordination of DERs has focused on distributed control methodologies to turn large-scale aggregations of DERs into dispatchable grid assets (similar to [82–84]). Since the aggregation of DERs is dispatched as a single entity by a centralized coordinator and is subject to power and energy limits, the DER fleet is often referred to as a "virtual battery" (VB) [20, 21, 142].

To avoid violating operational limits of the grid and to ensure system reliability with DERs at scale, coordination between a DSO and DER owners and aggregators will become critical. This has spurred a multitude of concepts and models for how DSOs can interact with DERs, aggregators, and whole-sale (transmission) markets [87–89].In this section, we focus on the so-called "Market DSO" model, e.g., see [87], where the DSO performs coordination and aggregation of DERs to deliver grid services. While such a setup could preclude independent DER aggregators (i.e., increases regulatory complexity), the model simplifies the interaction between wholesale market signals and the DSO and the ideas herein can be adapted further to enable independent "grid-aware" DER aggregators [90].

To address challenges concerning optimal, and network-admissible coordination of VBs and physical batteries, this section presents a method for coordinating demand-side flexibility in the form of VBs or physical batteries, which can be a part of a hierarchical multi-layer DSO framework (please see Fig. 3.29). The coordination method consists of a novel, convex OPF relaxation, which is provably tight at optimality under realistic conditions and generates grid-aware, feasible set-points for the VBs plus physical batteries. The optimization method is represented by the box "Optimal VB set-point dispatcher" in Fig. 3.29.

Unlike most of the existing literature, the presented method explicitly and effectively accounts for AC (radial) networks and energy-constrained VB resources.

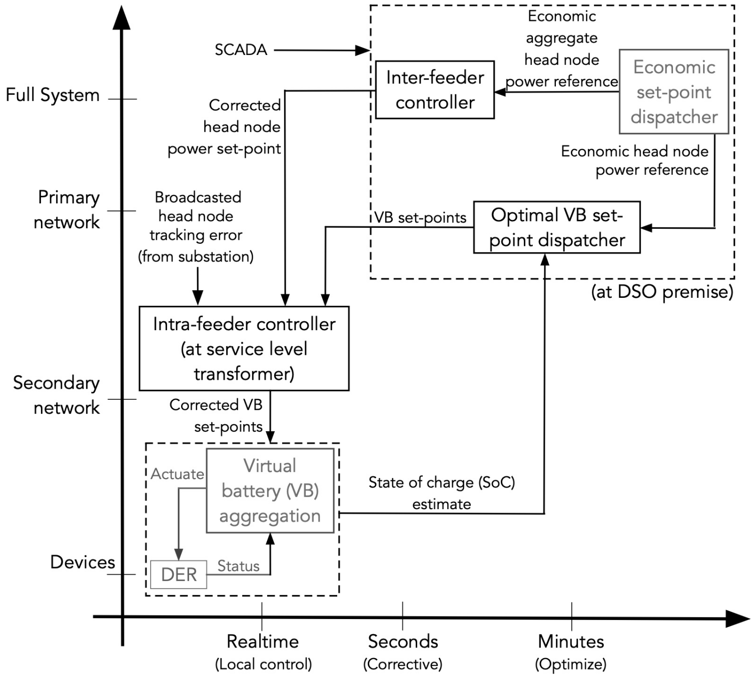

Figure 3.29: The multi-layer VB coordination framework. The optimal VB dispatcher forms the focus of this section, whereas the blocks with the inter- and intra-feeder controllers deal with grid disturbance and are discussed in detail in [10]. The DSO runs an AC OPF about every minute to dispatch VBs with optimal set-points.

Similar to [21, 143], we consider VBs at the scale of 100-200 DERs per VB that are managed locally (e.g., from the same neighborhood) via load control (with full state information) and subject to lags from device dispatch and communications.

Prior work on hierarchical control of DERs in microgrids (e.g. [96]) has mainly considered using frequency and voltage droop characteristics to generate active and reactive power set-points for DERs using local measurements of frequency and voltage and compensating for the deviations, but in this work, we compensate for the deviation in the head node power of the feeder from the economic set-point, thus taking into account the economic trajectory.

To be more specific, the “optimal VB set-point dispatcher" in Fig. 3.29 considers a convex relaxation of the (balanced) AC network model. Furthermore, the convex

OPF formulation is proven tight at optimality, which guarantees that the prediction of future physical operating states of the grid and the VBs are accurate. This is achieved by decomposing the feeder head-node (i.e., substation) economic reference into the aggregate VB dispatch, net-demand, and approximated total feeder line losses. The key feature here is the use of a first-order prediction model for the line losses to simplify the problem. It is shown through analysis and with simulations that this VB-plus-losses reference can achieve a tight optimal solution under practical conditions. To provide the formulation with updated estimates of feeder losses and network topology, it is assumed that a distribution system state estimator (DSSE) is available [144] (not considered in this work).

3.4.1.2 Original Contributions

In summary, the main contributions of this work are as follows:

- A novel second-order conic AC OPF formulation of a multi-period optimization of VBs designed for tracking the desired power reference at the head-node of the feeder. In this formulation, the feeder structure is taken into account and the second-order cone relaxation is proven to be exact even under significant reverse power flow and with a non-monotonic cost function, which is an improvement over the present state-of-science in radial network OPF presented in [102].
- Systematic, simulation-based analysis on IEEE distribution feeders is performed, illustrating the validity of the approach.

3.4.1.3 Practical implementation and Data management

In this subsection, we explain how the presented OPF formulation (shown as a block in Fig. 3.29) can be feasibly implemented in a practical scheme. In the proposed

DSO-centric methodology, we assume that the Market DSO acts as the coordinator and aggregator of DERs and manages the entire scheme. The DSO may also use technology services to manage the DERs via a software interface (e.g., the VB-DER interface in Fig. 3.29), but this is to help the DSO reduce costs and manage constraints. The DSO runs an OPF every minute or so for each feeder based on the economic head node power reference. In this regard, it is reasonable to assume that the DSO has access to SCADA data and is aware of the grid topology and receives VB state of charge (SoC) estimates from the VB-DER interface to run the AC OPF. For the VB interface, the only information required is the corrected VB power set-point. Apart from this, the VB interface does not require any other information and it is not involved in solving an OPF.

3.4.2 Convex OPF formulation for reference tracking

3.4.2.1 Mathematical Notation

In this section, we consider a radial, balanced distribution network as modeled by the *DistFlow* equations for radial networks and shown in section 2.2.

3.4.2.2 Virtual battery model

In this work, a VB is considered an energy-based model of a dispatchable aggregation of a relatively small number of controllable DERs (e.g., 100-200 distributed loads like ACs). This representation of DERs as an aggregate VB is adequate, based on several works in the literature (e.g., [20, 21, 145]). Moreover, while doing this aggregation, it is important to consider the human-in-the-loop in these flexible demand resources, which manifests itself in the form of State-of-Charge (SoC) of VBs [22], based on Quality of Service (QoS) constraints (e.g., temperature/comfort limits). It is assumed that the DERs reside in the low-voltage secondary network, while the local VB coordination (computation and control) takes place at a nearby primary service transformer node. Owing to the small scale of aggregation, the DERs that make up a VB are controlled directly via utility Gigabit ethernet (e.g., IEC 61850) or wireless cellular/Wi-Fi connection. From literature, it has been shown that a VB endowed with a DER control policy, such as a priority-based switching of DERs [146], can be well-described by a first-order dynamic model of the VB's energy state, (e.g., see [20, 21, 23]):

$$\dot{B}_i(t) = -\alpha_{\mathrm{b},i} B_i(t) - p_{\mathrm{b},i}(t) \tag{3.21}$$

$$\tau_i \dot{p}_{\mathrm{b},i}(t) = -p_{\mathrm{b},i}(t) + p_{\mathrm{in},i}(t - T_{d,i}) \tag{3.22}$$

$$\underline{B_i} \leq B_i(t) \leq \overline{B_i} \tag{3.23}$$

$$\underline{p_{\mathrm{b},i}} \leq p_{\mathrm{in},i}(t) \leq \overline{p_{\mathrm{b},i}}, \tag{3.24}$$

where at node $i \in \mathcal{N}^+$, $B_i(t)$ is the VB's state of charge (SoC), $p_{\mathrm{b},i}(t)$ its active power output, and $p_{\mathrm{in},i}(t)$ its desired total active power. The upper (lower) bound of the SoC is given by $\overline{B_i}$ ($\underline{B_i}$) while the VB's upper (lower) power limits are denoted $\overline{p_{\mathrm{b},i}}$ ($\underline{p_{\mathrm{b},i}}$). Note that (3.21) captures the SoC dynamics with $\alpha_{\mathrm{b},i}$ as the energy dissipation rate. The coupling between the VB's ability to change output power and the VB's control and communication of DERs and their response is generalized with (3.22) as a lag-and-delay model. In that model, $T_{\mathrm{d},i}$ is the time delay associated with communicating with the ith VB and τ_i is the time constant of the first-order model (similar to [147] for example). Specifically, (3.22) was formed by taking note of the following facts: *i*) The DERs that compose a VB turn on/off (possibly) sequentially, and there are power electronic components present inside each VB, both of which contribute to a net lag τ_i; *ii*) There are communication delays (generally of the order of 200 ms) between the head node of the feeder and each VB [148, 149], and delays associated with disaggregating the control signal into device-level signals [146]. The delays we consider in the VB model are in fact both these types of delays lumped together. For this work, the battery charge and discharge efficiencies are assumed to be unity. Inclusion of non-unity battery efficiency requires binary variables to avoid simultaneous charging and discharging. A detailed description of the battery model with non-unity efficiency and analysis on avoiding simultaneous charging and discharging is provided in [7, 150]. For the optimal dispatch, we optimize the VB set-points on a minutely timescale and $\alpha_{\mathrm{b},i} \approx 0$ in realistic settings, it is reasonable to consider a simplified, discretized VB model for set-point optimization. This reduced, predictive model is below:

$$B_i[k+1] = B_i[k] - \Delta t p_{\mathrm{b},i}[k] \tag{3.25}$$

$$\underline{B_i} \leq B_i[k] \leq \overline{B_i}, \quad \underline{p_{\mathrm{b},i}} \leq p_{\mathrm{b},i}[k] \leq \overline{p_{\mathrm{b},i}} \tag{3.26}$$

valid for any k and where Δt is the discretization timestep. Next, we augment the discrete-time VB model with the AC network model to formulate the feeder head-node reference power tracking OPF problem.

3.4.2.3 Conventional convex formulation

Convex relaxation techniques have gained popularity recently due to the existence of global optimality guarantees for AC OPF problems [53, 102]. In this subsection, we present a traditional second-order cone programming (SOCP) relaxation of the AC power flow equations to formulate a convex, multi-period reference tracking OPF problem, (P1). Decoupling the cost function in the form: $\sum_{i\in\mathcal{N}} f_i(p_i[k]) = (p_0[k] - p_0^{\text{econ}}[k])^2 + (p_{\text{VB}}^{\text{econ}}[k] - \sum_{i\in\mathcal{N}^+} p_{\text{b},i}[k])^2$, the optimization problem can be expressed as:

$$
\begin{aligned}
\text{(P1)} \qquad & \min_{p_{\text{b},i}[k]} \sum_{i\in\mathcal{N}} f_i(p_i[k]) && \text{(3.27a)}\\
& \text{s.t.}: \quad (3.25) - (3.26) && \text{(3.27b)}\\
S_{ij}[k] =& s_i[k] + \sum_{h:h\to i} (S_{hi}[k] - z_{hi} l_{hi}[k]), \quad \forall (i,j)\in\mathcal{E} && \text{(3.27c)}\\
0 =& s_0[k] + \sum_{h:h\to 0} (S_{h0}[k] - z_{h0} l_{h0}[k]) && \text{(3.27d)}\\
v_i[k] - v_j[k] =& 2\text{Re}(\overline{z}_{ij} S_{ij}[k]) - |z_{ij}|^2 l_{ij}[k], \quad \forall (i,j)\in\mathcal{E} && \text{(3.27e)}\\
& p_i[k] = p_{\text{b},i}[k] - P_{\text{L},i}[k] + P_{\text{S},i}[k], \quad \forall i\in\mathcal{N}^+ && \text{(3.27f)}\\
& q_i[k] = -Q_{\text{L},i}[k], \quad \forall i\in\mathcal{N}^+ && \text{(3.27g)}\\
& l_{ij}[k] \geq \frac{|S_{ij}[k]|^2}{v_i[k]}, \quad \forall (i,j)\in\mathcal{E} && \text{(3.27h)}\\
& s_i[k] \in \mathcal{S}_i, \quad i\in\mathcal{N}^+ && \text{(3.27i)}\\
& \underline{v_i} \leq v_i[k] \leq \overline{v_i}, \quad i\in\mathcal{N}^+ && \text{(3.27j)}
\end{aligned}
$$

for discrete time-step $k \in \mathcal{T}$ over a prediction horizon $\mathcal{T} := \{0, \ldots, T-1\}$ and where the power injection s_i at a node $i \in \mathcal{N}^+$ is constrained to be in a pre-specified, compact, convex set $\mathcal{S}_i \in \mathbb{C}$. The prediction horizon length T is chosen subject to availability of forecasts and depending upon the dynamics of VBs [20]. In our formulation, we choose $T = 10$. The set $\mathcal{S}_i \in \mathbb{C}$ depends upon the VB constraints, e.g., in case of inverters this set is given by: $\{(p_i, q_i) | p_i^2 + q_i^2 \leq \overline{S_i^2}\}$, where $\overline{S_i}$ is the apparent power limit of the inverter. In (3.27), the cost function (3.27a) minimizes the deviation of the head-node power $p_0[k] \in \mathbb{R}$ from the economic head-node reference trajectory $p_0^{\text{econ}}[k] \in \mathbb{R}$, which is composed of: *i*) desired economic aggregate VB dispatch, $p_{\text{VB}}^{\text{econ}}[k] \in \mathbb{R}$; *ii*) total predicted losses, $L[k] := \sum_{(i,j)\in\mathcal{E}} r_{ij} l_{ij}[k]$; and *iii*) total forecasted net-demand, $\sum_{i\in\mathcal{N}^+}(P_{\text{L},i}[k] - P_{\text{S},i}[k])$, where $P_{\text{L},i}[k] \in \mathbb{R}$ is the active power demand at node $i \in \mathcal{N}^+$, and $P_{\text{S},i}[k] \in \mathbb{R}_+$ is the solar PV generation at node $i \in \mathcal{N}^+$. We are optimizing over the VB dispatch, $p_{\text{b},i}[k] \in \mathbb{R} \quad \forall i \in \mathcal{N}^+$, which appears in power balance constraint (3.27f) while reactive power demand, $Q_{\text{L},i}[k] \in \mathbb{R}$, is used in (3.27g). The second-order cone relaxation of the nonlinear equation (2.5) is given in (3.27h); (3.27i) and (3.27j) provide constraints on power injection and voltage magnitudes.

Several works in literature such as [102] provide conditions under which the second-order cone relaxation is exact for distribution networks. If an optimal solution of (P1) $w^* = (s^*, S^*, v^*, l^*, s_0^*)$ is feasible for OPF, i.e., w^* satisfies (2.5), then w^* is global optimum of OPF and (P1) is said to be exact. Theorem 1 in [102] provides conditions for the SOCP problem in (P1) to be exact, however, it requires the part of cost function $f_0(p_0) = (p_0 - p_0^{\text{econ}})^2$ to be strictly increasing, which is not the case when tracking a reference power signal. Thus, even under the conditions provided in [102], (P1) may not be exact. To overcome these shortcomings of (P1), we propose a novel method for convexifying the AC OPF while ensuring an exact solution at optimality.

Specifically, we utilize a linearized approximation of line losses and through this obtain a cost function that is strictly increasing in p_0 in order to satisfy the conditions in [102].

3.4.2.4 Reformulated convex formulation

To reformulate (P1), we consider each piece of the two-part composition of feeder's predicted head-node power, $p_0[k] \approx -\sum_{i\in\mathcal{N}^+} p_i[k] + L_1[k]$. Specifically, we employ a first-order approximation of total predicted line losses, $L_1[k]$, in the cost function (via p_i-to-loss sensitivity factors, which we denote by ζ_i), and prove that with approximated losses, the solution is tight at optimality. Thus, the predicted grid response to an optimized VB dispatch is AC feasible. To achieve the above, we use $p_{\mathrm{VB}}^{\mathrm{econ}}$ and p_0^{econ} mentioned earlier. This leads to a multi-objective reference tracking problem, similar to the form of a linear quadratic regulator (LQR) from optimal control [151]:

$$\text{(P2)} \quad \min_{p_{\mathrm{b},i}[k]} \sum_{k=1}^{T} f_{\mathrm{HN}}[k]^2 + \alpha f_{\mathrm{VB}}[k]^2 + \epsilon p_0[k] \tag{3.28a}$$

subject to:

$$f_{\mathrm{HN}}[k] = \sum_{i\in\mathcal{N}^+} \left(p_{\mathrm{b},i}[k] + P_{\mathrm{S},i}[k] - P_{\mathrm{L},i}[k]\right) - L_1[k] - p_0^{\mathrm{econ}}[k] \tag{3.28b}$$

$$f_{\mathrm{VB}}[k] = p_{\mathrm{VB}}^{\mathrm{econ}}[k] - \sum_{i\in\mathcal{N}^+} p_{\mathrm{b},i}[k] \tag{3.28c}$$

$$L_1[k] = L_{0,k} + \sum_{i\in\mathcal{N}^+} \zeta_i \Delta p_i[k] \tag{3.28d}$$

$$\text{(3.27c)-(3.27e), (3.25), (3.26), and (3.27f)-(3.27j),} \tag{3.28e}$$

for discrete time-step $k \in \mathcal{T}$ over a prediction horizon $\mathcal{T} := \{0, \ldots, T-1\}$. The parameters α, $\epsilon \in \mathbb{R}_+$ are chosen appropriately with $\epsilon \ll 1$; $L_1[k] \in \mathbb{R}$ is the first-order estimate of the total feeder line losses at time-step k and $L_{0,k} \in \mathbb{R}_+$ is the loss estimated for the operating point at time k. The term ϵp_0 results in a tight relaxation as will be shown next in Theorem 2, whereas the term $\zeta_i \Delta p_i[k] = \zeta_i(p_i[k] - p_i[0])$ represents the change in network loss due to change in active power injection at node $i \in \mathcal{N}^+$, with $p_i[0]$ being the nominal injection. The factors $\zeta_i \in \mathbb{R}$ provide the first-order change in feeder losses due to changes in VB power injections. Similar *power transfer distribution factors* are often used in transmission system analysis but have recently been adapted for distribution networks [152].

Remark 5. *The formulation in (P2) can easily be extended to account for solar curtailment as a control variable resulting in a more general formulation. If* $P_C^{econ} \in \mathbb{R}_+$ *represents the curtailment reference trajectory and* $P_{C,i} \in \mathbb{R}_+$ *represents the solar curtailment at node* $i \in \mathcal{N}^+$, *then* $\sum_{i \in \mathcal{N}^+}(P_{S,i} - P_{C,i})$ *is the net solar output and* $\sum_{i \in \mathcal{N}^+} P_{C,i} - P_C^{econ}$ *is the error in tracking the curtailment trajectory.*

In the next section, Theorem 2 proves that under practical conditions, the (P2) has a zero duality gap.

3.4.2.5 Exactness of reformulation

In order to explain the notation in Theorem 2, consider $\mathcal{L} := \{l \in \mathcal{N} | \not\exists k \in \mathcal{N} \text{ such that } k \to l\}$, which denotes the collection of leaf nodes in the network. For a leaf node $l \in \mathcal{L}$, let $n_l + 1$ denote the number of nodes on path $\mathcal{P}_l$, and suppose

$$\mathcal{P}_l = \{l_{n_l} \to l_{n_{l-1}} \to \dots l_1 \to l_0\}$$

with $l_{n_l} = l$ and $l_0 = 0$.

Also, define $a^+ := \max\{a, 0\}$ for $a \in \mathbb{R}$ and let I_2 denote the 2×2 identity matrix, and define vectors $u_i := \mathrm{col}\{r_{ij}, x_{ij}\}$ and matrices

$$\underline{A}_i := I_2 - \frac{2}{\underline{v_i}} \begin{bmatrix} r_{ij} \\ x_{ij} \end{bmatrix} \begin{bmatrix} \hat{P}^+_{ij}(\overline{p}) & \hat{Q}^+_{ij}(\overline{q}) \end{bmatrix}$$

for $(i, j) \in \mathcal{E}$ where $\hat{P}^+_{ij}(\overline{p})$ and $\hat{Q}^+_{ij}(\overline{q})$ are upper bounds on P_{ij} and Q_{ij} and are chosen so that $\underline{A}_i$ only depends on the SOCP parameters $(r, x, \overline{p}, \overline{q}, \underline{v})$.

Furthermore, let $(\hat{S}, \hat{v})$ denote the solution of the Linear DistFlow model, then

$$\hat{S}_{ij}(s) = \sum_{h: i \in \mathcal{P}_h} s_h, \quad \forall (i, j) \in \mathcal{E} \tag{3.29}$$

$$\hat{v}_i(s) := v_0 + 2 \sum_{(j,k) \in \mathcal{P}_i} \mathrm{Re}(\overline{z}_{jk} \hat{S}_{jk}(s)), \quad \forall i \in \mathcal{N}^+ \tag{3.30}$$

where $\mathcal{P}_i$ denotes the unique path from node i to node 0. Since the network is radial, the path $\mathcal{P}_i$ exists and is unique. Physically, $\hat{S}_{ij}(s)$ denotes the sum of power injections s_h towards node 0 that go through line (i, j). Note that $(\hat{S}(s), \hat{v}(s))$ is affine in s, and equals (S, v) if and only if line loss $z_{ij} l_{ij}$ is 0 for $(i, j) \in \mathcal{E}$. Then based on the DistFlow model define:

$$\mathcal{S}_{\text{volt}} := \{s \in \mathbb{C}^n | \hat{v}_i(s) \leq \overline{v_i} \quad \forall i \in \mathcal{N}^+\} \tag{3.31}$$

which denotes the power injection region where $\hat{v}(s)$ is upper bounded by $\overline{v}$. Since $v(s) \leq \hat{v}(s)$ (Lemma 1 in [102]), the set $\mathcal{S}_{\text{volt}}$ is a power injection region where voltage upper bounds do not bind. Then based on this notation, Theorem 2 below proves the exactness of (P2).

Theorem 2. *The SOCP problem (P2) is exact if the C1 and C2 conditions given in Theorem 1 of [102] are satisfied:*

***C1**: $\underline{A}_{l_s}\underline{A}_{l_{s+1}}\dots\underline{A}_{l_{t-1}}u_{l_t} > 0$ for any $l \in \mathcal{L}$ and any s, t such that $1 \leq s \leq t \leq n_l$;*

***C2**: Every optimal solution $w^* = (s^*, S^*, v^*, l^*, s_0^*)$ satisfies $s^* \in \mathcal{S}_{volt}$*

Proof. The cost function of the optimization problem (P2) can be expressed as:

$$f_0(p_0) = \epsilon p_0 \tag{3.32}$$

$$f_i(p_i) = f_{\text{HN}}^2 + \alpha f_{\text{VB}}^2 \qquad \forall i \in \mathcal{N}^+ \tag{3.33}$$

As f_0 in the cost function in (3.28a) is strictly increasing, the SOCP formulation satisfies all the conditions provided in Theorem 1 of [102] and hence the proof is a direct application of Theorem 1 in [102] under conditions C1 and C2. This concludes the proof. □□□

The term ϵp_0 is added to satisfy the additional condition in Theorem 1 of [102], where the cost function must be increasing with respect to p_0. Note that the inclusion of this term in the cost function affects the optimal solution. However, $\epsilon > 0$ can now be made arbitrarily small (per the proof of Theorem 2), which ensures that the impact on the optimal solution is negligible.

C1 can be checked apriori and efficiently since $\underline{A}$ and u are simple function of $(r, x, \overline{p}, \overline{q}, \underline{v})$ that can be computed in $\mathcal{O}(n)$ time and there are no more than $n(n+1)/2$ inequalities in C1. For practical parameters ranges of $(r, x, \overline{p}, \overline{q}, \underline{v})$, line resistance and reactance $r_{ij}, x_{ij} << 1$ per unit for $(i, j) \in \mathcal{E}$, line flow $\hat{P}_{ij}(\overline{p}), \hat{Q}_{ij}(\overline{q})$ are on the order of 1 per unit for $(i, j) \in \mathcal{E}$ and voltage lower bound $\underline{v}_i \approx 1$ per unit for $i \in \mathcal{N}^+$. Hence,

$\underline{A}_i$ is close to I for $i \in \mathcal{N}^+$, and therefore C1 is likely to hold. As has been shown in [102], C1 holds for several test networks, including those with high penetration of renewables. This is further illustrated by results in Fig. 3.30a that shows the condition C1 holds even for extremely large VB injections (nearly 40 times the demand).

To show the practical restriction of condition C2, Fig. 3.30b shows the increase in $\hat{v}$ with increase in reverse power flow due to increased VB injections. From the figure, it can be seen that the condition is valid for VB injections up to more than 400% of demand, compared to the base case of 20%. It can also be seen from Fig. 3.30b that $\hat{v}$ matches the actual voltage v very closely due to the low impedance of the IEEE-37 node system resulting in small loss term $z_{ij}l_{ij}$. However, with solar PV penetration and an increase in impedance values, the maximum VB injection limit will reduce. To check the sensitivity of these conditions to network parameters, we have provide checks on conditions C1 and C2 under different (r, x) values. Figure 3.31a shows the VB injections for which C1 holds for different (r, x) values, whereas Fig. 3.31b shows the VB injections for which C2 holds for different (r, x) values. These results show that conditions C1 and C2 (especially C1) are expected to hold for a practical distribution system over a wide range of VB injections. Furthermore, condition C2 seems to be a more relevant condition to consider as it will be the first to be violated under large reverse power flows.

The next section presents simulation results that illustrate the effectiveness of (P2).

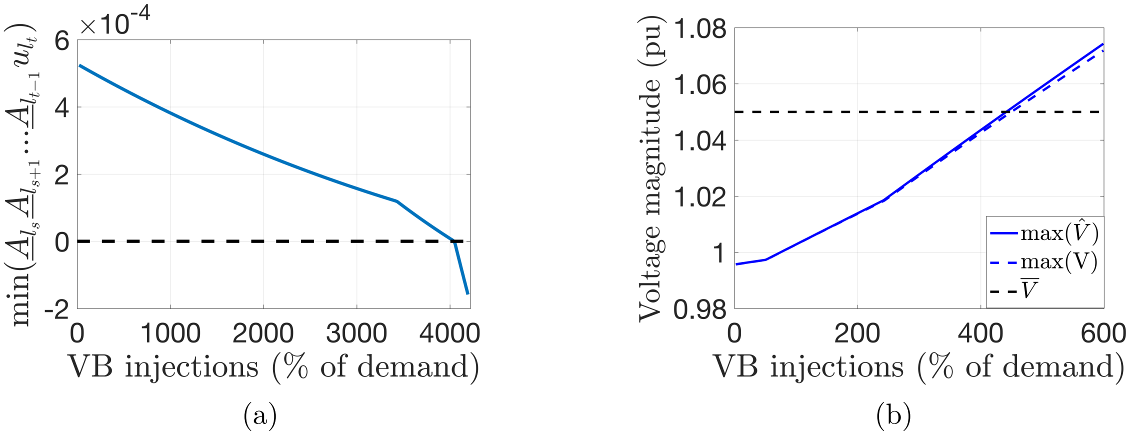

Figure 3.30: Conditions C1 and C2 for exactness of (P2): (a) Conditions C1 holds under large reverse power flow from VB injections, (b) Condition C2 holds under large reverse power flow from VB injections up to around 400% of demand.

3.4.2.6 Optimal VB dispatch and head node tracking simulation

Simulation tests for the optimal reference tracking with VBs were conducted on the balanced version of the IEEE-37 node test feeder [132] to compare the conventional (P1) and the proposed (P2) formulations against the actual AC load flow from Matpower [153]. Simulation results in Fig. 3.32a show the reference tracking results in Matpower achieved through the flexibility of VBs using (P1) and (P2). The figure shows that (P2) can track the reference trajectory whereas (P1) cannot. For (P2), the error in tracking at each step change in the reference trajectory is due to the first-order loss approximation used in (P2). Since the loss approximation is updated every time-step, the effect on tracking error is small and corrected quickly as shown in Fig. 3.32a, which means that (P2) represents a reference-tracking OPF formulation that can effectively dispatch VBs while guaranteeing network admissibility. On the other hand, for the convex (P1), the non-zero duality gap creates a mismatch between the predicted power flow values and the actual AC power flow, which results in the

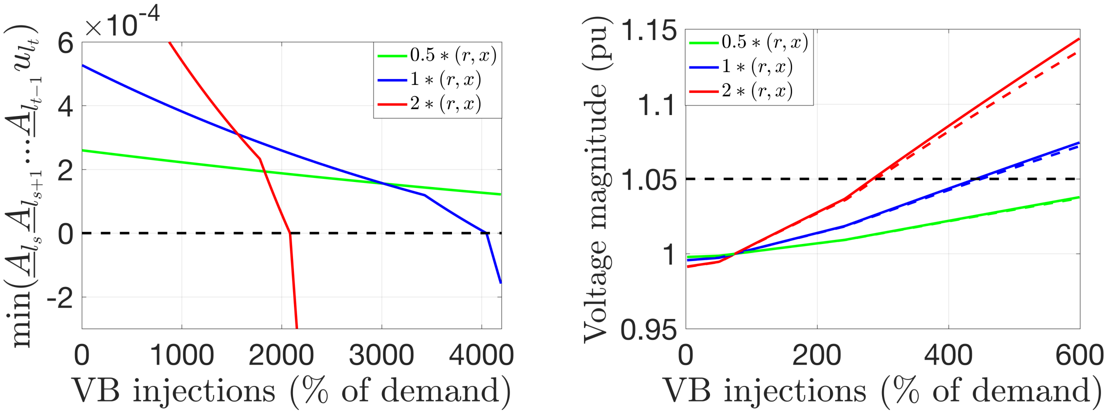

(a) (b)

Figure 3.31: (a) Condition C1 holds under large reverse power flow for different (r, x) *values, (b) Condition C2 holds under large reverse power flow for different* (r, x) *values.*

sub-par tracking illustrated in Fig. 3.32a. Specifically, (P1) predicts perfect tracking, but the realized AC head node power does not match the grid reference, which results in suboptimal use of VB resources. The comparison of the aggregate State of Charge (SoC) obtained through (P1) and (P2) is shown in Fig. 3.32b. Clearly, (P1) predicts a different SoC trajectory than (P2) due to the non-physical solution of (P1).

Remark 6 (High voltage conditions)**.** *The voltage condition in Theorem 2 (C2) is not restrictive for practical distribution networks as can be seen from Fig. 3.30b. Importantly, condition (C2) can still be satisfied under large reverse power flows, which occurs in feeders with significant penetrations of batteries or solar PV generation. To illustrate the effect of reverse power flows, we present simulation results in Fig. 3.33. For example, in Figs. 3.33a and 3.33b, it is shown that the predicted active head-node power matches the actual power while satisfying the voltage constraints. Of course, reverse power flows and high voltage conditions are related, which means that we are assuming that appropriate DER hosting capacity studies have been conducted to inform operations and avoid high voltage conditions. Nonetheless, theoretically, there*

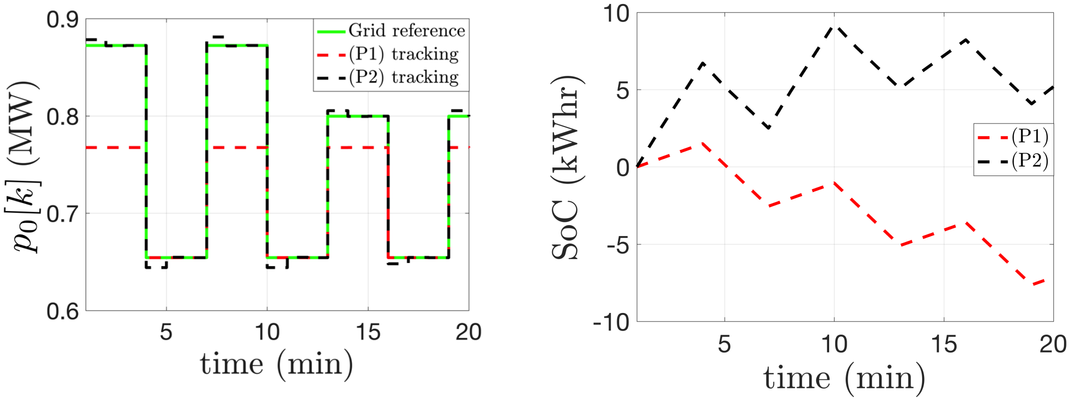

(a) (b)

Figure 3.32: Comparing the tracking performance of (P1) vs (P2); (b) Comparison of predicted SoC between (P1) and (P2) over the prediction horizon.

are reverse power flows for which condition (C2) is violated at optimality, which means that the convex relaxation in (P2) may not be tight. Figs. 3.33c and 3.33d illustrate the effects of a non-tight solution and show that the mismatch between the predicted and actual head-node power can lead to voltage violations due to predicted (relaxed, fictitious) losses that ensure a feasible solution in (P2), but are not realized in the physical feeder and, thus, reduce the head-node power further. To guarantee an exact solution that is always physically meaningful, we could include additional constraints to (P2) that capture condition (C2) implicitly (e.g., augment (P2) with the LinDist formulation's voltage variables, $\hat{v}_i$, and $\hat{v}_i$'s upper voltage bound), which ensures that $v < \bar{v}_i$, if (P2) is feasible [102]. Alternatively, we could just project (P2)'s optimal solution onto the AC feasible set and accept the loss of optimality.

Note that the solve time for the above optimization problem is typically less than a second for a feeder with 37 nodes. Our prior work on large scale three-phase systems has shown that the OPF scales well and can be solved in under a minute [150].

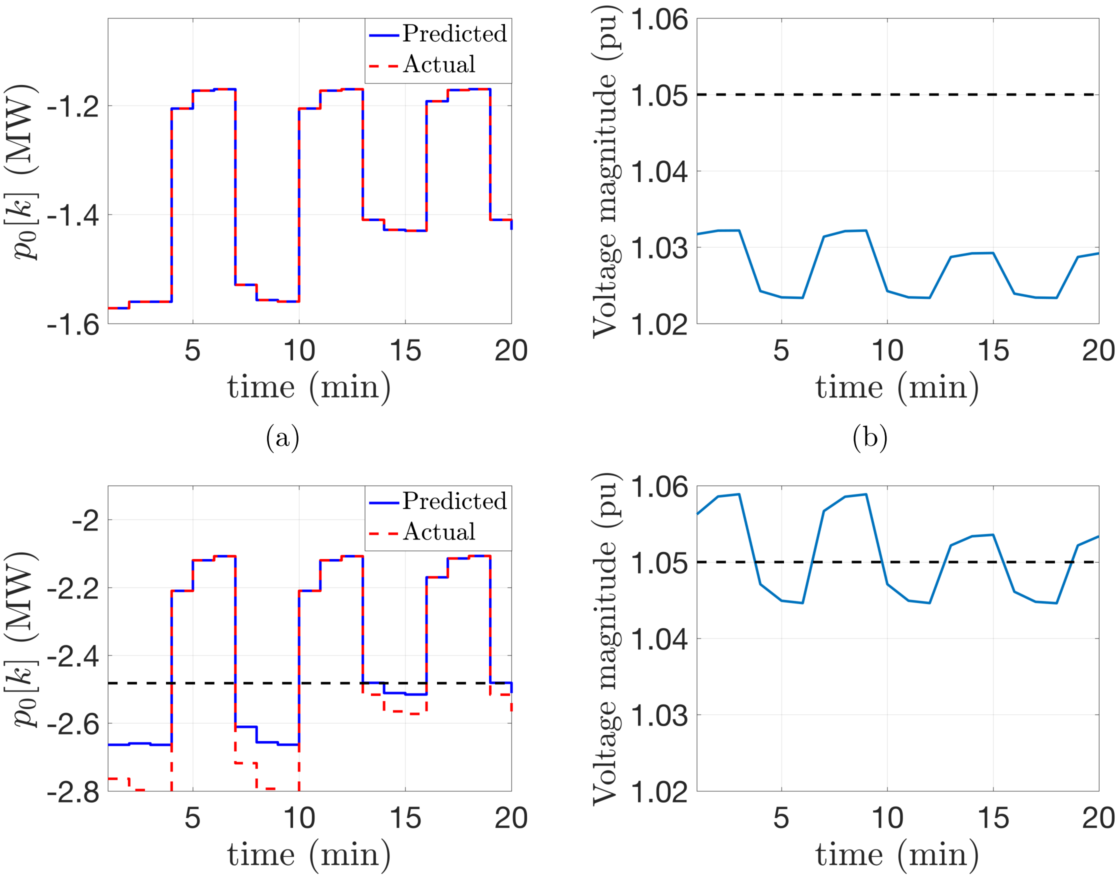

(a) (b)

(c) (d)

Figure 3.33: Reverse power flow studies on (P2): (a) Comparison between predicted and actual head-node power under reverse power flow when C2 holds which leads to an exact solution, (b) Admissible voltages under reverse power flow when C2 holds, (c) Comparison between predicted and actual head-node power when C2 does not hold (C2 limit shown by black dotted line), leading to a solution that is non-exact, (d) Voltage violation due to the solution being non-exact when C2 does not hold.

3.4.3 Conclusions

In this section, analysis and simulation results have been presented in support of a novel framework for large-scale coordination of DERs to support deep penetration of renewable energy. The explicit consideration of (temporal) energy and (spatial) grid constraints and the economic and reference-tracking (techno-economic) objectives have been achieved via a spatio-temporal decomposition approach that leverages information on demand-side flexibility to disaggregate grid economic trajectory into reference control signals for virtual batteries in distribution feeders. A convex optimal power flow (OPF) formulation has been presented that ensures a provably tight optimal dispatch of virtual batteries (VBs) to track an economic power trajectory. To show the effectiveness of the decomposition approach, simulation results have been conducted on a modified IEEE-37 test system.

3.5 FUTURE WORK ON OPTIMAL POWER FLOW IN DISTRIBUTION SYSTEMS

Future work on three-phase multi-period OPF will focus on reducing the optimality gap by using stronger relaxations of the power flow equations. We will also try and provide guarantees for a feasible solution to the decoupled NLP given an initialized SOCP solution. Extending the work to different grid objectives and including mechanical voltage control devices such as transformers and capacitor banks is another scope for improvement. Providing bounds on the gap between voltages obtained from the SOCP solver and a power flow solution is also an avenue for future work. Further analysis on the phenomenon of simultaneous charging and discharging is required as described in Section 3.2.3

Future work on Stochastic OPF will study the trade-off between performance and security in chance-constrained problems. Studying the uncertainty associated with demand and solar forecast and developing accurate distributions to represent the forecast errors leading to improved performance is another important area of research. The reasons behind a reduction in network imbalance in the stochastic method over the deterministic methods will also be analyzed.

Future work with reference to coordination of VBs will incorporate reactive power control of VBs and extend the regulation of voltage with inverters. Further, the market economic problem will be considered explicitly [154] to study the coupling between the market layer economic problem and the feeder constraint aware dispatch. Future work will also try to extend this approach to the three-phase unbalanced system operation [150]. Finally, we are interested in extending the multi-period OPF to a robust formulation to trade off conservativeness of dispatch and the probability of voltage and VB violations [155].

CHAPTER 4

TOWARDS REAL-TIME OPF WITH CONVEX INNER APPROXIMATIONS

In this section, a more aggregator-centric approach is followed, where an aggregator is an entity that represents an aggregation of many diverse DERs or a Virtual Battery (VB). In this approach, it is the role of the aggregator to dispatch DERs, whereas the utility provides certain bounds and limits (calculated offline), which the aggregator (which dispatches resources in real-time) must operate under. The benefits of such an approach lie in improved data-privacy and real-time admissible dispatch. In order to realise such a formulation, in section 4.1 we introduce the convex inner approximation method and show its advantages in comparison to linear OPF and convex relaxation based OPF. Then in section 4.2 we utilize the devised convex inner approximation for the dispatch of discrete devices such as OLTCs and capacitor banks in order to position the voltages close to nominal. Finally in section 4.3 we employ the convex inner approximation method in order to achieve network admissible aggregation and disaggregation of flexibility, paving the way for real-time dispatch of DERs.

4.1 INTRODUCTION TO CONVEX-INNER APPROXIMATION

This work presents a method to obtain a convex inner approximation that aims to improve the feasibility of optimal power flow (OPF) models in distribution feeders. For a resistive distribution network, both real and reactive power effect the node voltages and this makes it necessary to consider both when formulating the OPF problem. Inaccuracy in linearized OPF models may lead to under and over voltages when dispatching flexible demand, at scale, in response to whole-sale market or grid conditions. In order to guarantee feasibility, this work obtains an inner convex set in which the dispatchable resources can operate, based on their real and reactive power capabilities, that guarantees network voltages to be feasible. Test simulations are conducted on a standard IEEE distribution test network to validate the approach.

4.1.1 INTRODUCTION

With the increasing penetration of renewable generation and demand side flexibility in distribution networks, network constraints such as voltage limits could be violated. Traditional optimization techniques for dispatching resources include linear OPF based on *LinDist* models [27]. However, these linear models only work well close to the operating point and as the system is stressed to its extremes due to increasing penetration of DERs, they break down.

In order to improve the feasibility of OPF solutions in distribution systems with extreme penetration of renewables, this work aims to develop a method that guarantees the feasibility of optimized solutions. In order to achieve this, a convex inner approximation is developed to determine the feasible operating region for the dispatchable resources in the distribution network. Previous works in literature such as [6, 99] have developed techniques to determine error bounds in linear power flow approximations. This paper builds upon these works but develops a convex inner approximation for determining the operating region of dispachable resources that guarantees feasibility of solution.

As the proportion of dispatchable demand-side resources increases in the distribution network, they are expected to provide flexibility to the grid in the form of valuable energy services [88]. These flexible resources could be a fleet of DERs that constitute a virtual battery (VB), solar PV arrays, or advanced distribution feeders schemes act as a VB resource. In either case, these resources in aggregate are expected to provide certain energy services and participate in ISO markets, such as real-time or ancillary market services. However, the resulting ISO market-based dispatch signal does not consider the underlying distribution network and nodal constraints. Disaggregating the market-based dispatch signal at a nodal resource level, in real time, to account for local constraints and grid conditions represents a challenging problem. The key contribution of this paper is a convex formulation that provides an aggregator with the ability to disaggregate a fleet-wide dispatch signal into a feasible nodal dispatch across a distribution network as depicted in Fig. 4.1. Specifically, this paper develops a technique to determine a feasible operating region of these dispatchable resources which does not violate local network constraints. This is achieved by developing a provable convex inner approximation of the feasible region. Simulation tests are conducted on IEEE-13 node system [132] to show the effectiveness and validity of the

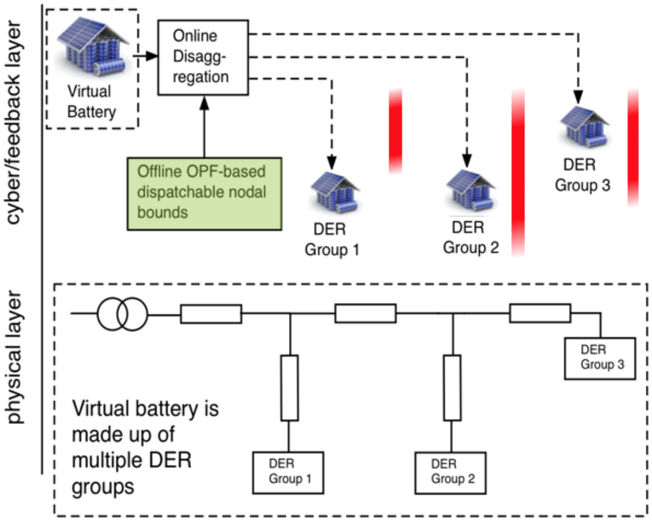

Figure 4.1: A schematic representation of the network model. The physical layer represents the circuit that connects the different DER groups into an aggregate virtual battery, whereas the cyber layer represents the disaggregation of the virtual battery market signal to the DER groups based on the feasible nodal bounds that are determined offline.

approach. The main contributions of this work are follows:

1. Through a motivating example, this paper explains the shortcomings of linear OPF approximations and how they can violate network constraints.
2. The problem of determining the feasible operating region of dispactchable resources is re-formulated as an inner convex optimization that respects network constraints.

The rest of this section is organized as follows: Section 4.1.2 illustrates the shortcomings of linear OPF under high renewable penetration in distribution networks. Section 4.1.3 develops the mathematical model for the optimization problem of determining the operating region of dispatchable resources, whereas section 4.1.4 provides the convex inner approximation of the feasible space. Simulation results showing the validity of the approach are given in section 4.1.5 and finally conclusions are provided in section 4.1.6.

4.1.2 Shortcomings of linear OPF

This section presents the shortcomings of linear OPF approximations under certain conditions in distribution networks. Simulations are run on the modified IEEE-13 node test case to check the effect of real and reactive power variation on nodal voltages. The IEEE-13 node test case with a DER at node 6 capable of four-quadrant operation is shown in Fig. 4.2. For the purpose of this study, the switching devices in the network (switches, capacitor banks, transformers) are assumed to be fixed at their nominal values. The real and reactive power injections of the DER are varied independently to observe the effect on node voltages. The results are shown in Fig. 4.3a and Fig. 4.3b. From the figures it can be observed that changes in real and reactive power injections at one node have significant effect on voltages at other nodes, especially the nodes which are "down-hill" from the injection node. Unlike transmission systems, where the coupling between real power and voltage is minimal, in distribution systems, changes in real power injection can cause significant(if not as much as reactive power) change in node voltages. From these results it becomes clear that the effect of both real and reactive power needs to be considered in order to correctly control voltages in distribution systems. However, in most linear power flow approximations, the affect of real power variations on the nodal voltages is often neglected, which could result in violation of voltage constraints.

To further illustrate this point, a two node model with DERs, solar and demand, as shown in Fig. 4.4 and parameters given in Table 4.1 is considered. For this system,

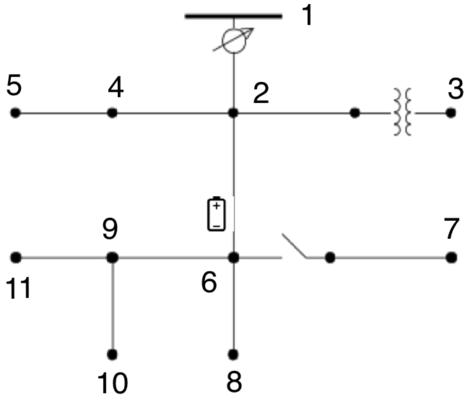

Figure 4.2: Modified IEEE-13 node test system with DER capable of four-quadrant operation at node 6*. The switch between nodes* 6 *and* 7 *is assumed to be closed and the transformer between nodes* 2 *and* 3 *is assumed to be ideal with unity turns ratio*

the net power injection at node j, p_j, which represents the net effect of DERs, solar and demand, is varied over a range to find the corresponding voltages obtained from *LinDist* and *DistFlow*. From Fig. 4.5a it can be seen that the linear model and nonlinear *DistFlow* model do not match and this could lead to operating the system at set-points that violate the voltage constraints as can be seen from Fig. 4.5a, where the voltage violation occurs when the system is operated at the lower voltage limit. This implies that when formulating an OPF model, it is important to consider the effect of the non-linear terms in the power flow equations in order to ensure feasibility.

The proposed approach in this paper, takes a worst case of the non-linear terms in the power flow equations and develops a feasible model for determining the real power limit bounds on the net power injections, which in turn can be used to determine the bounds on the flexible resources assuming demand and solar forecast are known. This means that the technique guarantees node voltages to be within their limits for the

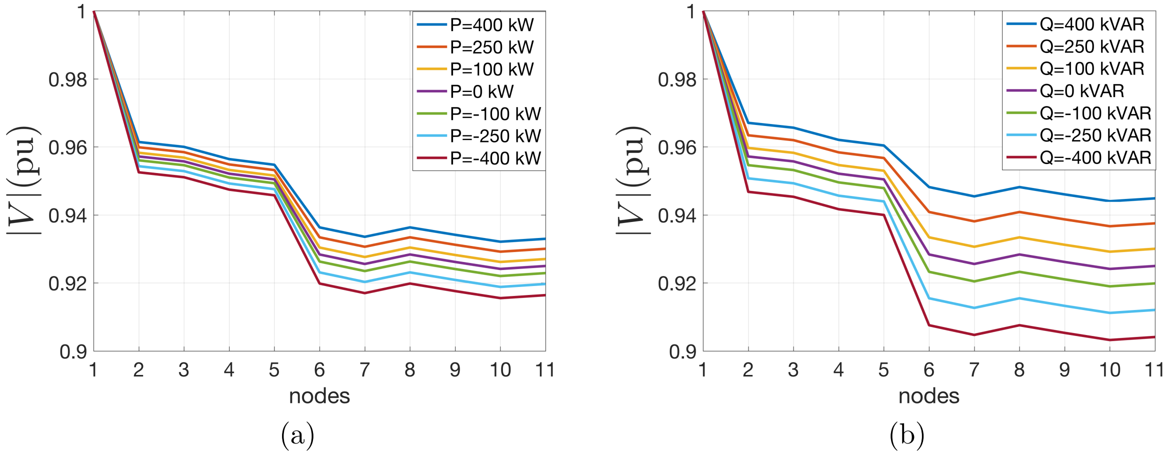

Figure 4.3: (a) Variation of node voltage with change in real power injection at node 6, (b) Variation of node voltage with change in reactive power injection at node 6.

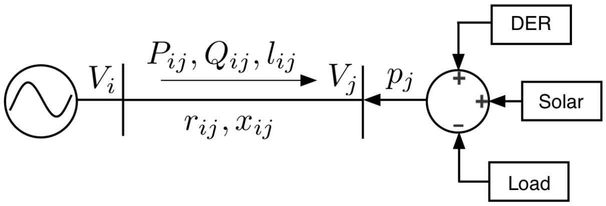

Figure 4.4: Two node model with demand side power source.

determined power bounds, while at the same time keeping the convex form of the formulation.

4.1.3 FORMULATION OF THE OPTIMIZATION PROBLEM

The aim of this work is to formulate an optimization scheme to provide feasible operating limits to the dispatchable resources based on the real and reactive power capabilities of the network, in order to satisfy the nodal voltage constraints. The input to this allocation problem is the real and reactive power capabilities of each

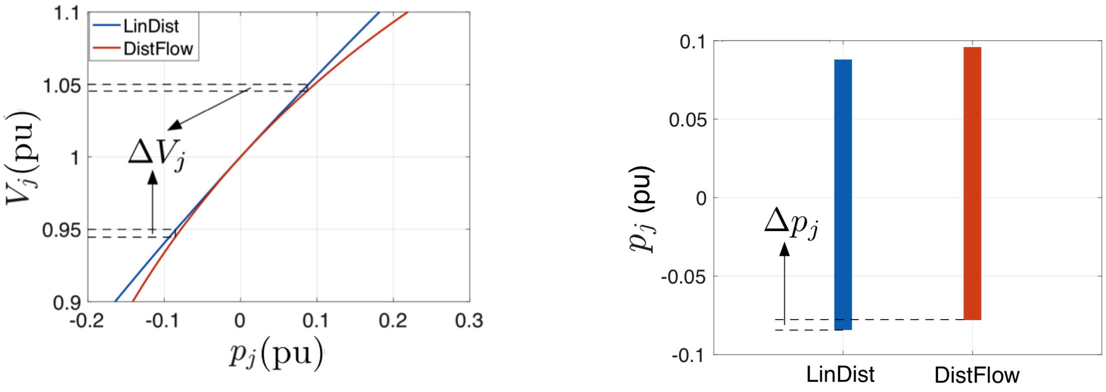

(a) (b)

Figure 4.5: (a) Comparison in change in node voltage with change in real power set-points between DistFlow and LinDist for two node system. The two models result in different voltages and if design is based on linear model then network voltages limit will be violated if p_j is operated at its lower limit, (b) Comparison of feasible region obtained from LinDist and DistFlow models for two node model.

Table 4.1: Parameters of the 2-node, 1-line system

Symbol	Type	Bounds/Values
l_{ij}	Variable	[0,0.5] p.u
V_j	Variable	[0.95,1.05] p.u
P_{ij}	Variable	[-5,5] MW
Q_{ij}	Variable	[-5,5] MVar
p_j	Variable	[-1,1] MW
V_i	Data	1 p.u
$r_{ij} + jx_{ij}$	Data	10+j15 ohm
V_{base}	Data	4.16 kV
S_{base}	Data	1 MVA

node and the output is the real power operating region where each node can operate while satisfying the network constraints. In order to increase the operating region of the resources, the optimization scheme is posed as a power bound maximization problem. *DistFlow* equations as given in [27] are used to solve the optimization problem. However, *DistFlow* equations are non-linear which takes the problem outside the realm of convex optimization. Linearized *LinDist* models are often used, but they are accurate only close to the operating point voltages. As the system starts operating away from the nominal voltage, the errors could become large [156]. In this work we develop a feasible convex formulation by modifying the *LinDist* equations. However, the techniques presented here can easily be extended to other single phase and multi-phase linearized power flow models in literature such as [157, 158].

4.1.3.1 Mathematical model

In this section we consider a radial distribution network modeled using the matrix notation as shown in section 2.2.1. Based on this modeling, the power flow equations can be represented as:

$$P = p + AP - ARl \tag{4.1}$$

$$Q = q + AQ - AXl \tag{4.2}$$

$$V = v_0 \mathbf{1}_n + M_{\mathrm{p}} p + M_{\mathrm{q}} q - Hl \tag{4.3}$$

$$l_{ij}[k] = \frac{|S_{ij}[k]|^2}{v_i[k]}, \quad \forall (i,j) \in \mathcal{E} \tag{4.4}$$

where the matrices $C, D_{\mathrm{R}}, D_{\mathrm{X}}, M_{\mathrm{p}}, M_{\mathrm{q}}$ and H depend upon the network impedance and incidence matrix and are defined in section 2.2.1.

Apart from the nonlinear relation (4.4) of l to P, Q and V, (4.3) is a linear relationship between the nodal power injections p, q and node voltages V. The nonlinearity in the network is represented by (4.4), as the current term l is related to the power

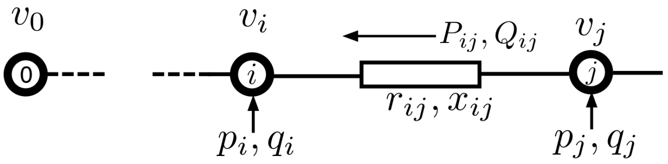

Figure 4.6: Diagram of a radial distribution network [6].

injections and node voltages in a nonlinear fashion. Including this term into the optimization model would render the optimization problem NP hard, however, neglecting this term could result in infeasible solutions from the linearized OPF model.

4.1.3.2 Optimization problem formulation

The problem being addressed in this paper is to determine the convex feasible operating region of dispatchable resources that respects the network voltage constraints. Let $\Delta p := p^+ - p^-$ be the feasible operating region of the net power injections. If the feasible region of the net power injections is found, then the feasible operating region of the flexible resources can be easily determined assuming the demand and solar power forecast are known. Based on these assumptions, (4.3) can be applied at p^+ and p^- as:

$$V^+ = v_0\mathbf{1} + M_\mathrm{p}p^+ + M_\mathrm{q}q^+ - Hl^+ \tag{4.5}$$

$$V^- = v_0\mathbf{1} + M_\mathrm{p}p^- + M_\mathrm{q}q^- - Hl^- \tag{4.6}$$

where $V^+ := V(p^+)$, $q^+ := q(p^+)$, and $l^+ := l(p^+)$ are the respective variable values at p^+, and, $V^- := V(p^-), q^- := q(p^-), l^- := l(p^-)$ are the values of the variables at p^-. Next, we modify (4.5) and (4.6) to obtain the feasible operating region as:

$$M_{\mathrm{p}}p^{+} = V^{+} - v_0\mathbf{1} - M_{\mathrm{q}}q^{+} + Hl^{+} \tag{4.7}$$

$$M_{\mathrm{p}}p^{-} = V^{-} - v_0\mathbf{1} - M_{\mathrm{q}}q^{-} + Hl^{-} \tag{4.8}$$

Based on (4.7) and (4.8), the optimization problem to determine the maximum feasible operating region of the network can be obtained from the solution of the two optimization problems shown below for p^{+} and p^{-}:

$$\text{(P1)} \quad \max_{V^{+},p^{+},q^{+},l^{+}} \sum_{i=1}^{n} \log(p_i^{+}) \tag{4.9a}$$

$$\text{subject to :} \quad (4.7), (4.4) \tag{4.9b}$$

$$\underline{S_i} \leq f(p_i^{+}, q_i^{+}) \leq \overline{S_i} \forall i \in \mathcal{N} \tag{4.9c}$$

$$\underline{V} \leq V^{+} \leq \overline{V} \tag{4.9d}$$

$$\underline{l} \leq l^{+} \leq \bar{l} \tag{4.9e}$$

where $f(p_i^{+}, q_i^{+})$ represents the type of apparent power constraint on the nodal injections that is required to satisfy the bounds $\underline{S_i} \in \mathcal{R}$ and $\overline{S_i} \in \mathbb{R}$ at node i. $f(p_i^{+}, q_i^{+})$ could represent box constraints on active and reactive power or it could represent a quadratic apparent power constraint in the case of an inverter. $\underline{V} \in \mathbb{R}^n$ and $\overline{V} \in \mathbb{R}^n$ are the voltage magnitude square lower and upper limits, $\underline{l} \in \mathbb{R}^n$ and $\bar{l} \in \mathbb{R}^n$ are the current magnitude square lower and upper limits. The optimization problem (4.9) determines the maximum power that can be supplied by the dispatchable resources in the distribution network. The optimization problem to find the minimum power that can be supplied can similarly be determined based on *(P2)*.

$$\text{(P2)} \quad \max_{V^-, p^-, q^-, l^-} \quad \sum_{i=1}^{n} \log(-p_i^-) \tag{4.10a}$$

$$\text{subject to :} \quad (4.8), (4.4) \tag{4.10b}$$

$$\underline{S_i} \leq f(p_i^-, q_i^-) \leq \overline{S_i} \quad \forall i \in \mathcal{N} \tag{4.10c}$$

$$\underline{V} \leq V^- \leq \overline{V} \tag{4.10d}$$

$$\underline{l} \leq l^- \leq \bar{l} \tag{4.10e}$$

It is assumed that $p_i^- < 0, \forall i \in \mathcal{N}$. Optimization problems *(P1)* and *(P2)* are nonconvex due to the constraint (4.4) which is a nonlinear relationship. In the next section we will provide a formulation for these problems that is a linear inner approximation.

4.1.4 CONVEX INNER APPROXIMATION FORMULATION

In order to obtain a convex inner approximation of *(P1)* and *(P2)*, we need to approximate the nonlinear relationship in (4.4). This is obtained by considering the worst case of l in order to obtain a conservative estimate of Δp (i.e., $l_{\min}$ in *(P1)* and $l_{\max}$ in *(P2)*). Based on this approximation, a conservative estimate of Δp, $\Delta p_{\mathrm{c}} = p_{\mathrm{c}}^+ - p_{\mathrm{c}}^-$ can be obtained, where $p_{\mathrm{c}}^+, p_{\mathrm{c}}^-$ are the inner approximations of p^+, p^-.

$$M_{\mathrm{p}} p^+ \geq V^+ - v_0 \mathbf{1} - M_{\mathrm{q}} q^+ + H l_{\min} = M_{\mathrm{p}} p_c^+ \tag{4.11}$$

$$M_{\mathrm{p}} p^- \leq V^- - v_0 \mathbf{1} - M_{\mathrm{q}} q^- + H l_{\max} = M_{\mathrm{p}} p_c^- \tag{4.12}$$

Based on the above inner approximations, *(P1)* and *(P2)* can now be modified to a convex inner approximation model shown below, if $l_{\min}, l_{\max}$ can be found *a-priori* based on the network capacity.

$$\text{(P3)} \max_{V^+, p_{\text{c}}^+, q^+} \sum_{i=1}^{n} \log(p_{i,\text{c}}^+) \tag{4.13a}$$

$$\text{subject to :} \quad (4.11), (4.9c) - (4.9d) \tag{4.13b}$$

$$\text{(P4)} \max_{V^-, p_{\text{c}}^-, q^-} \sum_{i=1}^{n} \log(-p_{i,\text{c}}^-) \tag{4.14a}$$

$$\text{subject to :} \quad (4.12), (4.10c) - (4.10d) \tag{4.14b}$$

The optimization problems *(P3)* and *(P4)* are convex and determine an inner approximation of the feasible operating region of the nodal injections that satisfy the network constraints. The problem then is to determine the the worst cases of l, i.e., $l_{\min}$ and $l_{\max}$, which is discussed in the next section.

4.1.4.1 Determining the worst-case bounds for l

In this section we present a method to calculate the worst case of l, i.e., $l_{\min}$ and $l_{\max}$, which results in a feasible convex inner approximation. $l_{\min}$ and $l_{\max}$ are calculated based on the real and reactive power capacity of the nodal injections, which in turn is determined based on the demand and solar profile and DER capacities at a particular node. Before solving the optimization problems *P3* and *P4*, we determine $l_{\min}$ and $l_{\max}$ by solving a power flow based on the real and reactive power capacity of the nodal injections as depicted by the block diagram in Fig. 4.7 that outlines the steps to solve the optimization problem. For simplicity, in this paper we set $l_{\min}$ to zero, which reduces *P3* to the *LinDist* model. $l_{\max}$ is obtained by solving a power flow where the dispatchable resources are set to their capacity to determine the worst case of l. Based on this $l_{\max}$, *(P4)* is solved to obtain a value of p_c^- that respects network constraints, which could be violated if *LinDist* model was used instead. Based on these results, a Δp_c which represents a feasible operating region of the network can be obtained. Simulation results are presented in the next section to show the validity of the proposed approach.

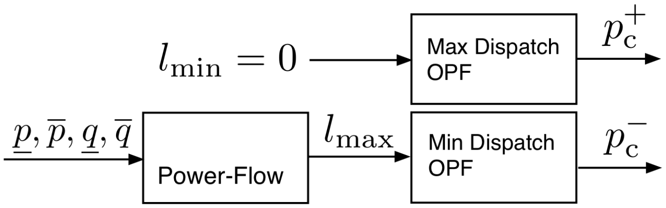

Figure 4.7: Block diagram of the optimization problem to obtain the maximum dispatchable operating region.

4.1.5 SIMULATION RESULTS

In this section, simulation results on a standard IEEE-test network will be presented to show the the efficacy of the proposed approach. A comparison between the results of the convex inner approximation and the linearized OPF (*LinDist*) is presented. However, the techniques presented here can be extended to improve any linearized OPF model. It is shown that the convex inner approximation results in a feasible solution when the *LinDist* model may result in an infeasible solution. Simulation tests are conducted on the IEEE-13 node test case [132] using optimization solver SDPT3 [159] in CVX, with validation of the results performed through Matpower [153]. The block diagram in Fig. 4.7 shows the steps to determine the feasible operating region from the proposed inner convex approximation.

For the purpose of comparison between the convex inner approximation and the linearized OPF model, three test scenarios are considered as shown in Table 4.2. In each of the three test scenarios, the operating regions obtained from the *LinDist* OPF model and the convex inner approximation are obtained and then the feasibility of the operating regions is compared through powerflow solutions.

Table 4.2: Types of apparent power constraints

Case no.	Case description	Bounds ($f(p_i, q_i)$)
1	Unity power factor	$q_i = \gamma_i p_i$
2	Box constraint	$\underline{q_i} \leq q_i \leq \overline{q_i}$
3	Quadratic constraint	$p_i^2 + q_i^2 \leq \overline{S_i}$

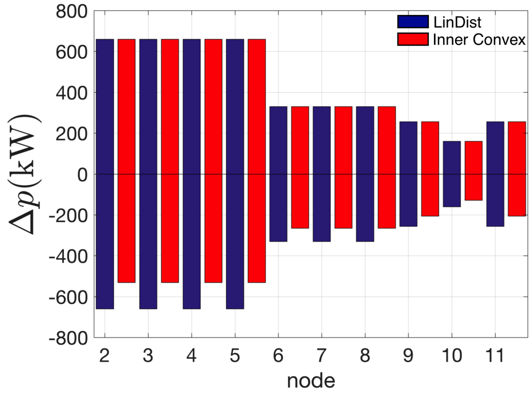

Figure 4.8: Comparison of the feasible operating regions for Case 1 (unity power factor) between LinDist and convex inner approximation showing the conservativeness of the inner convex approximation over LinDist. Based on this, the feasible operating region of flexible dispatchable resources can be obtained by subtracting solar and demand forecast.

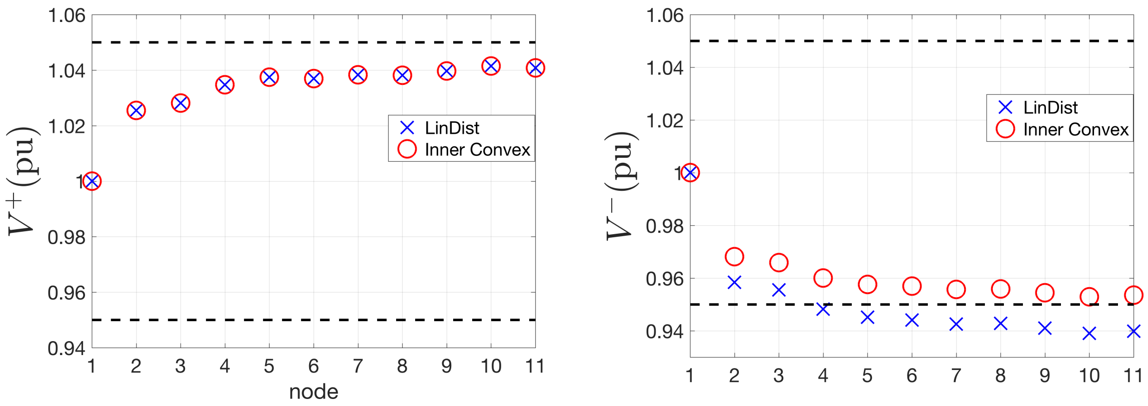

(a) (b)

Figure 4.9: (a) Comparison of the Voltages (V^+) for Case 1 (unity power factor) obtained through Matpower for the optimized set-points from LinDist and convex inner approximation showing that the voltages match (as $l_{min} = 0$ and are within the bounds, (b) Comparison of the Voltages (V^-) for Case 1 (unity power factor) obtained through Matpower for the optimized set-points from LinDist and convex inner approximation showing that the voltages violate the bounds when using LinDist model, which is avoided when using the convex inner approximation.

4.1.5.1 Case 1: Constant power factor

In this case, the relation between real and reactive power injection for the flexible resource is given by a constant power factor, $PF_i := \cos(\phi_i)$, at node i:

$$q_i = \gamma_i p_i \quad \forall i \in \mathcal{N} \tag{4.15}$$

where $\gamma_i := \sqrt{(1 - PF_i^2)/PF_i^2}$. For this test case, we consider the flexible resource to be an aggregation of resistive water heaters, which results in unity power factor, i.e., $cos(\phi_i) = 1, \forall i \in \mathcal{N}$.

Figure 4.8 shows the comparison of the feasible region obtained from *LinDist* model and from the proposed convex inner approximation for the constant power

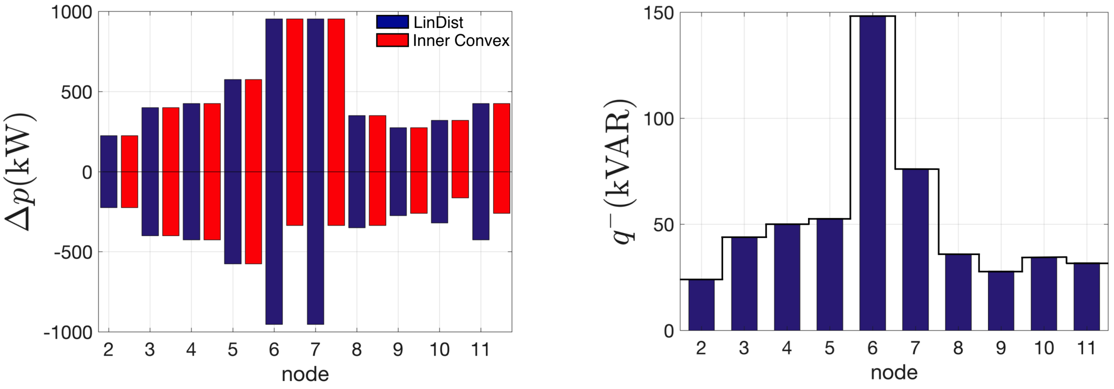

(a) (b)

Figure 4.10: (a) Comparison of the feasible operating regions for Case 2 (box constraints) between LinDist and convex inner approximation showing the conservativeness of the inner convex approximation over LinDist, (b) Reactive power injection (blue bars) in LinDist for Case 2 (box constraints) showing that the reactive power is at its limit (black lines) and hence the voltage infeasibility cannot be improved through more injection of reactive power, highlighting the need for a conservative estimate of Δp.

factor case. It can be seen from Fig. 4.8 that the convex inner approximation provides conservative lower bounds on the feasible region. Figure 4.9a and Fig. 4.9b show the comparison of the voltages obtained through Matpower for the set-points shown in Fig. 4.8. As can be clearly seen from Fig. 4.9b, in case of the *LinDist* model the voltages obtained when determining the lower limit of the operating region violate network bounds, whereas the convex inner approximation due to its conservative approach is able to obtain a feasible solution.

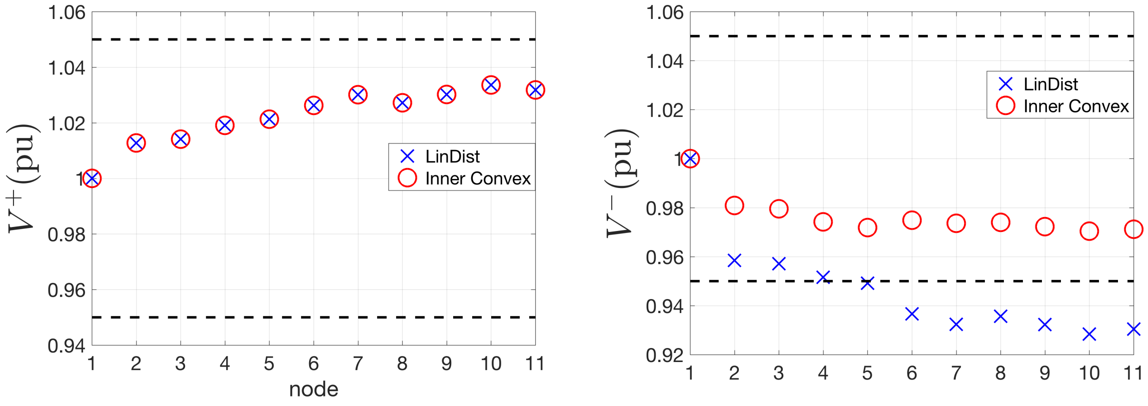

(a) (b)

Figure 4.11: (a) Comparison of the Voltages (V^+) for Case 2 (box constraints) obtained through Matpower for the optimized set-points from LinDist and convex inner approximation, (b) Comparison of the Voltages (V^-) for Case 2 (box constraints) obtained through Matpower for the optimized set-points from LinDist and convex inner approximation showing that the voltage bounds are violated when using the LinDist model, which is avoided when using the convex inner approximation.

4.1.5.2 Case 2: Box constraints on reactive power

In this case, simulation results are conducted with box constraints on reactive power as shown below:

$$\underline{q_i} \leq q_i \leq \overline{q_i} \quad \forall i \in \mathcal{N} \tag{4.16}$$

where $\underline{q} \in \mathbb{R}$ is the lower limit of the reactive power injection and $\overline{q} \in \mathbb{R}$ is the upper limit, at node i. From Fig. 4.10a it can be seen that the convex inner approximation provides a conservative estimate to the feasible region. Figure 4.11a shows the comparison of the voltages at the upper limit of the feasible region, whereas Fig. 4.11b shows the comparison of the voltages at the lower limit of the feasible region. As can be seen the figures, the convex inner approximation is able to provide a feasible

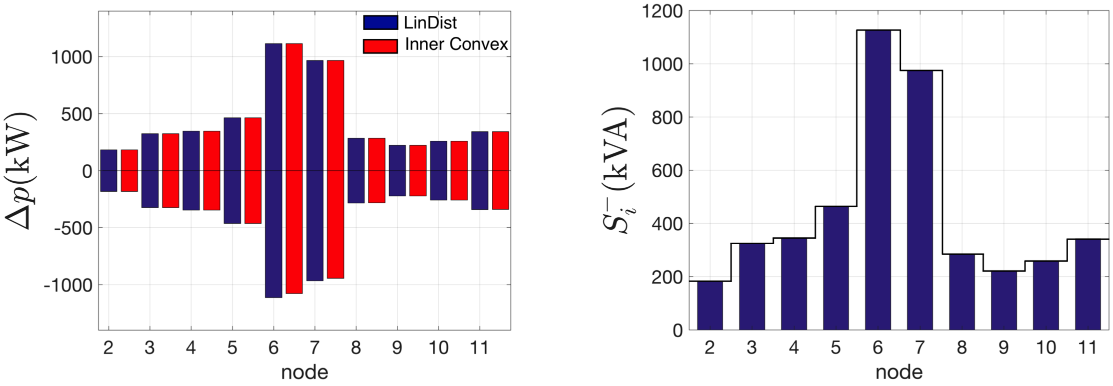

(a)

(b)

Figure 4.12: (a) Comparison of the feasible operating regions for Case 3 (quadratic apparent power constraint) between LinDist and convex inner approximation showing the conservativeness of the inner convex approximation over LinDist, (b) Apparent power injection in LinDist (blue bars) for Case 3 (quadratic apparent power constraint) shows that the apparent power is at its limit (black line) and hence a voltage infeasibility cannot be improved through additional injection of reactive power, highlighting the need for a conservative estimate of Δp*.*

solution, while the *LinDist* model results in violation of constraints. Figure 4.10b shows that the violation of voltage constraints in *LinDist* model is due to the operating region of real power injection Δp, as the reactive power injection is at its limit and cannot provide any further voltage support. This is also proved in Theorem 5 in Appendix 5.C that shows for the *LinDist* model the reactive power at optimality is always at the boundary of the constraint.

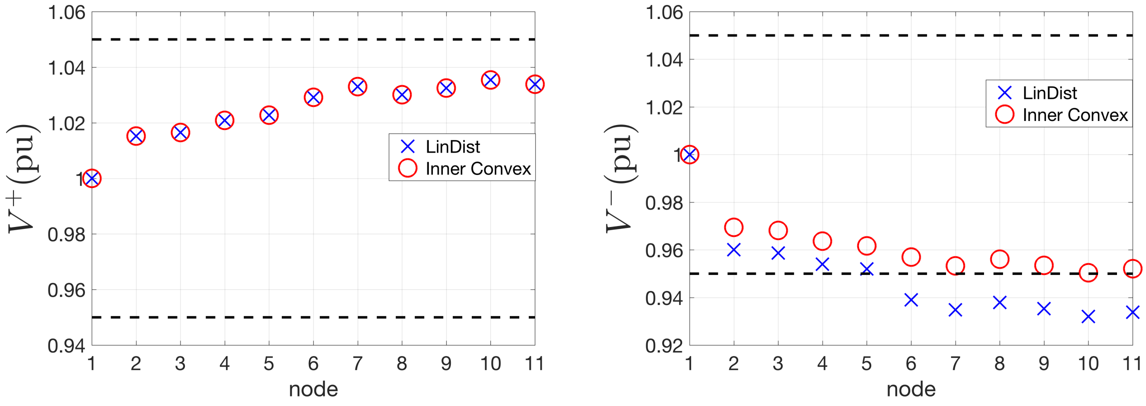

(a) (b)

Figure 4.13: (a) Comparison of the Voltages (V^+) for Case 3 (quadratic apparent power constraint) obtained through Matpower for the optimized set-points from LinDist and convex inner approximation, (b) Comparison of the Voltages (V^-) for Case 3 (quadratic apparent power constraint) obtained through Matpower for the optimized set-points from LinDist and convex inner approximation showing that the voltage bounds are violated when using the LinDist model, which is avoided when using the convex inner approximation.

4.1.5.3 Case 3: Apparent power constraint

In this case the real and reactive power injections at each node are bound by the following quadratic apparent power constraint:

$$p_i^2 + q_i^2 \leq \overline{S_i} \quad \forall i \in \mathcal{N} \tag{4.17}$$

This is the case when flexible resources are connected to the grid through inverters. From Fig. 4.12a it can be seen that the convex inner approximation provides a conservative estimate of the feasible region. The comparison of the voltages in Fig. 4.13a and Fig. 4.13b shows that at the lower limit of the feasible region, the *LinDist* model does not result in a feasible solution, which on the other hand is provided by the convex inner approximation. Furthermore, Fig. 4.12b shows that the nodal injections are at their apparent power limits without any margin to provide reactive power support. Theorem 5 in Appendix 5.C presents a formal proof that shows that this condition always holds.

These simulation results illustrate how the convex inner approximation compares against the linearized OPF models with respect to modeling errors, and hence ensuring robust and resilient operation of distribution feeders. To verify the feasibility guarantee of the convex inner approximation, Monte Carlo methods are employed to sample 10,000 different combinations of the DER operating regions and simulate the resulting AC load flow with Matpower to determine nodal voltages with distribution as shown in Fig. 4.14. From the figure, it is clear that voltages are within limits for all combinations.

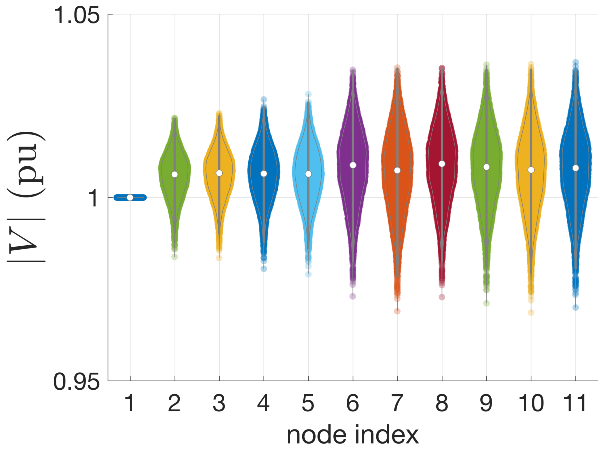

Figure 4.14: Violin plot of the voltage magnitudes from 10,000 Monte-Carlo simulations using the operation regions obtained from the convex inner approximation.

4.1.6 CONCLUSIONS

This paper presents a convex inner approximation of the optimal power flow problem that determines the feasible operating region of the dispatchable resources while respecting the network constraints. Through illustrative examples, the shortcomings of linear OPF techniques is explained. The mathematical formulation of the convex inner approximation is developed and through simulations on an IEEE test network, the advantage of using this formulation is presented.

4.2 VOLTAGE POSITIONING OF DISCRET DEVICES THROUGH CONVEX INNER APPROXIMATION

With increasing penetration of solar PV, some distribution feeders are experiencing highly variable net-load flows and even reverse flows. To optimize distribution systems under such conditions, the scheduling of mechanical devices, such as OLTCs and capacitor banks, needs to take into account forecasted solar PV and actual grid conditions. However, these legacy switching assets are operated on a daily or hourly timescale, due to the wear and tear associated with mechanical switching, which makes them unsuitable for real-time control. Therefore, there is a natural timescale-separation between these slower mechanical assets and the responsive nature of inverter-based resources. In this work, we present a network admissible convex formulation for holistically scheduling controllable grid assets to position voltage optimally against solar PV. An optimal hourly schedule is presented that utilizes mechanical resources to position the predicted voltages close to nominal values, while minimizing the use of inverter-based resources (i.e., DERs), making them available for control at a faster time-scale (after the uncertainty reveals itself). A convex, inner approximation of the OPF problem is adapted to a mixed-integer linear program that minimizes voltage deviations from nominal (i.e., maximizes voltage margins). The resulting OPF solution respects all the network constraints and is, hence, robust against modeling simplifications. Simulation based analysis on IEEE distribution feeders validates the approach.

4.2.1 Introduction

With the increasing penetration of renewable resources in the distribution grid, maintaining system voltages within acceptable limits (i.e., minimizing voltage deviations), is a major challenge [109,160]. The intermittent nature of solar energy can cause under and over-voltages in the system [35–38] leading to unacceptable operation. However, solar PV resources are inverter interfaced and can provide responsive reactive power resources, which can be used in active network management [161]. Besides these inverter-interfaced resources, the distribution grid also includes traditional mechanical devices, such as on-load tap changing (OLTC) transformers, cap banks, reactors, etc. These discrete mechanical assets are subject to physical wear and tear and, thus, are usually only operated a few times during the day with heuristic open-loop policies [39]. However, with increasing solar PV penetration, it becomes important to optimize the schedule for the mechanical assets against bidirectional and variable power flows [40]. However, the mechanical switching is not suitable for real-time conditions and control and should, therefore, be utilized on slower timescales to position the predicted voltage profile (i.e., increase voltage margins) against predicted solar PV generation. In fact, inverter-interfaced assets, such as solar PV generation and battery storage, can effectively supply controllable reactive resources appropriate for these faster time-scales. Therefore, there is a natural timescale-separation between (slow) mechanical and (fast) inverter-based controllable grid assets. DER resources on slow time-scale act as a form of reactive reserve, allowing the DERs to fully participate in valuable market services on a fast timescale. This way mechanical assets maximize margins and optimize value of DERs. This leads to the challenge of co-optimization of different types of controllable reactive power resources. Thus, for the scheduling on slower time-scales, it is desirable to maximize utilization of the mechanical assets to keep voltages close to desirable nominal values while using as little as possible of the responsive inverter-interfaced reactive resources. This effectively prioritizes the responsive reactive resources for the faster time-scales to counter variability in net-load (demand minus solar PV).

The aim of this work is then to present a convex OPF formulation where the objective function seeks to minimize the deviation of the predicted nodal voltages from their nominal values. The nonlinear power flow equations relate the voltages in the network with the complex power injections. This work uses a convex approximation of the power flow equations that results in a network-admissible solution, i.e., all physical network limits are respected at (global) optimality, while solving in polynominal time. Hence, the method is robust against modeling errors introduced from approximations of the non-linear power flow equations.

Discrete devices like the capacitor/reactor banks and line regulators (ON/OFF) and load-tap-changing (LTC) transformers are an integral part of distribution system operations. Due to the discrete nature of these devices, including them into an optimization problem renders the problem NP-hard [42]. This work leverages the notion that discrete devices and continuous resources can offer their flexibility at different time-scales, which gives rise to a natural prioritization of reactive power resources.

This section focuses on optimizing discrete control assets in the grid to maximize both the voltage margins and the availability of reactive reserves for the faster timescales. This maximization of voltage margins[1] is illustrated in Fig. 4.15 which

---

[1] Minimizing voltage deviations from nominal can be viewed as maximizing voltage margins.

depicts larger voltage margins as we move closer to the nominal. Recent works in literature such as [11,29,162] have developed control schemes that achieve voltage regulation through dispatch of flexible resources in real-time. The work in this section could provide prediction schedules for voltage control at faster timescales.

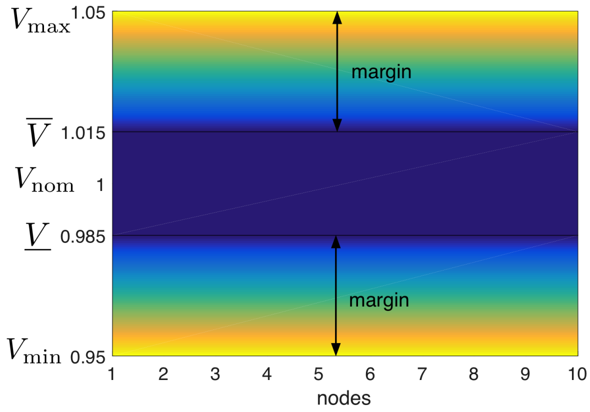

Figure 4.15: Illustrating the relationship between voltage margin, nominal voltage and voltage bounds. Lighter colors represent larger margins.

In general, employing convex relaxations with an objective that minimizes voltage deviations will lead to a non-zero duality gap [163], due to being non-monotonic. More general conditions for the exactness of the convex relaxation are shown in [95, 102]. This makes it challenging to use convex relaxations to formulate the optimization problem. In many applications, providing network admissibility guarantees are more valuable than solving to a globally optimal solution [164]. This work uses the convex inner approximation method of the OPF problem that exhibits computational solve times similar to that of linear formulations with the added and crucial benefit that the formulation guarantees admissible solutions. Furthermore, the utilization of reactive power from flexible inverter-interfaced DERs should be minimized, so that this resource can be better utilized at the faster time-scale. Previous work on minimizing both voltage deviations and reactive power use has been shown in [165], where a trade-off parameter is used between the two competing objectives. Unlike [165], this work considers control scheme for the integration of existing discrete mechanical assets and flexible inverters and provides a systematic method to select the trade-off parameter. To summarize, main contributions of this work are the following:

- A convex inner OPF formulation is developed for the problem of minimizing voltage deviations from nominal in a distribution system with guarantees on admissiblility and scalability.
- A voltage positioning optimization (VPO) method is developed that holistically optimizes the schedule of discrete mechanical assets while systematically minimizing the need for continuous inverter-interfaced reactive DERs.
- Simulation based analysis is leveraged to select trade-off parameters between the use of continuous reactive resources and voltage margins, which are then utilized to validate the performance on IEEE test feeders.

The rest of the section is organized as follows: Section 4.2.2 develops the voltage positioning optimization (VPO) formulation to include discrete mechanical assets as a mixed integer program in order to position the nodal voltages. Section 4.2.3 develops the mathematical formulation of the convex inner approximation OPF problem that is then used in the VPO problem to obtain a MILP based VPO. Simulation results on IEEE test feeders are discussed in Section 4.2.4 and finally conclusions are summarized in Section 4.2.5.

4.2.2 Voltage Positioning Optimization

This section develops the voltage positioning optimization problem as a mixed integer program (MIP). The nonlinearity associated with modeling discrete mechanical devices, such as On-load tap changers (OLTCs) and capacitor banks (CBs), is expressed with an equivalent piece-wise linear formulation to engender the MIP.

4.2.2.1 Distribution Grid Model

In this section we consider a radial distribution network modeled using the matrix notation as shown in section 2.2.1. Based on this modeling, the power flow equations can be represented as:

$$P = p + AP - ARl \tag{4.18}$$

$$Q = q + AQ - AXl \tag{4.19}$$

$$V = v_0 \mathbf{1}_n + M_{\mathrm{p}} p + M_{\mathrm{q}} q - Hl \tag{4.20}$$

$$l_{ij}[k] = \frac{|S_{ij}[k]|^2}{v_i[k]}, \quad \forall (i,j) \in \mathcal{E} \tag{4.21}$$

where the matrices $C, D_{\mathrm{R}}, D_{\mathrm{X}}, M_{\mathrm{p}}, M_{\mathrm{q}}$ and H depend upon the network impedance and incidence matrix and are defined in section 2.2.1.

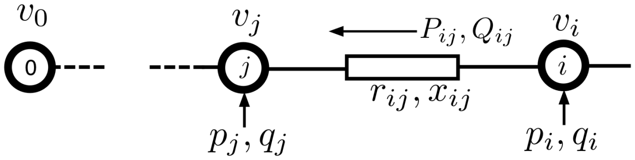

Figure 4.16: Diagram of a radial distribution network from [6].

Apart from the nonlinear relation (4.21) of l to P, Q and V, (4.18), (4.19) and (4.20) is a linear relationship between the nodal power injections p, q, the branch power flows P ,Q and node voltages V. The nonlinearity in the network is represented by (4.21), as the current term l is related to the power injections and node voltages in a nonlinear fashion. Including this term into the optimization model would render the optimization problem non-convex, however, neglecting this term could result in an inadmissible linear OPF solution. In the next section, we model the discrete grid resources such as OLTCs and capacitor banks, which will then be used to formulate the voltage positioning optimiazation problem.

4.2.2.2 Discrete device nomenclature

For this work we utilize the discrete device models of OLTCs and capacitor banks derived and explained in section 2.3.

4.2.2.3 Voltage positioning optimization formulation

The focus of this work is to maximize both the voltage margins and the availability of reactive reserves for the faster timescales i.e., position voltages within tighter bounds $\underline{V}$ and $\overline{V}$, and prioritize the use of mechanical (discrete) assets over more flexible reactive resources, q_{g}. Hence the objective minimizes a function of q_{g} and the voltage deviation terms for the upper and lower bounds, V_{v}^{+} and V_{v}^{-}, respectively. The VPO formulation is described next.

Given a radial, balanced, and single-phase equivalent representation of a distribution feeder, denote the VPO problem as (P1), which is expressed as a mixed-integer nonlinear program (MINLP) as follows:

$$\textbf{(P1)} \qquad \min_{q_{\mathrm{g},i}, n_m^{\mathrm{tr}}, n_i^{\mathrm{cp}}} \sum_{i=1}^{n} q_{\mathrm{g},i}^2 + \alpha_i (V_{\mathrm{v},i}^+ + V_{\mathrm{v},i}^-) \tag{4.22a}$$

subject to:

$$V = v_0 \mathbf{1}_n + M_{\mathrm{p}} p + M_{\mathrm{q}} q - Hl \tag{4.22b}$$

$$l_{ij} v_i = P_{ij}^2 + Q_{ij}^2 \qquad \forall (i,j) \in \mathcal{E} \tag{4.22c}$$

$$q = q_{\mathrm{g}} - Q_{\mathrm{L}} + Q^{\mathrm{cp}} \tag{4.22d}$$

$$0 = v_i - t_m^2 v_j \quad \forall m \in \mathcal{T} \tag{4.22e}$$

$$0 = t_m - (1 + \tau_m n_m^{\mathrm{tr}}) \quad \forall m \in \mathcal{T} \tag{4.22f}$$

$$0 = Q_i^{\mathrm{cp}} - v_i b_i \quad \forall i \in \mathcal{C} \tag{4.22g}$$

$$0 = b_i - y_{\mathrm{c},i} n_i^{\mathrm{cp}} \quad \forall i \in \mathcal{C} \tag{4.22h}$$

$$V_{\min} \leq V \leq V_{\max} \tag{4.22i}$$

$$\underline{V} - V_{\mathrm{v}}^- \leq V \leq \overline{V} + V_{\mathrm{v}}^+ \tag{4.22j}$$

$$V_{\mathrm{v}}^+ \geq 0, \ V_{\mathrm{v}}^- \geq 0 \tag{4.22k}$$

$$\underline{q_{\mathrm{g},i}} \leq q_{\mathrm{g},i} \leq \overline{q_{\mathrm{g},i}} \quad \forall i \in \mathcal{D} \tag{4.22l}$$

$$\underline{n_m^{\mathrm{tr}}} \leq n_m^{\mathrm{tr}} \leq \overline{n_m^{\mathrm{tr}}} \quad \forall m \in \mathcal{T} \tag{4.22m}$$

$$\underline{n_i^{\mathrm{cp}}} \leq n_i^{\mathrm{cp}} \leq \overline{n_i^{\mathrm{cp}}} \quad \forall i \in \mathcal{C} \tag{4.22n}$$

$$n_m^{\mathrm{tr}}, \, n_i^{\mathrm{cp}} \in \mathbb{Z} \quad \forall m \in \mathcal{T}, \forall i \in \mathcal{C} \tag{4.22o}$$

where $q_{\mathrm{g},i}$ is the DER reactive power generation at node i and $V_{\mathrm{v},i}^+$ and $V_{\mathrm{v},i}^-$ represents the voltage violation terms for the upper and lower bound respectively, at node

i. The parameter α is chosen to trade-off between the use of flexible reactive resources and maximizing voltage margins. The equality constraints (4.20) and (4.21) represent the power flow equations relating the voltages and currents in the network to the power injections, whereas (4.22d) represents the nodal reactive power balance, with Q_{L} being the reactive net-demand and $p = -P_{\mathrm{L}}$ with P_{L} being the active net-demand. The constraints (4.22e) and (4.22f) define the relation between the tap ratio and the tap position with $\tau_m \in \mathbb{R}$ being the tap step, whereas the limits in (4.22m) define bounds on OLTC tap position with $\underline{n_m^{\mathrm{tr}}}$ and $\overline{n_m^{\mathrm{tr}}}$ being the lower and upper tap position limit. The relation between capacitor bank admittance (b_i) and reactive power injected by capacitor banks (Q_i^{cp}) is given by (4.22g), whereas the relation between capacitor bank admittance and number of capacitor bank units with $y_{\mathrm{c},i} \in \mathbb{R}$ being the admittance of a single capacitor bank unit is given by (4.22h) and (4.22n) gives bounds on the capacitor bank units with $\underline{n_i^{\mathrm{cp}}}$ and $\overline{n_i^{\mathrm{cp}}}$ being the lower and upper bound on number of capacitor bank units. The box constraints in (4.22i) are the network voltage limits with $V_{\min}$ and $V_{\max}$ being the lower and upper network voltage limit. The constraint in (4.22j) represents the tighter voltage bound constraints that seek to position the voltage close to nominal using the tighter inner voltage bounds $\underline{V}$ and $\overline{V}$. This ensures that the reactive power resources are utilized to position the voltage within the tighter voltage bounds. The box constraints (4.22l) represents the DER reactive power generation limits for each generator node with $\underline{q_{\mathrm{g},i}}$ and $\overline{q_{\mathrm{g},i}}$ being the lower and upper limit on generation and finally, (4.22o) constrains the transformer tap positions and the number of capacitor bank units to be discrete set of integers.

(P1) represents the VPO problem for a radial distribution network. Note that nonlinear equality constraints (4.4), (4.22e) and (4.22g) and the integer constraint

(4.22o) represent non-convex constraints and make the OPF problem NP-hard. The nonlinearity related to the transformer taps and the bilinear term for the capacitor banks are approximated with piecewise linear (PWL) constraints as shown in the next section, whereas the nonlinearity due to the powerflow equations represented by (4.21) is dealt with through convex inner approximation illustrated in section 4.2.3

4.2.2.4 OLTC and capacitor bank modeling

Based on the transformer modeling in section 2.3.2, the voltage relation between the nodes across an OLTC is given by:

$$v_i = t_{m,0}^2 v_j + \sum_{p=1}^{K} \Delta v_p^m \tag{4.23a}$$

$$0 \leq \Delta v_p^m \leq s_p^m \overline{v} \Delta t_{m,p} \tag{4.23b}$$

$$\Delta t_{m,p}(v_j - (1 - s_p^m)\overline{v}) \leq \Delta v_p^m \leq \Delta t_{m,p} v_j \tag{4.23c}$$

$$s_{p+1}^m \leq s_p^m,\ p = 1, 2, \ldots, K - 1. \tag{4.23d}$$

Similarly, the realtion between capacitor bank admittance(b_i) and reactive power injected by capacitor banks (Q_i^{cp}) is given by:

$$Q_i^{\mathrm{cp}} = \sum_{p=1}^{K} Q_{i,p}^{\mathrm{s}} \tag{4.24a}$$

$$0 \leq Q_{i,p}^{\mathrm{s}} \leq u_p^i \overline{v} b_{i,p} \tag{4.24b}$$

$$b_{i,p}(v_i - (1 - u_p^i)\overline{v}) \leq Q_{i,p}^{\mathrm{s}} \leq v_i b_{i,p} \tag{4.24c}$$

$$u_{p+1}^i \leq u_p^i,\ p = 1, 2, \ldots, K - 1. \tag{4.24d}$$

Details about this OLTC and capacitor bank modeling can be found in section 2.3.2.

Based on the linear modeling of OLTCs and capacitor banks in this section, we now present the mixed-integer program to solve the voltage positioning problem with the piecewise linear formulation of OLTCs and capacitor banks as shown in (P2).

$$\textbf{(P2)} \qquad \min_{q_{\mathrm{g},i}, s_p, u_p} \sum_{i=1}^{n} q_{\mathrm{g},i}^2 + \alpha_i (V_{\mathrm{v},i}^{+} + V_{\mathrm{v},i}^{-}) \tag{4.25a}$$

$$\text{subject to: } (4.22b) - (4.22d), (4.22i) - (4.22o) \tag{4.25b}$$

$$(4.23a) - (4.23d), (4.24a) - (4.24d) \tag{4.25c}$$

The VPO problem presented in (P2) is convex in the continuous variables except for the nonlinear constraint in (4.22c). One possible solution is to employ convex relaxation techniques to the nonlinear constraints and obtain an SDP or SOCP formulation. However, several works in literature such as [163], have shown that employing convex relaxations with an objective that minimizes voltage deviations will lead to a non-zero duality gap. On the other hand, linearized OPF techniques, even though computationally efficient, do not provide guarantees on feasibility or bounds on optimality.

To overcome these challenges associated with the nonlinearity of the power flow equations, the next section describes the convex inner approximation method of the OPF problem.

4.2.3 FORMULATION OF THE CONVEX INNER APPROXIMATION

To obtain the convex inner approximation, the approach presented bounds the nonlinear terms in the power flow equations and develops an admissible model that is robust against modeling errors due to the nonlinearity. This means that the technique ensures that nodal voltages, branch power flows, and current magnitudes are within their limits at optimality.

The optimization problem (P2) is non-convex due to the constraint (4.21). In order to obtain an inner convex approximation of (P2), we bound the nonlinearity introduced due to (4.21). Let $l_{\min} \in \mathbb{R}^n$ and $l_{\max} \in \mathbb{R}^n$ be the lower and upper bound on $l \in \mathbb{R}^n$, respectively. Then based on these values and provided that the matrices D_R, D_X, M_p ,M_q and H are positive for an inductive radial network [166], define:

$$V^{+} := v_0 \mathbf{1}_n + M_{\mathrm{p}} p + M_{\mathrm{q}} q - H l_{\min} \tag{4.26}$$

$$V^{-} := v_0 \mathbf{1}_n + M_{\mathrm{p}} p + M_{\mathrm{q}} q - H l_{\max}. \tag{4.27}$$

If $l_{\min}$ and $l_{\max}$ are known, then the optimization problem (P2) can be modified to a convex inner approximation of the OPF problem. In the proceeding analysis we will provide a method to obtain an accurate representation of these bounds. In section 4.1, we provided conservative bounds on the nonlinearity based on worst case net-demand forecasts. In this section, we present rigorous analysis to obtain tighter lower and upper bounds on the nonlinearity using local bounds.

Consider the nonlinear term in the power flow equations given by (4.21). From the second-order Taylor series expansion, l_{ij} can be expressed as:

$$l_{ij} \approx l_{ij}^0 + \mathbf{J}_{\mathbf{ij}}^\top \delta_{\mathbf{ij}} + \frac{1}{2}\delta_{\mathbf{ij}}^\top \mathbf{H}_{\mathrm{e},\mathbf{ij}} \delta_{\mathbf{ij}} \tag{4.28}$$

where l_{ij}^0 is the value of l_{ij} at the forecast net-demand and $\delta_{\mathbf{ij}}$, the Jacobian $\mathbf{J}_{\mathbf{ij}}$ and the Hessian $\mathbf{H}_{\mathrm{e},\mathbf{ij}}$ are defined below.

$$\delta_{\mathbf{ij}} := \begin{bmatrix} P_{ij} - P_{ij}^0 \\ Q_{ij} - Q_{ij}^0 \\ v_i - v_i^0 \end{bmatrix} \qquad \mathbf{J}_{\mathbf{ij}} := \begin{bmatrix} \frac{2P_{ij}^0}{v_i^0} \\ \frac{2Q_{ij}^0}{v_i^0} \\ -\frac{(P_{ij}^0)^2+(Q_{ij}^0)^2}{(v_i^0)^2} \end{bmatrix} \tag{4.29}$$

$$\mathbf{H}_{\mathrm{e},\mathbf{ij}} := \begin{bmatrix} \frac{2}{v_i^0} & 0 & \frac{-2P_{ij}^0}{(v_i^0)^2} \\ 0 & \frac{2}{v_i^0} & \frac{-2Q_{ij}^0}{(v_i^0)^2} \\ \frac{-2P_{ij}^0}{(v_i^0)^2} & \frac{-2Q_{ij}^0}{(v_i^0)^2} & 2\frac{(P_{ij}^0)^2+(Q_{ij}^0)^2}{(v_i^0)^3} \end{bmatrix} \tag{4.30}$$

where the superscript 0, $(.)^0$, denotes the nominal values at the forecasted net demand for all variables (.) in (4.29) and (4.30). The eigenvalues of the Hessian $\mathbf{H}_{\mathrm{e},\mathbf{ij}}$ are all non-negative, with two of the eigenvalues being strictly positive and one is zero. As the Hessian is positive semi-definite, the nonlinear function l_{ij} is convex. If a function is convex then the linear approximation underbounds the nonlinear function [119], i.e.,

$$l_{ij} \geq l_{ij}^0 + \mathbf{J}_{\mathbf{ij}}^\top \delta_{\mathbf{ij}} =: l_{\min,ij} \qquad \forall (i,j) \in \mathcal{L} \tag{4.31}$$

The upper bound on the nonlinearity is obtained next and the convex inner approximation based on these bounds is presented. Applying Taylor's theorem to the expansion, the upper bound on the nonlinear function l_{ij} is given by:

$$
\begin{aligned}
|l_{ij}| &\approx |l^0_{ij} + \mathbf{J}^\top_{\mathbf{ij}}\delta_{\mathbf{ij}} + \frac{1}{2}\delta^\top_{\mathbf{ij}}\mathbf{H}_{\mathrm{e},\mathbf{ij}}\delta_{\mathbf{ij}}| && (4.32)\\
&\leq |l^0_{ij}| + |\mathbf{J}^\top_{\mathbf{ij}}\delta_{\mathbf{ij}}| + |\frac{1}{2}\delta^\top_{\mathbf{ij}}\mathbf{H}_{\mathrm{e},\mathbf{ij}}\delta_{\mathbf{ij}}| && (4.33)\\
&\leq l^0_{ij} + \max\{2|\mathbf{J}^\top_{\mathbf{ij}}\delta_{\mathbf{ij}}|, |\delta^\top_{\mathbf{ij}}\mathbf{H}_{\mathrm{e},\mathbf{ij}}\delta_{\mathbf{ij}}|\} =: l_{\max,ij} && (4.34)
\end{aligned}
$$

The conditions for the upper bound hold if we can neglect the third order term in (4.28), i.e., the expression is cubic order accurate or the order of accuracy is $\mathcal{O}(||\delta||^3_\infty)$. A comparison of the actual expression of l (calculated using (4.21)) with its second order Taylor approximation (calculated using (4.28)) in Fig. 4.17. From the figure, it is clear that the second-order Taylor approximation is sufficiently accurate over a wide range of DER operation (from -1000 kVAr to +1000 kVAr), which is much larger than the actual DER operation range used herein (i.e., from -100 kVAr to +100 kVAr).

Based on this upper and lower bound determined, we can now formulate the complete convex inner approximation VPO problem by modifying (P2) as:

$$
\textbf{(P3)} \qquad \min_{q_{\mathrm{g},i}, s_p, u_p} \sum_{i=1}^{n} q^2_{\mathrm{g},i} + \alpha_i(V^+_{\mathrm{v},i} + V^-_{\mathrm{v},i}) \tag{4.35a}
$$

$$
\text{subject to: } (4.26), (4.27), (4.31), (4.34) \tag{4.35b}
$$

$$
(4.23a) - (4.23d), (4.24a) - (4.24d) \tag{4.35c}
$$

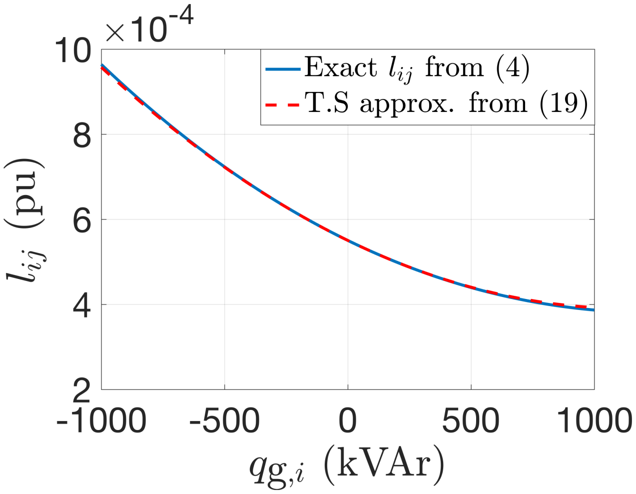

Figure 4.17: Comparison of the second-order Taylor series (T.S.) approximation from (4.28) of the updated manuscript with the original (nonlinear) expression of l *in (4.21) of the updated manuscript. In this experiment, the reactive power of DER at node* 2 *of the IEEE-13 node system is varied from -1000 to +1000 kVAr and the accuracy of the second-order approximation of* l_{ij} *branch* $(1,2)$ *is illustrated.*

$$V_{\min} \leq V^{-}; V^{+} \leq V_{\max} \tag{4.35d}$$

$$\underline{V} - V_{\mathrm{v}}^{-} \leq V^{-}; V^{+} \leq \overline{V} + V_{\mathrm{v}}^{+} \tag{4.35e}$$

$$(4.22d), (4.22k) - (4.22o) \tag{4.35f}$$

The optimization problem (P3) represents the convex inner approximation of the VPO problem that provides a network admissible solution. This formulation includes discrete mechanical assets resulting in mixed-integer linear program (MILP) Voltage Positioning Optimization problem.

4.2.3.1 Iterative algorithm for improving solution

In this section, we present an iterative algorithm that achieves tighter bounds on the non-linearity. The lower and upper bounds obtained in previous section can be conservative depending upon the initial net-demand forecast. Without Algorithm 1, if we only solved (P3) once, it could result in a conservative inner approximation, which would lead to reduced performance. This is because the operating point x_0 could be close to the no-load condition, i.e., $P^0_{ij} = Q^0_{ij} \approx 0$, which means that the Jacobian would be close to zero per (4.29) and the first-order estimate of $l_{\min}$ and $l_{\max}$ would be close to l_0 per (4.31) and (4.34). This results in conservative feasible set for (P3) and Algorithm 1 overcomes this by successively enhancing the feasible solutions by updating the operating point and the Jacobian (and the Hessian) with the optimized decision variables, sometimes called the convex-concave procedure [119]. Algorithm 1 shows the steps involved in the proposed iterative scheme, where $q^*_{\mathrm{g}}(k)$ and $Q^{\mathrm{cp}*}(k)$ represent the solution of (P3) for the kth iteration of Algorithm 1, whereas $q(k)$ represents the net-reactive power injection at iteration k. It is assumed that the initial operating point satisfies q_{g} and Q^{cp} both being zero and, hence, $q(0) = -Q_{\mathrm{L}}$. Finally the result of Algorithm 1 is given by the cumulative sum of the iterates, i.e., $q_{\mathrm{g}} = \sum_{i=1}^{k-1} q^*_{\mathrm{g}}(i)$, $Q^{\mathrm{cp}} = \sum_{i=1}^{k-1} Q^{\mathrm{cp}*}(i)$.

Algorithm 1: Successive feasible solution enhancement

```
Result: $q_{\mathrm{g}}$, $Q^{\mathrm{cp}}$, $n^{\mathrm{tr}}$
Input: $Q_{\mathrm{L}}$, $f(x_0)$, $\epsilon$
Run AC load flow with $q(0) = -Q_{\mathrm{L}} \Rightarrow \mathbf{J}(0), \mathbf{H}_{\mathrm{e}}(0)$
Initialize $k = 1$, $error(0) = \infty$
while $error(k-1) > \epsilon$ do
    Solve (P3) $\Rightarrow q^*_{\mathrm{g}}(k), Q^{\mathrm{cp}*}(k), n^{\mathrm{tr}*}(k), f(x^*_k)$
    Update $\sum_{i=1}^{k}(q^*_{\mathrm{g}}(i) + Q^{\mathrm{cp}*}(i)) - Q_{\mathrm{L}} \Rightarrow q(k)$
    Run AC load flow with $q(k) \Rightarrow \mathbf{J}(k), \mathbf{H}_{\mathrm{e}}(k)$
    Update $error(k) = ||f(x^*_k) - f(x^*_{k-1})||_\infty$
    $k := k + 1$
end
$q_{\mathrm{g}} = \sum_{i=1}^{k-1} q^*_{\mathrm{g}}(i)$, $Q^{\mathrm{cp}} = \sum_{i=1}^{k-1} Q^{\mathrm{cp}*}(i)$, $n^{\mathrm{tr}} = n^{\mathrm{tr}*}(k-1)$
```

Theorem 3 proves the feasibility and convergence of solutions obtained through Algorithm 1.

Theorem 3. *Every iterate of Algorithm 1 is AC feasible and the iterates converge to a locally optimal solution.*

Proof. Let χ be the feasible set of the underlying, nonconvex ACOPF from (P1) with convex objective function $f(.)$ given in (11a) and let $x_0 = \begin{bmatrix} P(p,q) & Q(p,q) & V(p,q) & l(p,q) \end{bmatrix}^\top$ be a feasible AC operating point, i.e., $x_0 \in \chi$, that depends on (p,q) injections. Also, define the feasible set of the convex inner approximation (P3) based on x_0 as $\Psi_0(x_0)$. Now, let x_1^* be the optimal solution of (P3), then $x_1^* \in \Psi_0(x_0)$ and $x_0 \in \Psi_0(x_0)$ and by definition of inner approximation $\Psi_0(x_0) \subseteq \chi$. Also since x_1^* is the optimal solution, then $f(x_1^*) \leq f(x_0)$. This process can be repeated so that, for the kth iteration ($k \in \mathbb{N}_+$), $\Psi_{k-1}(x_{k-1}^*) \subseteq \chi$ is the feasible set of (P3) and $x_k^* \in \Psi_{k-1}(x_{k-1}^*)$ is the optimal solution of (P3) with $f(x_k^*) \leq f(x_{k-1}^*)$. This implies that each iterate is an improved solution that is feasible and continuing this process yields a non-increasing sequence: $\{f(x_k^*)\}_{k\in\mathbb{N}_+}$ that is bounded below by zero (since $f(x) \geq 0 \; \forall x \in \chi$). Thus, by the greatest-lower-bound property of real numbers, we know $\inf_{k\in\mathbb{N}_+}\{f(x_k^*)\} \in [0, f(x_0)]$ exists. Since $\{f(x_k^*)\}_{k\in\mathbb{N}_+}$ is non-increasing and bounded below, by the monotone convergence theorem [167], $error(k) := ||f(x_k^*) - f(x_{k-1}^*)||_\infty \to 0$ as $k \to \infty$. Thus, we have proven that application of Algorithm 1 converges to an AC feasible, locally optimal solution, x^*, through a sequence of successively improved AC-feasible iterates, x_k^*, and that x^* improves on the original objective by $||f(x_1^*) - f(x^*)||_\infty$. □□□

Since the above problem is convex in the continuous variables, the MILP can be solved effectively and provide good feasible solutions [168]. The formulation (P3) minimizes the utilization of reactive power from flexible DERs, prioritizing mechanical assets as a result. The formulation positions the voltage within the tighter voltage bounds, close to nominal, while the voltage violation terms V_{v}^{+} V_{v}^{-} ensure feasibility of the solution.

In Section 4.2.4, simulations involving standard IEEE test networks, e.g., see [132], show that the results of this analysis holds for these radial distribution network. Simulation-based analysis is conducted on IEEE-13 node and IEEE-37 node system to check the validity of the approach on standard networks and analyze how tighter voltage bounds affect the utilization of DER reactive power at optimality.

4.2.4 Simulation Results

In this section, simulation tests are conducted on IEEE test cases and validation of the results is performed with Matpower [153] on a standard MacBook Pro laptop with 2.2 GHz of processor speed and 16 GB RAM. Simulation results illustrate the validity of the VPO problem (P3). The optimization problem is solved using GUROBI 8.0 [126], whereas the simulation is performed with AC load flows in Matpower. In all the simulation results, the system was solved to a MIP gap of under 0.01%.

For the IEEE-13 node shown in Fig. 4.18 and IEEE-37 node test case shown in Fig. 4.23, optimal reactive dispatch schedules from (P3) are fed to an AC load flow in Matpower. The IEEE-13 node test case is modified to include capacitor banks at nodes 7 and 11, besides having an OLTC connecting nodes 3 and 12. Each capacitor bank operates with 10 increments with each increment being 50 kVAr. Apart from these mechanical resources, DERs are placed at leaf nodes 5, 7, 8, 10, 11 and 12 with each DER $q_{\mathrm{g},i}$ at node i having a range of -100 to +100 kVAr. In all the test cases

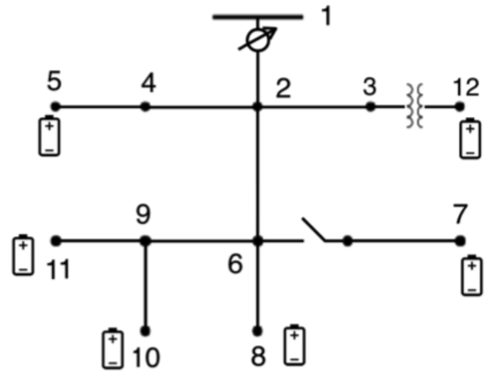

Figure 4.18: IEEE-13 node distribution network with added DERs at leaf nodes.

the value of α is chosen to be .001.

The comparison of the output voltages of the optimizer (upper and lower bounds) and the AC power flow solver over two iterations are shown in Fig. 4.19a and 4.19b respectively. The optimal value changes from 3.6414×10^{-6} (pu) to 3.196×10^{-6} (pu), while the OLTC tap position stays fixed at position 2. From the figures, it is shown that the actual voltages are within the determined bounds and the voltage bounds converge to the AC power flow solution.

In another simulation conducted on the IEEE-13 node system, we study the sensitivity on the reactive power utilization and the voltage violation term. Fig. 4.20a shows the variation in the total flexible reactive power consumption as the parameter α is varied, with the nominal value of α being highlighted. Similarly, Fig. 4.20b shows the change in the total voltage violation term as we sweep across α, illustrating that as α increases the voltage violation term reduces as expected.

Fig. 4.21a shows the variation of the total flexible reactive power as the lower

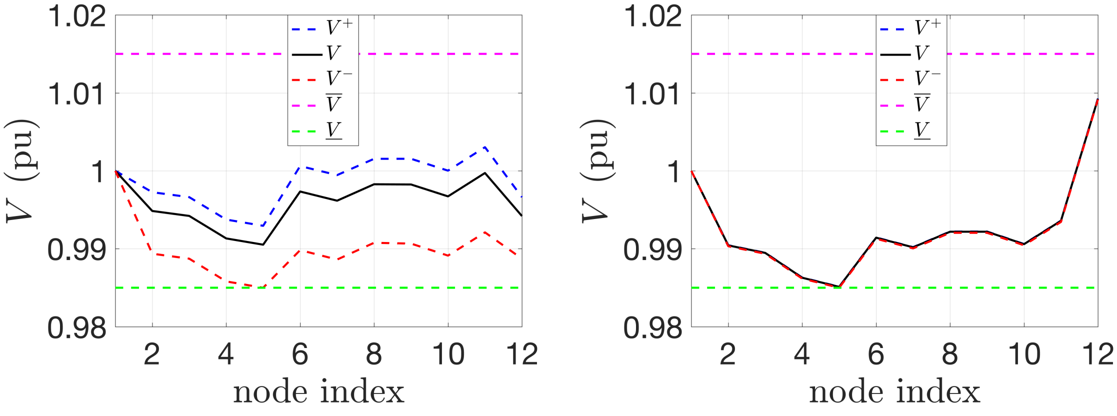

(a) (b)

Figure 4.19: (a) Comparison of the actual nodal voltage with the upper and lower bound voltages for the first iteration. (b) Comparison of the actual nodal voltage with the upper and lower bound voltages for the second iteration. The objective value changed from 3.614$\times10^{-}6$ *to 3.196* $\times10^{-}6$ *with a value of* α *chosen being* 0.001 *and the OLTC tap position at tap position 2 in both iterations.*

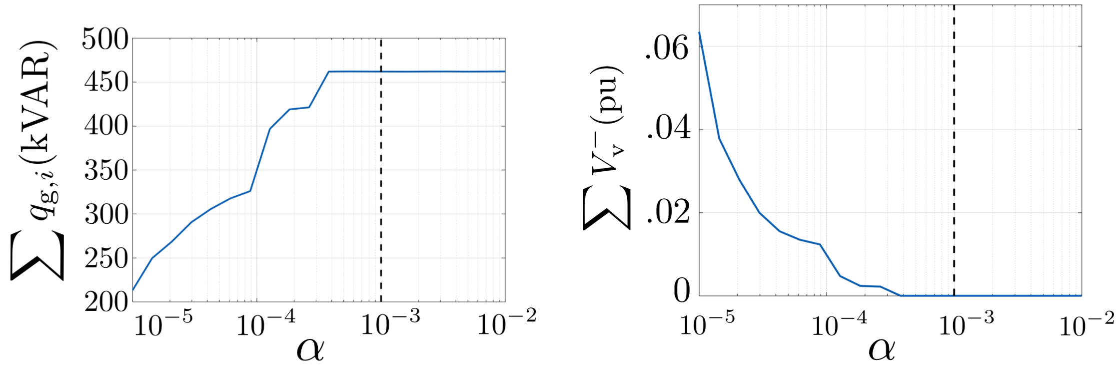

(a) (b)

Figure 4.20: (a) Variation in the total flexible reactive power consumption with change in α*, (b) Variation in the total lower voltage violation term with change in* α*.*

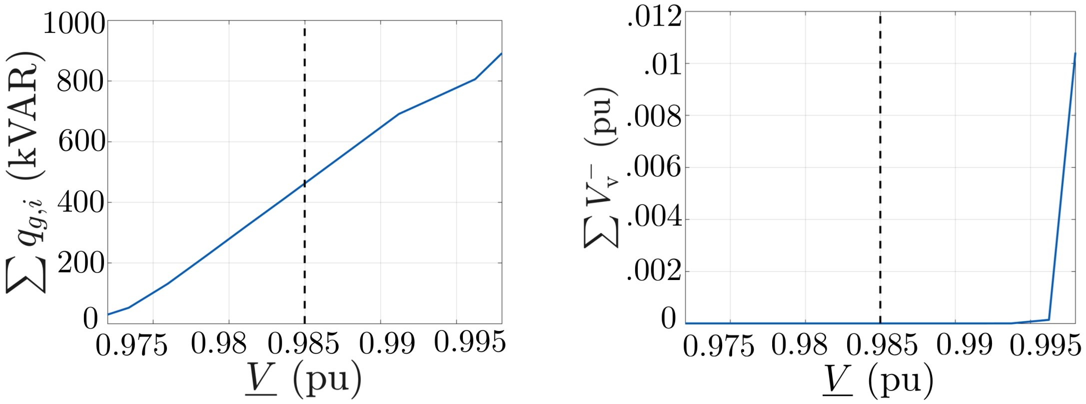

(a) (b)

Figure 4.21: (a) Variation in the total flexible reactive power consumption with change in $\underline{V}$, (b) Variation in the total lower voltage violation term with change in $\underline{V}$.

voltage bound is increased, showing the trade off between positioning voltage closer to nominal and the utilization of flexible reactive power resources, with the nominal value of $\underline{V}$ used being highlighted. Similarly, Fig. 4.21b shows the variation in the total voltage violation with the increase in the lower voltage bound, showing a similar trend.

Simulations are also conducted by considering a daily predicted 24-hour load profile shown in Fig. 4.22a obtained from real load data measured from feeders near Sacramento, CA during the month of August, 2012 [169]. Figure 4.22b shows the predicted aggregated reactive power supply from DERs over the horizon, whereas Fig. 4.22c shows the predicted aggregate cap bank reactive power supply, illustrates that as the load in the system increases, the aggregate utilization of reactive power from capacitor banks also increases and follows a similar trend. Figure 4.22d shows the optimal OLTC tap positions over the prediction horizon.

Fig. 4.24a shows the comparison between the reactive power supply between the

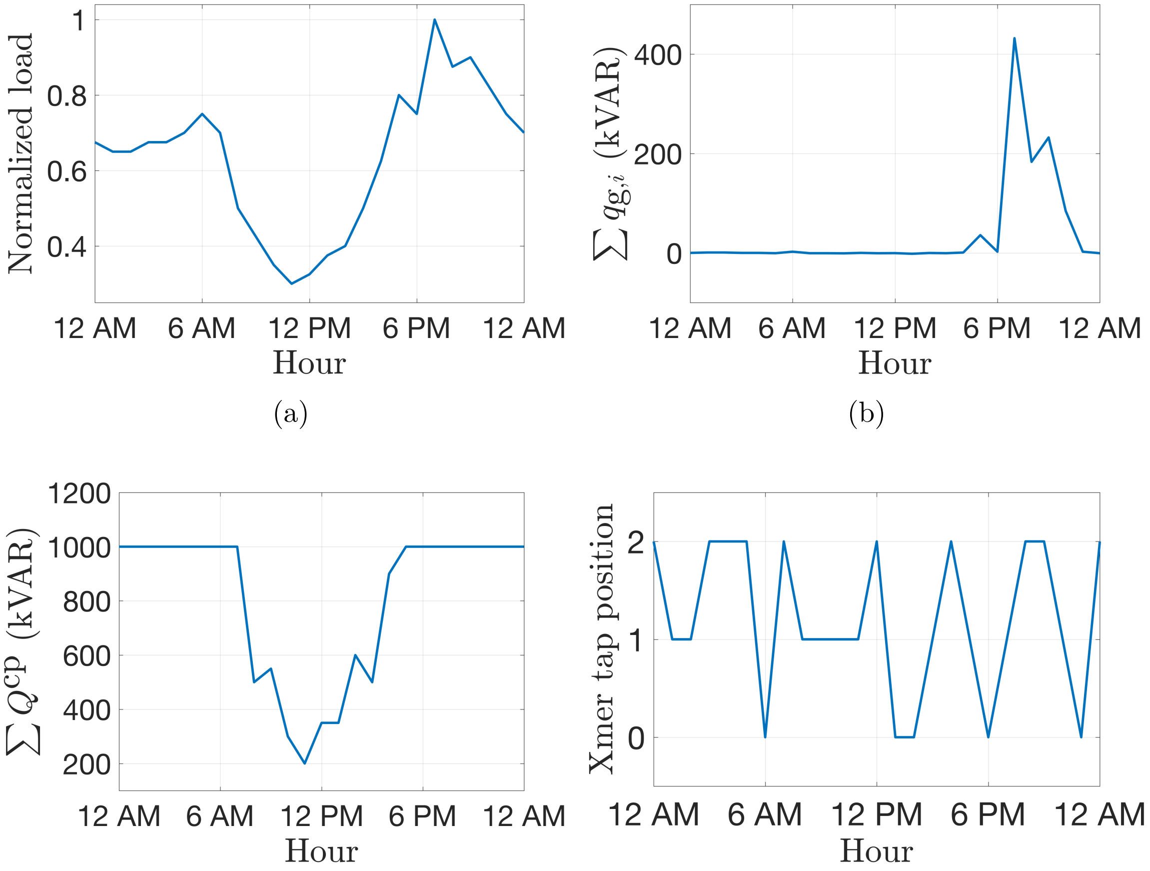

(a) (b)

(c) (d)

Figure 4.22: (a) Predicted 24-hour normalized load profile, (b) optimized schedule of aggregate reactive power from DERs utilized over the 24-hour horizon for IEEE-13 node system, (c) optimized schedule of the total reactive power from capacitor banks (at 1 p.u voltage) over the 24-hour horizon, (d) optimized OLTC tap position for IEEE-13 node system over the 24-hour horizon.

case using capacitor banks and the case without the use of capacitor banks, showing that capacitor banks supply part of the reactive power reducing the burden on DERs. Fig. 4.24b shows the comparison between the voltage violation terms between the case using capacitor banks and the case without capacitor banks, showing that the voltage violations are very small and hence the system violations are within the specified tighter voltage bounds.

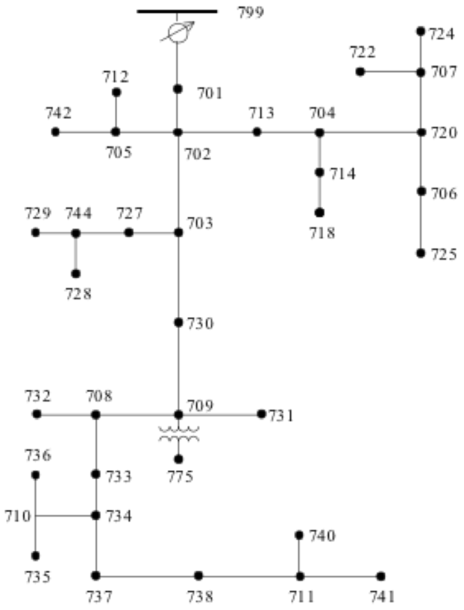

Figure 4.23: IEEE-37 node distribution network [11].

Further simulations are conducted on IEEE-37 node system shown in Fig. 4.23. In this case cap banks are positioned at nodes 724, 725, 728, 732, 736 and 741, whereas flexible DERs are placed at leaf nodes 714, 731, 734, 744 and 775 and the load profile shown in Fig. 4.22a is used. For the IEEE-37 node system also, each capacitor bank operates with 10 increments with each increment being 10 kVAr and each DER has a range of -100 to +100 kVAr. Similar results are observed with regards to the reduction in reactive power utilization from flexible resources with the

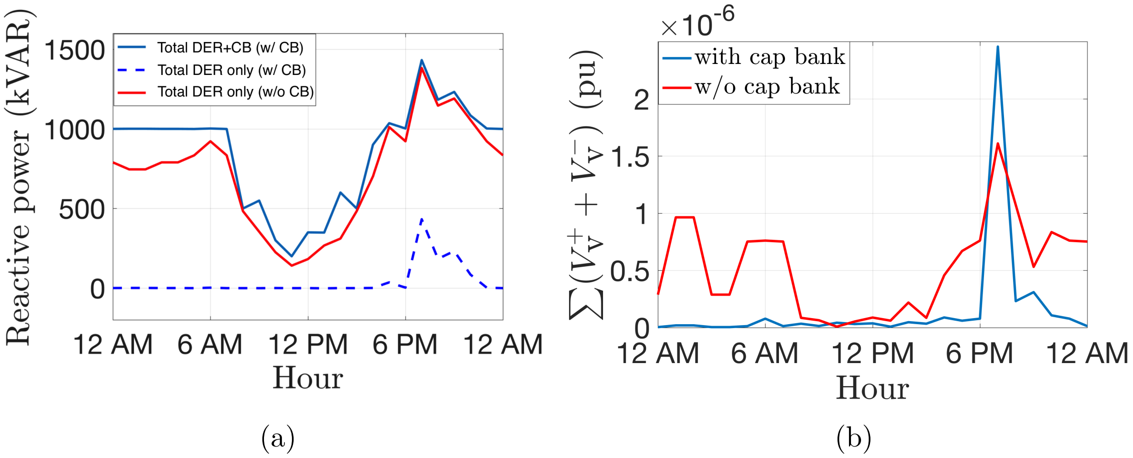

Figure 4.24: (a) Comparison of reactive power supply between the case using capacitor banks and without capacitor banks for IEEE-13 node system. The figure compares the total reactive power supply from DERs and cap banks (Total DER+CB (w/ CB)) with the reactive power supply only from DERs when cap banks are utilized (Total DER only (w/ CB)) and with DER reactive power supply when cap banks are not utilized (Total DER only (w/o CB)) , (b) Comparison of total voltage violation over time between the case using capacitor banks and without capacitor banks for IEEE-13 node system.

inclusion of capacitor banks as shown in Fig. 4.25a. Similarly, Fig. 4.25b shows the comparison of the voltage violation terms illustrating that the tighter voltage bounds are maintained. Further, Fig. 4.26a shows the optimal OLTC tap positions over the prediction horizon, whereas Fig. 4.26b shows the comparison between voltages obtained from the optimzer (upper and lower bound) and Matpower at node 775 of the IEEE-37 node system over the prediction horizon.

Finally, Fig. 4.27 shows the increase in solve time (over one iteration) as the number of devices increases in the network. It can be seen that the convex formulation scales well with the increase in problem size.

Through these simulation results, it is observed that the voltage positioning algorithm results in a network admissible solution that prioritizes the utilization of

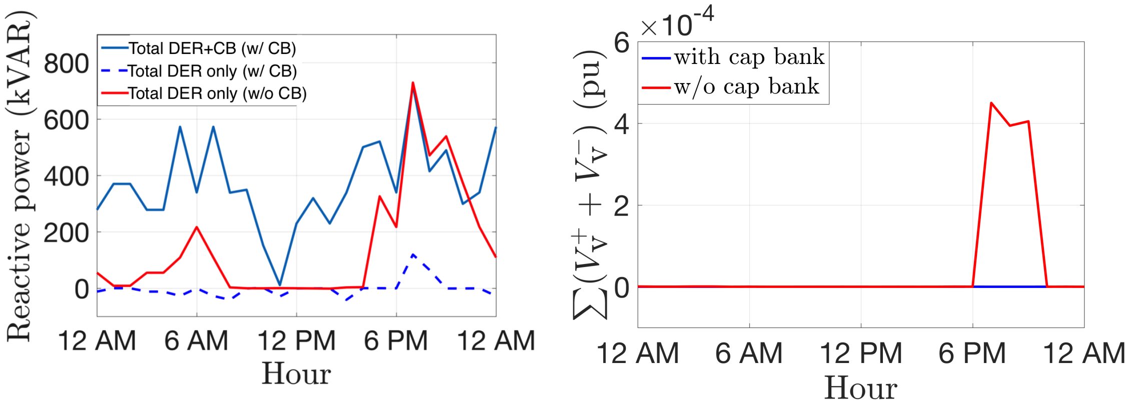

(a) (b)

Figure 4.25: (a) Comparison of reactive power supply between the case using capacitor banks and without capacitor banks for IEEE-37 node system. The figure compares the total reactive power supply from DERs and cap banks (Total DER+CB (w/ CB)) with the reactive power supply only from DERs when cap banks are utilized (Total DER only (w/ CB)) and with DER reactive power supply when cap banks are not utilized (Total DER only (w/o CB)) , (b) Comparison of total voltage violation over time between the case using capacitor banks and without capacitor banks for IEEE-37 node system.

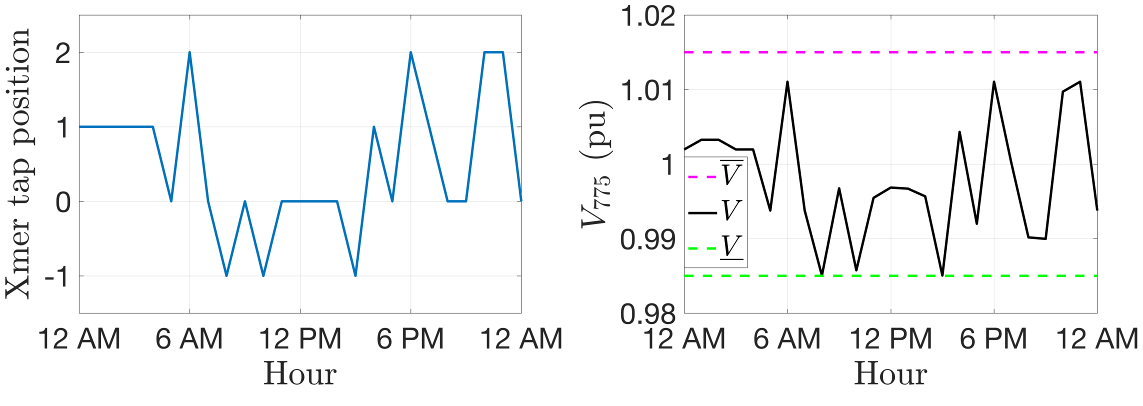

(a) (b)

Figure 4.26: (a) Predicted OLTC tap position for IEEE-37 node system over the 24-hour horizon. (b) Comparison of the actual nodal voltage at node 775 with the upper and lower bounds over a 24-hour horizon for IEEE-37 node system

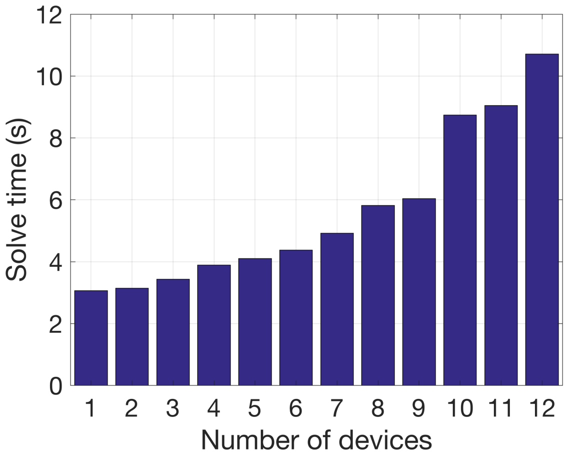

Figure 4.27: Solve time for IEEE-37 node system with number of devices (capacitor banks) in the network over one iteration.

mechanical assets over flexible resources to position the voltage close to nominal and hence could be utilized for voltage control of mechanical assets in distribution networks.

4.2.5 CONCLUSIONS

This section introduces a holistic voltage positioning algorithm to optimally schedule mechanical switching devices, such as on-load tap changing transformers and capacitor banks, together with more responsive DERs in a distribution grid. The optimization program makes maximum use of mechanical resources to position the voltage close to nominal using tighter inner voltage bounds to counter the predicted hourly variation of renewable generation. At the same time, the scheduling of responsive reactive resources from DERs is reduced, making them available at the faster time-scale to counter fast minute-to-minute variation inherent to renewable generation. The optimization problem is formulated as a MILP through an convex inner approximation of the OPF ensuring network admissible solutions. The optimization problem is validated via simulations on the IEEE-13 node and IEEE-37 node test feeders and the results are compared with AC load flows from Matpower. The results validate the approach.

4.3 Grid-aware aggregation and disaggregation of flexibility

Dispatching a large fleet of distributed energy resources (DERs) in response to wholesale energy market or regional grid signals requires solving a challenging disaggregation problem when the DERs are located within a distribution network. This work presents a computationally tractable convex inner approximation for the optimal power flow (OPF) problem that characterizes a feeders aggregate DERs hosting capacity and enables a realtime, grid-aware dispatch of DERs for radial distribution networks. The inner approximation is derived by considering convex envelopes on the nonlinear terms in the AC power flow equations. The resulting convex formulation is then used to derive provable nodal injection limits, such that any combination of DER dispatches within their respective nodal limits is guaranteed to be AC admissible. These nodal injection limits are then used to construct a realtime, open-loop control policy for dispatching DERs at each location in the network to collectively deliver grid services. The IEEE-37 distribution network is used to validate the technical results and highlight various use-cases.

4.3.1 Introduction

The distribution system was engineered under the assumption that residential and commercial customers would only have power directed to them from the bulk grid. However, the increasing penetration of solar PV in distribution feeders has created so-called “prosumers” who (at times) can supply the grid with energy rather than just consume it. This leads to *reverse power flows* that can result in unexpected violations of voltage and transformer constraints, which may negatively impact system reliability [109]. Furthermore, the significant variability inherent to solar PV generation challenges traditional distribution system operating paradigms. Furthermore, with ubiquitous connectivity, smart appliances and DERs behind the meter (BTM) will soon underpin a demand that becomes inherently flexible. The optimal power flow (OPF) represents an opportunity for algorithms to improve reliability and responsiveness of the grid and the dispatch of flexible resources (e.g., batteries, PV inverters). However, due to the sub-minutely timescale of the solar PV variability, these algorithms must be computationally tractable and, yet, representative of the physics. That is, grid optimization algorithms can ensure admissible network operations [88].

Since Carpentier's original OPF formulation [50] and subsequent improvements in optimization solvers, the OPF problem has become a powerful methodology for optimizing the dispatch of various grid resources. This is because OPF-based methods can account for the underlying grid physics, static network constraints on voltages and apparent branch flows, and resource limitations. However, it was also recognized early on that the nonlinear AC power flow equations that model the underlying grid physics render the AC OPF non-convex [97]. In many practical applications, guaranteeing network admissibility is more critical than finding the globally optimal solution.

The work herein presents a novel convex approximation of the AC OPF problem to quantify the network-admissible range of DER nodal injections. In general, obtaining a convex inner approximation is NP-hard [170], however, the work herein uses the nonlinear branch-flow model (BFM) formulation of the AC power flow equations to define a convex envelope on the nonlinear terms relating the branch current,

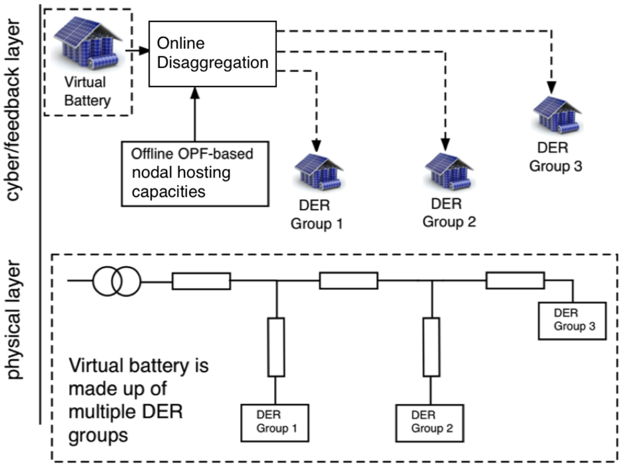

Figure 4.28: A schematic representation of the network model. The physical layer represents the circuit that connects the different DER groups into an aggregate virtual battery, whereas the cyber layer represents the disaggregation of the virtual battery market signal to the DER groups based on the nodal hosting capacities that are determined offline. VB image source: https://esdnews.com.au/

nodal voltages, and apparent power flows that is combined with the remaining linear relationships of the BFM to form a convex inner approximation. This convex inner approximation ensures that all feasible (and, hence, optimal) solutions in the convex OPF are also feasible in the non-convex AC OPF formulation. We denote such a solution as *network admissible* or *AC admissible.* From this approach, we achieve an OPF formulation that exhibits computational solve times similar to that of linear formulations with the added (and crucial benefit) that the formulation guarantees admissible solutions. This convex inner approximation is then utilized to determine the admissible DER dispatch ranges for nodes over a network, i.e., any combination of dispatching nodes across the network is admissible as long as each node is dispatched within its provided DER capacigy. This methodology represents a major shift in how to dispatch networked grid assets in distribution feeders and it overcomes practical limitations of methods that rely on repeatedly solving full, centralized AC OPFs at each time-step [171] or require extensive, realtime communication, grid data, and DER data [26].

The main contributions of this work are as follows:

- This work improves over section 4.2 to generalize a convex inner approximation of the AC OPF problem that is applicable to any radial, balanced distribution feeder, such as those with a mix of inductive and capacitive branches and with branch current and nodal voltage constraints.
- The generalized convex inner approximation is employed to optimize the feeder's DER nodal capacities, which represent the ranges of admissible injections for DERs at each node in the network such that all branch flows and nodal voltages are within limits (i.e., network admissible). Thus, the optimized DER nodal capacities can then be trivially aggregated to form the network's range of admissible flexibility. Provable guarantees are provided for admissibility over the entire range of DER nodal dispatch.
- Different reactive power DER control strategies are investigated to enlarge the range of a feeder's aggregate DER nodal capacity.
- The admissible DER nodal capacities are used within an open-loop, realtime disaggregation policy to account for network constraints while providing fast grid services.

The remainder of the section is organized as follows. Section 4.3.2 develops the mathematical formulation of the convex inner approximation for the OPF problem using the robust bounds on nonlinear terms. Section 4.3.3 provides admissibility guarantees for the obtained DER nodal capacity and proposes an iterative algorithm that enlarges the admissible range. In Section 4.3.4, we present and analyze the effect of different nodal reactive power control policies to enlarge the range of admissible flexibility for the feeder, whereas Section 4.3.5 describes a realtime dispatch policy that disaggregates flexibility over a network in an admissible manner using the DER nodal capacity obtained through the convex inner approximation. Finally, section 4.3.7 provides the conclusions.

4.3.2 FORMULATING THE CONVEX INNER APPROXIMATION

The nonlinear *DistFlow* model is often used to represent the underlying physics for a radial, balanced AC distribution network [27]. However, embedding this model within an AC OPF setting results in a non-convex formulation due to the nonlinear equations that map branch currents to branch power flows and nodal voltages. Common techniques that employ linear or convex relaxations are only valid under certain technical assumptions or near a pre-defined operating point. In this section, we develop a novel convex inner approximation of the AC OPF that is used to compute the range of allowable nodal net injections, such that any combination of nodal injections within those ranges are guaranteed to satisfy AC limits for voltages and branch flows.

4.3.2.1 Mathematical model

In this section we consider a radial distribution network modeled using the matrix notation as shown in section 2.2.1.

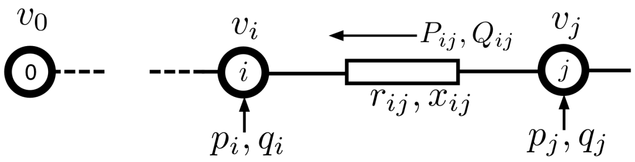

Figure 4.29: Nomenclature for a radial distribution network [6].

The goal of this work is to maximize the range of active power DER injections, p_g, from a given feasible operating point with $p_{\mathrm{g},j} = 0$, $q_{\mathrm{g},j} = 0\ \forall j \in \mathcal{N}$, such that all voltages v_j and currents l_{ij} are within their respective limits (i.e., $v_j \in [\underline{v}_j, \overline{v}_j]\ \forall j \in \mathcal{N}$ and $l_{ij} \in [\underline{l}_{ij}, \bar{l}_{ij}]\ \forall (i,j) \in \mathcal{L}$).

However, finding such a range is challenging due to the non-linear nature of (4.36c). For clarity, we provide definitions of the following key terms used in the manuscript.

Definition 1 (AC Admissibility)**.** *A solution of a convex OPF problem is AC admissible, if the solution applied to the original, non-convex AC OPF, which uses DistFlow, is feasible.*

Definition 2 (Nodal capacity)**.** *Nodal capacity is the range of AC admissible active power injections* $\Delta p_{g,j} := [p^-_{g,j}, p^+_{g,j}]\,\forall j \in \mathcal{N}$ *with lower and upper bounds* $p^-_{g,j} \leq 0$ *and* $p^+_{g,j} \geq 0$*, respectively. That is, for all nodes* j*, all injections* $p_{g,j} \in \Delta p_{g,j}$ *are AC admissible.*

In the next section we use a simple 3-node system to motivate the need for analyzing nodal capacity in distribution systems.

4.3.2.2 Motivating example on nodal capacity

Consider the 3-node system shown in Fig. 4.30. Each branch of the system has an impedance of $z = 0.55 + 1.33j$pu. Node 2 has a load injection $s_{\mathrm{L},2} = -0.02 +$

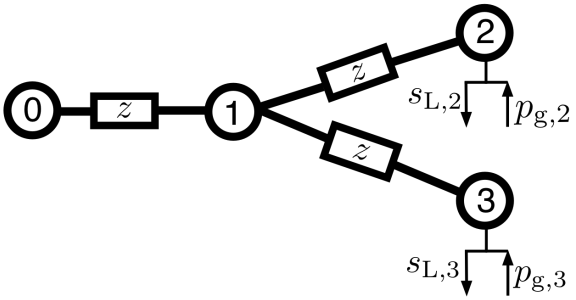

Figure 4.30: The 3-node network used as a motivating example.

$0.005j$pu and node 3 has a load injection $s_{\mathrm{L},3} = -0.015 + 0.001j$pu. Flexible resources $p_{\mathrm{g},2}$ and $p_{\mathrm{g},3}$ are assumed to be located at nodes 2 and 3. Only the active power of resources at nodes 2 and 3 is assumed to be controllable. Based on the sweep of power flow solutions obtained through Matpower [153], by varying $p_{\mathrm{g},2}$ and $p_{\mathrm{g},3}$, Fig. 4.31 shows the set of the AC OPF for the 3-node system. As can be seen from Fig. 4.31, the admissible set is non-convex and contains “holes”. Hence, it is important when dispatching $p_{\mathrm{g},2}$ and $p_{\mathrm{g},3}$, to choose the right trajectory in order to maintain AC admissibility. Fig. 4.31 shows that trajectory A is within the admissible set and, hence, the network voltages obtained as we traverse this dispatch trajectory, whereas Path B passes through a “hole” and results in voltage violations. Even though trajectory A is AC admissible it requires $p_{\mathrm{g},2}$ and $p_{\mathrm{g},3}$ to be coordinated (i.e., stay on the trajectory) to ensure admissibility, so they cannot be manipulated independently. This means that any changes in either requires a change in the other and, thus, they are not nodal capacities. This simple example shows the need to develop tools that determines nodal capacities for any radial, balanced network. Towards that objective, the next section develops a convex inner approximation of the non-convex *DistFlow* formulation.

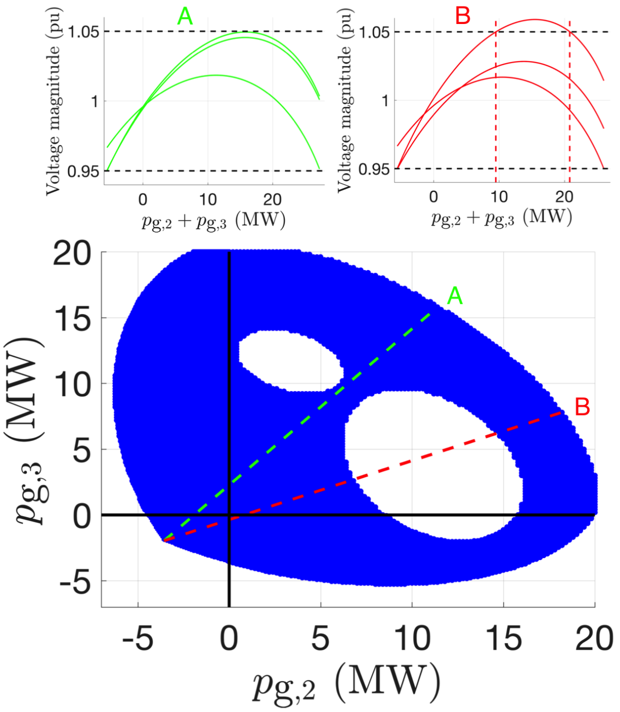

Figure 4.31: Analysis of 3-node motivating example. (Bottom) The set of admissible injections is non-convex with trajectories A and B showing admissible (green) and inadmissible (red) dispatch, respectively. (Top) Voltage profiles from sweeping $(p_{g,2}, p_{g,3})$ along admissible trajectory A and inadmissible trajectory B.

4.3.2.3 Convex Inner Approximation Preliminaries

In this section, we first present a compact matrix representation of the linear components as given in section 2.2.1. Then, we bound the nonlinear branch current terms, $l_{ij}(P_{ij}, Q_{ij}, v_j)$, by a convex envelope, which leads to a convex inner approximation of the *DistFlow* model.

First, define vectors $P := [P_{ij}]_{(i,j)\in\mathcal{L}} \in \mathbb{R}^N$, $Q := [Q_{ij}]_{(i,j)\in\mathcal{L}} \in \mathbb{R}^N$, $V := [v_i]_{i\in\mathcal{N}} \in \mathbb{R}^N$, $p := [p_i]_{i\in\mathcal{N}} \in \mathbb{R}^N$, $p_{\mathrm{g}} := [p_{\mathrm{g},i}]_{i\in\mathcal{N}} \in \mathbb{R}^N$, $P_{\mathrm{L}} := [P_{\mathrm{L},i}]_{i\in\mathcal{N}} \in \mathbb{R}^N$, $q := [q_i]_{i\in\mathcal{N}} \in \mathbb{R}^N$, $Q_{\mathrm{L}} := [Q_{\mathrm{L},i}]_{i\in\mathcal{N}} \in \mathbb{R}^N$, and $l := [l_{ij}]_{(i,j)\in\mathcal{L}} \in \mathbb{R}^N$ and matrices $R := \mathrm{diag}\{r_{ij}\}_{(i,j)\in\mathcal{L}} \in \mathbb{R}^{N\times N}$, $X := \mathrm{diag}\{x_{ij}\}_{(i,j)\in\mathcal{L}} \in \mathbb{R}^{N\times N}$, $Z^2 := \mathrm{diag}\{z_{ij}^2\}_{(i,j)\in\mathcal{L}} \in \mathbb{R}^{N\times N}$, and $A :=$

$[0_N \quad I_N]B - I_N$, where I_N is the $N \times N$ identity matrix and 0_N is a column vector of N rows. Then, directly applying [6], we get the following expression for P, Q, V:

$$V = v_0 \mathbf{1}_N + M_\mathrm{p} p + M_\mathrm{q} q - Hl, \tag{4.36a}$$

$$P = Cp - D_\mathrm{R} l, \qquad Q = Cq - D_\mathrm{X} l, \tag{4.36b}$$

$$l_{ij}[k] = \frac{|S_{ij}[k]|^2}{v_i[k]}, \quad \forall (i,j) \in \mathcal{E} \tag{4.36c}$$

where matrices $M_\mathrm{p} := 2C^T RC, \quad M_\mathrm{q} := 2C^T XC, \quad H := C^T(2(RD_\mathrm{R} + XD_\mathrm{X}) + Z^2)$ and $C := (I_N - A)^{-1}$, $D_\mathrm{R} := (I_N - A)^{-1}AR$, and $D_\mathrm{X} := (I_N - A)^{-1}AX$ describe the network topology and impedance parameters. Note that it is shown in section 2.2.1 that the matrix $(I_N - A)$ is non-singular for radial and balanced distribution networks. Furthermore, the convex inner approximation in section 4.2 is valid only for purely inductive, radial, and balanced networks. In the current manuscript, we extend the convex formulation to any radial and balanced network, including those with mixed inductive and capacitive branches.

Clearly, (4.36a) and (4.36b) represent linear relationships between the nodal power injections, (p, q), the branch power flows, (P, Q), and node voltages V. However, setting $l = 0$ and neglecting (4.36c), as done with the commonly used *LinDist approximation*, can result in overestimating the nodal capacities [166]. Next, we present methods for bounding the nonlinearity $l_{ij}(P_{ij}, Q_{ij}, v_j)$ from above and below.

Based on the description of voltages in (4.36a) and branch flows in (4.36b), denote l_lb and l_ub as lower and upper bounds on l. Then, we can define the corresponding upper $(.)^+$ and lower $(.)^-$ bounds of P, Q and V as follows:

$$P^+ := Cp - D_\mathrm{R} l_\mathrm{lb} \tag{4.37a}$$

$$P^- := Cp - D_\mathrm{R} l_\mathrm{ub} \tag{4.37b}$$

$$Q^+ := Cq - D_{\mathrm{X}_+} l_\mathrm{lb} - D_{\mathrm{X}_-} l_\mathrm{ub} \tag{4.37c}$$

$$Q^- := Cq - D_{\mathrm{X}_+} l_\mathrm{ub} - D_{\mathrm{X}_-} l_\mathrm{lb} \tag{4.37d}$$

$$V^+ := v_0 \mathbf{1}_n + M_\mathrm{p} p + M_\mathrm{q} q - H_+ l_\mathrm{lb} - H_- l_\mathrm{ub} \tag{4.37e}$$

$$V^- := v_0 \mathbf{1}_n + M_\mathrm{p} p + M_\mathrm{q} q - H_+ l_\mathrm{ub} - H_- l_\mathrm{lb}, \tag{4.37f}$$

where D_{X_+} and H_+ include the non-negative elements of D_X and H, respectively, and D_{X_-} and H_- are the corresponding negative elements. For example, if the network is purely inductive, then $D_{\mathrm{X}_-} = H_- = 0$ and the formulation reduces to the one presented in [141]. These upper and lower bounds in (4.37) satisfy $P^- \leq P \leq P^+$, $Q^- \leq Q \leq Q^+$ and $V^- \leq V \leq V^+$. Note that the bounds $l_\mathrm{lb}, l_\mathrm{ub}$ in (4.37) effectively allow us to neglect the nonlinear (4.36c). Thus, if we can find convex representations of these bounds, the corresponding OPF formulation will be a convex inner approximation. This is described next.

Equation (4.37) provides a linear formulation for bounding the AC power flow equations in terms of bounds $l_\mathrm{lb}, l_\mathrm{ub}$ and controllable injections. This was first presented in [141], where bounds $l_\mathrm{lb}, l_\mathrm{ub}$ were derived based on a nominal operating point and used to maximize voltage margins with mechanical grid assets (e.g., LTCs and capacitor-banks). Next, we summarize the derivation of these bounds and leverage them to formulate a novel convex inner approximation of the AC OPF to determine the nodal capacities for any radial, balanced network.

Based on any nominal or predicted operating point $x^0_{ij} := \mathrm{col}\{P^0_{ij}, Q^0_{ij}, v^0_j\} \in \mathbb{R}^3$, the second-order Taylor series approximation for (4.36c) can be expressed as:

$$l_{ij} \approx l^0_{ij} + \mathbf{J}^\top_{\mathbf{ij}} \delta_{\mathbf{ij}} + \frac{1}{2} \delta^\top_{\mathbf{ij}} \mathbf{H}_{\mathrm{e},\mathbf{ij}} \delta_{\mathbf{ij}} \tag{4.38}$$

where $l^0_{ij} := l_{ij}(P^0_{ij}, Q^0_{ij}, v^0_j)$ are branch current flows at the operating point and $\delta_{\mathbf{ij}}(P_{ij}, Q_{ij}, v_j, x^0_{ij}) := \mathrm{col}\{P_{ij}, Q_{ij}, v_j\} - x^0_{ij}$ and the Jacobian $\mathbf{J_{ij}}$ and the Hessian $\mathbf{H}_{\mathrm{e},\mathbf{ij}}$ are defined accordingly and detailed in [141]. Specifically, [141] shows that $\mathbf{H}_{\mathrm{e},\mathbf{ij}}$ is positive semi-definite, which, together with (4.38), means that the lower and upper bounds of l_{ij} for all $(i, j) \in \mathcal{L}$ are given by:

$$l_{ij} \geq l^0_{ij} + \mathbf{J_{ij+}}^\top \delta^-_{\mathbf{ij}} + \mathbf{J_{ij-}}^\top \delta^+_{\mathbf{ij}} =: l_{\mathrm{lb},ij} \tag{4.39}$$

$$l_{ij} \leq l^0_{ij} + \max\{2|\mathbf{J_{ij+}}^\top \delta^+_{\mathbf{ij}} + \mathbf{J_{ij-}}^\top \delta^-_{\mathbf{ij}}|, \psi_{\mathbf{ij}}\} =: l_{\mathrm{ub},ij}, \tag{4.40}$$

where $\mathbf{J_{ij+}}$ and $\mathbf{J_{ij-}}$ includes the positive and negative elements of $\mathbf{J_{ij}}$, $\delta^+_{\mathbf{ij}} := \delta_{\mathbf{ij}}(P^+_{ij}, Q^+_{ij}, v^+_j, x^0_{ij})$ and $\delta^-_{\mathbf{ij}} := \delta_{\mathbf{ij}}(P^-_{ij}, Q^-_{ij}, v^-_j, x^0_{ij})$, and $\psi_{\mathbf{ij}} := \max\{(\delta_{\mathbf{ij}}{}^{+,-})^\top \mathbf{H}_{\mathrm{e},\mathbf{ij}} (\delta_{\mathbf{ij}}{}^{+,-})\}$, which represents the largest of eight possible combinations of $P/Q/v$ terms in $\delta_{\mathbf{ij}}$ with mixed $+, -$ superscripts. Note that from (4.39), the lower bound $l_{\mathrm{lb},ij}$ may become negative, however, we know from physics that $l_{ij} \geq 0$, which means the $l_{\mathrm{lb},ij}$ may be overly conservative. To alleviate this shortcoming, Algorithm 1 in Section 4.3.3.2 presents an iterative approach that improves the nodal capacity. Thus, from (4.37), (4.39) and (4.40) we have a convex inner approximation of *DistFlow* that can be used to determine the nodal capacities.

4.3.2.4 Optimizing DER nodal capacity

The bounds from (4.39) and (4.40) allow us to omit (4.36c) entirely and replace the original variables P, Q, and V with their corresponding upper and lower bounds $(.)^+$ and $(.)^-$ in (4.37). Since $(.)^+$ and $(.)^-$ are outer approximations, using them in an OPF formulation results in a feasible set that is contained in the original, non-convex AC OPF, which means that (P1) below represents a convex inner approximation and can be used to determine nodal hosting capacities:

$$\text{(P1)} \quad \min_{p_{\mathrm{g},i}, q_{\mathrm{g},i}} \sum_{i=1}^{N} f_i(p_{\mathrm{g},i}) \tag{4.41}$$

$$\text{s.t.} \quad (4.37a) - (4.37f), (4.39), (4.40) \tag{4.42}$$

$$p = p_{\mathrm{g}} - P_{\mathrm{L}} \quad q = q_{\mathrm{g}} - Q_{\mathrm{L}}, \tag{4.43}$$

$$\underline{V} \leq V^-(p,q) \quad V^+(p,q) \leq \overline{V} \tag{4.44}$$

$$l_{\mathrm{ub}} \leq \bar{l} \quad \underline{q_{\mathrm{g}}} \leq q_{\mathrm{g}} \leq \overline{q_{\mathrm{g}}} \tag{4.45}$$

where (4.44) and (4.45) ensure that any feasible dispatch p_{g} from (P1) satisfies nodal voltages and branch flows in the original AC OPF based on *DistFlow* model. To determine the nodal capacity (i.e., the range $[p^-_{\mathrm{g},i}, p^+_{\mathrm{g},i}]$ of admissible net injections at each node i), we must solve (P1) once for the lower range, p^-_{g}, and once for the upper range, p^+_{g}. Thus, the objective function components, $f_i(p_{\mathrm{g},i})$, must be designed to engender $p^-_{\mathrm{g},i}$ and $p^+_{\mathrm{g},i}$. For example, to compute $p^-_{\mathrm{g},i}$, we can choose $f_i(p_{\mathrm{g},i}) := \alpha_i p_{\mathrm{g},i}$ and, for $p^+_{\mathrm{g},i}$, we can designate $f_i(p_{\mathrm{g},i}) := -\alpha_i p_{\mathrm{g},i}$, where α_i is the relative priority of nodal capacity at node i. Clearly, the choice of objective function determines how flexibility is allocated over the network nodes, e.g., choosing objective function such as $\pm\alpha_i \log(p_{\mathrm{g},i})$ could result in a different allocation of nodal capacity over the nodes as compared with $\pm\alpha_i p_{\mathrm{g},i}$. The design of the objective function represents an interesting future extension into energy policy and incentive mechanism and rate design [172].

While (P1) ensures AC admissibility at the nodal capacity values, it is natural to consider what happens when the nodal flexibility is below the rated capacity. That is, are all injections within the hosting capacity range guaranteed to be admissible across all the nodes? The next section answers this question by providing analytical guarantees of admissibility for the nodal hosting capacity, Δp_{g}, and then presents an iterative algorithm to successively improve Δp_{g}.

4.3.3 Analysis of convex inner approximation

In this section, we analyze (P1) and prove that any $p_{\mathrm{g}} \in \Delta p_{\mathrm{g}}$ is network admissible.

4.3.3.1 Admissibility guarantees

To prove admissibility claims below, we only present nodal voltages (as the case of branch flows is similar). Theorem 4 shows that the range Δp_{g} obtained through (P1) results in an AC admissible load flow solution.

Theorem 4. *Under conditions C1)* $\frac{\partial V^+}{\partial p_{g,i}} \geq 0$*, C2)* $\frac{\partial V^-}{\partial p_{g,i}} \geq 0$, $\forall i \in \mathcal{N}$*, if* Δp_g *is the DER nodal capacity obtained via (P1), then* $\forall p_g \in \Delta p_g$ *and* $p(p_g) = p_g - P_L$*, we have*

$$\underline{V} \leq V^-(p) \leq V(p) \leq V^+(p) \leq \overline{V},$$

where $V(p)$ *represents the actual nodal voltages from DistFlow model.*

Proof. Consider two cases: Case 1: $0 \leq p_{\mathrm{g}} \leq p_{\mathrm{g}}^{+}$; and Case 2: $0 \geq p_{\mathrm{g}} \geq p_{\mathrm{g}}^{-}$.

Proof of Case 1: Using (4.37e) at p_{g}^{+} yields:

$$V^{+}(p^{+}) = v_0 \mathbf{1}_n + M_{\mathrm{p}} p^{+} + M_{\mathrm{q}} q^{+} - H_{+} l_{\mathrm{lb}} - H_{-} l_{\mathrm{ub}} \leq \overline{V} \tag{4.46}$$

where $p^{+} = p_{\mathrm{g}}^{+} - P_{\mathrm{L}}$ and $q^{+} = q_{\mathrm{g}}^{+} - Q_{\mathrm{L}}$. Now, consider any $p_{\mathrm{g}} \in \Delta p_{\mathrm{g}}$ such that $0 \leq p_{\mathrm{g}} \leq p_{\mathrm{g}}^{+}$ and using C1, then

$$V^{+}(p) = v_0 \mathbf{1}_n + M_{\mathrm{p}} p + M_{\mathrm{q}} q^{+} - H_{+} l_{\mathrm{lb}}(p) - H_{-} l_{\mathrm{ub}}(p) \leq \overline{V} \tag{4.47}$$

where $p = p_{\mathrm{g}} - P_{\mathrm{L}}$. The actual voltage according to (4.36a) at p is

$$V(p) = v_0 \mathbf{1}_n + M_{\mathrm{p}} p + M_{\mathrm{q}} q^{+} - H_{+} l(p) - H_{-} l(p) \tag{4.48}$$

Then, subtracting (4.47) from (4.48) gives:

$$V^{+}(p) - V(p) = H_{+}\left(l(p) - l_{\mathrm{lb}}(p)\right) + H_{-}\left(l(p) - l_{\mathrm{ub}}(p)\right) \tag{4.49}$$

Using (4.39) and (4.40) we get, $l_{\mathrm{lb}}(p) \leq l(p) \leq l_{\mathrm{ub}}(p)$ and that $V^{+}(p) - V(p) \geq 0 \implies V(p) \leq V^{+}(p) \leq \overline{V}$.

Proof of Case 2: Using (4.37f) at p_{g}^{-} yields:

$$V^{-}(p^{-}) = v_0 \mathbf{1}_n + M_{\mathrm{p}} p^{-} + M_{\mathrm{q}} q^{-} - H_{+} l_{\mathrm{ub}} - H_{-} l_{\mathrm{lb}} \geq \underline{V} \tag{4.50}$$

where $p^{-} = p_{\mathrm{g}}^{-} - P_{\mathrm{L}}$ and $q^{-} = q_{\mathrm{g}}^{-} - Q_{\mathrm{L}}$. Now, consider any $p_{\mathrm{g}} \in \Delta p_{\mathrm{g}}$ such that

$0 \geq p_{\mathrm{g}} \geq p_{\mathrm{g}}^{-}$ and C2, then

$$V^{-}(p) = v_0 \mathbf{1}_n + M_{\mathrm{p}} p + M_{\mathrm{q}} q^{-} - H_{+} l_{\mathrm{ub}}(p) - H_{-} l_{\mathrm{lb}}(p) \geq \underline{V} \tag{4.51}$$

where $p = p_{\mathrm{g}} - P_{\mathrm{L}}$. The actual voltage according to (4.36a) at p is

$$V(p) = v_0 \mathbf{1}_n + M_{\mathrm{p}} p + M_{\mathrm{q}} q^{-} - H_{+} l(p) - H_{-} l(p) \tag{4.52}$$

Then, subtracting (4.51) from (4.52) gives:

$$V^{-}(p) - V(p) = H_{+} \left(l(p) - l_{\mathrm{ub}}(p) \right) + H_{-} \left(l(p) - l_{\mathrm{lb}}(p) \right) \tag{4.53}$$

Using (4.39) and (4.40) we get, $l_{\mathrm{lb}}(p) \leq l(p) \leq l_{\mathrm{ub}}(p)$, and that $V^{-}(p) - V(p) \leq 0 \implies V(p) \geq V^{-}(p) \geq \underline{V}$. Case 1 and Case 2 complete the proof. □□□

Theorem 4 significantly improves over the result provided in [141], since it guarantees that the full range, Δp_{g}, is admissible rather than just the solutions, p_{g}^{+} and p_{g}^{-}. Importantly, this is *exactly* why Δp_{g} can be used to represents the nodal hosting capacity. As with any convex inner approximation, the results can be conservative. Thus, in the next section, a new iterative algorithm is presented that successively increases the nodal capacity.

4.3.3.2 Iterative Algorithm for nodal capacity improvement

The lower and upper bounds obtained in section 4.3.2.3 can be conservative initially depending upon the nominal operating point, x^0. Without Algorithm 2, when we solve (P1) to determine p_{g}^{+} and p_{g}^{-}, the nodal capacities can be significantly underestimated.

This is because the operating point x^0 in certain situations could be such that, $P_{ij}^0 = Q_{ij}^0 \approx 0$, which means that the Jacobian would be close to zero and the first-order estimate of $l_{\mathrm{lb},ij}$ and $l_{\mathrm{ub},ij}$ would be close to l_{ij}^0 per (4.39) and (4.40). Algorithm 2 overcomes this by successively improving the operating point and the Jacobian (and Hessian) based on each optimal solution. This successive approach is related to the convex-concave procedure [173]. Algorithm 2 outlines the steps involved in the proposed scheme.

Algorithm 2: Successive enhancement of DER nodal capacity Δp_{g} (unity power factor case)

```
Result: Admissible range $\Delta p_{\mathrm{g}} = [p_{\mathrm{g}}^-, p_{\mathrm{g}}^+]$
Input: $P_L, Q_L \in \mathbb{R}^N$, convex $f_i(p_{\mathrm{g},i})$ $\forall i \in \mathcal{N}$, and $\epsilon > 0$
Run Load flow w/ $P_L, Q_L, p_{\mathrm{g}}(0) = 0 \Rightarrow \mathbf{J}(0), \mathbf{H}_{\mathrm{e}}(0)$
for $m = 1:2$ do
    if $m = 1$ then
        $p_{\mathrm{g},i} \to p_{\mathrm{g},i}^+$, Cond($i$)$\to$ Check $\frac{\partial V^+}{\partial p_{\mathrm{g},i}} \geq 0 \quad \forall i \in \mathcal{N}$
    else
        $p_{\mathrm{g},i} \to p_{\mathrm{g},i}^-$, Cond($i$)$\to$ Check $\frac{\partial V^-}{\partial p_{\mathrm{g},i}} \geq 0 \quad \forall i \in \mathcal{N}$
    end
    Initialize $k = 1$, $error(0) = \infty$
    while $\exists i$, s.t. Cond(i) holds $\wedge$ $error(k-1) > \epsilon$ do
        for $i = 1:N$ do
            if Cond(i) does not hold then
                Set $p_{\mathrm{g},i}(k) = 0$
            end
        end
        Solve (P1) $\Rightarrow p_{\mathrm{g},i}(k), f_i(p_{\mathrm{g},i}(k)),\ \forall i \in \mathcal{N}$
        Run load flow w/ $P_L - p_{\mathrm{g}}(k), Q_L \Rightarrow \mathbf{J}(k), \mathbf{H}_{\mathrm{e}}(k)$
        Update Cond($i$) $\forall i \in \mathcal{N}$
        Update error:
        $error(k) = \max_{i \in \mathcal{N}} |f_i(p_{\mathrm{g},i}(k)) - f_i(p_{\mathrm{g},i}(k-1))|$
        $k \to k + 1$
    end
end
```

Next, we apply Algorithm 2 to the motivating example from Fig. 4.30 to present how the nodal capacity is improved. Note that reactive power net injections, $q_{\mathrm{g},i}$, are decision variables in (P1), however, in the proceeding analysis and simulations, we set $q_{\mathrm{g},i} = 0$.[2] Later in Section 4.3.4, we analyze the role of reactive power strategies in enabling greater DER nodal capacities. For the sake of simplicity, we neglect the branch limit constraint (4.45) in (P1) and assume an oversized substation transformer, which is a common practice in the US. The focus is on voltage because that is often the primary concern of utilities in the US [174]. However, the formulation in (P1) and the analysis therein hold for branch limit constraints as well. Future work will analyze and provide simulation results on this extension.

If Algorithm 2 is applied to determine p_{g}^{+} and p_{g}^{-} without considering C1 and C2 (i.e, omit lines 12-14 in Algorithm 2), then the admissible set for $p_{\mathrm{g},2}$ and $p_{\mathrm{g},3}$ is shown by the blue region in Fig. 4.32. When the conditions C1 and C2 are considered in Algorithm 2, then the green region in Fig. 4.32 is the admissible set. As can be seen from the figure, the green region is a convex set that is contained in the blue set as expected from being a convex inner approximation. The successive iterative solutions obtained through Algorithm 2 are also marked in Fig. 4.32. It is clear from the non-convex nature of the blue set that operating in that region would require coordination between different nodes in order to ensure AC admissibility (i.e., to stay on the piecewise linear trajectory provided by the iterates with the black dotted line in Fig. 4.32). On the other hand, since the green set is a hypercube, no coordination between nodes is necessary in order to guarantee AC admissibility. Due to these reasons, further analysis in this work will consider this hypercube AC admissible region only. The

---

[2] For this manuscript, any mechanical devices such as tap-changers, capacitor banks and switches are assumed to be fixed at their nominal values and are not part of the optimization problem.

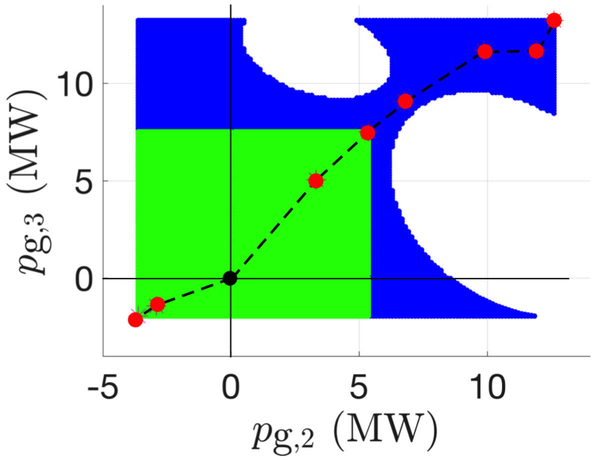

Figure 4.32: The set of admissible injections for the 3-node network is non-convex (blue). Algorithm 2 can find maximal admissible injections via iterations (red dots), but monotonicity conditions $C1$ and $C2$ in Theorem 4 define the convex inner approximation (green), which gives nodal capacity Δp_g.

analysis shown here provides a mechanism to update the operating point to achieve larger DER nodal capacity.

Remark 7. ***AC power flow solvability:*** *The analysis presented herein assumes that the AC power flow equations for radial networks are solvable, i.e., there exists a unique solution. Previous works in literature such as [175] and [176] have studied the conditions for the existence and uniqueness of solutions to AC power flow equations in radial networks. The solvability of the AC power flow equations is also closely related to the voltage collapse phenomenon [177] and thus has great theoretical and practical significance. Incorporating the power flow solvability into convex inner approximation formulation is an important extension that will be considered in future works.*

Next, we present Case Study 1, which employs Algorithm 2 to determine the solar PV hosting capacity for a distribution network.

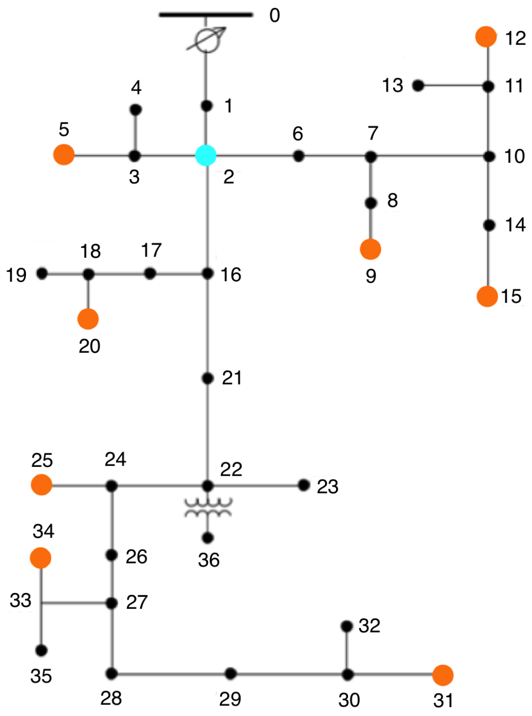

Figure 4.33: Single-phase version of the IEEE-37 node distribution network from [11].

Case study 1

Algorithm 2 is applied to the IEEE-37 node distribution feeder shown in Fig. 4.33 for three different scenarios to determine $p^{+}_{\mathrm{g},i}$. In this context, $p^{+}_{\mathrm{g},i}$ can effectively be considered the solar PV hosting capacity.

The three different scenarios are specified in Table 4.3. In scenarios A (linear objective) and B (logarithmic objective), the solar PV units may be installed at the leaf nodes with the largest demand, whereas in scenario C (linear objective), solar PV is only allowed at node 702 (e.g., utility-scale solar PV array). The optimization problem (P1) is solved with Gurobi 9.1 in Julia 1.1 in less than 1 sec and the solution is validated with Matpower [153] on a standard MacBook Pro laptop with 2.2GHz

Table 4.3: PV hosting capacity scenarios

Scenario	Nodes with PVs	Objective function
A	$\{5, 9, 12, 15, 20, 25, 31, 34\}$	$f_i(p_{\mathrm{g},i}) = -p_{\mathrm{g},i}$
B	$\{5, 9, 12, 15, 20, 25, 31, 34\}$	$f_i(p_{\mathrm{g},i}) = -\log(p_{\mathrm{g},i})$
C	$\{2\}$	$f_i(p_{\mathrm{g},i}) = -p_{\mathrm{g},i}$

CPU and 16GB RAM. The comparison of the resulting solar PV hosting capacity from each scenario using Algorithm 2 is shown in Fig. 4.34a, with the stacked bars showing the hosting capacity at the different nodes with DERs in the system. It can be seen that having a single centralized solar unit allows greater total solar PV capacity as compared to the distributed cases. The reason for this is that Scenario C has fewer network limit constraints to consider than the distributed case. This can be seen from Fig. 4.34b which shows voltages obtained for the three scenarios at the first iteration PV hosting capacity and after repeated iterations through Algorithm 2. As can be seen from the figure, voltages are at their upper limit at multiple nodes for scenarios A and B, but only at the head-node (node 2) for scenario C. As a result, the distributed case (case A and B) has more active constraints and hence more conservative solution as compared to the case with a single central PV (case C). Furthermore, scenario B favors a more equitable allocation (log objective) that results in smaller net solar PV capacity ($\sum_i p_{\mathrm{g},i}$), leading to reduced overall performance as compared to scenario A. The results show the admissibility of the PV hosting capacity solution both by using (P1) once or repeatedly through Algorithm 2.

Remark 8 (Adapting analysis to distribution planning)**.** *It is important to note that the nodal capacity in this network can incorporate both generation (*$p_g^+ > 0$*) and flexible demand (*$p_g^- < 0$*), but that* Δp *is with respect to a particular operating*

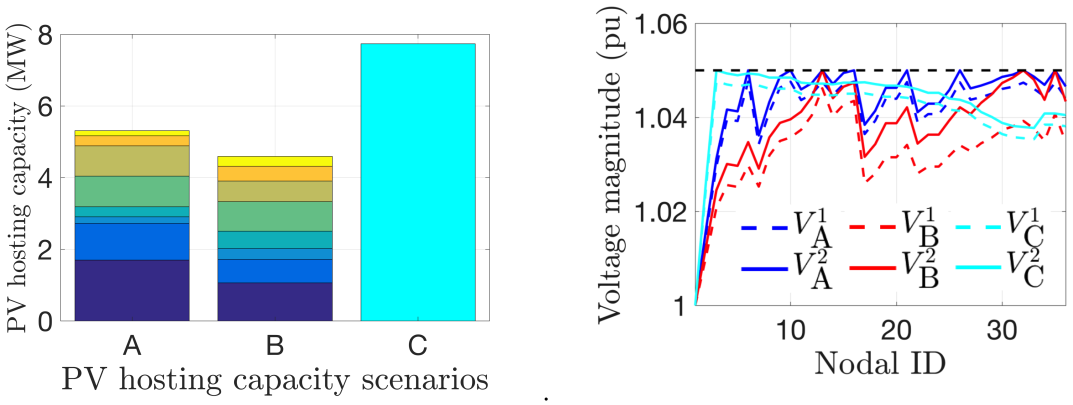

(a)

(b)

Figure 4.34: Case study 1 on IEEE-37 node network for the three PV scenarios. (a) Shows the feeder's solar PV hosting capacity with Algorithm 2. (b) illustrates admissibility of PV hosting capacity via voltage profiles, where V_A^1, V_B^1, V_C^1 results from first iteration and V_A^2, V_B^2, V_C^2 are from final iteration of Algorithm 2.

point, (P_L, Q_L). This is different from conventional PV hosting capacity studies that consider a representative annual, hourly demand profile [174]. In future work, we will adapt (P1) and Algorithm 2 for multi-hour planning problems and incorporate battery storage and flexible demand to determine the "dynamic hosting capacity" of a feeder from quasi-static timeseries (QSTS) demand profiles.

The analysis and simulation results presented in case study 1 have used $q_g = 0$, e.g., unity power factor solar PV arrays. However, the role of reactive power management in optimizing DER nodal capacities is important and the focus of the next section.

4.3.4 ROLE OF REACTIVE POWER

Reactive power, q_g, can be utilized to increase the nodal capacity, $[p_g^-, p_g^+]$. Different reactive power control schemes are analyzed in this section. Specifically, we will compare between DERs that are operated at unity power factor, fixed power factor, and those with reactive power control capability, where the power factor is allowed to vary according to advanced inverter capabilities, such as IEEE Standard 1547 [178]. The different reactive power schemes along with the relevant relations between q_{g} and p_{g} are provided in Table 4.4. For each particular scheme, the corresponding constraints are added to (P1) when determining the nodal capacity.

Fig. 4.35a compares the feeder's solar PV hosting capacities, $\sum_i p^{+}_{\mathrm{g},i}$, resulting from the different reactive power schemes applied to Scenario A of Case Study 1. The stacked bar chart in Fig. 4.35a also shows the hosting capacity at the different nodes with DERs in this system. Scheme UPF represents the hosting capacity with unity power factor, which matches the result from Scenario A in Fig. 4.34a and serves as the base-case for comparison. Scheme LAG employs a lagging power factor of 0.95 ($\gamma_i = -0.33$), while LEAD uses a leading power factor of 0.95 ($\gamma_i = +0.33$). Scheme QVP employs a common volt-VAr policy with $\beta^0_i = 0$ and $\beta^1_i = -0.073$, while QCON represents advanced inverter capability with quadratic constraints and $\bar{S}_{\mathrm{g},i} = 2\mathrm{MVA}$ and a minimum power factor of 0.95. The results show that for scheme LEAD, the hosting capacity is reduced while schemes LAG, QCON and QVP increase hosting capacity. In LEAD, this is due to reactive power injections increasing with active power injections resulting in larger v and, hence, reduces p^{+}_{g}. The opposite occurs in the other schemes. Interestingly, QCON achieves the same nodal capacity as LAG at minimum power factor (0.95). This shows that reactive power scheme in QCON chooses the minimum power factor injection in order to maximize nodal capacity. The voltage profiles at the hosting capacities for the different schemes are compared in Fig. 4.35b and are clearly AC admissible.

Table 4.4: DER reactive power schemes

Scheme	Description	Constraint $(g_i(p_{\mathrm{g},i}, q_{\mathrm{g},i}, v_i))$
UPF	Unity power factor	$q_{\mathrm{g},i} = 0$
LAG	Lagging power factor	$q_{\mathrm{g},i} = -\gamma_i p_{\mathrm{g},i}$
LEAD	Leading power factor	$q_{\mathrm{g},i} = \gamma_i p_{\mathrm{g},i}$
QVP	Volt-VAr policy	$q_{\mathrm{g},i} = \beta_i^0 + \beta_i^1 v_i$
QCON	Quadratic constraint	$p_{\mathrm{g},i}^2 + q_{\mathrm{g},i}^2 \leq \overline{S}_{\mathrm{g},i}^2$

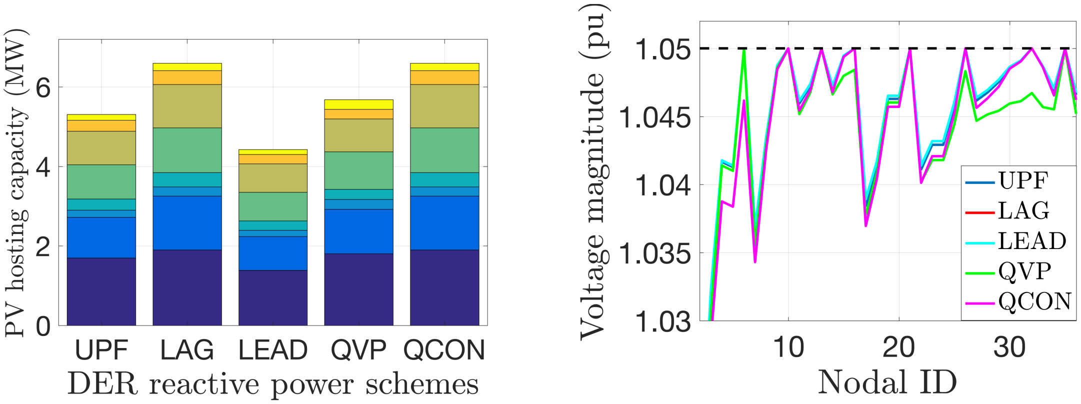

(a) (b)

Figure 4.35: Reactive power schemes for case Study 1 (Scenario A) on the IEEE-37 node network for five different reactive power schemes: (a) Solar PV hosting capacity for each reactive power scheme after employing Algorithm 2 (b) Illustrating admissibility with voltage profiles for the final iterate from Algorithm 2.

The next section employs the nodal capacities, $\Delta p_{\mathrm{g},i}$, to develop a simple, open-loop, decentralized DER control policy for the realtime, grid-aware disaggregation of a (net) demand reference signal. This turns the whole feeder into a responsive grid resource with *a-priori* AC admissibility guarantees that can provide fast grid services in wholesale markets.

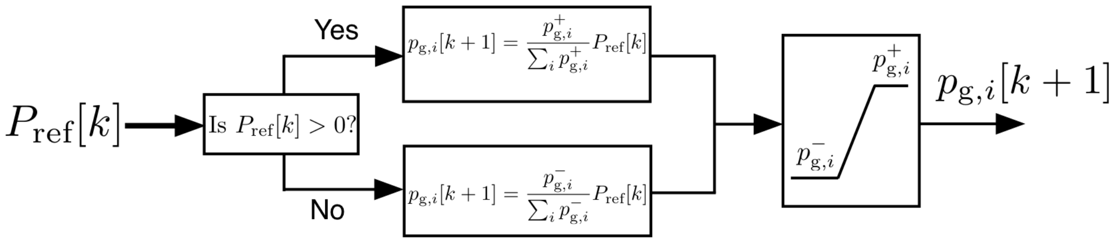

Figure 4.36: Realtime open-loop, proportional nature of disaggregation of flexibility at an aggregator. The aggregator only requires the market signal to be tracked from the ISO and does not need to coordinate with other aggregators in order to ensure network AC admissibility. This is achieved through the saturation block that ensures the nodal flexibility within the admissible range $p^+_{g,i}$ and $p^-_{g,i}$.

4.3.5 REALTIME GRID-AWARE DISAGGREGATION

Dispatching a set of networked DERs in response to a fast, time-varying wholesale market signal while guaranteeing admissible operations is challenging. However, it is necessary to solve this problem before aggregators can safely coordinate millions of behind-the-meter DERs without jeopardizing reliability of the grid. Thus, after computing the available nodal capacity (offline), as shown in Fig. 4.28, this section proposes a simple, grid-aware controller to allocate the required flexibility among the available resources in the network (i.e., disaggregate the signal) in realtime. The realtime disaggregation mechanism is shown in Fig. 4.36.

The necessary parameters to execute the realtime, grid-aware disaggregation in Fig. 4.36 are $p^+_{\mathrm{g},i}$ and $p^-_{\mathrm{g},i}$ and can be updated every 15-60 minutes by the grid operator running Algorithm 2, which is the timescale of the baseline of the aggregate uncontrollable net-demand.

The realtime disaggregation can then be solved as shown in Fig. 4.36 by a DER aggregator to provide fast grid service without the need to include *any* information about the underlying grid parameters. That is, the nodal capacities embed the AC OPF constraints to simplify the aggregator's dispatch. The next case study shows the effectiveness of the proposed disaggregation technique in having DERs collectively respond to grid service signals while guaranteeing AC admissibility.

Case study 2

The effectiveness of the offline Algorithm 2 and the online disaggregation shown in Fig. 4.36 is illustrated in a second case study with the IEEE-37 node system where we use the nodal capacities defined by Scenario A. The case study shows that the feeder is being managed within its limits at all times despite providing a large range of flexibility from the responsive DERs. Fig. 4.37a shows a reference grid service signal and the aggregate response from dispatching the DERs. It can be seen that the reference market signal is tracked well when the reference is within the admissible range and the grid-aware dispatch is AC-admissible as shown in Fig. 4.37b. In a practical setting, the DER aggregator should only offer what can be delivered, but the case study is meant to illustrate how the realtime dispatch is grid-aware and how the nodal capacities can be used to easily define the admissible range. Clearly, if the aggregator was not grid aware and just coordinated DERs to ensure perfect tracking, then such a "greedy" version of the realtime DER control leads to violations in network voltages, as seen by the blue dots in Fig. 4.37b. Thus, the proposed open-loop control scheme is grid-aware and scalable across a network of DERs by just broadcasting a single scalar grid service reference.

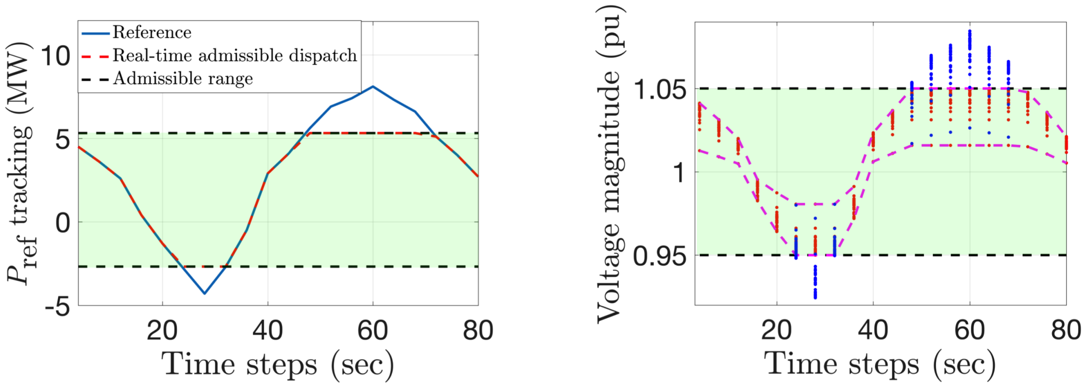

(a) (b)

Figure 4.37: Case study 2: (a) tracking performance of the realtime disaggregation policy shown in Fig. 4.36 for IEEE-37 node system (b) Voltage profile of the IEEE-37 node network over the time steps showing the admissibility of the solution when following the disaggregation policy (red) and voltage violations when following the greedy approach (blue). The greedy approach results in a maximum voltage violation of 0.03 *pu at time-step* 60.

4.3.6 SENSITIVITY ANALYSIS

The above analysis on hosting capacity is based on the assumption that the system parameters such as the line impedance and uncontrollable demand are accurate and known to the distribution system operator (DSO). However, in practice, often times these parameter values are either not known or are mis-recorded. Hence, in practice, an estimate of these parameter values is used to solve the optimization problem. For the 3-node network shown in Fig. 4.30, the changes in the admissible set as the uncontrollable demand is reduced is depicted in Fig. 4.38. It shows how the admissible set changes with changes in uncontrollable demand. Similar results are obtained for the case when the impedance values are varied as depicted in Fig. 4.39 for increase in impedance values of 1%, 5%, 10% and 20%.

As depicted by the changing admissible set and the fact that these estimated

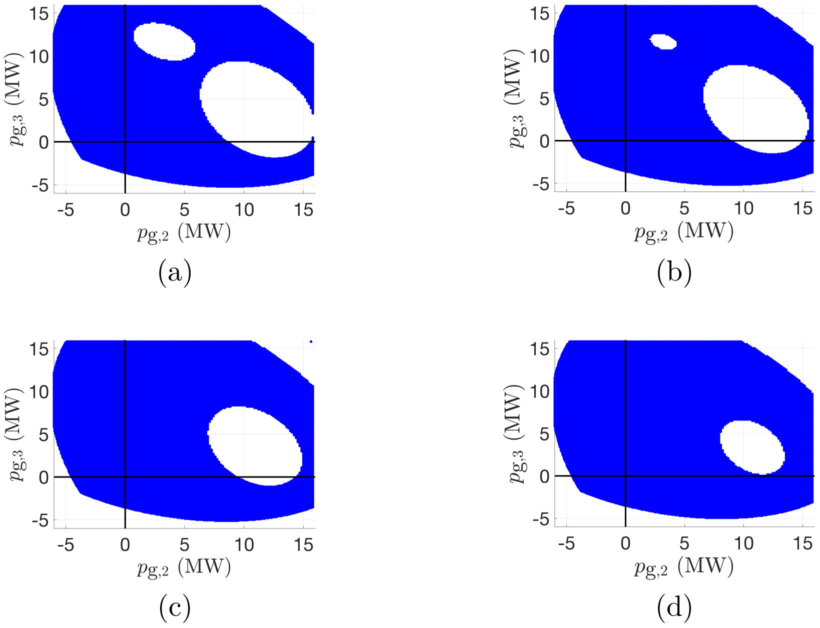

(a) (b) (c) (d)

Figure 4.38: Admissible set for 3-node system when demand is reduced by: (a) +1%; (b) +5%; (c) +10%; (d) +20%.

parameter values can be inaccurate, it is important to determine the sensitivity of the hosting capacity results to changes in system parameters (line impedances and uncontrollable demand). To achieve this, we vary the demand and impdedance values over a uniform distribution of 1%, 5%, 10% and 20%. Sampling over this distribution, we calculate the changes in hosting capacity at node i as:

$$\text{\% hosting capacity change (i)} = \frac{HC_{\mathrm{uni},i} - HC_{\mathrm{base},i}}{HC_{\mathrm{base},i}} \times 100 \tag{4.54}$$

where $HC_{\mathrm{uni},i}$ is the hosting capacity at node i obtained when the system parameter values are sampled from a uniform distribution and $HC_{\mathrm{base},i}$ is the base case hosting capacity at node i.

Simulation results for the sensitivity analysis are conducted on the IEEE-37 node

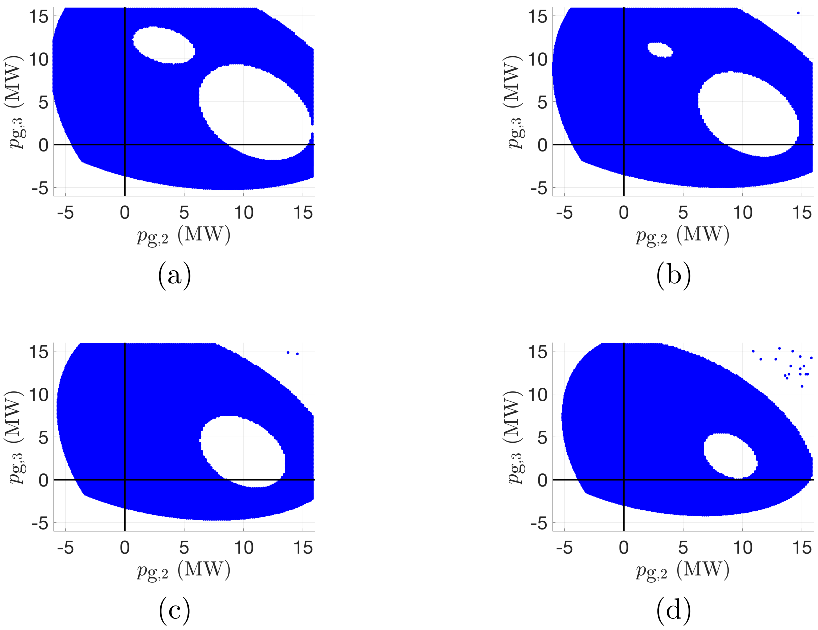

Figure 4.39: Admissible set for 3-node system when impedance is increased by: (a) +1%; (b) +5%; (c) +10%; (d) +20%.

system shown in Fig. 4.33 under Scenario A with PV units having unity power factor placed at leaf nodes only. Figure 4.40 shows the histogram of the distribution of change in uncontrollable active and reactive demand, illustrating that it belongs to a uniform distribution. Corresponding to this distribution in uncontrollable demand, Fig. 4.41 shows the histogram of percentage change in nodal hosting capacities resulting from the change in demand. We also plot the distribution of the aggregate change in hosting capacity, calculated as:

$$\% \text{ hosting capacity change} = \frac{HC_{\text{uni}} - HC_{\text{base}}}{HC_{\text{base}}} \times 100 \tag{4.55}$$

where HC_{uni} is the aggregate hosting capacity obtained when the system parameter values are sampled from a uniform distribution and HC_{base} is the base case hosting capacity. The histogram of the aggregate hosting capacity change is shown in Fig. 4.42.

Next we also conduct sensitivity analysis for the hosting capacity problem to the changes in line impedance values. Figure 4.43 shows the histogram of the change in resistance and reactance values of the IEEE-37 node system, illustrating that they belong to a uniform distribution. Sampling from this distribution, Fig. 4.44 shows the histogram of the percentage change in nodal hosting capacities resulting from the variation in the line impedance values, whereas Fig. 4.45 shows the histogram of the change in aggregate hosting capacities.

The mean and standard deviation of the changes in nodal hosting capacities is shown in Table 4.5, whereas these values for changes in aggregate hosting capacity is given in Table 4.6. From these values we can obtain a rule of thumb metric for changes in nodal hosting capacity, e.g., a background demand change of $x\%$ results in nodal hosting capacity change with standard deviation of $\frac{x}{10}\%$. In case of change in impedance, this metric is around $\frac{x}{2}\%$. Similar metrics can be calculated for the aggregate hosting capacity.

Remark 9. *From the results in Table 4.5 and 4.6, it can be seen that the nodal hosting capacity is not super-sensitive to the changes in background demand. This implies that we do not need to update the nodal hosting capacities at a fast timescale. An update every 5 minutes would be reasonable. Future work will further investigate the relationship between input and output uncertainty in distribution networks through uncertainty quantification.*

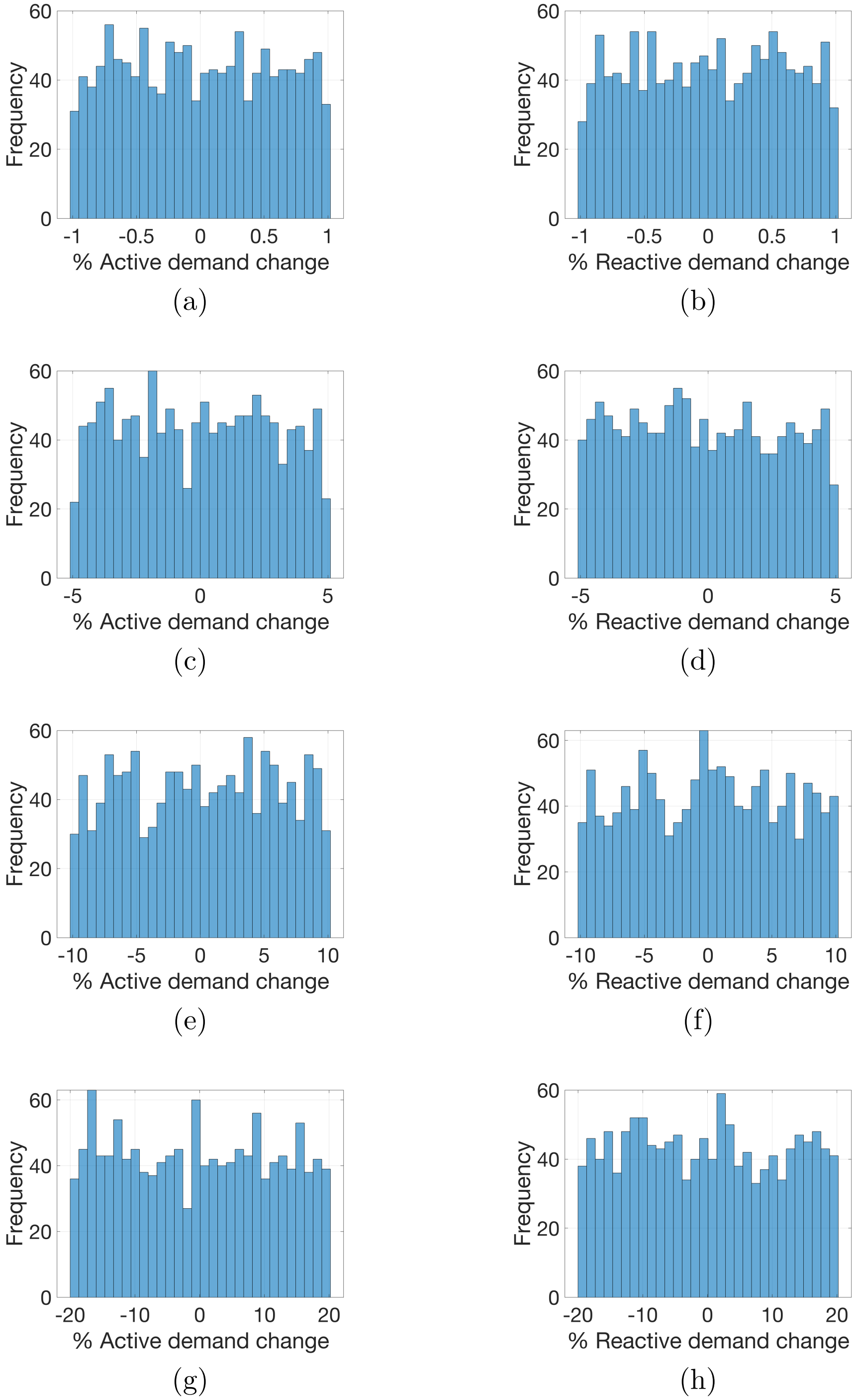

Figure 4.40: Histograms of the percentage change in active and reactance demand values resulting from variation in demand in a uniform distribution of : (a), (b) 1% error; (c), (d) 5% error; (e), (f) 10% error; (g), (h) 20% error.

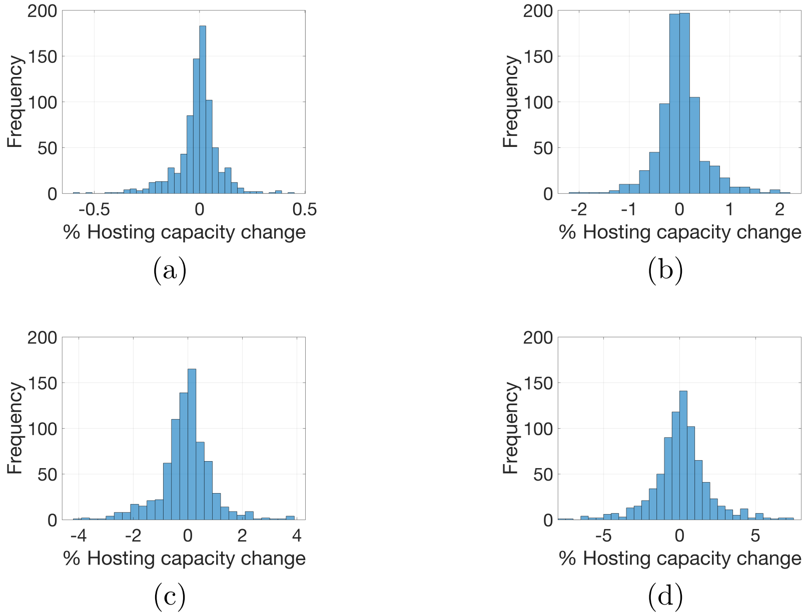

(a) (b) (c) (d)

Figure 4.41: Histograms of the change in nodal hosting capacity from variation in demand belonging to a uniform distribution of : (a) 1%; (b) 5%; (c) 10%; (d) 20%.

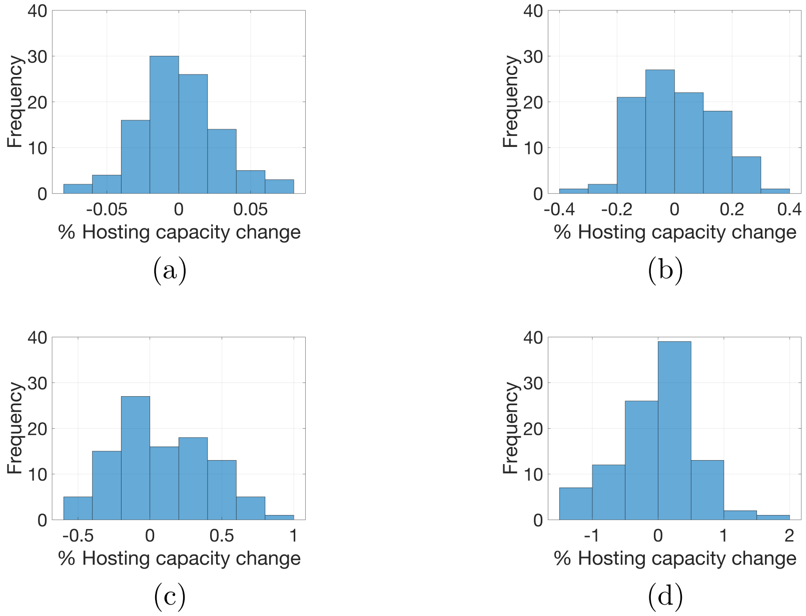

(a) (b) (c) (d)

Figure 4.42: Histograms of the change in aggregate hosting capacity from variation in demand belonging to a uniform distribution of : (a) 1%; (b) 5%; (c) 10%; (d) 20%.

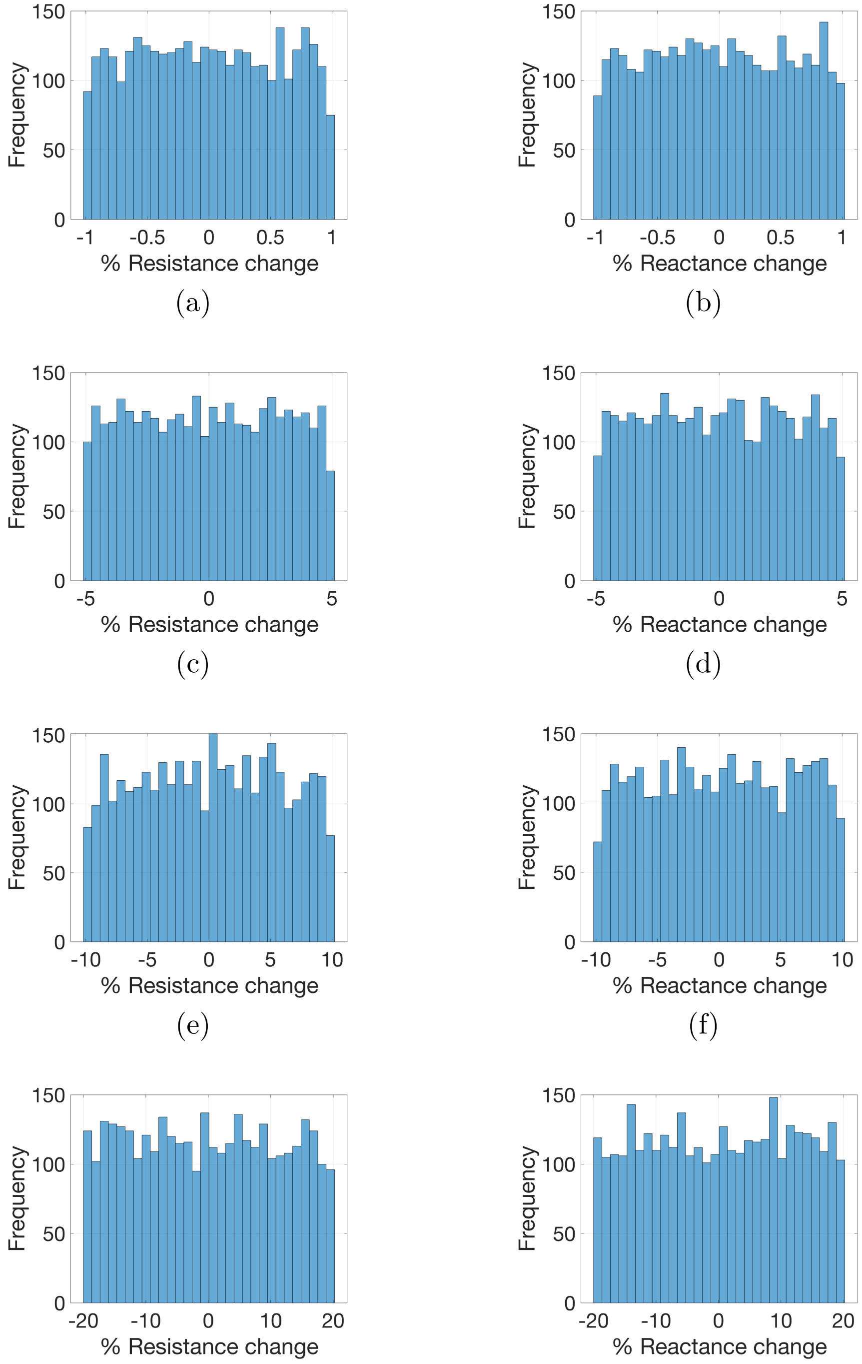

(a) (b)

(c) (d)

(e) (f)

(g) (h)

Figure 4.43: Histograms of the percentage change in resistance and reactance values resulting from variation in the line impedance values belonging to a uniform distribution of : (a) 1% error; (b) 5% error; (c) 10% error; (d) 20% error.

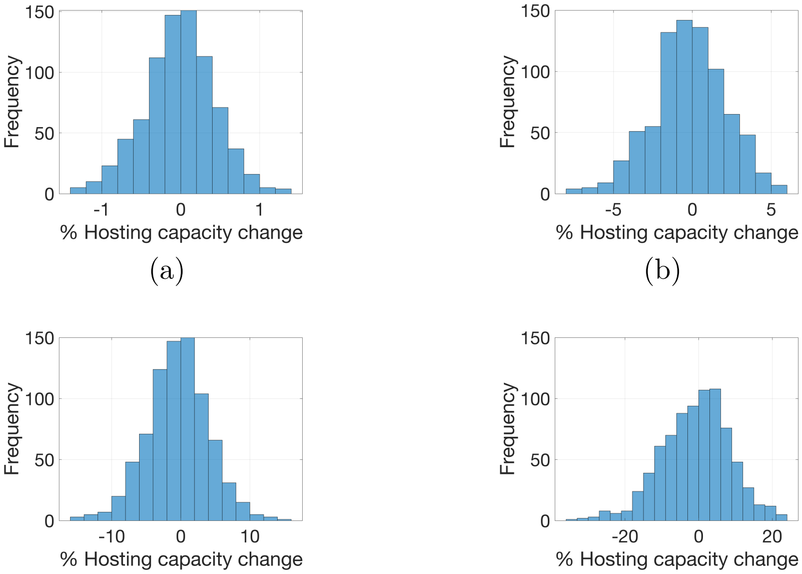

(a) (b) (c) (d)

Figure 4.44: Histograms of the change in nodal hosting capacity from variation in line impedance belonging to a uniform distribution of : (a) 1%; (b) 5%; (c) 10%; (d) 20%.

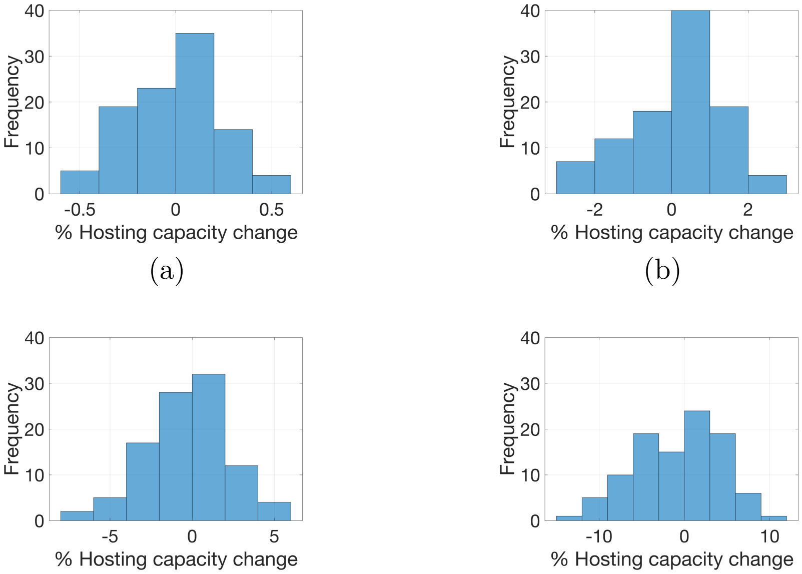

(a) (b) (c) (d)

Figure 4.45: Histograms of the change in aggregate hosting capacity from variation in line impedance belonging to a uniform distribution of : (a) 1%; (b) 5%; (c) 10%; (d) 20%.

Table 4.5: Mean and standard deviation (S.D.) of the percent changes in nodal hosting capacities resulting from uniformly distributed deviations in demand and line parameter values (R,X).

% change	Mean (demand)	S.D. (demand)	Mean (line)	S.D. (line)
1%	0.00	0.09	-0.01	0.44
5%	-0.04	0.46	-0.03	2.17
10%	0.03	0.96	0.37	4.26
20%	0.02	1.86	-0.53	9.20

Table 4.6: Mean and standard deviation (S.D.) of the percent changes in aggregate feeder hosting capacities resulting from uniformly distributed deviations in nodal demand and line parameter values (R,X).

% change	Mean (demand)	S.D. (demand)	Mean (line)	S.D (line)
1%	0.00	0.03	-0.01	0.24
5%	0.01	0.13	0.11	1.22
10%	0.06	0.31	-0.30	2.45
20%	-0.01	0.56	-0.74	5.10

4.3.7 CONCLUSIONS

This manuscript presents a convex inner approximation of the AC OPF problem. Leveraging convex lower and upper bounds on the nonlinear branch flow terms in the AC formulation, the inner approximation ensures an AC admissible optimal solution. A novel algorithm is presented to successively improve the nodal capacity values of a feeder. Reactive power control schemes are then presented and volt-VAr and smart inverter schemes are shown to further improve the nodal capacity. Finally, a realtime disaggregation scheme is presented for dispatching flexible demand in realtime across the network, while respecting the grid constraints and providing fast grid services.

CHAPTER 5

FUTURE WORK

5.1 EXTENSION OF CONVEX INNER APPROXIMATION TO OTHER APPLICATIONS

The convex inner approximation technique presented in section 4 implicitly embeds the grid physics into the nodal capacity limits and thus enables real-time grid-aware control of DERs, without having to solve a computationally costly multi-period OPF at every market update. This has the potential to solve many challenging problems in energy systems. An immediate extension of the work on CIA, would be to include complex network topologies such as meshed networks and three-phase networks within the this framework. Furthermore, there could also be applications in specific domains such as wind farms and other radial distribution networks. Similar to determining the DER flexibility bounds, CIA can also be utilized to provide reactive power flexibility bounds in certain applications.

With the proliferation of flexible energy storage across distribution networks in the form of either physical batteries, thermostatically controlled loads (TCLs) or electric vehicles (EVs), it is also important for the distribution system operator (DSO) to be aware of the aggregate system level available energy storage. Knowledge of the aggregate level energy storage is critical in the ability of feeders to participate in energy markets. For this application, convex inner approximation can be extended to the multi-period domain in order to determine network aggregate energy storage. Extension to multi-period domain will also consider the challenging problem of disaggregating a reference trajectory over time across energy-constrained nodes on a network. Furthermore, while we focus on feasible disaggregation at the nodal level (to ensure constraints are not violated), we also need to consider an optimal disaggregation policy that allows an aggregator to steer the system response along an (online) OPF solution.

Future work on the Voltage positioning optimization (VPO) will focus on the multi-period extension by considering the time-coupling introduced due to energy storage and ramp-rate limits. Of particular interest is the problem of restricting the frequent tap changes of OLTCs in distribution networks that has been previously highlighted in [40]. The VPO formulation is well-suited for limiting the switching of tap-changers by introducing tap change rate constraints in the multi-period optimization formulation. Furthermore, we are seeking to extend the results to consider the effects of uncertainty in the VPO. It is important to note that the VPO work considers radial, balanced, and inductive distribution feeders. However, realistic distribution feeders are sometimes meshed, often unbalanced, and usually a mix of inductive and capacitative lines, which means that extending this work to a full, three-phase AC formulation is valuable towards utility practice.

Traditional approach in accounting for forecast uncertainty involve transformation of the uncertainty in generation over a nonlinear network in order satisfy network constraints such as voltage limits and line power flow limits. Due to the nonlinearity of the network, reformulating this stochastic problem into a determinstic form is a challenge [179]. Through the formulation of convex inner approximation, we are able to transform the network constraints (such as voltage and line power flow constraints), into nodal level generation and flexibility constraints. As a result, we only require nodal level uncertainty constraints, which are linear and do not need to transform the uncertainty distribution over a nonlinear network. Hence, reformulation to a deterministic form (through techniques such as chance constraints) is simple and does not require any simplifying assumption (such as linearization).

Apart from the above mentioned applications, convex inner approximation also opens up many avenues in real-time control of DERs. Solving DER dispatch within milliseconds enables their use for frequency response. Hence, through CIA frequency response can be made grid-aware in distribution systems. Furthermore, CIA can also be extended to determine dynamic hosting capacity and thus enable larger penetration of renewable generation, which as of now is limited by the hosting capacity determined based on the worst case over a year. Such advancements will greatly help the planning, sizing and siting of new renewable generation and grid-size energy storage.

5.2 Physics based machine learning for DER dispatch

Ensuring acceptable performance of energy systems involves optimizing a large number of controllable inputs efficiently at different timescales, while respecting the operational and solve time limit constraints of the system. This requires solving a challenging non-convex optimal power flow problem. This problem is further exacerbated by the fact that the distribution system topology is either complex (such as meshed and multi-phase) or unknown to the system operator due to changes in system topology and outdated records of an aging infrastructure [180]. Furthermore, the system parameters (such as impedance values and energy resource parameters such as power and energy limits) are often unknown or misrecorded and the system topology is often times subject to change due to various plug-and-play devices such as electric vehicles (EVs) [181]. Often times the optimization models developed, end up being non-convex which due to the large number of controllable inputs, increases the complexity and solve-time of the problem to such an extent that traditional optimization techniques become intractable [182]. As a result, we might have to limit the growth of resources, not take advantage of their full capabilities, or will need to overbuild the system to handle more extreme operating conditions [183].

All these challenges highlight the shortcomings of traditional model-based optimization techniques and pave the way for the development of data-driven methods to leverage an increasingly large number of measurements. With the advent of "Big Data", recent literature has shown the benefit of applying machine learning to many fields, including energy systems [184]. However, due to the safety critical nature of such systems, these methods have failed to receive support in industry applications as of yet. Many open problems remain when it comes to the application of machine learning to such complex systems [185]. Providing performance guarantees using these methods is one such important challenge. To overcome these practical challenges and given the availability of historical data and a growing set of measurements from smart meters, such as AMI and inverters, many works in literature have proposed machine learning methods to solve optimization problems [186–188]. Furthermore, recent works leveraging machine learning have incorporated the system physics into their formulation thereby providing a more interpretable and physics-based solution [189, 190].

Machine learning methods can find application in planning and design of distribution systems, such as the sizing and siting of solar PV units and energy storage units, by solving hosting capacity problems. The methods developed in this work in section 4.1, 4.2 and 4.3 rely on precise system models, which might not be available in practice. Utilizing data-driven methods, can be used to estimate hosting capacity in cases where system models may be unreliable, often changing or highly complex.

BIBLIOGRAPHY

[1] J. Farrell, "Solving solar's variability with more solar." `https://ilsr.org/solving-solars-variability-more-solar`, 2011.

[2] K. Desrochers, V. Hines, F. Wallace, J. Slinkman, A. Giroux, A. Khurram, M. Amini, M. Almassalkhi, and P. D. Hines, "Real-world, full-scale validation of power balancing services from packetized virtual batteries," in *2019 IEEE Power & Energy Society Innovative Smart Grid Technologies Conference (ISGT)*, pp. 1–5, IEEE, 2019.

[3] A. Zare *et al.*, *Multistage Expansion Planning of Active Distribution Systems: Towards Network Integration of Distributed Energy Resources.* PhD thesis, University of Saskatchewan, 2018.

[4] I. A. Hiskens and R. J. Davy, "Exploring the power flow solution space boundary," *IEEE Power Engineering Review*, vol. 21, no. 8, pp. 57–57, 2001.

[5] W. Post, "The vagaries of solar in new england." `https://www.windtaskforce.org/profiles/blogs/the-vagaries-of-solar-in-new-england?xg_source=activity`, 2020.

[6] R. Heidari, M. M. Seron, and J. H. Braslavsky, "Non-local approximation of power flow equations with guaranteed error bounds," in *Control Conference (ANZCC), 2017 Australian and New Zealand*, pp. 83–88, 2017.

[7] M. R. Almassalkhi and I. A. Hiskens, "Model-predictive cascade mitigation in electric power systems with storage and renewables—part i: Theory and implementation," *IEEE Transactions on Power Systems*, vol. 30, no. 1, pp. 67–77, 2015.

[8] B. Stellato, "Data-driven chance constrained optimization," Master's thesis, ETH-Zürich, 2014.

[9] M. Amini and M. Almassalkhi, "Optimal corrective dispatch of uncertain virtual energy storage systems," *IEEE Transactions on Smart Grid*, pp. 1–1, 2020.

[10] S. Brahma, N. Nazir, H. Ossareh, and M. Almassalkhi, "Optimal and resilient coordination of virtual batteries in distribution feeders," *arXiv preprint arXiv:2010.03063*, 2020.

[11] K. Baker, A. Bernstein, E. Dall'Anese, and C. Zhao, "Network-cognizant voltage droop control for distribution grids," *IEEE Transactions on Power Systems*, vol. 33, no. 2, pp. 2098–2108, 2018.

[12] U. N. E. Program, "The emissions gap report 2017: A un environment synthesis report," tech. rep., United Nations Environment Program, Nairobi, Kenya, June 2019.

[13] W. J. Cole and A. Frazier, "Cost projections for utility-scale battery storage," tech. rep., National Renewable Energy Lab.(NREL), Golden, CO (United States), 2019.

[14] R. Hledik, A. Faruqui, T. Lee, and J. Higham, "The national potential for load flexibility: Value and market potential through 2030," tech. rep., The Brattle Group, Boston, Massachussetts, June 2019.

[15] C. Goldenberg, M. Dyson, and H. Masters, "Demand flexibility: the key to enabling a low-cost, low-carbon grid," *Insight Brief, Rocky Mountain Institute*, 2018.

[16] IEA, "Digitalisation and energy, iea, paris," 2017.

[17] "Distributed energy resources: Connection, modeling and reliability considerations," tech. rep., North American Electric Reliability Council (NERC), 11 2016.

[18] J. Singer, *Enabling Tomorrow's Electricity System: Report of the Ontario Smart Grid Forum.* Independent Electricity System Operator, 2009.

[19] T. Ackermann, T. Prevost, V. Vittal, A. J. Roscoe, J. Matevosyan, and N. Miller, "Paving the way: A future without inertia is closer than you think," *IEEE Power and Energy Magazine*, vol. 15, no. 6, pp. 61–69, 2017.

[20] H. Hao, B. M. Sanandaji, K. Poolla, and T. L. Vincent, "Aggregate flexibility of thermostatically controlled loads," *IEEE Transactions on Power Systems*, vol. 30, no. 1, pp. 189–198, 2014.

[21] J. T. Hughes, A. D. Domínguez-García, and K. Poolla, "Identification of virtual battery models for flexible loads," *IEEE Transactions on Power Systems*, vol. 31, no. 6, pp. 4660–4669, 2016.

[22] M. B. Kane and K. Sharma, "Data-driven identification of occupant thermostat-behavior dynamics," *arXiv preprint arXiv:1912.06705*, 2019.

[23] I. Chakraborty, S. P. Nandanoori, and S. Kundu, "Virtual battery parameter identification using transfer learning based stacked autoencoder," in *2018 17th IEEE International Conference on Machine Learning and Applications (ICMLA)*, pp. 1269–1274, IEEE, 2018.

[24] J. D. Taft, "Grid architecture 2," tech. rep., Pacific Northwest National Lab.(PNNL), Richland, WA (United States), 2016.

[25] P. De Martini, L. Kristov, and L. Schwartz, "Distribution systems in a high distributed energy resources future," tech. rep., Lawrence Berkeley National Lab.(LBNL), Berkeley, CA (United States), 2015.

[26] E. Dall'Anese, S. S. Guggilam, A. Simonetto, Y. C. Chen, and S. V. Dhople, "Optimal regulation of virtual power plants," *IEEE Transactions on Power Systems*, vol. 33, no. 2, pp. 1868–1881, 2017.

[27] M. Baran and F. F. Wu, "Optimal sizing of capacitors placed on a radial distribution system," *IEEE Transactions on power Delivery*, vol. 4, no. 1, pp. 735–743, 1989.

[28] R. A. Jabr, "Modeling network losses using quadratic cones," *IEEE Transactions on Power Systems*, vol. 20, no. 1, pp. 505–506, 2005.

[29] X. Zhou, E. Dall'Anese, L. Chen, and K. Baker, "Incentive-based voltage regulation in distribution networks," in *American Control Conference (ACC), 2017*, pp. 2732–2738, IEEE, 2017.

[30] E. Dall'Anese, S. Guggilam, A. Simonetto, Y. C. Chen, and S. V. Dhople, "Optimal regulation of virtual power plants," *IEEE Transactions on Power Systems*, 2017.

[31] K. Baker, A. Bernstein, E. Dall'Anese, and C. Zhao, "Network-cognizant voltage droop control for distribution grids," *arXiv preprint arXiv:1702.02969*, 2017.

[32] M. Sinha, F. Dörfler, B. B. Johnson, and S. V. Dhople, "Virtual oscillator control subsumes droop control," in *American Control Conference (ACC), 2015*, pp. 2353–2358, IEEE, 2015.

[33] D. Cai, E. Mallada, and A. Wierman, "Distributed optimization decomposition for joint economic dispatch and frequency regulation," *IEEE Transactions on Power Systems*, 2017.

[34] E. Mallada, "idroop: A dynamic droop controller to decouple power grid's steady-state and dynamic performance," in *Decision and Control (CDC), 2016 IEEE 55th Conference on*, pp. 4957–4964, IEEE, 2016.

[35] T. Stetz, F. Marten, and M. Braun, "Improved low voltage grid-integration of photovoltaic systems in germany," *IEEE Transactions on sustainable energy*, vol. 4, no. 2, pp. 534–542, 2013.

[36] North American Electric Reliability Corporation, "1,200 mw fault induced solar photovoltaic resource interruption disturbance report," *NERC*, 2017.

[37] B. Bayer, P. Matschoss, H. Thomas, and A. Marian, "The german experience with integrating photovoltaic systems into the low-voltage grids," *Renewable energy*, vol. 119, pp. 129–141, 2018.

[38] Y. Guangya, F. Marra, M. Juamperez, S. B. Kjær, S. Hashemi, J. Østergaard, H. H. Ipsen, and K. H. Frederiksen, "Voltage rise mitigation for solar pv integration at lv grids," *Journal of Modern Power Systems and Clean Energy*, vol. 3, no. 3, pp. 411–421, 2015.

[39] R. Sanghi, "Chemistry behind the life of a transformer," *Resonance*, vol. 8, no. 6, pp. 17–23, 2003.

[40] J. A. Kersulis and I. A. Hiskens, "Renewable voltage regulation and the transformer tapping trade-off," in *2016 IEEE Innovative Smart Grid Technologies-Asia (ISGT-Asia)*, pp. 960–965, IEEE, 2016.

[41] S. Paudyal, C. A. Canizares, and K. Bhattacharya, "Three-phase distribution opf in smart grids: Optimality versus computational burden," *Innovative Smart Grid Technologies (ISGT Europe), 2nd IEEE PES International Conference and Exhibition on*, 2011.

[42] B. A. Robbins, H. Zhu, and A. D. Domínguez-García, "Optimal tap setting of voltage regulation transformers in unbalanced distribution systems," *IEEE Transactions on Power Systems*, vol. 31, no. 1, pp. 256–267, 2016.

[43] G. P. McCormick, "Computability of global solutions to factorable nonconvex programs: Part I—convex underestimating problems," *Mathematical programming*, vol. 10, no. 1, pp. 147–175, 1976.

[44] N. Nazir and M. Almassalkhi, "Receding-horizon optimization of unbalanced distribution systems with time-scale separation for discrete and continuous control devices," in *2018 Power Systems Computation Conference (PSCC)*, pp. 1–7, IEEE, 2018.

[45] E. Briglia, S. Alaggia, and F. Paganini, “Distribution network management based on optimal power flow: Integration of discrete decision variables,” *Information Sciences and Systems (CISS), 51st Annual Conference on*, pp. 1–6, 2017.

[46] Z. Yang, A. Bose, H. Zhong, N. Zhang, Q. Xia, and C. Kang, “Optimal reactive power dispatch with accurately modeled discrete control devices: a successive linear approximation approach,” *IEEE Trans. Power Syst*, vol. 32, no. 3, pp. 2435–2444, 2017.

[47] S. R. Shukla, S. Paudyal, and M. Almassalkhi, “Efficient distribution system optimal power flow with discrete control of load tap changers,” *IEEE Transactions on Power Systems*, pp. 1–1, 2019.

[48] H. Nagarajan, M. Lu, E. Yamangil, and R. Bent, “Tightening mccormick relaxations for nonlinear programs via dynamic multivariate partitioning,” in *International Conference on Principles and Practice of Constraint Programming*, pp. 369–387, Springer, 2016.

[49] A. Falsone, K. Margellos, and M. Prandini, “A decentralized approach to multi-agent milps: finite-time feasibility and performance guarantees,” *arXiv preprint arXiv:1706.08788*, 2017.

[50] J. Carpentier, “Contribution to the economic dispatch problem,” *Bulletin de la Societe Francoise des Electriciens*, vol. 3, no. 8, pp. 431–447, 1962.

[51] M. Haque, “Load flow solution of distribution systems with voltage dependent load models,” *Electric Power Systems Research*, vol. 36, no. 3, pp. 151–156, 1996.

[52] D. K. Molzahn, B. C. Lesieutre, and C. L. Demarco, “Approximate Representation of ZIP Loads in a Semidefinite Relaxation of the OPF Problem,” *IEEE Transactions on Power Systems*, vol. 29, pp. 1864–1865, July 2014.

[53] J. Lavaei and S. H. Low, “Zero duality gap in optimal power flow problem,” *IEEE Transactions on Power Systems*, vol. 27, no. 1, pp. 92–107, 2012.

[54] J. Lavaei, D. Tse, and B. Zhang, “Geometry of power flows and optimization in distribution networks,” *IEEE Transactions on Power Systems*, vol. 29, no. 2, pp. 572–583, 2014.

[55] R. A. Jabr, “Radial distribution load flow using conic programming,” *IEEE Transactions on Power Systems*, vol. 21, no. 3, pp. 1458–1459, 2006.

[56] M. Farivar, C. R. Clarke, S. H. Low, and K. M. Chandy, "Inverter var control for distribution systems with renewables," *Smart Grid Communications (SmartGridComm), IEEE International Conference on*, pp. 457–462, 2011.

[57] P. Roux, Y.-L. Voronin, and S. Sankaranarayanan, "Validating numerical semidefinite programming solvers for polynomial invariants," *International Static Analysis Symposium*, pp. 424–446, 2016.

[58] R. A. Jabr, "Optimal power flow using an extended conic quadratic formulation," *IEEE Transactions on Power Systems*, vol. 23, no. 3, pp. 1000–1008, 2008.

[59] R. Madani, S. Sojoudi, and J. Lavaei, "Convex relaxation for optimal power flow problem: Mesh networks," *IEEE Transactions on Power Systems*, vol. 30, no. 1, pp. 199–211, 2015.

[60] B. C. Lesieutre, D. K. Molzahn, A. R. Borden, and C. L. DeMarco, "Examining the limits of the application of semidefinite programming to power flow problems," in *Communication, Control, and Computing (Allerton), 2011 49th Annual Allerton Conference on*, pp. 1492–1499, IEEE, 2011.

[61] D. K. Molzahn, B. C. Lesieutre, and C. L. DeMarco, "Investigation of non-zero duality gap solutions to a semidefinite relaxation of the optimal power flow problem," in *System Sciences (HICSS), 2014 47th Hawaii International Conference on*, pp. 2325–2334, IEEE, 2014.

[62] D. K. Molzahn and I. A. Hiskens, "Sparsity-exploiting moment-based relaxations of the optimal power flow problem," *IEEE Transactions on Power Systems*, vol. 30, no. 6, pp. 3168–3180, 2015.

[63] C. Coffrin, H. L. Hijazi, and P. Van Hentenryck, "The qc relaxation: A theoretical and computational study on optimal power flow," *IEEE Transactions on Power Systems*, vol. 31, no. 4, pp. 3008–3018, 2016.

[64] S. Bolognani and F. Dörfler, "Fast power system analysis via implicit linearization of the power flow manifold," in *Communication, Control, and Computing (Allerton), 2015 53rd Annual Allerton Conference on*, pp. 402–409, IEEE, 2015.

[65] S. Bolognani and S. Zampieri, "On the existence and linear approximation of the power flow solution in power distribution networks," *IEEE Transactions on Power Systems*, vol. 31, no. 1, pp. 163–172, 2016.

[66] S. Karagiannopoulos, P. Aristidou, and G. Hug, "A centralised control method for tackling unbalances in active distribution grids," in *2018 Power Systems Computation Conference (PSCC)*, pp. 1–7, IEEE, 2018.

[67] W. Wang and N. Yu, "Chordal conversion based convex iteration algorithm for three-phase optimal power flow problems," *IEEE Transactions on Power Systems*, vol. 33, no. 2, pp. 1603–1613, 2018.

[68] F. Katiraei, C. Sun, and B. Enayati, "No inverter left behind: protection, controls, and testing for high penetrations of pv inverters on distribution systems," *IEEE Power and Energy Magazine*, vol. 13, no. 2, pp. 43–49, 2015.

[69] M. D. Sankur, R. Dobbe, E. Stewart, D. S. Callaway, and D. B. Arnold, "A linearized power flow model for optimization in unbalanced distribution systems," *arXiv preprint arXiv:1606.04492*, 2016.

[70] B. A. Robbins and A. D. Domínguez-García, "Optimal reactive power dispatch for voltage regulation in unbalanced distribution systems," *IEEE Transactions on Power Systems*, vol. 31, no. 4, pp. 2903–2913, 2016.

[71] E. Dall'Anese, H. Zhu, and G. B. Giannakis, "Distributed optimal power flow for smart microgrids," *IEEE Transactions on Smart Grid*, vol. 4, no. 3, pp. 1464–1475, 2013.

[72] L. Gan and S. H. Low, "Convex relaxations and linear approximation for optimal power flow in multiphase radial networks," *Power Systems Computation Conference (PSCC)*, pp. 1–9, 2014.

[73] A. S. Zamzam, N. D. Sidiropoulos, and E. Dall'Anese, "Beyond relaxation and newton-raphson: Solving ac opf for multi-phase systems with renewables," *IEEE Transactions on Smart Grid*, 2016.

[74] D. Gayme and U. Topcu, "Optimal power flow with large-scale storage integration," *IEEE Transactions on Power Systems*, vol. 28, no. 2, pp. 709–717, 2013.

[75] A. Gopalakrishnan, A. U. Raghunathan, D. Nikovski, and L. T. Biegler, "Global optimization of multi-period optimal power flow," *American Control Conference*, pp. 1157–1164, 2013.

[76] J. F. Marley, D. K. Molzahn, and I. A. Hiskens, "Solving Multiperiod OPF problems using an AC-QP algorithm Initialized with an SOCP relaxation," *IEEE Transactions on Power Systems*, vol. 32, no. 5, pp. 3538–3548, 2017.

[77] Z. Li, Q. Guo, H. Sun, and J. Wang, "Sufficient conditions for exact relaxation of complementarity constraints for storage-concerned economic dispatch," *IEEE Transactions on Power Systems*, vol. 31, no. 2, pp. 1653–1654, 2016.

[78] Z. Zhao and L. Wu, "Impacts of high penetration wind generation and demand response on lmps in day-ahead market," *IEEE Transactions on Smart Grid*, vol. 5, no. 1, pp. 220–229, 2014.

[79] F. C. Schweppe, R. D. Tabors, J. L. Kirtley, H. R. Outhred, F. H. Pickel, and A. J. Cox, "Homeostatic utility control," *IEEE Transactions on Power Apparatus and Systems*, no. 3, pp. 1151–1163, 1980.

[80] A. Brooks, E. Lu, D. Reicher, C. Spirakis, and B. Weihl, "Demand dispatch," *IEEE Power and Energy Magazine*, vol. 8, no. 3, pp. 20–29, 2010.

[81] D. S. Callaway and I. A. Hiskens, "Achieving controllability of electric loads," *Proceedings of the IEEE*, vol. 99, no. 1, pp. 184–199, 2010.

[82] J. L. Mathieu, M. Kamgarpour, J. Lygeros, G. Andersson, and D. S. Callaway, "Arbitraging intraday wholesale energy market prices with aggregations of thermostatic loads," *IEEE Transactions on Power Systems*, vol. 30, no. 2, pp. 763–772, 2014.

[83] S. P. Meyn, P. Barooah, A. Bušić, Y. Chen, and J. Ehren, "Ancillary service to the grid using intelligent deferrable loads," *IEEE Transactions on Automatic Control*, vol. 60, no. 11, pp. 2847–2862, 2015.

[84] M. Almassalkhi, L. D. Espinosa, P. D. H. Hines, J. Frolik, S. Paudyal, and M. Amini, *Asynchronous Coordination of Distributed Energy Resources with Packetized Energy Management*, pp. 333–361. New York, NY: Springer New York, 2018.

[85] S. H. Tindemans, V. Trovato, and G. Strbac, "Decentralized control of thermostatic loads for flexible demand response," *IEEE Transactions on Control Systems Technology*, vol. 23, no. 5, pp. 1685–1700, 2015.

[86] F. L. Müller, J. Szabó, O. Sundström, and J. Lygeros, "Aggregation and disaggregation of energetic flexibility from distributed energy resources," *IEEE Transactions on Smart Grid*, vol. 10, no. 2, pp. 1205–1214, 2017.

[87] P. D. Martini, L. Kristov, and L. Schwartz, "Distribution systems in a high distributed energy resources future: Planning, market design, operation and oversight," tech. rep., Lawrence Berkeley National Laboratory, 10 2015.

[88] L. Kristov, P. De Martini, and J. D. Taft, "A tale of two visions: Designing a decentralized transactive electric system," *IEEE Power and Energy Magazine*, vol. 14, no. 3, pp. 63–69, 2016.

[89] conEdison, "Consolidated edison distributed system implementation plan," in *Con Edison DSIP filing*.

[90] N. Nazir and M. Almassalkhi, "Convex inner approximation of the feeder hosting capacity limits on dispatchable demand," in *2019 IEEE 58th Conference on Decision and Control (CDC)*, pp. 4858–4864, 2019.

[91] K. Kok and S. Widergren, "A society of devices: Integrating intelligent distributed resources with transactive energy," *IEEE Power and Energy Magazine*, vol. 14, pp. 34–45, May 2016.

[92] M. S. Nazir and I. A. Hiskens, "A dynamical systems approach to modeling and analysis of transactive energy coordination," *IEEE Transactions on Power Systems*, 2018.

[93] E. Dall'Anese, S. S. Guggilam, A. Simonetto, Y. C. Chen, and S. V. Dhople, "Optimal regulation of virtual power plants," *IEEE Transactions on Power Systems*, vol. 33, no. 2, pp. 1868–1881, 2018.

[94] D. B. Arnold, M. D. Sankur, M. Negrete-Pincetic, and D. S. Callaway, "Model-free optimal coordination of distributed energy resources for provisioning transmission-level services," *IEEE Transactions on Power Systems*, vol. 33, no. 1, pp. 817–828, 2018.

[95] Q. Li and V. Vittal, "Convex hull of the quadratic branch ac power flow equations and its application in radial distribution networks," *IEEE Transactions on Power Systems*, vol. 33, no. 1, pp. 839–850, 2018.

[96] A. Bidram and A. Davoudi, "Hierarchical structure of microgrids control system," *IEEE Transactions on Smart Grid*, vol. 3, no. 4, pp. 1963–1976, 2012.

[97] D. K. Molzahn, "Computing the feasible spaces of optimal power flow problems," *IEEE Transactions on Power Systems*, vol. 32, no. 6, pp. 4752–4763, 2017.

[98] D. K. Molzahn and I. A. Hiskens, "A Survey of Relaxations and Approximations of the Power Flow Equations," *Foundations and Trends in Electric Energy Systems*, vol. 4, pp. 1–221, 2 2019.

[99] K. Dvijotham and D. K. Molzahn, "Error bounds on the DC power flow approximation: A convex relaxation approach," in *Decision and Control (CDC), 2016 IEEE 55th Conference on*, pp. 2411–2418, 2016.

[100] D. B. Arnold, M. Sankur, R. Dobbe, K. Brady, D. S. Callaway, and A. Von Meier, "Optimal dispatch of reactive power for voltage regulation and balancing in unbalanced distribution systems," in *2016 IEEE Power and Energy Society General Meeting (PESGM)*, pp. 1–5, IEEE, 2016.

[101] J. A. Taylor, *Convex optimization of power systems.* Cambridge University Press, 2015.

[102] L. Gan, N. Li, U. Topcu, and S. H. Low, "Exact convex relaxation of optimal power flow in radial networks," *IEEE Transactions on Automatic Control*, vol. 60, no. 1, pp. 72–87, 2015.

[103] S. Huang, Q. Wu, J. Wang, and H. Zhao, "A sufficient condition on convex relaxation of ac optimal power flow in distribution networks," *IEEE Transactions on Power Systems*, vol. 32, no. 2, pp. 1359–1368, 2017.

[104] D. Molzahn and L. A. Roald, "Grid-aware versus grid-agnostic distribution system control: A method for certifying engineering constraint satisfaction," in *Proceedings of the 52nd Hawaii International Conference on System Sciences*, 2019.

[105] D. Lee, H. D. Nguyen, K. Dvijotham, and K. Turitsyn, "Convex restriction of power flow feasibility sets," *IEEE Transactions on Control of Network Systems*, vol. 6, no. 3, pp. 1235–1245, 2019.

[106] D. Lee, K. Turitsyn, D. K. Molzahn, and L. Roald, "Feasible path identification in optimal power flow with sequential convex restriction," *IEEE Transactions on Power Systems*, 2020.

[107] M. Nick, R. Cherkaoui, J.-Y. Le Boudec, and M. Paolone, "An exact convex formulation of the optimal power flow in radial distribution networks including transverse components," *IEEE Transactions on Automatic Control*, vol. 63, no. 3, pp. 682–697, 2017.

[108] S. C. Ross and J. L. Mathieu, "A method for ensuring a load aggregator's power deviations are safe for distribution networks," *Electric Power Systems Research*, vol. 189, p. 106781, 2020.

[109] J. Driesen and R. Belmans, "Distributed generation: Challenges and possible solutions," in *Power Engineering Society General Meeting, 2006. IEEE*, pp. 8–pp, IEEE, 2006.

[110] UMBRELLA-F97-Project, "Toolbox for common forecasting, risk assessment, and operational optimisation in grid security cooperations of transmission system operators(tsos)," in *[Online]. Available:http://www.e-umbrella.eu.*

[111] T. Summers, J. Warrington, M. Morari, and J. Lygeros, "Stochastic optimal power flow based on conditional value at risk and distributional robustness," *International Journal of Electrical Power & Energy Systems*, vol. 72, pp. 116–125, 2015.

[112] E. Dall'Anese, K. Baker, and T. Summers, "Chance-constrained ac optimal power flow for distribution systems with renewables," *IEEE Transactions on Power Systems*, vol. 32, no. 5, pp. 3427–3438, 2017.

[113] J. F. Marley, M. Vrakopoulou, and I. A. Hiskens, "Towards the maximization of renewable energy integration using a stochastic ac-qp optimal power flow algorithm," in *10th IREP Symp. Bulk Power Syst. Dynamics Control*, 2017.

[114] A. Venzke, L. Halilbasic, U. Markovic, G. Hug, and S. Chatzivasileiadis, "Convex relaxations of chance constrained ac optimal power flow," *IEEE Transactions on Power Systems*, vol. 33, no. 3, pp. 2829–2841, 2017.

[115] L. Roald and G. Andersson, "Chance-constrained ac optimal power flow: Reformulations and efficient algorithms," *IEEE Transactions on Power Systems*, vol. 33, no. 3, pp. 2906–2918, 2017.

[116] J. Peppanen, C. Rocha, J. A. Taylor, and R. C. Dugan, "Secondary low-voltage circuit models—how good is good enough?," *IEEE Transactions on Industry Applications*, vol. 54, no. 1, pp. 150–159, 2017.

[117] N. Nazir, P. Racherla, and M. Almassalkhi, "Optimal multi-period dispatch of distributed energy resources in unbalanced distribution feeders," *IEEE Transactions on Power Systems*, pp. 1–1, 2020.

[118] T. Fujimoto and R. R. Ranade, "Two characterizations of inverse-positive matrices: the hawkins-simon condition and the le chatelier-braun principle," *Electronic Journal of Linear Algebra*, vol. 11, no. 1, p. 6, 2004.

[119] S. Boyd and L. Vandenberghe, *Convex optimization.* Cambridge university press, 2004.

[120] R. T. Rockafellar, “Lagrange multipliers and optimality,” *SIAM review*, vol. 35, no. 2, pp. 183–238, 1993.

[121] G. Kron, *Tensor analysis of networks.* New York: J. Wiley & Sons, Incorporated, 1939.

[122] S. Blumsack, P. Hines, M. Patel, C. Barrows, and E. C. Sanchez, “Defining power network zones from measures of electrical distance,” in *2009 IEEE Power Energy Society General Meeting*, pp. 1–8, 2009.

[123] F. Dorfler and F. Bullo, “Kron reduction of graphs with applications to electrical networks,” *IEEE Transactions on Circuits and Systems I: Regular Papers*, vol. 60, no. 1, pp. 150–163, 2012.

[124] “Robust and resilient coordination of feeders with uncertaindistributed energy resources: from real-time control to long-term planning,” tech. rep., Department of Energy (DOE), 12 2020.

[125] K. Garifi, K. Baker, D. Christensen, and B. Touri, “Convex relaxation of grid-connected energy storage system models with complementarity constraints in dc opf,” *IEEE Transactions on Smart Grid*, vol. 11, no. 5, pp. 4070–4079, 2020.

[126] L. Gurobi Optimization, “Gurobi optimizer reference manual,” 2018.

[127] J. Singer, *Enabling Tomorrow’s Electricity System: Report of the Ontario Smart Grid Forum.* Independent Electricity System Operator, 2010.

[128] D. P. Chassin, K. Schneider, and C. Gerkensmeyer, “GridLAB-D: An open-source power systems modeling and simulation environment,” in *Transmission and distribution conference and exposition, 2008. t&d. IEEE/PES*, pp. 1–5, IEEE, 2008.

[129] Y. Atwa, E. El-Saadany, M. Salama, and R. Seethapathy, “Optimal renewable resources mix for distribution system energy loss minimization,” *IEEE Transactions on Power Systems*, vol. 25, no. 1, pp. 360–370, 2010.

[130] B. Kocuk, S. S. Dey, and X. A. Sun, “Strong SOCP relaxations for the optimal power flow problem,” *Operations Research*, vol. 64, no. 6, pp. 1177–1196, 2016.

[131] R. A. Horn and C. R. Johnson, *Matrix analysis.* Cambridge university press, 2012.

[132] W. H. Kersting, “Radial distribution test feeders,” in *Power Engineering Society Winter Meeting, 2001. IEEE*, vol. 2, pp. 908–912, IEEE, 2001.

[133] J. Bing, P. Krishnani, O. Bartholomy, T. Hoff, and R. Perez, "Solar monitoring, forecasting, and variability assessment at smud," in *Proceedings of the World Renewable Energy Forum*, 2012.

[134] I. Dunning, J. Huchette, and M. Lubin, "Jump: A modeling language for mathematical optimization," *SIAM Review*, vol. 59, no. 2, pp. 295–320, 2017.

[135] A. Wächter and L. T. Biegler, "On the implementation of an interior-point filter line-search algorithm for large-scale nonlinear programming," *Mathematical programming*, vol. 106, no. 1, pp. 25–57, 2006.

[136] HSL, "A Collection of Fortran codes for large-scale scientific computation," *See http://www.hsl.rl.ac.uk*, 2007.

[137] S. E. Haupt, B. Kosovic, T. Jensen, J. Lee, P. Jimenez, J. Lazo, J. Cowie, T. Mccandless, J. Pearson, G. Weiner, S. Alessandrini, L. D. Monache, S. Miller, M. Rogers, and L. Hinkleman, "The Sun4cast® Solar Power Forecasting System: the Results of the Public-private-academic Partnership to Advance Solar Power Forecasting," *Ams*, pp. 1–5, 2013.

[138] R. Perez, J. Schlemmer, K. Hemker, S. Kivalov, A. Kankiewicz, and J. Dise, "Solar energy forecast validation for extended areas & economic impact of forecast accuracy," *Conference Record of the IEEE Photovoltaic Specialists Conference*, vol. 2016-Novem, pp. 1119–1124, 2016.

[139] M. Amini and M. Almassalkhi, "Trading off robustness and performance in receding horizon control with uncertain energy resources," in *2018 Power Systems Computation Conference (PSCC)*, pp. 1–7, IEEE, 2018.

[140] A. Bernstein, C. Wang, E. Dall'Anese, J.-Y. Le Boudec, and C. Zhao, "Load flow in multiphase distribution networks: Existence, uniqueness, non-singularity and linear models," *IEEE Transactions on Power Systems*, vol. 33, no. 6, pp. 5832–5843, 2018.

[141] N. Nazir and M. Almassalkhi, "Voltage positioning using co-optimization of controllable grid assets," *arXiv preprint arXiv:1911.00338*, 2019.

[142] L. Duffaut Espinosa, A. Khurram, and M. Almassalkhi, "A Virtual Battery Model for Packetized Energy Management," in *IEEE Conference on Decision and Control (to appear)*, 2020.

[143] L. Zhao, W. Zhang, H. Hao, and K. Kalsi, "A geometric approach to aggregate flexibility modeling of thermostatically controlled loads," *IEEE Transactions on Power Systems*, vol. 32, pp. 4721–4731, Nov 2017.

[144] K. Dehghanpour, Z. Wang, J. Wang, Y. Yuan, and F. Bu, "A survey on state estimation techniques and challenges in smart distribution systems," *IEEE Transactions on Smart Grid*, vol. 10, no. 2, pp. 2312–2322, 2018.

[145] S. P. Nandanoori, I. Chakraborty, T. Ramachandran, and S. Kundu, "Identification and validation of virtual battery model for heterogeneous devices," *arXiv preprint arXiv:1903.01370*, 2019.

[146] S. P. Nandanoori, S. Kundu, D. Vrabie, K. Kalsi, and J. Lian, "Prioritized threshold allocation for distributed frequency response," in *2018 IEEE Conference on Control Technology and Applications (CCTA)*, pp. 237–244, IEEE, 2018.

[147] S. S. Sami, M. Cheng, J. Wu, and N. Jenkins, "A virtual energy storage system for voltage control of distribution networks," *CSEE Journal of Power and Energy Systems*, vol. 4, pp. 146–154, June 2018.

[148] B. Naduvathuparambil, M. C. Valenti, and A. Feliachi, "Communication delays in wide area measurement systems," in *Proceedings of the Thirty-Fourth Southeastern Symposium on System Theory (Cat. No. 02EX540)*, pp. 118–122, IEEE, 2002.

[149] M. Amini and M. Almassalkhi, "Investigating delays in frequency-dependent load control," in *2016 IEEE Innovative Smart Grid Technologies-Asia (ISGT-Asia)*, pp. 448–453, IEEE, 2016.

[150] N. Nazir, P. Racherla, and M. Almassalkhi, "Optimal multi-period dispatch of distributed energy resources in unbalanced distribution feeders," *IEEE Transactions on Power Systems*, vol. 35, no. 4, pp. 2683–2692, 2020.

[151] H. Kwakernaak and R. Sivan, *Linear optimal control systems*, vol. 1. Wiley-interscience New York, 1972.

[152] K. Christakou, J. LeBoudec, M. Paolone, and D. Tomozei, "Efficient computation of sensitivity coefficients of node voltages and line currents in unbalanced radial electrical distribution networks," *IEEE Transactions on Smart Grid*, vol. 4, pp. 741–750, June 2013.

[153] R. D. Zimmerman, C. E. Murillo-Sánchez, R. J. Thomas, *et al.*, "Matpower: Steady-state operations, planning, and analysis tools for power systems research and education," *IEEE Transactions on power systems*, vol. 26, no. 1, pp. 12–19, 2011.

[154] C. Ji, M. Hajiesmaili, D. F. Gayme, and E. Mallada, "Coordinating distribution system resources for co-optimized participation in energy and ancillary service transmission system markets," in *2019 American Control Conference (ACC)*, pp. 1315–1322, IEEE, 2019.

[155] N. Nazir and M. Almassalkhi, "Stochastic multi-period optimal dispatch of energy storage in unbalanced distribution feeders," in *2020 Power Systems Computation Conference (PSCC)*, pp. 1–7, 2020.

[156] S. Alyami, Y. Wang, C. Wang, J. Zhao, and B. Zhao, "Adaptive real power capping method for fair overvoltage regulation of distribution networks with high penetration of PV systems," *IEEE Transactions on Smart Grid*, vol. 5, no. 6, pp. 2729–2738, 2014.

[157] Z. Yang, H. Zhong, A. Bose, T. Zheng, Q. Xia, and C. Kang, "A linearized OPF model with reactive power and voltage magnitude: A pathway to improve the MW-only DC OPF," *IEEE Transactions on Power Systems*, vol. 33, no. 2, pp. 1734–1745, 2018.

[158] A. Bernstein and E. Dall'Anese, "Linear power-flow models in multiphase distribution networks," in *2017 IEEE PES Innovative Smart Grid Technologies Conference Europe (ISGT-Europe)*, pp. 1–6, 2017.

[159] R. H. Tütüncü, K.-C. Toh, and M. J. Todd, "Solving semidefinite-quadratic-linear programs using sdpt3," *Mathematical programming*, vol. 95, no. 2, pp. 189–217, 2003.

[160] R. J. Bravo, R. Salas, T. Bialek, and C. Sun, "Distributed energy resources challenges for utilities," in *Photovoltaic Specialist Conference (PVSC), 2015 IEEE 42nd*, pp. 1–5, IEEE, 2015.

[161] T. S. Basso and R. DeBlasio, "Ieee 1547 series of standards: interconnection issues," *IEEE Transactions on Power Electronics*, vol. 19, no. 5, pp. 1159–1162, 2004.

[162] S. Bolognani, R. Carli, G. Cavraro, and S. Zampieri, "Distributed reactive power feedback control for voltage regulation and loss minimization," *IEEE Transactions on Automatic Control*, vol. 60, no. 4, pp. 966–981, 2015.

[163] Q. Li and V. Vittal, "Non-iterative enhanced sdp relaxations for optimal scheduling of distributed energy storage in distribution systems," *IEEE Transactions on Power Systems*, vol. 32, no. 3, pp. 1721–1732, 2017.

[164] D. Lee, K. Turitsyn, D. K. Molzahn, and L. Roald, "Feasible path identification in optimal power flow with sequential convex restriction," *IEEE Transactions on Power Systems*, pp. 1–1, 2020.

[165] C. Wu, G. Hug, and S. Kar, "Distributed voltage regulation in distribution power grids: Utilizing the photovoltaics inverters," in *American Control Conference (ACC), 2017*, pp. 2725–2731, IEEE, 2017.

[166] N. Nazir and M. Almassalkhi, "Convex inner approximation of the feeder hosting capacity limits on dispatchable demand," in *2019 IEEE 58th Conference on Decision and Control (CDC)*, pp. 4858–4864, IEEE, 2019.

[167] M. Rosenlicht, *Introduction to analysis.* Courier Corporation, 1986.

[168] M. Lubin, E. Yamangil, R. Bent, and J. P. Vielma, "Extended formulations in mixed-integer convex programming," in *International Conference on Integer Programming and Combinatorial Optimization*, pp. 102–113, Springer, 2016.

[169] J. Bank and J. Hambrick, "Development of a high resolution, real time, distribution-level metering system and associated visualization, modeling, and data analysis functions," tech. rep., National Renewable Energy Lab.(NREL), Golden, CO (United States), 2013.

[170] J.-S. Chang and C.-K. Yap, "A polynomial solution for the potato-peeling problem," *Discrete & Computational Geometry*, vol. 1, no. 2, pp. 155–182, 1986.

[171] N. Nazir, P. Racherla, and M. Almassalkhi, "Optimal multi-period dispatch of distributed energy resources in unbalanced distribution feeders," *IEEE Transactions on Power Systems*, pp. 1–1, 2020.

[172] I. J. Pérez-Arriaga, J. D. Jenkins, and C. Batlle, "A regulatory framework for an evolving electricity sector: Highlights of the MIT utility of the future study," *Economics of Energy & Environmental Policy*, vol. 0, no. Number 1, 2017.

[173] T. Lipp and S. Boyd, "Variations and extension of the convex–concave procedure," *Optimization and Engineering*, vol. 17, no. 2, pp. 263–287, 2016.

[174] K. A. Horowitz, A. Jain, F. Ding, B. Mather, and B. Palmintier, "A techno-economic comparison of traditional upgrades, volt-var controls, and coordinated distributed energy resource management systems for integration of distributed photovoltaic resources," *International Journal of Electrical Power & Energy Systems*, vol. 123, p. 106222, 2020.

[175] C. Wang, A. Bernstein, J. Le Boudec, and M. Paolone, “Explicit conditions on existence and uniqueness of load-flow solutions in distribution networks,” *IEEE Transactions on Smart Grid*, vol. 9, no. 2, pp. 953–962, 2018.

[176] A. Bernstein, C. Wang, E. Dall’Anese, J. Le Boudec, and C. Zhao, “Load flow in multiphase distribution networks: Existence, uniqueness, non-singularity and linear models,” *IEEE Transactions on Power Systems*, vol. 33, no. 6, pp. 5832–5843, 2018.

[177] B. Cui and X. A. Sun, “Solvability of power flow equations through existence and uniqueness of complex fixed point,” *arXiv preprint arXiv:1904.08855*, 2019.

[178] “IEEE standard for interconnection and interoperability of distributed energy resources with associated electric power systems interfaces,” *IEEE Std 1547-2018 (Revision of IEEE Std 1547-2003)*, April 2018.

[179] T. Mühlpfordt, L. Roald, V. Hagenmeyer, T. Faulwasser, and S. Misra, “Chance-constrained ac optimal power flow: A polynomial chaos approach,” *IEEE Transactions on Power Systems*, vol. 34, no. 6, pp. 4806–4816, 2019.

[180] D.-H. Choi and L. Xie, “Impact analysis of locational marginal price subject to power system topology errors,” in *2013 IEEE International Conference on Smart Grid Communications (SmartGridComm)*, pp. 55–60, IEEE, 2013.

[181] M. D. Galus, R. A. Waraich, F. Noembrini, K. Steurs, G. Georges, K. Boulouchos, K. W. Axhausen, and G. Andersson, “Integrating power systems, transport systems and vehicle technology for electric mobility impact assessment and efficient control,” *IEEE Transactions on Smart Grid*, vol. 3, no. 2, pp. 934–949, 2012.

[182] B. D. Kroposki, E. Dall-Anese, A. Bernstein, Y. Zhang, and B. S. Hodge, “Autonomous energy grids,” tech. rep., National Renewable Energy Lab.(NREL), Golden, CO (United States), 2017.

[183] R. H. Wiser, A. Mills, J. Seel, T. Levin, and A. Botterud, “Impacts of variable renewable energy on bulk power system assets, pricing, and costs,” tech. rep., Lawrence Berkeley National Lab.(LBNL), Berkeley, CA (United States), 2017.

[184] S. Karagiannopoulos, P. Aristidou, and G. Hug, “Data-driven local control design for active distribution grids using off-line optimal power flow and machine learning techniques,” *IEEE Transactions on Smart Grid*, vol. 10, no. 6, pp. 6461–6471, 2019.

[185] Y. Chen, Y. Tan, and D. Deka, "Is machine learning in power systems vulnerable?," in *2018 IEEE International Conference on Communications, Control, and Computing Technologies for Smart Grids (SmartGridComm)*, pp. 1–6, IEEE, 2018.

[186] A. S. Zamzam, X. Fu, and N. D. Sidiropoulos, "Data-driven learning-based optimization for distribution system state estimation," *IEEE Transactions on Power Systems*, vol. 34, no. 6, pp. 4796–4805, 2019.

[187] M. K. Singh, S. Gupta, V. Kekatos, G. Cavraro, and A. Bernstein, "Learning to optimize power distribution grids using sensitivity-informed deep neural networks," *arXiv preprint arXiv:2007.03728*, 2020.

[188] D. Biagioni, P. Graf, X. Zhang, and J. King, "Learning-accelerated admm for distributed optimal power flow," *arXiv preprint arXiv:1911.03019*, 2019.

[189] F. L. Lewis and D. Vrabie, "Reinforcement learning and adaptive dynamic programming for feedback control," *IEEE circuits and systems magazine*, vol. 9, no. 3, pp. 32–50, 2009.

[190] J. Ostrometzky, K. Berestizshevsky, A. Bernstein, and G. Zussman, "Physics-informed deep neural network method for limited observability state estimation," *arXiv preprint arXiv:1910.06401*, 2019.

APPENDIX

5.A PROOF OF THEOREM 1

Proof. Since the SOCP optimization problem is convex and Slater's condition holds trivially, the KKT optimality conditions are both necessary and sufficient. Thus, for the KKT conditions, let

- $\mathcal{L}$ be the Lagrangian.
- $\lambda_{\mathrm{p}} \in \mathbb{R}$ be the Lagrange multiplier for (3.2e).
- $\lambda_{\mathrm{s}} \in \mathbb{R}_{+}$ be the Lagrange multiplier for inequality (3.2j).
- $\underline{\lambda_{\mathrm{d}}}, \overline{\lambda_{\mathrm{d}}} \in \mathbb{R}_{+}$ be Lagrange multipliers associated with the lower bound and upper bound of inequality (3.2m), respectively.
- $\underline{\lambda_{\mathrm{c}}}, \overline{\lambda_{\mathrm{c}}} \in \mathbb{R}_{+}$ be Lagrange multipliers for the lower and upper bounds of inequality (3.2n), respectively.

Note that P^{c} and P^{d} are the charging and discharging rates for the battery at node n, phase ϕ at time t and represent primal variables and $\eta_{\mathrm{c}}, \eta_{\mathrm{d}} \in (0, 1]$ are the charging and discharging efficiencies.

From the KKT optimality conditions, the following relation is obtained from the Lagrangian with respect to P^{c}, i.e., $\frac{\partial \mathcal{L}}{\partial P^{\mathrm{c}}} \equiv 0$:

$$\frac{\partial f(x)}{\partial P^{\mathrm{c}}} - \underline{\lambda_{\mathrm{c}}} + \overline{\lambda_{\mathrm{c}}} - \eta_{\mathrm{c}}\Gamma(t)\Delta t + \lambda_{\mathrm{p}} - 2\lambda_{\mathrm{s}}(P^{\mathrm{d}} - P^{\mathrm{c}}) = 0. \tag{5.1}$$

With respect to P^{d}, KKT conditions give $\frac{\partial \mathcal{L}}{\partial P^{\mathrm{d}}} \equiv 0$:

$$\frac{\partial f(x)}{\partial P^{\mathrm{d}}} + \alpha(\frac{1}{\eta_{\mathrm{d}}} - \eta_{\mathrm{c}}) - \underline{\lambda_{\mathrm{d}}} + \overline{\lambda_{\mathrm{d}}} + \frac{\Gamma(t)\Delta t}{\eta_{\mathrm{d}}} - \lambda_{\mathrm{p}} + 2\lambda_{\mathrm{s}}(P^{\mathrm{d}} - P^{\mathrm{c}}) = 0. \tag{5.2}$$

Adding (5.1) and (5.2) gives:

$$\underline{\lambda_{\mathrm{c}}} + \underline{\lambda_{\mathrm{d}}} = \overline{\lambda_{\mathrm{c}}} + \overline{\lambda_{\mathrm{d}}} + (\alpha + \Gamma(t)\Delta t)\left(\frac{1}{\eta_{\mathrm{d}}} - \eta_{\mathrm{c}}\right) + \frac{\partial f(x)}{\partial P^{\mathrm{c}}} + \frac{\partial f(x)}{\partial P^{\mathrm{d}}} \tag{5.3}$$

In order to avoid SCD, the right hand side of equation (5.3) needs to be strictly positive. In the above equation $\overline{\lambda_{\mathrm{c}}} \geq 0$ and $\overline{\lambda_{\mathrm{d}}} \geq 0$, which changes (5.3) to the following inequality:

$$\underline{\lambda_{\mathrm{c}}} + \underline{\lambda_{\mathrm{d}}} \geq (\alpha + \Gamma(t)\Delta t)\left(\frac{1}{\eta_{\mathrm{d}}} - \eta_{\mathrm{c}}\right) + \frac{\partial f(x)}{\partial P^{\mathrm{c}}} + \frac{\partial f(x)}{\partial P^{\mathrm{d}}} \tag{5.4}$$

It can be seen that condition C1 is satisfied by the given objective functions, e.g. for objective $(P^{\mathrm{d}} - P^{\mathrm{c}} - P^{\mathrm{ref}})^2$, $\frac{\partial f(x)}{\partial P^{\mathrm{c}}} + \frac{\partial f(x)}{\partial P^{\mathrm{d}}} = -2(P^{\mathrm{d}} - P^{\mathrm{c}} - P^{\mathrm{ref}}) + 2(P^{\mathrm{d}} - P^{\mathrm{c}} - P^{\mathrm{ref}}) = 0$. Based on these facts, (5.4) gives:

$$\underline{\lambda_{\mathrm{c}}} + \underline{\lambda_{\mathrm{d}}} \geq (\alpha + \Gamma(t)\Delta t)\left(\frac{1}{\eta_{\mathrm{d}}} - \eta_{\mathrm{c}}\right) \tag{5.5}$$

Based on the value of $\Gamma(t)$, the problem is divided into two cases:

1. $\Gamma(t) \geq 0$: This is the case where the battery does not hit its upper capacity limit which makes $\Gamma(t) \geq 0$ and as a result, the right hand side of (5.5) is strictly positive due to condition C2. Hence, if efficiencies are non-unity, simultaneous charging and discharging is avoided in this case. If efficiencies are unity, SCD fictitious losses are zero, so it is always exact.

2. $\Gamma(t) < 0$: this implies that the battery must hit its upper limit of state of charge at least once over the prediction horizon. In this case, the battery may waste energy through SCD in order to lower its state of charge. Parameter α is added to discourage SCD in the battery. When battery is at its lower limit, SCD may occur at optimality to consume more power. The α term acts as a penalty to discourage SCD. In this case, α would have to be chosen in such a way that condition C3 is satisfied. Hence, conditions C1, C2, and C3 represent sufficient conditions for avoiding SCD.

$\square\square\square$

5.B AVOIDING SCD WHEN TRACKING A DESIRED BATTERY STATE OF CHARGE

For the objective function: $f(B_{n,T}) = \left(B_{n,T} - B^{\mathrm{d}}\right)^2$, where $B_{n,T} = B_{n,t} + \Delta t \sum_{\tau=t}^{T-1} \left(\eta_{\mathrm{c},n} P^{\mathrm{c}}_{n,\tau} - \frac{1}{\eta_{\mathrm{d},n}} P^{\mathrm{d}}_{n,\tau}\right)$, Corollary 1 provides conditions for the relaxation to be exact. These conditions are more restrictive than the ones required in Theorem 1.

Corollary 1. *For the objective function $f(B_{n,T})$, the relaxation is exact under the following conditions:*

A1: $\lambda_p \geq 0$.

A2: $\alpha > 0$

Proof. Let $P^{\mathrm{c}} \geq P^{\mathrm{d}}$, then using KKT conditions, $\underline{\lambda_{\mathrm{c}}} = 0$, $\overline{\lambda_{\mathrm{c}}} \geq 0$ and the following equation is obtained from the Lagrangian with respect to P^{c}:

$$\Gamma(t)\Delta t \geq \frac{1}{\eta_{\mathrm{c}}}(\lambda_{\mathrm{p}} + \frac{\partial f(B_{n,T})}{\partial P^{\mathrm{c}}} - 2\lambda_{\mathrm{s}}(P^{\mathrm{d}} - P^{\mathrm{c}})) \tag{5.6}$$

Since $\overline{\lambda_{\mathrm{d}}} \geq 0$, with respect to P^{d}, the following KKT condition results:

$$\Gamma(t)\Delta t \leq \eta_{\mathrm{d}}(\lambda_{\mathrm{p}} - \alpha(\frac{1}{\eta_{\mathrm{d}}} - \eta_{\mathrm{c}}) + \underline{\lambda_{\mathrm{d}}} - \frac{\partial f(B_{n,T})}{\partial P^{\mathrm{d}}} - 2\lambda_{\mathrm{s}}(P^{\mathrm{d}} - P^{\mathrm{c}})) \tag{5.7}$$

Comparing (5.6) and (5.7) gives:

$$\begin{split}\eta_{\mathrm{d}}\underline{\lambda_{\mathrm{d}}} \geq \alpha(1 - \eta_{\mathrm{d}}\eta_{\mathrm{c}}) + \lambda_{\mathrm{p}}(\frac{1}{\eta_{\mathrm{c}}} - \eta_{\mathrm{d}}) + 2\lambda_{\mathrm{s}}(\frac{1}{\eta_{\mathrm{c}}} - \eta_{\mathrm{d}})(P^{\mathrm{c}} - P^{\mathrm{d}}) \\ + \eta_{\mathrm{d}}\frac{\partial f(B_{n,T})}{\partial P^{\mathrm{d}}} + \frac{1}{\eta_{\mathrm{c}}}\frac{\partial f(B_{n,T})}{\partial P^{\mathrm{c}}}\end{split} \tag{5.8}$$

Using conditions A1, A2 and the fact that $\frac{\partial f(B_{n,T})}{\partial P^{\mathrm{c}}} = 2\eta_{\mathrm{c}}(B_{n,T} - B^{\mathrm{d}})$, $\frac{\partial f(B_{n,T})}{\partial P^{\mathrm{d}}} = -\frac{2}{\eta_{\mathrm{d}}}(B_{n,T} - B^{\mathrm{d}})$ and $\lambda_{\mathrm{s}} \geq 0$ in (5.8) gives $\underline{\lambda_{\mathrm{d}}} > 0$ and hence $P^{\mathrm{d}} = 0$, provided $\eta_{\mathrm{c}}, \eta_{\mathrm{d}} < 1$ and $P^{\mathrm{c}} \geq P^{\mathrm{d}}$. A similar procedure can be used to show that when $P^{\mathrm{c}} < P^{\mathrm{d}}$, then $P^{\mathrm{c}} = 0$. Hence, $P^{\mathrm{d}}P^{\mathrm{c}} \equiv 0$ is enforced. □□□

5.C LinDist model at optimality

Based on the mathematical modeling presented in section 4.1.3.1, the optimization problem to determine the operating region of dispatchable resources using *LinDist* model can be expressed as:

$$\text{(P5)} \quad \max_{V,p,q} \sum_{i=1}^{n} \log(p_i) \tag{5.9a}$$

$$\text{subject to :} \quad M_{\mathrm{p}} p = V - v_0 \mathbf{1} - M_{\mathrm{q}} q \tag{5.9b}$$

$$\underline{S}_i \leq f(p_i, q_i) \leq \overline{S}_i \quad \forall i \in \mathcal{N} \tag{5.9c}$$

$$\underline{V} \leq V \leq \overline{V} \tag{5.9d}$$

Theorem 5. *With the LinDist model applied to a radial, inductive distribution feeder, the constraints related to reactive power injections from the dispatchable demand-side resources are all active (i.e., $f(p_i, q_i) = \underline{S}_i$ or $f(p_i, q_i) = \overline{S}_i$ for all i).*

Proof. (by contradiction): Assume that at optimality the reactive power is not at its constraint (i.e., $\exists\, i, \text{s.t } \underline{S_i} < f(p_i, q_i) < \overline{S_i}$). Then, the Lagrange multiplier associated with (5.9c) is zero and, hence, this constraint will not show up in the KKT conditions.

The voltage constraint in (5.9d) can be expressed as:

$$\underline{V} \leq M_{\mathrm{p}} p + M_{\mathrm{q}} q + v_0 \mathbf{1} \leq \overline{V} \tag{5.10}$$

Let $\underline{\lambda} \in \mathbb{R}^n$ and $\overline{\lambda} \in \mathbb{R}^n$ be the Lagrange multipliers associated with (5.9d) and let $\mathcal{L}$

be the Lagrangian. From the KKT conditions, the following relations are obtained:

$$\frac{\partial \mathcal{L}}{\partial p_i} = \frac{1}{p_i} - \underline{\lambda}^i [M_{\mathrm{p}}]_i + \overline{\lambda}^i [M_{\mathrm{p}}]_i = 0 \tag{5.11}$$

$$\frac{\partial \mathcal{L}}{\partial q_i} = - \underline{\lambda}^i [M_{\mathrm{q}}]_i + \overline{\lambda}^i [M_{\mathrm{q}}]_i = 0 \tag{5.12}$$

where $[M_{\mathrm{p}}]_i$ and $[M_{\mathrm{q}}]_i$ are the sums of the ith columns of M_{p} and M_{q}, respectively. From (5.12), since $[M_{\mathrm{q}}]_i > 0$ for inductive networks, we have that $\alpha_i \overline{\lambda}^i - \beta_i \underline{\lambda}^i = 0$ for some $\alpha_i, \beta_i > 0$, which implies that $\overline{\lambda}^i = \underline{\lambda}^i = 0$. Substituting this result in (5.11), gives $\frac{1}{p_i} = 0$, which is not possible for p_i finite. Thus, we reach a contradiction. Hence, constraint (5.9c) must be active. In other words, the reactive power at optimality is always at the boundary of its constraint. □□□